UNIVERSITY OF NAPLES FEDERICO II

Doctorate in Earth, Environmental and Resource Sciences

Doctoral thesis in Stratigraphy and Tectonics

(Cycle XXXIII)

CONSTRAINING THE ONSET OF FLEXURAL SUBSIDENCE AND THE RATE OF FOREBULGE-FOREDEEP MIGRATION IN THE FORELAND BASIN SYSTEM OF THE CENTRAL-SOUTHERN APENNINE BELT (ITALY) BY SR-ISOTOPE STRATIGRAPHY

Supervisor

Prof. Mariano Parente

Co-supervisors

Prof. Stefano Tavani

Prof. Stefano Vitale

Ph.D. Candidate

Monia Sabbatino

Head of Doctorate

Prof. Maurizio Fedi

Academic Year 2019/2020

A mio padre, la roccia che ha ispirato la mia vita

To my father, my rock and inspiration

Table of Contents

ABSTRACT

In fold and thrust belts developing at convergent margins, the migration of the advancing wedge is accompanied by bulging of the downgoing plate, followed by the development of a foredeep basin filled by a thick succession of syn-orogenic sediments. The transition from forebulge to foredeep marks a key moment in the evolution of the orogenic system. In deep-water environments, the record of this transition is typically complete and progressive. Conversely, in the shallow-water/continental environment of many collisional systems, the uplift of the forebulge area can imply emersion and erosion, obliterating the stratigraphic record of key steps of the evolution of the orogenic system.

The Apennines are a retreating collisional belt where the foreland basin system, in large domains, is floored by a subaerial forebulge unconformity developed due to bulge uplift and erosion. This unconformity is overlain by a diachronous sequence of three lithostratigraphic units made of: (i) shallow-water carbonates, (ii) hemipelagic marls and shales, and (iii) siliciclastic turbidites. Typically, the latter have been interpreted regionally as the onset of syn-orogenic deposition in the foredeep depozone, while little attention has been given to the underlying units. Accordingly, the rate of migration of the southern Apennine foreland basin-belt system has been constrained, so far, exclusively considering the age of the turbidites, which largely postdate the onset of sedimentation in the foredeep depozone.

This thesis provides new high-resolution ages obtained by strontium isotope stratigraphy applied to the low-Mg calcite of bivalve shells sampled at the base of the first syn-orogenic deposits overlying the Eocene-Cretaceous pre-orogenic substratum. This new regional dataset of high-resolution ages obtained from the detailed analysis of 203 samples collected from 15 sites (37 sub-sites) across the central-southern Apennines, integrated with previously published data, provide a comprehensive spatial-temporal evolutive model of the Apennine belt and foreland basin system from the early Miocene to the

Recent. In particular, this dataset indicates progressive rejuvenation of the strata sealing the forebulge unconformity toward the outer portions of the belt. Plotting the data on a restored section of the pre-orogenic Adria passive margin reveals that the age of the forebulge unconformity linearly scales with the position of the analyzed sites in their pre-orogenic position, pointing to an overall constant velocity of migration of the forebulge wave in the last 25 Myr. A comparative analysis of previously used datasets reveals that dating the base of the post-bulging carbonates represents the best tool to constrain the style and rate of the foreland flexuring.

CHAPTER 1. GENERAL INTRODUCTION

1.1 Rationale – Foreland flexure and syn-orogenic sedimentation: the need for high-resolution age constraints

Foreland basins are key portions of orogenic systems, forming ahead and above of thrust belts due to the downward flexing of the lithosphere during convergence (Allen et al., 1986; DeCelles and Giles, 1996). Information about the timing of the thrust belt – foreland basin system development has been derived mainly by the age of syn-orogenic deposits filling the fossil foreland basins (Ori et al., 1986; Cipollari and Cosentino, 1995; Cavinato and DeCelles, 1999; Bigi et al., 2009; Vezzani et al., 2010; Vitale and Ciarcia, 2013). Indeed, the architecture and stratigraphy of foreland basins provide constraints on the evolution of the associated thrust belts and on the migration rate of the subduction hinge (e.g., Allen et al., 1986; Ori et al., 1986; DeCelles and Giles, 1996; DeCelles and DeCelles, 2001; DeCelles, 2012). Typically, foreland basin systems host four depozones: wedge-top, foredeep, forebulge, and back-bulge (DeCelles and Giles, 1996). Accordingly, numerous studies have documented the genetic linkages between thrust belt kinematics, orogenic loading, and flexural subsidence in foreland basins. Flexural loading of an ideal elastic plate results in a rapidly damped sinusoidal profile with a large magnitude negative flexure adjacent to the load (the foredeep depozone), a medial positive flexural bulge (the forebulge), and a secondary negative depression in the most distal region (the back-bulge depozone) (DeCelles, 2012). The amplitude of deflection (negative or positive) decreases by roughly three orders of magnitude from the foredeep to the back-bulge depozone. Typical flexural loading of continental lithosphere produces a foredeep depression that scales horizontally with $\pi\alpha$, where α is defined as the flexural parameter (Turcotte and Schubert, 2006):

$$\alpha = \left[\frac{4D}{\Delta\rho g}\right]^{1/4}$$

where D is the flexural rigidity of the lithosphere, g is the acceleration of gravity, and $\Delta\rho$ is the difference in density between the mantle and the basin fill ($\simeq$ 3200 – 2800 kg/m^3). The flexure of the lithosphere depends on: (i) the lithosphere elastic thickness (usually referred to as effective elastic thickness of the lithosphere or stiffness, T_e), (ii) the elastic properties of the lithosphere, and (iii) the applied load or force (Turcotte and Schubert, 1982). The flexural rigidity of the lithosphere is determined by the Young's modulus (E = 6.5x 10^{10} Pa), Poisson's ratio (ν = 0.25) and the elastic thickness of the lithosphere according to the following equation:

$$\mathrm{D} = \frac{ET_e{}^3}{12(1-\nu^2)}$$

Typical values of D for continental lithosphere range between ~5x10^{22}Nm and 4x10^{24}Nm (corresponding to elastic thicknesses of 20–90km; e.g., Jordan, 1981; Lyon-Caen and Molnar, 1985; Watts, 2001; Roddaz et al., 2005). The basic flexural equation predicts that the foredeep depozones are typically 100-300 km wide and 2-8km thick (DeCelles and Giles, 1996). The forebulge in a typical flexural basin filled to the crest of the forebulge should be of the order of 60–470 km wide, and a few tens to a few hundred meters high (DeCelles and Giles, 1996). Broken plates and plates with lower flexural rigidity should have higher, narrower forebulges than infinite plates and more rigid plates (Turcotte and Schubert, 1982).

Incorporation of the four-part foreland basin system into palinspastic restorations allows for better constrained estimates of flexural wave migration because both the foredeep and forebulge may be used to position the flexural wave through time within the context of palinspastically restored foreland basin stratigraphy. Also, the distance of flexural wave migration can be used to determine total amount of shortening, especially in orogenic belts where the total amount of shortening cannot be reliably estimated from balanced regional cross sections (DeCelles and DeCelles, 2001).

Depending on the tectonic setting where a foreland basin system develops, the foreland basin depozones develop different characteristics. Accordingly, three main types of contractional foreland basin settings can be defined: retroarc, collisional, and collisional with retreating subducting slabs (DeCelles 2012, pp. 411–416, for a detailed review).

Collisional tectonic settings characterized by a subduction rate exceeding the regional convergence rate, produce particular orogenic chains called retreating collisional belts (DeCelles, 2012). In these chains, the orogenic evolution is driven by the roll-back mechanism (e.g., Malinverno and Ryan, 1986), where the hinge line of the subducting plate rolls through the plate in opposite direction to the direction of subduction.

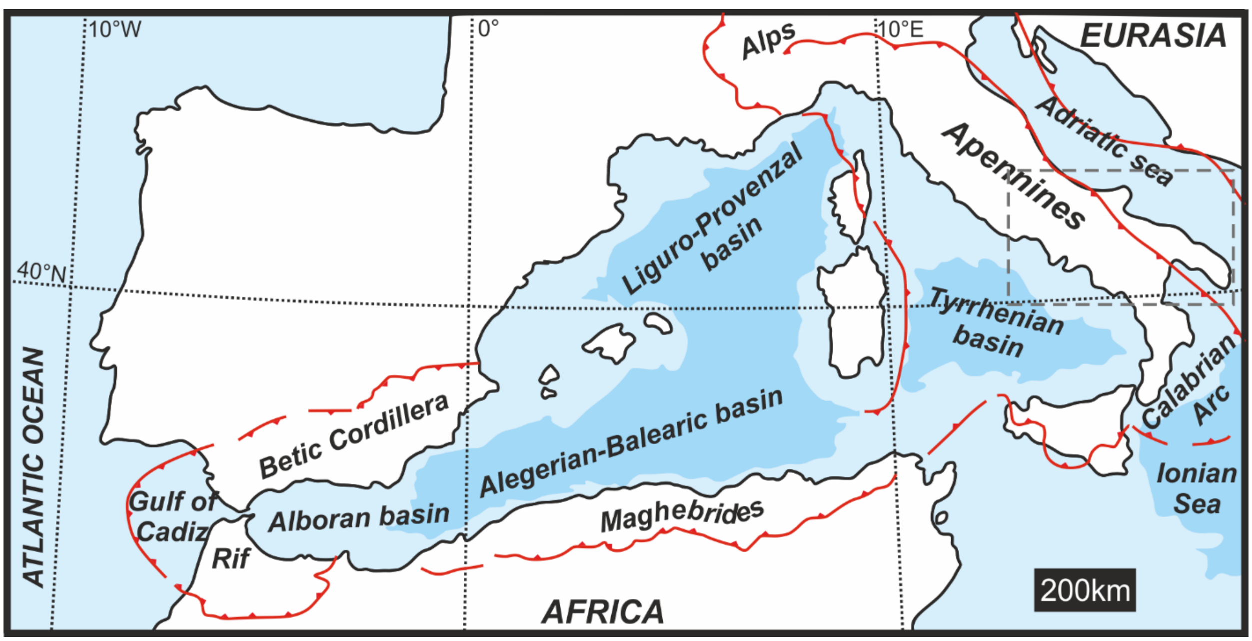

Figure 1.1. Tectonic sketch map of the Western Mediterranean subduction zone.

The Apennines are a classic example of a retreating collisional belt developing in the framework of the Western Mediterranean subduction zone (Fig. 1.1) (Royden and Faccenna, 2018 and references therein), characterized by narrow but thick foredeep and wedge-top depozones, and very narrow forebulge and back-bulge depozones (DeCelles, 2012). In such a context, during the accretionary wedge migration, following the slab retreat (Fig. 1.2), the foreland undergoes to bending, with uplift, erosion and extension (stage 2; peripheral bulge or forebulge; Fig. 1.2), generally accompanied by faulting and fracturing in the upper crust (Tavani et al., 2015a). The stratigraphic expression of this stage is a forebulge unconformity at the top of the passive margin megasequence (Crampton and Allen, 1995). Subsequently, flexural subsidence causes the drowning of the previously emerged and eroded forebulge zone and the deposition of unconformable sediments of the foreland basin megasequence, first in shallow-water (stage 3, post-forebulge transgression; Fig. 1.2) and afterwards in hemipelagic setting (stage 4; Fig. 1.2). The system evolves with the deposition of siliciclastics (stage 5; Fig. 1.2), deriving from the erosion of the orogenic belt and secondarily by the foreland and syn-orogenic volcaniclastic and calciclastic sediments. Finally, foredeep deposits get incorporated into the accretionary wedge and overlain by unconformable sediments deposited in wedge-top basins (stage 6; Fig. 1.2). The vertical stacking pattern of this syn-orogenic sequence follows the Walther's law of foreland basin stratigraphy (DeCelles, 2012).

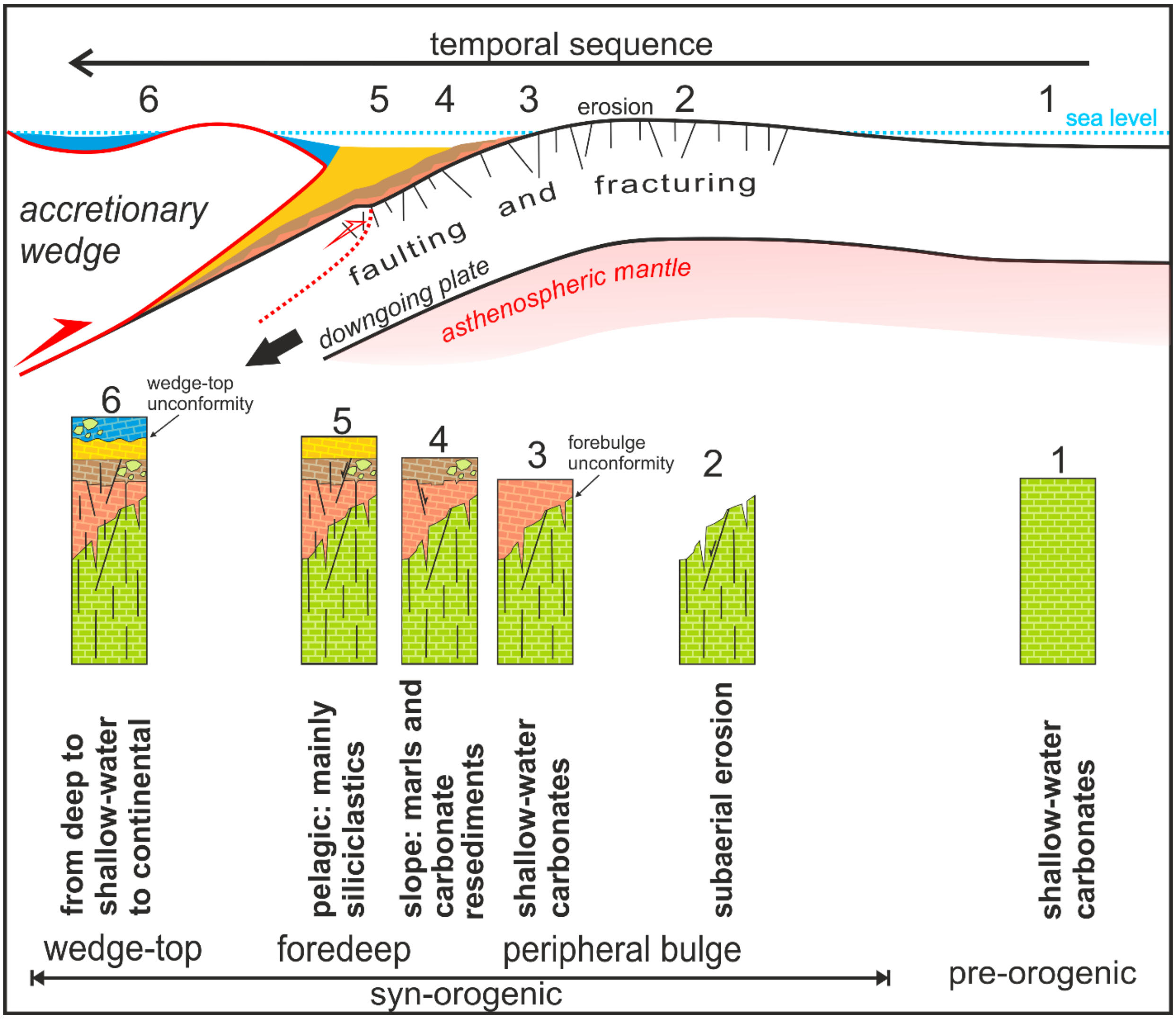

Figure 1.2. Schematic tectonostratigraphic evolution of a foreland basin system in response to the accretionary wedge migration. The scheme refers to a basin where the forebulge unconformity develops in subaerial condition and the syn-orogenic sedimentation in the foredeep depozone starts in shallow-water carbonate system**.**

The architecture and stratigraphy of the central and southern Apennines, including its fossil foreland basins, have been extensively studied in the last decades (e.g., Patacca and Scandone, 2007; Cosentino et al., 2010; Vezzani et al., 2010; Critelli et al., 2011; Vitale and Ciarcia, 2013 among others). Typically, the timing of migration and deformation of the Apennine belt-foreland basin system has been constrained using the ages of the siliciclastic turbidites filling the foredeep and wedge-top depozones. However, those strata do not represent the first syn-orogenic depositional event on the foreland plate. In fact, the earliest stage of a foreland basin system history predates the passage of the forebulge and it is recorded by the slow accumulation in the back-bulge depozone, which, in retreating collisional settings like the Apennines, is generally removed by erosion during passage of the forebulge itself (e.g., DeCelles, 2012). During forebulge uplift, the lithosphere flexes upward, causing stratigraphic condensation, erosion, and development of a forebulge unconformity in shallow-water settings (Crampton and Allen, 1995). In these cases, the deposits directly overlying the unconformity constitute the first record of syn-orogenic deposition associated with the most distal portion of the foredeep depozone, not reached by siliciclastic input.

To date, the early evolutionary stage in the syn-orogenic history of the central-southern Apennines has not been investigated in detail: filling this gap constitutes the main aim of this thesis. In particular, the main goal is precisely constraining the age of the onset of flexural subsidence by dating the first datable carbonate sediments overlying the forebulge along a large transect of the orogenic belt, extending from inner to outer sectors (i.e., from W to E/NE; Fig. 1.3). This goal is achieved by means of Strontium Isotope Stratigraphy (SIS) (Chapters 4 and 6). This method is particularly suitable for high-resolution dating and correlation of Miocene marine carbonates because the reference curve for this stratigraphic interval is characterized by a very narrow statistical uncertainty and by a very high slope (i.e., rapid unidirectional change of $^{87}Sr/^{86}Sr$ ratio of the ocean through time) (McArthur, 1994). For these reasons, a resolution of up to 0.1 Ma can be potentially attained in Miocene marine deposits. Moreover, Miocene shallow-water carbonate units of the Apennines contain low-Mg calcite shells of pectinid and ostreid bivalves, which are one of the best materials for SIS (McArthur et al., 2020 and references therein; see further details in Chapter 2). Besides constraining the timing of the onset of syn-orogenic sedimentation, the secondary aim of this research is to study in detail the transition from pre-orogenic to syn-orogenic sequences and the forebulge unconformity. Such transition can be either extremely abrupt or witnessed by a more complete sedimentary record, largely depending on the depositional environment of the forebulge area itself (Crampton and Allen, 1995). In fact, when bulging occurs in sub-marine environments, the first phase of syn- to post-forebulge sedimentation occurs generally in a deep-water setting, such as in the Aruma Group on Wasia-Aruma Break in Oman-UAE (Robertson, 1987; Boote et al., 1990; Robertson and Searle, 1990; Cooper et al., 2014), and in the Gurpi-Pabdeh Group in Zagros (Vergés et al., 2011; Saura et al., 2015). In these settings the stratigraphic interval associated with the flexural bulge is fully registered by sediments. In tectonic settings involving mostly subaerial peripheral bulge areas, distinctive and articulated forebulge unconformities can develop through erosion and karst, such as on top of passive margin rocks of the Adriatic carbonate platform (Otoničar, 2007).

In most parts of the central-southern Apennines, a paraconformity/disconformity separates the shallow-water carbonates of the pre-orogenic sequence from syn-orogenic open marine carbonate ramp strata. Only in a few areas, red beds followed by very proximal marine or paralic deposits, witnessing the first stage of the syn-orogenic transgression, have been preserved. These deposits contain rich foraminiferal assemblages commonly dominated by specimens of the genus *Ammonia,* a benthic foraminifer typically dwelling in littoral and neritic environments (Chapter 5).

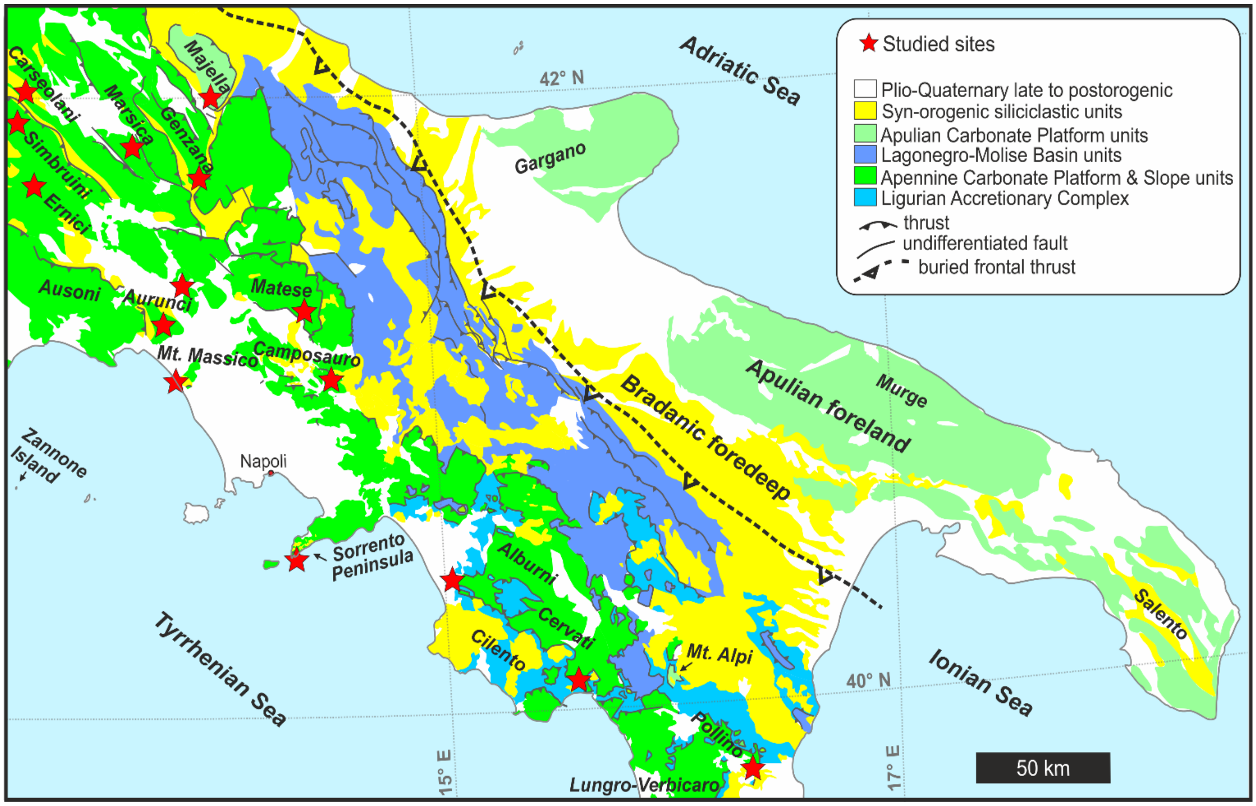

Figure 1.3. Schematic geological map of the central and southern Apennines showing the locations of the studied sites (modified after Vitale and Ciarcia, 2013).

For this project I have assembled a regional dataset consisting of high-resolution Sr-isotopes ages of the first datable syn-orogenic strata in 15 sites (37 sub-sites) across the central-southern Apennines (Fig. 1.3). This dataset, based on the analysis of 203 samples, has been integrated with previously published ages of syn-orogenic deposits and used to build a comprehensive spatial-temporal evolutive model of the Apennine belt and foreland basin system from the early Miocene to the Recent. Plotting the data for the studied localities on a restored section of the pre-orogenic Adria passive margin, reveals that, among the different lithostratigraphic units of the foreland megasequence, dating the base of the post-bulging carbonates represents the best tool to constrain the style and rate of the foreland flexuring (Chapter 6).

Overall, this research, providing these unprecedented age constraints, helps to define for the first time the onset of deformation in the forebulge area, and thus better constrain the amount and rate of shortening and trench retreat in the Apennine fold and thrust belt. Ultimately, the workflow used in this thesis can be applied to other fold and thrust belts where subaerial exposure has produced an incomplete record of the transition from bulging to foredeep.

1.2 Thesis outline

This thesis is organized into 6 chapters. Besides this first introductory Chapter 1, Chapter 2 is a summary of the geological setting including all the studied locations in the central-southern Apennines. In section 3 the main methods leading this research are outlined. Chapters 4, 5 and 6 are the three papers containing the main results of the thesis. The first two are published (Ch. 4 in Sedimentary Geology, Ch. 5 in Palaeogeography, Palaeoclimatology, Palaeoecology); the third one (Ch. 6) is under review in Basin Research.

1.3 Note to the reader

This work is part of the research project ApMioFore (scientific coordinator Mariano Parente), funded by the University of Naples Federico II under the scheme “Progetto di Ricerca di Ateneo” (ID number: E62F17000190005). The chapters 5 to 7 in this thesis should be seen and read as individual studies that are all part of the larger research project. This implies that each chapter can be read individually. This also implies that there may be some overlap in the explained methodologies and geological settings. The sequence of chapters has to be seen as a progressive upscaling of the targeted goal, from a localized study area to a regional transect. To make easier the understanding of the whole study area from the beginning, the geological setting of the whole central-southern Apennines is presented in the following section.

1.4 Data availability

Most of the results, methods, and interpretations presented in this thesis are available in the form of research articles. For each chapter/article and supplementary information, the generated DOI can be found in the respective data availability sections.

CHAPTER 2. GEOLOGICAL SETTING: THE CENTRAL-SOUTHERN APENNINES

The Apennines are part of the Western Mediterranean subduction zone that evolved in the framework of the Alpine-Himalayan geodynamic system (Fig. 1.1) (e.g., Faccenna et al., 2001; Royden and Faccenna, 2018). The orogenic system formed by the westward subduction of Adria beneath Europe (Malinverno and Ryan, 1989) and evolved in the context of a retreating collisional system, characterized by a progressive arching of an originally nearly linear belt, following the E-ward retreat of the trench and the opening of the Tyrrhenian back-arc basin (e.g., Dewey et al., 1989; Malinverno and Ryan, 1986; Doglioni, 1991; Mazzoli and Helman, 1994; Faccenna et al., 2014). During such convergence, several tectonic units, originally deposited in a system of carbonate platforms and intervening deep basins that developed on the southern margin of the Alpine Tethys ocean since the Triassic (Bosellini, 2004), were imbricated to form the Apennine thrust belt.

In more detail, the Apennines can be further subdivided into two main arcs: the northern and the southern Apennines, which connect in the central Apennines. The present-day tectonic architecture of the southern Apennines is made up of the thrust sheets of the Mesozoic Lagonegro-Molise Basin successions, sandwiched between thrust sheets composed of the overlying Apennine and underlying Apulian Mesozoic shallow-water platforms. The Apennine platform is in turn overthrust by the deep basinal units of the Ligurian accretionary complex, which was deposited on top of the Jurassic oceanic and thinned continental crust and exhumed oceanic lithosphere (Fig. 1.3) (e.g., Cello and Mazzoli, 1998; Mazzoli et al., 2008, Tavani et al., 2021). The western part of the Apulian platform is deformed under a thick tectonic pile, and is now exposed in the Mount Alpi, in the southern Apennines, and Majella Mountains in the central Apennines. The outer (eastern) sector of the Apulian platform is exposed in the foreland region of the southern Apennines to the NE, where it is locally buried underneath a Plio-Pleistocene sedimentary cover (Fig. 1.3).

The foreland basin, which developed ahead of the central-southern Apennine tectonic edifice, was progressively filled with syn-orogenic sediments, following a younging trend toward the east/north-east. The Miocene to Pleistocene syn-orogenic carbonates, object of this study, unconformably overlie the Apennine and Apulia carbonate platform pre-orogenic units. The Apennine and Apulia platform units represent allochthonous, and (partly) autochthonous, respectively, paleogeographic domains witnessing a long-term record of pre-orogenic passive margin shallow-water carbonate sedimentation. Thick platform successions (up to 6000m; Ricchetti et al., 1988) developed from the Late Triassic to the Late Cretaceous (Bernoulli, 2001), with the only long-lasting interruption by prolonged subaerial exposure recorded in some areas by 'middle' Cretaceous karst bauxites (Mindszenty et al., 1995). Shallow-water carbonate sedimentation resumed in some sparse areas in the Paleogene and is now represented by much less widespread, thin, and stratigraphically discontinuous deposits (Selli, 1962; Chiocchini et al., 1994) overlying unconformably Upper Cretaceous platform carbonates. In the southern Apennines, this stratigraphic interval is represented by an up to 150 m-thick sequence of lower-middle Eocene limestones, known as the Trentinara Formation (Selli, 1962), which is widely exposed in the Alburno-Cervati (Cilento Promontory) and Pollino Mountains (Fig. 1.3). In the central Apennines analogous facies, described as "Spirolina sp. Limestones" (Chiocchini and Mancinelli, 1977; Romano and Urgera, 1995; Vecchio et al., 2007), are much less widespread and reach a maximum thickness of about 30 m (Romano and Urgera, 1995). After this prolonged phase of passive margin sedimentation and a long-lasting Cretaceous/Eocene to Miocene hiatus, a new phase of shallow-water carbonate sedimentation occurred starting from the early Miocene, related to the development of the Apennine belt. A long-lasting hiatus separates the pre-orogenic Cretaceous/Eocene deposits of the Apennine and Apulia platforms from the Neogene syn-orogenic shallow-water carbonates. The history entailed by such a long hiatus has not been unraveled yet and its causative processes are still debated. The most accepted scenarios invoke either subaerial erosional processes and/or by-pass and erosion in a submarine environment (Damiani et al., 1992; Cipollari and Cosentino, 1995; Brandano, 2017).

2.1 The central-southern Apennine foreland basin system

Starting from the Miocene, the foreland of the central-southern Apennines has experienced pre-thrusting bulging, uplift, and erosion, caused by the bending of the subducting lithosphere and by the E/NE-ward migration of the accretionary wedge (e.g., Doglioni, 1995). This tectonic stage is recorded by a regional unconformity, by extensional fracturing and faulting in the uppermost part of the lithosphere, and by the onset of flexural subsidence, conforming to the models of foreland basin evolution in retreating collisional systems (Turcotte and Schubert, 1982; Bradley and Kidd, 1991; Crampton and Allen, 1995; Doglioni, 1995; DeCelles and Giles, 1996; DeCelles, 2012; Carminati et al., 2014). The onset of flexural subsidence is recorded by time-transgressive deposits overlying the pre-orogenic substrate. In absence of records of the earliest syn-orogenic back-bulge depozone, the Miocene shallow-water carbonates of the central-southern Apennines represent the base of the foreland basin mega-sequence (Sabbatino et al., 2020). The vertical stacking pattern of the Apennine foreland basin conforms to the "Waltherian sequence" of DeCelles (2012), recording the spatial-temporal evolution and migration of syn-orogenic depozones in front of the migrating orogenic belt. The sequence is composed of the basal subaerial forebulge unconformity at the top of the pre-orogenic passive margin megasequence, overlain by three diachronous lithostratigraphic units, which from bottom to top are: (i) a shallow-water carbonate unit, (ii) a hemipelagic marly unit, and (iii) a siliciclastic turbiditic unit (Fig. 1.2) ("underfilled trinity"; Sinclair, 1997).

The facies transition from pre-, syn-, and post- bulging is only sporadically fully recorded in the Apennines, such as in the Cilento area of southern Apennines (Boni, 1974) and in Scontrone and Palena areas of the central Apennines (Patacca et al., 2008; Carnevale et al., 2011). In most parts of the central-southern Apennines, a paraconformity/disconformity (Bassi et al., 2010; Brandano, 2017) is the only record left by the passage of the forebulge. The syn-orogenic shallow-water carbonate unit records the sedimentation on a carbonate ramp dominated by red algae and bryozoans, with variable amounts of benthic foraminifers. This fossil assemblage is typical of a temperate-type foramol (sensu Lees, 1975) or foramol/rhodalgal carbonate factory (*sensu* Carannante et al., 1988b). In the central-southern Apennines, these deposits are typically described under different lithostratigraphic units, such as the Cerchiara Fm., Roccadaspide Fm., Recommone Fm., Cusano Fm., Bryozoan and Lithothamnium Limestone, Lithothamnium Limestone, and Gravina Calcarenite (Selli, 1957; De Blasio et al., 1981; Carannante et al., 1988a; Taddei, 1996; Civitelli and Brandano, 2006; Brandano et al., 2012; Brandano et al., 2017a). The shallow-water carbonate ramp sedimentation was not able to keep up with accelerating flexural subsidence and it was eventually terminated by drowning below the photic zone, as recorded by the deposition of hemipelagic marls with planktonic foraminifera (Lirer et al., 2005). The switch from hemipelagic deposits to Mio-Pliocene turbiditic siliciclastics (Sgrosso, 1998; Patacca and Scandone, 2007) represents the further step within the frame of the above-mentioned evolution of an underfilled foreland basin (Sinclair, 1997). Finally, foredeep deposits were incorporated into the accretionary wedge and overlain by unconformable sediments deposited in wedge-top basins (e.g., Ascione et al., 2012). In the regional literature of the Apennines, different names have been used for lithostratigraphic units representing the same evolutive stage in different areas. To make easier the understanding of the Apennine foreland basin evolution, we group the different formations according to the above-mentioned nomenclature of Sinclair (1997). Groups of formations, biostratigraphic age, and related lithostratigraphic units are listed in the Table S6.1 of the Supporting information section in Chapter 6.

CHAPTER 3. MATERIAL AND METHODS

This research has involved the following main activities:

1. Fieldwork;
2. Samples preparation and laboratory investigations.

3.1 Fieldwork

The fieldwork plan was developed after geo-referencing of old and recent maps (when available), review of papers describing the stratigraphic interval of interest (many of them are very old and their descriptive indications of key localities often led to recent built walls or houses), and satellite and street-view interpretation in Google Earth (when available).

The fieldwork comprises three fundamental stages:

- Sedimentologic and stratigraphic analysis,
- Sampling of material for the SIS,
- Structural analysis.

A total of 15 localities (Fig. 1.3) including 37 field sites have been investigated for sedimentological/stratigraphic and structural analysis (Figs 3.1, 3.2, and 3.3).

Sedimentological and stratigraphic observations were made on outcrops where pre-orogenic to syn-orogenic successions are exposed (Figs 3.1a, d and 3.2a). The first step of fieldwork was a careful description of the syn-bulging erosional surface and of the underlying layers, looking for evidence of subaerial exposure, karst, bioerosion, etc. (Figs 3.1 and 3.2). The second step was the sedimentological description and sampling of the first beds of the Miocene carbonates overlying the unconformity. Both the uppermost beds of the Cretaceous/Paleogene limestones underlying the unconformity and the lowermost beds of the Miocene limestones overlying the unconformity were carefully sampled for biostratigraphy and SIS, collecting a total of 203 samples. To obtain very precise and accurate dating through SIS, it is important to select well-preserved shells of low-Mg calcite, which is the most suitable material for SIS, owing to its resistance to diagenetic alteration (McArthur, 1994). Pectinid and ostreid bivalves offer a good material in the Miocene carbonates (Fig. 3.1b).

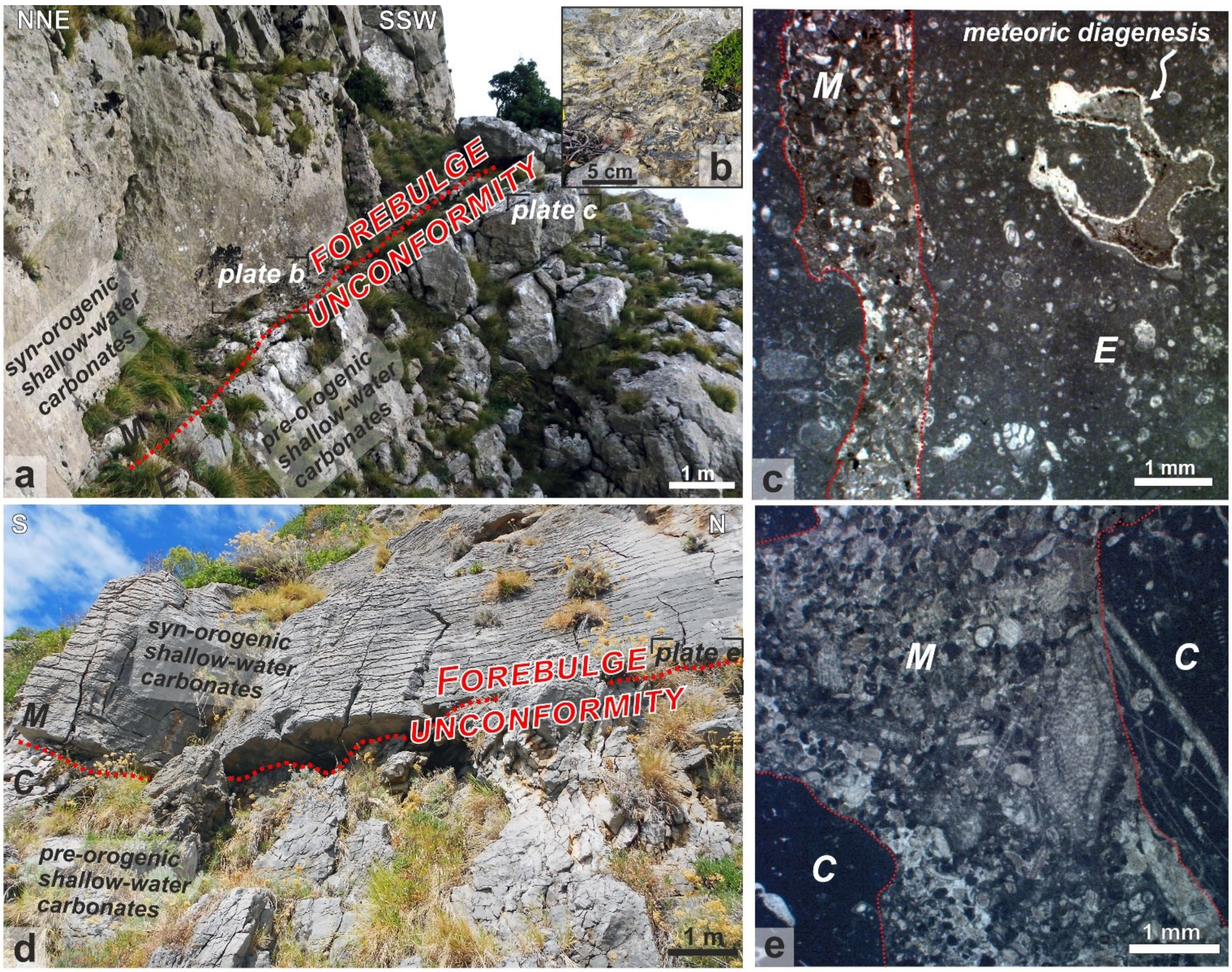

Figure 3.1. Investigated outcrops in the southern Apennines in which the forebulge unconformity (paraconformity at the outcrop scale) is exposed. a) Mt. Panno Bianco near Cerchiara di Calabria (Pollino Ridge): Eocene pre-orogenic carbonates (E) covered by Miocene syn-orogenic carbonates (M). The sharp contact is marked by ostreids bank in life-position. b) Detail of the ostreid bank. d) Recommone site at Sorrento Peninsula: Cretaceous pre-orogenic carbonates (C) covered by Miocene syn-orogenic carbonates (M). c,e) Thin section microphotographs of dykes of Miocene carbonate sediments within the top of the Eocene and Cretaceous rocks, respectively.

The structural analysis has consisted in collecting data on mesoscale extensional structures possibly associated with the forebulge-foredeep stage.

Generally, mesoscale structural data related to the forebulge-foredeep extension consists in extensional structures such as joints, veins, sedimentary dykes and faults, hosted in both the pre-orogen Cretaceous substrate and the syn-orogen transgressive Miocene calcarenites (Figs 3.1c, e, 3.2c, and 3.3). In the field, all mesostructures were analyzed, paying attention to the description of their abutting and cross-cutting relationships, their timing with respect to the deposition of the Miocene deposits and overprinting relations with the forebulge unconformity. A total of 1226 structural data has been collected in 37 field sites.

Although nearly always gently dipping, bedding attitudes were also collected in order to restore to the horizontal all the measured structures. This is a common procedure to evaluate fracture origin with respect to regional or local folding, restoring the fractures to the orientation at the time of their origin, and to compare structures hosted within differently dipping bedding. The presented data suggest that rotation around the vertical axis is instead not relevant among the studied localities.

Field observations on both pre-orogenic and syn-orogenic successions were necessary to discriminate forebulge and foredeep early extensional events, based on the orientations of the associated structures.

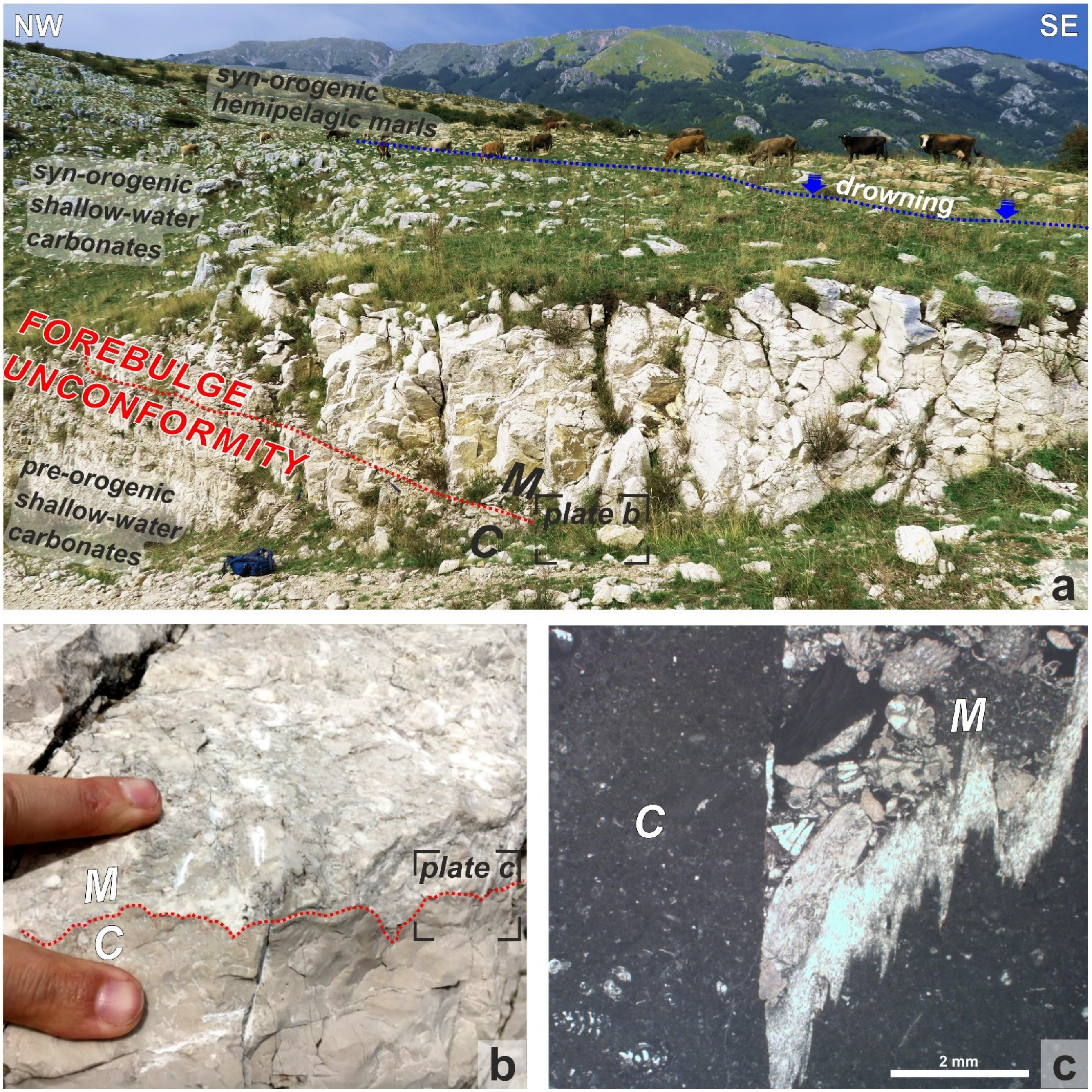

Figure 3.2. a) Matese Mts, southern Apennines: Cretaceous pre-orogenic carbonates (C) covered by Miocene syn-orogenic shallow-water carbonates (M) evolving upward to hemipelagic marls. b) detail of the forebulge unconformity. c) Thin section microphotograph of the contact between the Miocene carbonates and Cretaceous carbonates, marked by a stylolite.

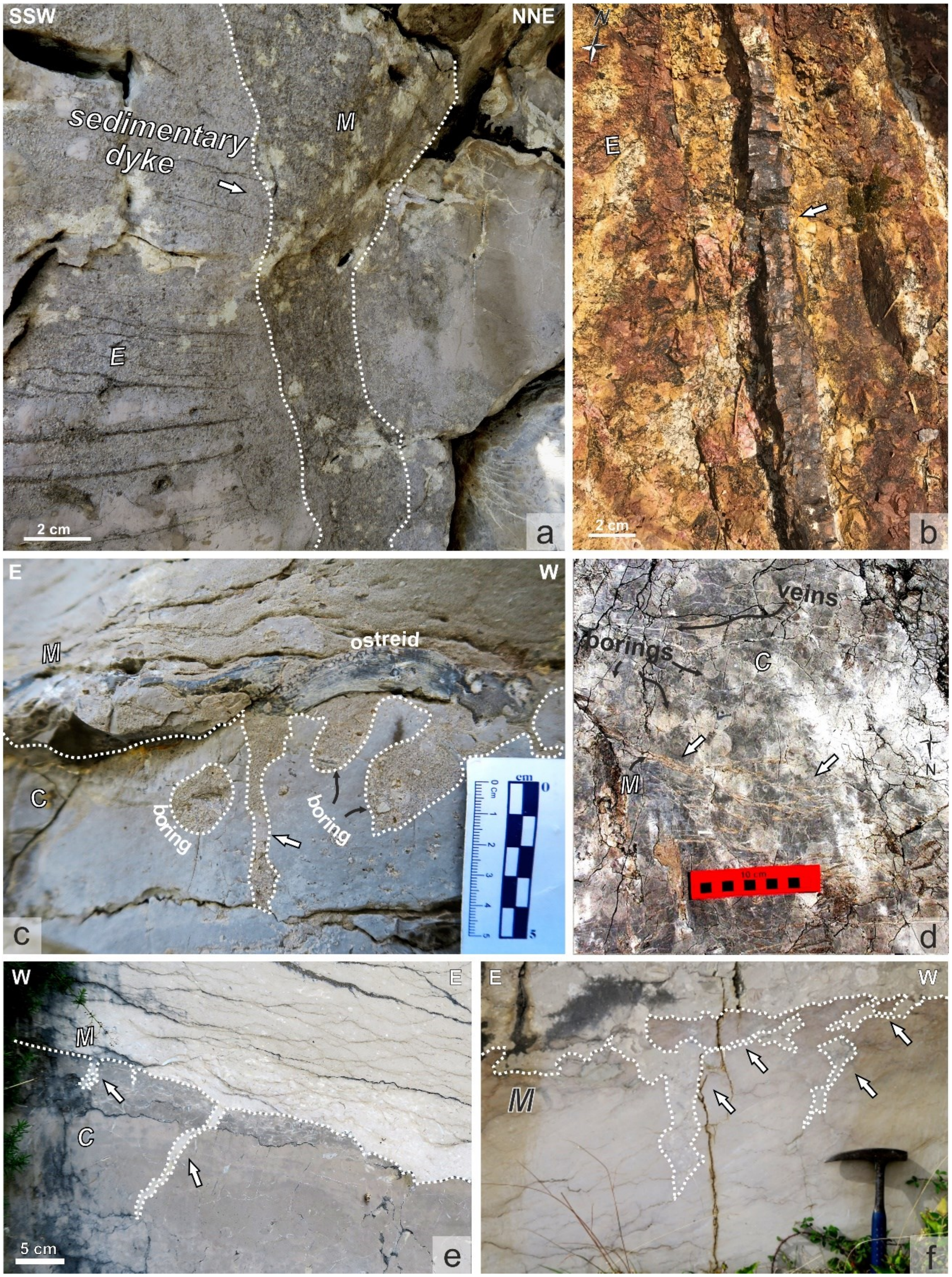

Figure 3.3. Sedimentary dykes (indicated by white arrows) within the top of the pre-orogenic substrate, Eocene (a, b) and Cretaceous (c,d,e) in age, and within the basal levels of Miocene syn-orogenic carbonates (f).

3.2 Laboratory work

Samples selected and collected in the field were processed through the following stages:

- Lab preparation,
- Optical microscopy,
- Cathodoluminescence,
- Scanning Electron Microscopy,
- Geochemical analysis for measuring trace and minor elements concentration and Sr isotope ratios.

Samples of rocks were cut and polished. The polished slabs were used to obtain thin sections for the biostratigraphic and sedimentologic analysis and carbonate powders, by means of microdrilling, for geochemical analysis. A total of 120 thin sections and 156 geochemical and isotopic analyses were obtained. From the total number of analyses, 111 data results were further considered from samples selected after the diagenetic screening (see Tables 4.1 and S6.3 in the Chapters 4 and 6, respectively).

Thin sections of Cretaceous, Eocene, and Miocene rocks were observed through the optical microscope in order to describe microfacies, biostratigraphic content and diagenetic features (i.e., traces of dissolution, recrystallization and cementation processes) (Figs 3.1c, e and 3.2c).

3.3 Strontium Isotope Stratigraphy (SIS)

Strontium isotope stratigraphy (SIS) is based on the empirical observation that the Sr-isotope ratio ($^{87}Sr/^{86}Sr$) of the ocean has varied through time, and on the assumption (verified in the modern ocean and consistent with the long residence time of Sr) that, at any moment in the geological past, the Sr-isotope ratio of the ocean was homogeneous (DePaolo and Ingram, 1985; McArthur, 1994). A reference curve, documenting the $^{87}Sr/^{86}Sr$ value of the ocean through geological time, has been assembled by means of well-dated and diagenetically pristine samples of marine precipitates (McArthur et al., 2001) and has been continuously refined and calibrated to the most recent geological time scale (McArthur et al., 2012; 2020) (Fig. 3.4a).

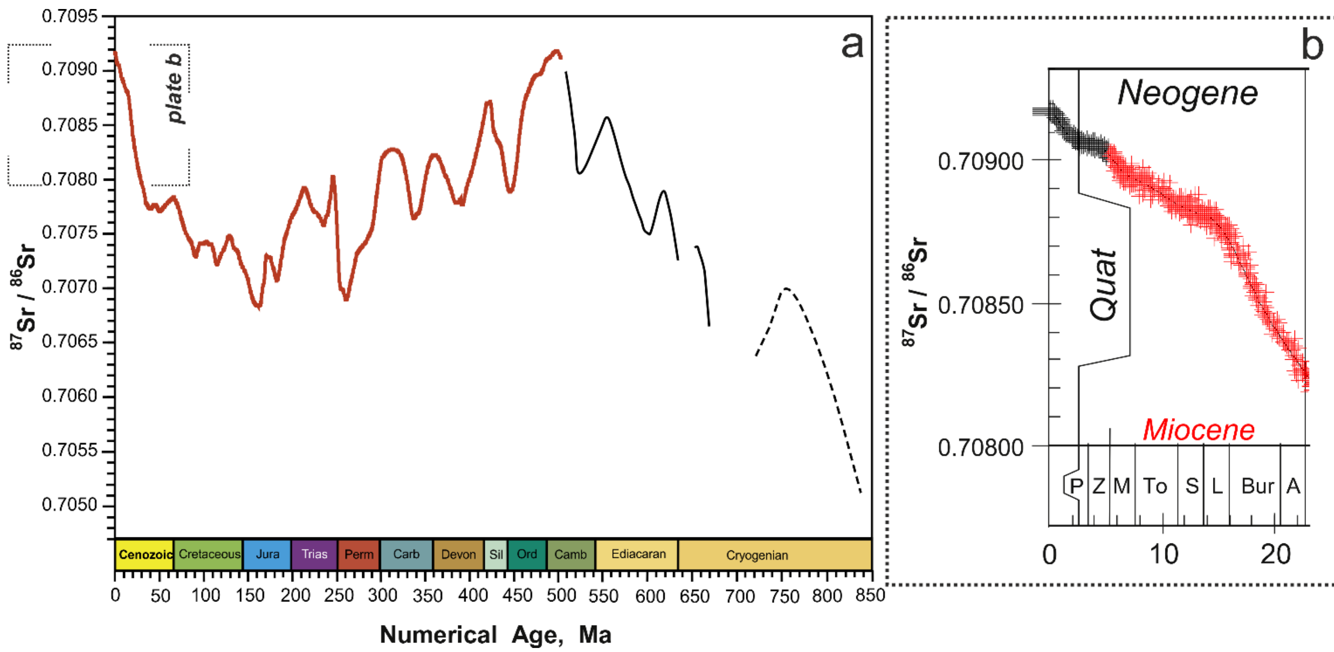

Figure 3.4. a) Reference curve of seawater Sr-isotope ratio through the Neoproterozoic and Phanerozoic times, and b) detail of the curve through the Neogene and Quaternary times (modified from McArthur, 2012, 2020).

SIS is particularly suitable for high-resolution dating and correlation of Miocene marine carbonates because the reference curve for this stratigraphic interval is characterized by a very narrow statistical uncertainty and by a very high slope (i.e., rapid unidirectional change of $^{87}Sr/^{86}Sr$ ratio of the ocean through time)

(Fig. 3.4b). For these reasons, a resolution of 0.1 Ma can be potentially attained in Miocene marine deposits. A prerequisite for successful application of SIS is to select unaltered marine precipitates that have retained their pristine Sr isotope ratio. Biotic low-Mg calcite is a suitable material because it is more resistant to diagenetic alteration and because its degree of diagenetic alteration can be checked with a suite of petrographic and geochemical analyses (McArthur, 1994; Ullmann and Korte, 2015). In Miocene shallow-water carbonate units of the Apennines, this material is provided by pectinid and ostreid bivalves.

3.3.1 SIS workflow

The best-preserved shells were selected in the field, using color preservation as a first guidance. The biotic calcite of pristine shells is generally honey colored to dark brown or dark grey, as opposed to the whitish or dull light grey color of shells replaced by diagenetic calcite. Then, the preservation of the original shell microstructure was checked with a low-magnification lens. For each stratigraphic level, at least 4-5 shells and/or shell fragments were collected, along with a sample of the bulk matrix enclosing the shells. Having more than one shell from a single bed is fundamental to generate a more robust isotopic dataset and to further assess the degree of diagenetic alteration. Different shells from the same bed (i.e., same age) should be characterized by a very narrow range of Sr isotope ratios (i.e., the Sr isotope ratio of marine water at the time of their precipitation), while diagenetic alteration would move the isotope ratio of the shells to different values. On the other hand, the bulk matrix represents a mixture dominated by diagenetic material (cements, recrystallized grains). Comparing its strontium isotope ratio with the ratio shown by the shells can be further used to assess their preservation (i.e., a shell that has a Sr isotope ratio very close to that of the matrix has been most probably altered by diagenesis).

From polished slabs of carbonate rocks containing shell material for the SIS, two halves were obtained. A half was used to obtain thin sections, whereas the other half was used to extract carbonate powders. Thin sections containing shells and shell fragments, or isolated shell fragments, were analyzed through microscopy to check the preservation of the shell microstructures of each sample to be used for the geochemical analysis (Fig. 3.5). The next step was to observe the material through cathodoluminescence microscopy. Cathodoluminescence (CL) microscopy is used to spatially resolve the degree of preservation of fossil shells (e.g., Ullmann and Korte, 2015 and references therein). Certain trace elements, especially Mn incorporated into calcite during alteration (Barbin, 2000), emit characteristic dull to bright radiation during cathodic excitation of the shell calcite and induce a typical orange to red color (Fig. 3.5), indicative of diagenetic alteration. CL microscopy operates with the assumption that this characteristic luminosity is absent in well-preserved biogenic calcite, showing a weak blue, “intrinsic” luminosity, which is related to structural defects in the calcite crystal lattice (Barbin, 2000). However, not always non-luminescence is a proof of good preservation because of the absence of “Mn-activators” in diagenetic fluids or of the “quenching” effect of Fe^{2+}, another diagenetic indicator, which suppresses luminescence. On the other hand, also luminescent material is not necessarily altered, because well-preserved shells and even modern shells can show bright luminescence, related to a variety of environmental controls (Ullman and Korte, 2015; Barbin, 2000). Therefore, together with cathodoluminescence, other screening techniques are necessary for a complete diagenetic evaluation. For instance, observation through scanning electron microscopy is also necessary. In fact, at the high magnification of a scanning electron microscope it is possible to observe in great detail the ultrastructure of the fossil shells. Generally, a perfectly pristine shell shows smooth surfaces of crystals fibers. In particular for the material of this study, ostreids and pectinids have well-recognizable lamellar and cross-lamellar microstructure (Fig. 3.5), respectively. Observed by SEM, altered material can show evidence of partial dissolution-recrystallization up to a complete recrystallization, with obliteration of the original shell microstructure (Fig. 3.5).

After selecting the best-preserved shells by optical and SEM petrography, the elemental (Mg, Sr, Mn, and Fe) composition of the shells, and of the micritic matrix of the samples, were analyzed as a further screening step. Powder for geochemical analyses was obtained by scraping the polished surfaces of rocks exposing bivalve shells by means of a hand-operated microdrill, equipped with thin tungsten drill bits (diameter = 0.5-1 mm). Before microdrilling the polished slabs and the isolated shell fragments were cleaned in an ultrasonic bath with a weak acid (acetic acid 4%), in order to remove surficial diagenetic coatings. Microsampling was performed under the binocular microscope, avoiding visibly altered portions of the rock, such as micro-veins and recrystallized calcite or interstitial cements, microborings filled by sediments. About 8-10 mg of calcite powder was obtained from each shell and matrix bulk sample for geochemical analyses.

The samples used for this thesis were analyzed in three different geochemistry laboratories using different analytical method protocols. Some samples were analyzed in the geochemical laboratories of the Centro Interdipartimentale Grandi Strumenti and the Department of Chemistry and Earth Science of the University of Modena and Reggio Emilia, some in the geochemical laboratory of the OV-INGV of Naples, and others in the laboratories of the Institut für Geologie, Mineralogie und Geophysik of the Ruhr-Universität of Bochum. An aliquot of each sampled carbonate powder was used for the minor and trace element analysis.

A first batch of carbonate powders was dissolved into an acid solution of 5 ml of 3N HNO_3 (i.e., nitric acid) and analyzed for the elemental concentration by means of an ICP-OES Perkin Elmer Optima 4200 DV and a quadrupole ICP-MS X Series II Thermo Fisher Scientific (at the Centro Interdipartimentale Grandi Strumenti of the University of Modena and Reggio Emilia). A second batch of carbonate powders was dissolved in 1 ml 3 M HNO_3 and then diluted with 2 ml H_2O for analysis with an ICP-OES Thermo Fisher Scientific iCAP6500 Dual View (at the Institut für Geologie, Mineralogie und Geophysik of the Ruhr-Universität of Bochum). The results are shown in table 4.1 and S6.3, in Chapter 4 and 6, respectively.

After this step, the residual aliquot of the carbonate powder was used for Sr-isotope ratio analyses.

In the laboratories of the University of Modena and Reggio Emilia, a batch of carbonate powders was rinsed three times with MilliQ-water. After drying, each sample was leached two times using a solution of 0.3% acetic acid, in order to sequentially dissolve the powdered material, as described in Li et al. (2011). Solutions were dried and then reacidified in 3 ml of 3 N HNO_3 and put into chromatographic columns. Sr was separated using standard ion exchange techniques. The solutions were loaded into 300 µl columns containing 100–150 µm particle size Sr-SPEC resin to isolate Sr from the interfering elements Ca, Rb, REE. The columns were washed before with 1 ml 3 N HNO_3 and 3 ml MilliQ-water and conditioned using 1 ml 3 N HNO_3. Strontium was eluted from the columns with 2.5 ml MilliQ-water. Final solutions were adjusted to a concentration of 4% HNO_3 and strontium isotope ratios were obtained using a high resolution multi collector inductively coupled plasma mass spectrometer HR-MC-ICPMS Thermo Scientific Neptune, located at Centro Interdipartimentale Grandi Strumenti CIGS Unimore.

In the OV-INGV laboratories, the analytical techniques were somehow different. A powder aliquot of each sample was digested in 2 ml of 2.5 N HCl. The solutions were dried and then reacidified in additional 500 µl of 2.5 N HCl. The solutions were then transferred to 15 ml centrifuge tubes and centrifuged for 10 minutes in order to separate the dissolved material from potential insoluble residues. Successively, the solutions were loaded into 300 ml columns and Sr was collected by cation exchange chromatography using Bio-Rad Dowex AG50W X-8 200–400 mesh exchange resin. The columns were washed before with 17 ml of 2.5 N HCl and Sr separation occurred by using 6 ml of 2.5 N HCl. The final solution was dried, and the resultant solid was then dissolved with 2 drops of pure 65% HNO_3 and dried again. The next step was to dilute the sample in 2 µl of 10% HNO_3 and to load the sample on outgassed Rhenium-filaments using tantalum chloride ($TaCl_5$) and phosphoric acid (H_3PO_4) as emitters. Strontium isotope ratios were measured using a Thermo Fisher Triton thermal ionization multi collector mass spectrometer, running in static mode.

In the laboratories of the Ruhr-Universität of Bochum, each sample was weighted in order to obtain an amount of powder containing 400 ppb of Sr (already known by the above-mentioned elemental concentration analysis). The powders were dissolved in 6N HNO_3 and dried. After, the dried samples were soluted again in 0.4 ml of 3N HNO_3 and they were loaded into chromatographic columns. Sr was separated using standard ion exchange techniques. Before separation, 3.6 ml of 3N HNO_3 were passed through each column for removing the waste, and Strontium was eluted from the columns with 2 ml of MilliQ-water. Finally, 0.5 ml of MilliQ-water plus 0.5 of ultrapure nitric acid were added to the final solutions that were dried, diluted again with 6N HCl, and loaded on Rhenium-filaments. Strontium isotope ratios were obtained using a Finnigan MAT 262 thermal ionization mass spectrometer.

All Sr-isotopes data obtained in different analytical sessions are reported in Table 4.1 and S6.3 of the Chapters 4 and 6, respectively.

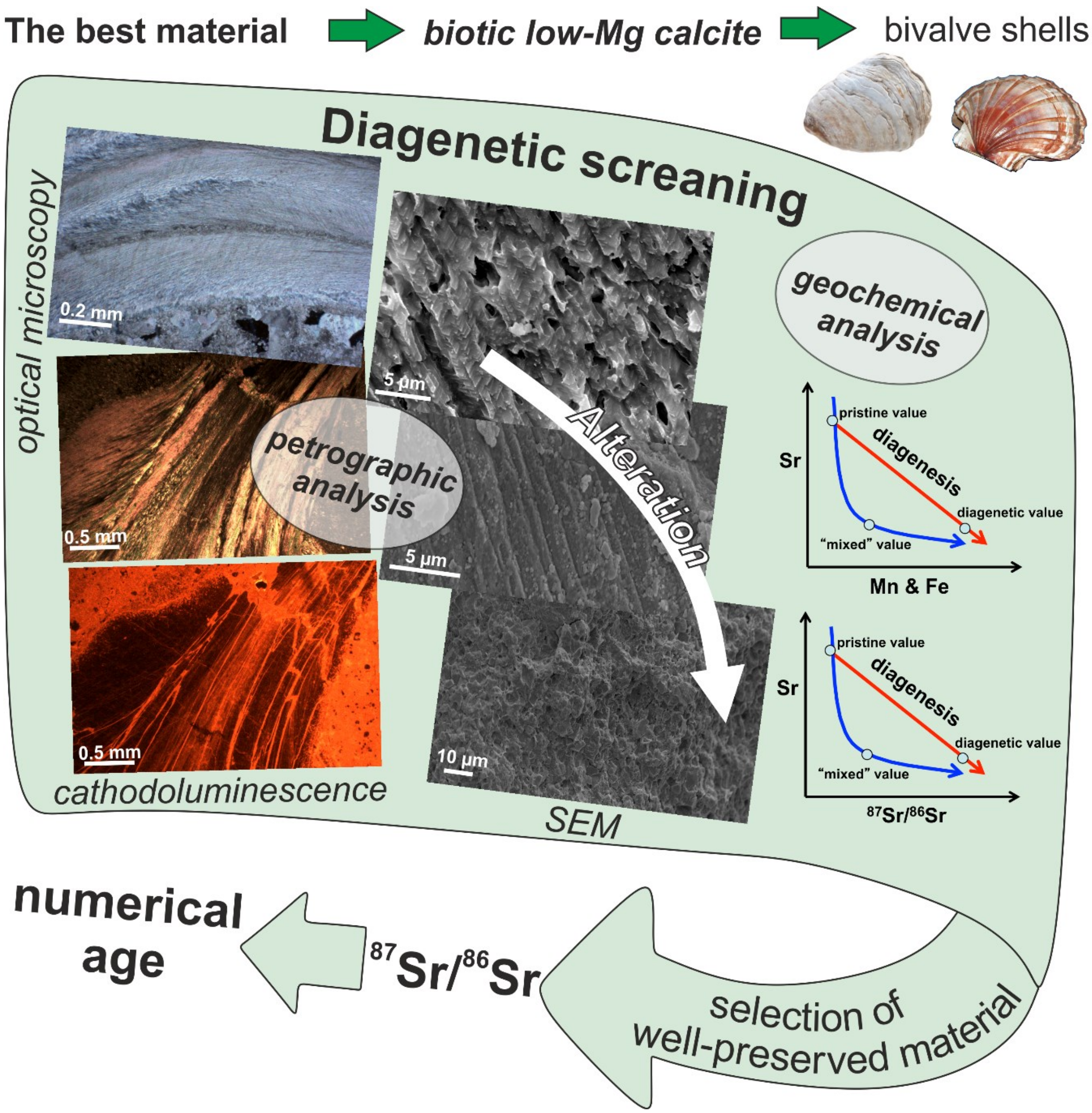

Figure 3.5. Summary of the SIS workflow.

CHAPTER 4. CONSTRAINING THE ONSET OF FLEXURAL SUBSIDENCE AND PERIPHERAL BULGE EXTENSION IN THE MIOCENE FORELAND OF THE SOUTHERN APENNINES (ITALY) BY SR-ISOTOPE STRATIGRAPHY

Sabbatino, M., *Vitale, S., Tavani, S., Consorti, L., Corradetti, A., Cipriani, A., Arienzo, I., & Parente, M.*

This chapter has been published in *Sedimentary Geology* **401**, (2020).

Abstract

In fold and thrust belts developing at convergent margins, the migration of the advancing wedge is accompanied by bulging of the downgoing plate, followed by the development of a foredeep basin filled by a thick succession of syn-orogenic sediments. The transition from forebulge to foredeep marks a key moment in the evolution of the orogenic system. In deep water environments, the record of this transition is typically complete and progressive. Conversely, in the shallow-water/continental environment of many collisional systems, the uplift of the forebulge area can imply emersion and erosion, obliterating the stratigraphic record of key steps of the evolution of the orogenic system. The southern Apennines constitute one of these collisional fold and thrust belts where the development of the forebulge has implied emersion and erosion, with the development of a Miocene forebulge erosional unconformity, accompanied by extensional deformation associated with the bending of the lithosphere during the forebulge stage. In this paper, we use strontium isotope stratigraphy to constrain with unprecedented time-resolution the age of the forebulge unconformity in areas presently incorporated in the northern sector of the southern Apennines fold and thrust belt. Integration of our results and those of previous studies indicates, at the regional scale, a younging toward the foreland of the forebulge unconformity across the belt. Our high-resolution ages also reveal a diachronous onset of the flexural subsidence over short distances, associated with the occurrence of horst and graben structures, possibly resulting from inherited paleotopography along with forebulge extension. This work highlights how high-resolution dating is critical to unravel the evolution of foreland basin systems at different scales.

Key words: foreland basin system, forebulge unconformity, strontium isotope stratigraphy, forebulge extension, Miocene, southern Apennines (Italy)

4.1 Introduction

Foreland basins are key portions of orogenic systems, forming in front and above of thrust belts due to the downward flexing of the lithosphere during convergence (Allen et al., 1986; DeCelles and Giles, 1996). The forebulge is the outermost portion of the thrust belt-foreland basin system, dividing the foreland from the foredeep basin. The bulge consists of a small (generally in the order of less than a few hundreds of meters) and gentle rise of the topography, developing as an elastic response to the flexure of the lithosphere (Turcotte and Schubert, 1982). The first stratigraphic expression of the flexural stage is a regional unconformity between the pre-orogenic sequence and the syn-to post bulge sediments, commonly referred to as the forebulge unconformity (Crampton and Allen, 1995). The syn-orogenic deposits are wedge-shaped and forelandward thinning, and they are characterized by distinctive time-transgressive sedimentation toward the foreland, as found, for example, in the Carpathians (Leszczyński and Nemec, 2015), Dinarides (Babic and Zupanic, 2008, 2012), Himalayas (DeCelles et al., 1998), Northern Alps (Crampton and Allen, 1995; Sinclair, 1997), Oman-UAE (Glennie et al., 1973; Robertson, 1987; Corradetti et al., 2019), Pyrenees (Vergés et al., 1998), Taiwan (Yu and Chou, 2001), West Interior (White et al., 2002), and Zagros (Alavi, 2004; Saura et al., 2015). The transition from pre-orogenic to syn-orogenic sedimentation in the forebulge area can be either gradual or extremely abrupt, largely depending on the depositional environment of the forebulge area itself (Crampton and Allen, 1995). When bulging occurs in sub-marine environments, the first phase of syn- to post-forebulge sedimentation occurs generally in a deep-water setting such as in the Aruma Group on Wasia-Aruma Break in Oman-UAE (Robertson, 1987; Boote et al., 1990; Robertson and Searle, 1990; Cooper et al., 2014), and in the Gurpi-Pabdeh Group in Zagros (Vergés et al., 2011; Saura et al., 2015), hence the stratigraphic record associated with the flexural bulge is fully registered. In tectonic settings involving mostly subaerial peripheral bulge areas, distinctive and articulated forebulge unconformities can develop through erosion and karst such as on top of passive margin rocks of the Adriatic carbonate platform (Otoničar, 2007). Also, subsequent submarine erosion and sediment bypass in shallow-water environments, levelling the bulge unconformity and/or removing condensed forebulge deposits (DeCelles and Giles, 1996), may generate disconformities/paraconformities (White et al., 2002). In view of the above mentioned, in shallow-water/continental environments, the lack of a complete sedimentary record may hinder the full reconstruction of the tectono-sedimentary evolution of the forebulge/foredeep system. In fossil and dismembered foreland basins, the forebulge phase is recorded by the basal portion of the syn-orogenic sedimentary sequence, where time-transgressive unconformities and facies changes track the progressive evolution of the foreland-thrust wedge system (Fig. 4.1). High-resolution dating of these deposits provides constraints on the main steps of the tectono-sedimentary evolution of the dismembered foreland basin (Sinclair, 1997; Galewsky, 1998; Leszczyński and Nemec, 2015).

A typical example is the Miocene fossil foreland of the southern Apennine belt, which has experienced pre-thrusting bulging, uplift, and erosion, caused by the bending of the subducting lithosphere and the accretionary wedge migration (e.g., Doglioni, 1995), and has been subsequently dismembered and incorporated into the thrust belt during the E/NE-ward migration of the trench (e.g., Roure et al., 1991; Cello and Mazzoli, 1998; Vitale and Ciarcia, 2013; Faccenna et al., 2014). Patches of this foreland basin are now exposed at different localities of the central-southern Apennines. The timing of deformation and the shortening rate of the Apennine fold and thrust belt have been so far reconstructed using the ages of the first siliciclastic deposits of the foredeep and wedge-top basins (e.g., Cipollari and Cosentino, 1995; Bigi et al., 2009; Critelli et al., 2011; Vitale and Ciarcia, 2013). This approach has produced controversial results, since these deposits are poorly fossiliferous and usually dominated by reworked specimens (e.g., De Capoa et al., 2003). An alternative would be to use the age of the Miocene shallow-water carbonate deposits, which represent the base of the foreland basin megasequence, and record the first phase of foreland flexural subsidence during the Apennine thrust sheet belt emplacement. An additional advantage would be that shallow-water carbonates, being more sensitive to sea-level and paleoenvironmental changes compared to deep-water siliciclastics, could give a more detailed record of the first phases of foreland basin evolution (Dorobek, 1995; Galewsky, 1998; Bosence, 2005). However, the Miocene syn-orogenic shallow-water carbonates of the southern Apennines have been so far dated only by biostratigraphy, which is mainly based on miogypsinid larger foraminifera (Schiavinotto, 1979, 1985; Brandano et al., 2007), with limitations imposed by the sparse occurrence of these fossils, and by the low time resolution (not better than 2-4 Ma) and uncertain calibration of larger foraminiferal biozones to the geological time scale (Cahuzac and Poignant, 1997; Hilgen et al., 2012).

In this work, we aim to constrain the sequence of events recording the migration of the southern Apennines fold and thrust belt and of its foreland basin by dating with unprecedented high-resolution the basal levels of the Miocene syn-orogenic shallow-water carbonates. To overcome the above-mentioned limitations of biostratigraphy, we use strontium isotope stratigraphy (McArthur et al., 2012) on the biotic low-Mg calcite of well-preserved bivalve shells, attaining a resolution of 0.1-0.3 Ma.

In addition to the high-resolution dating, we report on joints and sedimentary dykes formed during the Miocene forebulge-related extension. The latter is associated with deformation occurring in the peripheral bulge area, as recognized worldwide in foreland basins (e.g., Tavani et al., 2015a; Martinelli et al., 2019). The timing of syn-orogenic sedimentation in relation to the development of extensional structures provides additional constraints for the reconstruction of the tectono-sedimentary evolution of a foreland basin.

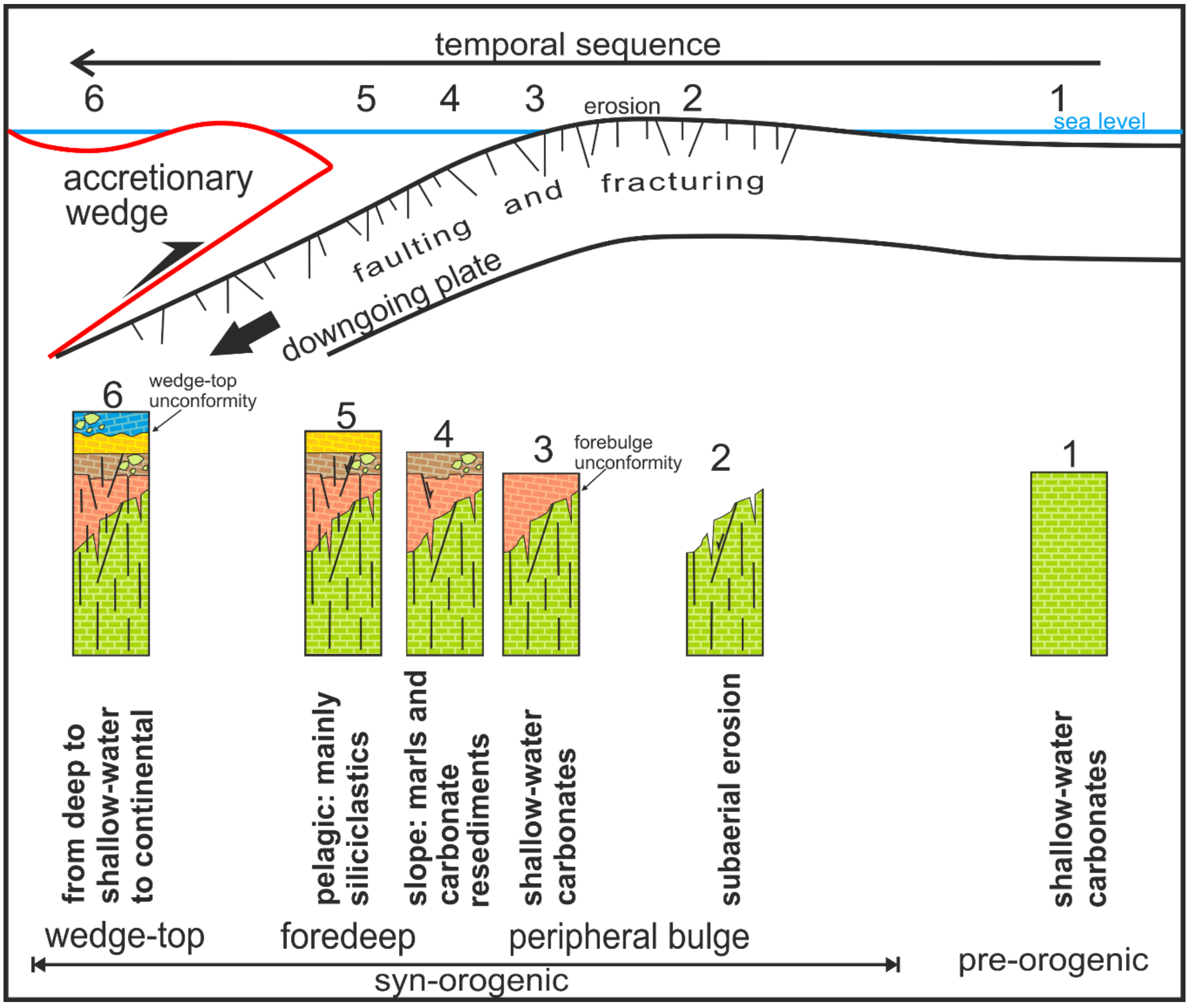

Figure 4.1. Schematic tectonostratigraphic evolution of a foreland basin system in response to the accretionary wedge migration. The scheme refers to a basin where syn-orogenic sedimentation in the forebulge area starts in shallow-water carbonate system, like the Apennine model.

4.2 Geological Setting

4.2.1 The Southern Apennines

The southern Apennines are one of the two arcs constituting the Neogene Apennines fold and thrust belt (Fig. 4.2a). This fold and thrust belt developed due to the W-ward subduction of the Adria plate underneath Europe. The collisional system was characterized by a progressive arching of an originally almost linear belt, due to the E-ward retreat of the trench and the opening of the Tyrrhenian back-arc basin (e.g., Malinverno and Ryan, 1986; Doglioni, 1991; Mazzoli and

Helman, 1994; Faccenna et al., 2014). The present-day configuration of the southern Apennines (Fig. 4.2b) is defined by the tectonic superposition of several thrust sheets, made up of Meso-Cenozoic sediments deposited in basins and carbonate platforms developed on the southern margin of the Alpine Tethys (i.e. in the Adria domain) since the Triassic (Bosellini, 2004). In the study area (Fig. 4.2b), the top of the tectonic pile is made of units belonging to the Apennine Carbonate Platform, and these units overthrust imbricated thrust sheets made up of deep-water sediments of the Lagonegro-Molise Basin. Before the onset of convergence, this basin was interposed between the Apennine Carbonate Platform to the west and the Apulian Carbonate Platform to the east. The Lagonegro units tectonically cover the Apulian Carbonate Platform, which is buried below the thrust belt and is exposed further to the E/NE, in the foreland region (Fig. 4.2).

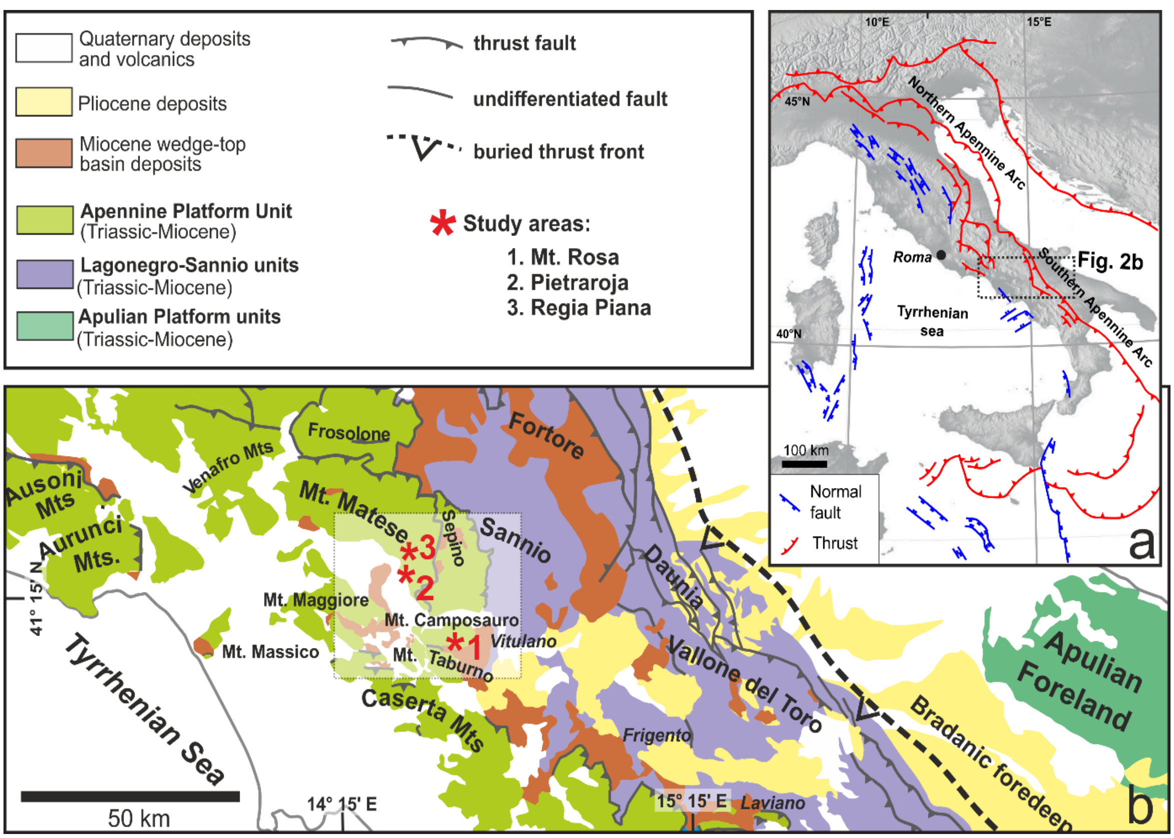

Figure 4.2. a) Structural scheme of Italy (modified after Tavani et al., 2015b); b) Schematic geological map of the northern sector of the southern Apennines showing the locations of the study areas (modified after Vitale and Ciarcia, 2013).

In the Apennine Carbonate Platform, which is the focus of this work, the pre-orogenic passive margin sedimentation was generally in shallow-water conditions and almost continuous from the Middle Triassic to the Late Cretaceous (Zamparelli et al., 1999; Bernoulli, 2001; Simone et al., 2003; Iannace et al., 2007 and references therein), with a long-lasting exposure recorded in some areas by Albian-Cenomanian karst bauxites (Mindszenty et al., 1995; Vitale et al., 2018). Passive margin shallow-water carbonate sedimentation was comparatively less widespread during the Paleogene and it is generally represented by thin and stratigraphically discontinuous deposits (Selli, 1962; Chiocchini et al., 1994). The last phase of shallow-water carbonate sedimentation is recorded during the Miocene by transgressive deposits overlying the Cretaceous or Paleogene substrate (Carannante and Simone, 1996). During the Miocene, the foreland of the central-southern Apennine fold and thrust belt has experienced pre-thrusting bulging, uplift, and erosion caused by the bending of the subducting lithosphere and the migration of the accretionary wedge (e.g., Doglioni, 1995). This tectonic stage is recorded by a regional unconformity, by extensional fracturing and faulting in the uppermost part of the lithosphere, and by the onset of flexural subsidence (e.g., Bradley and Kidd, 1991; Crampton and Allen, 1995; Tavani et al., 2015a). After the last phase of shallow-water carbonate sedimentation in the early Miocene, ongoing flexural subsidence is recorded by drowning of the early Miocene carbonate ramp, recorded by the deposition of hemipelagic marls with planktonic foraminifera (Lirer et al., 2005), followed by deposition of thick sequences of Mio-Pliocene turbiditic calci- and siliciclastic sediments both in foredeep and wedge-top basins (Sgrosso, 1998; Patacca and Scandone, 2007). The foredeep setting is mainly characterized by deposition of siliciclastics derived from the erosion of the orogenic belt and secondarily by volcaniclastic and calciclastic sediments. Finally, foredeep deposits are incorporated into the accretionary wedge and overlain by unconformable sediments deposited in wedge-top basins (e.g., Ascione et al., 2012; Vitale and Ciarcia, 2013, 2018). The temporal sequence of the tectonic pulses has been so far constrained by the biostratigraphic ages of the foredeep deposits and of the first unconformable wedge-top basin sediments (Ori et al., 1986; Cipollari and Cosentino, 1995; Bigi et al. 2009; Vitale and Ciarcia, 2013). Figure 1 shows a cartoon depicting the evolution of the syn-orogenic sedimentation associated with the slab retreat and the accretionary wedge migration.

4.2.2 Study area

Our study was performed in the localities of Pietraroja and Regia Piana in the Matese Mountains, and Mount Rosa in the Camposauro Mountain range, in the northern sector of the southern Apennines (Fig. 4.2b). There, the thick succession (>2000m) of Upper Triassic to Cretaceous shallow-water carbonate rocks of the Apennine Carbonate Platform is unconformably covered by the red algae and bryozoans limestones of the Burdigalian - Langhian Cusano Formation (Fm.) (Selli 1957; Carannante and Simone, 1996; Bassi et al., 2010), which pass upward to the hemipelagic Orbulina marls of the Longano Fm. (Selli, 1957), recording the drowning of the platform below the photic zone (Lirer et al., 2005). Above the Longano Fm., the middle Tortonian arenaceous-pelitic turbidites of the Pietraroja Fm. (Selli, 1957) mark the foredeep stage, while the unconformable upper Tortonian–lower Messinian clastic deposits of the Caiazzo Fm. record the wedge-top basin stage (Ogniben, 1958; Vitale et al., 2019).

As mentioned above, the shallow-water limestones of the Cusano Fm. represent the first deposits overlying the regional unconformity that developed during the emersion associated with the forebulge stage (Crampton and Allen, 1995). Together with the Recommone calcarenites, the Roccadaspide and Cerchiara Fms. in the southern Apennines (De Blasio et al., 1981; Carannante et al.,1988a; Carannante and Simone, 1996) and the Briozoi e Litotamni Fm. in the central Apennines (Brandano and Corda, 2002; Civitelli and Brandano, 2005; Brandano et al., 2010), the Cusano Fm. represents the base of the foreland basin mega-sequence of the central-southern Apennines. All these Miocene shallow-water carbonate units are characterized by benthic assemblages dominated by red algae and bryozoans, with variable amounts of larger benthic foraminifers, typical of a temperate-type foramol (*sensu* Lees, 1975) or foramol/rhodalgal carbonate factory (*sensu* Carannante et al., 1988b).

4.3. Material and methods

4.3.1 Fieldwork and stratigraphic and structural analysis

Field observations and sampling, aimed at sedimentological, biostratigraphical and structural analysis, were performed at the three localities (see Fig. 4.2b). Both the first beds of the Miocene carbonates overlying the forebulge unconformity and the top of the Cretaceous carbonates, just below the unconformity, were studied (see Fig. 4.3 for a detailed stratigraphy of the studied outcrops). A total of 32 limestone samples was collected from which 51 thin sections were prepared and studied under an optical microscope, in order to analyze the microfacies, fossil content, diagenetic features and the preservation of the microstructure of the shells or shell fragments to be used for geochemical analyses (Table 4.1). For the structural study, mesoscale structures were analyzed, such as fractures and sedimentary dykes hosted in both the pre-orogenic Cretaceous carbonates and the syn-orogenic transgressive Miocene limestones. The bedding orientations were also collected, in order to restore all the measured structures to the horizontal. During the data collection, particular attention was paid to the abutting and cross-cutting relationships. The analysis of these mesoscale structures was aimed at reconstructing the stress field orientation at the time of the unconformity development, to check its consistency with deformation expected in the forebulge area.

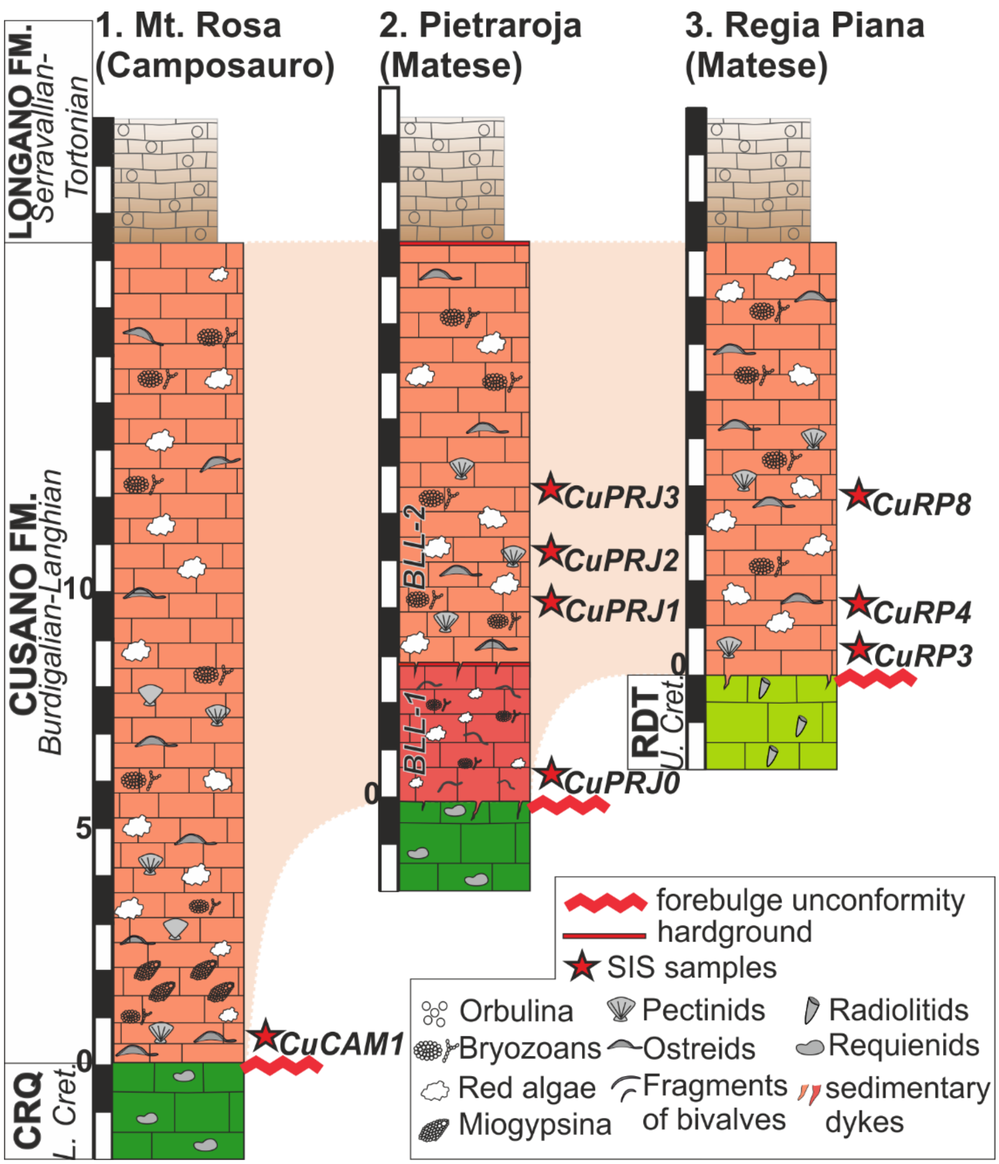

Figure 4.3. Stratigraphic logs of the studied sections, from left to right: Mt. Rosa (Camposauro Mountain range), Pietraroja and Regia Piana (both in the Matese Mts.).

4.3.2 Strontium isotope stratigraphy

Strontium isotope stratigraphy (SIS) is based on the empirical observation that the Sr-isotope ratio ($^{87}Sr/^{86}Sr$) of the ocean has varied through time, and on the assumption (verified in the modern ocean and consistent with the long residence time of Sr) that, at any moment in the geological past, the Sr-isotope ratio of the ocean was homogeneous (DePaolo and Ingram, 1985; McArthur, 1994). A reference curve documenting the $^{87}Sr/^{86}Sr$ value of the ocean through geological time, has been assembled by means of well-dated and diagenetically pristine samples of marine precipitates (McArthur et al., 2001) and has been continuously refined and calibrated to the most recent geological time scale (McArthur et al., 2012). SIS is particularly suitable for high-resolution dating and correlation of Miocene marine carbonates because the reference curve for this stratigraphic interval is characterized by a very narrow statistical uncertainty and by a very high slope (i.e., rapid unidirectional change of $^{87}Sr/^{86}Sr$ ratio of the ocean through time). For these reasons, a resolution of 0.1 Ma can be potentially attained in Miocene marine deposits. A prerequisite for successful application of SIS is to select unaltered marine precipitates that have retained their pristine Sr isotope ratio. Biotic low-Mg calcite is a suitable material because it is more resistant to diagenetic alteration and because its degree of diagenetic alteration can be checked with a suite of petrographic and geochemical analyses (McArthur, 1994; Ullmann and Korte, 2015). In Miocene shallow-water carbonate units of the Apennines, this material is provided in pectinid and ostreid bivalves.

The dataset used for SIS consists of 43 sub-samples, derived from 27 limestone samples containing shells or fragments of ostreids and pectinids collected from the base of Cusano Fm. (see Table 4.1 and Fig. 4.3 for details about locality, geographic coordinates, stratigraphic position, and type of material).

The preservation of the original microstructure of the bivalve shells was assessed by petrographic observation with a standard optical microscope and with a scanning electron microscope (SEM). Based on these observations, the state of preservation was recorded as “preserved” (Pr) or “altered” (A). The notation “partially altered” (PA) was used for shells that showed moderately well-preserved portions side by side with altered portions (Table 4.1).

In order to get a more complete understanding of the impact of diagenesis on the different components of the studied samples, all the shells, including the petrographically altered ones, and the matrix enclosing the shells, were measured for the concentration of minor and trace elements and for the Sr isotope ratio.

About 8-10 mg of calcite powder was obtained from each subsample by careful microdrilling with a tungsten bit under an optical microscope. Concentrations of Mg, Sr, Fe, and Mn (Table 4.1) were determined through inductively coupled plasma optical emission spectroscopy (ICP-OES) - UNICAM PU 7000 at the Institut für Geologie, Mineralogie und Geophysik of the Ruhr-Universität of Bochum (Germany) for some samples and by using an ICP-OES Perkin Elmer Optima 4200 DV at the Department of Chemistry and Earth Science of the University of Modena and Reggio Emilia (Italy), for the remaining set of samples.

Strontium isotope ratios were measured in three different laboratories. The first batch of samples was analyzed using a thermal-ionization mass spectrometer (TIMS) Finnigan MAT 262 at the Institut für Geologie, Mineralogie und Geophysik of the Ruhr-Universität of Bochum. The second one was analyzed by means of a high-resolution multi-collector inductively coupled plasma mass spectrometer (MC-ICP-MS) Thermo Scientific Neptune, at the Centro Interdipartimentale Grandi Strumenti (CIGS) of the University of Modena and Reggio Emilia. The third group of samples was analyzed with a ThermoFinnigan Triton multi-collector TIMS at the National Institute of Geophysics and Volcanology, Vesuvius Observatory in Naples (Italy). All geochemical data are given in Table 4.1, while details on sample preparation, analytical procedures, precision and reproducibility of the analyses and the values of the laboratory standards are given in the supplementary material. The $^{87}Sr/^{86}Sr$ values measured in the labs are considered to be free of inter-laboratory bias since, during the collection of isotopic data, replicate analyses of the standards were performed to check for external reproducibility. Sr isotope ratios were normalized to the value of the NIST–SRM 987 standard used by McArthur et al. (2001) for their compilation.

Only the Sr isotope ratios of the shells that are considered to have retained their pristine Sr isotope value were used for SIS. The diagenetic screening process followed the multistep procedure outlined in Frijia and Parente (2008) and Frijia et al. (2015), incorporating i. petrographic observation of the shell microstructure, ii.

sample by sample evaluation of the geochemical composition of the different components (well-preserved shells, altered shells and bulk matrix), and iii. internal consistency of the Sr isotope ratios of different shells from the same stratigraphic level.

Numerical ages were derived from the Sr isotope ratios by means of the look-up table of McArthur et al. (2001; version 5: 03/13). When more than one shell was available for the same stratigraphic level, the SIS age was derived from the mean value calculated from all the shells. Minimum and maximum ages were obtained by combining the statistical uncertainty of the samples, given by 2 standard error (2 s.e; McArthur, 1994) of the mean value, with the uncertainty of the reference curve (see Steuber 2003, for an explanation of the method). When less than four shells per level were analyzed, the precision of the mean value was considered to be not better than the average precision of single measurements, given as 2 s.e. of the mean value of the standards. The numerical ages obtained from the look-up table were translated into chronostratigraphic ages by reference to the Geological Time Scale of Gradstein et al. (2012) (hereinafter GTS2012), to which the look-up table is tied.

Table 4.1. Geochemistry of the basal levels of the Cusano Fm. in the studied localities. Pr = preserved, PA = partially altered, A = Altered.

Sample	Section locality	Latitude	Longitude	m from the base	Material	Mg (ppm)	Sr (ppm)	Fe (ppm)	Mn (ppm)	$^{87}Sr/^{86}Sr^{a}$	2 se (*10^{-6})	Preservation
CuPRJ0a	Pietraroja	41°20'59"N	14°33'09"E	0	bivalve shell	3390	445	136	13	0.708516	7	Pr
CuPRJ0b	Pietraroja	41°20'59"N	14°33'09"E	0	bivalve shell	3905	457	127	12	0.708506	7	Pr
CuPRJ0M	Pietraroja	41°20'59"N	14°33'09"E	0	matrix bulk	7381	375	191	21	0.708561	6	
CuPRJ1a	Pietraroja	41°20'59''N	14°33'08''E	4.5	pectinid shell	2088	632	82	14	0.708542	8	Pr
CuPRJ1b1	Pietraroja	41°20'59''N	14°33'08''E	4.5	pectinid shell	2399	566	148	27	0.708552	6	Pr
CuPRJ1b2	Pietraroja	41°20'59''N	14°33'08''E	4.5	pectinid shell	2987	444	77	33	0.708581	8	PA
CuPRJ1c	Pietraroja	41°20'59''N	14°33'08''E	4.5	pectinid shell	2000	772	63	11	0.708709	5	A
CuPRJ1d	Pietraroja	41°20'59''N	14°33'08''E	4.5	pectinid shell	2947	641	169	22	0.708562	7	Pr
CuPRJ1M	Pietraroja	41°20'59''N	14°33'08''E	4.5	matrix bulk	3232	335	99	30	0.708688	6	
CuPRJ2a	Pietraroja	41°20'59''N	14°33'06''E	5	pectinid shell	1886	509	65	33	0.708537	5	Pr
CuPRJ2b	Pietraroja	41°20'59''N	14°33'06''E	5	pectinid shell	1791	492	119	15	0.708541	5	Pr
CuPRJ2c	Pietraroja	41°20'59''N	14°33'06''E	5	pectinid shell	1767	554	87	17	0.708541	5	Pr
CuPRJ2M	Pietraroja	41°20'59''N	14°33'06''E	5	matrix bulk	3111	224	61	38	0.708605	6	
CuPRJ3a	Pietraroja	41°21'0"N	14°33'08''E	6	ostreid shell	1633	437	33	12	0.708712	5	A
CuPRJ3b	Pietraroja	41°21'0"N	14°33'08''E	6	ostreid shell	1716	409	32	11	0.708704	5	A
CuPRJ3c	Pietraroja	41°21'0"N	14°33'08''E	6	ostreid shell	1428	578	35	9	0.708506	5	A
CuPRJ3M	Pietraroja	41°21'0"N	14°33'08''E	6	matrix bulk	6813	376	133	21	0.708556	5	
CuRP3b	Regia Piana	41°21'46''N	14°32'09''E	0.2	ostreid shell	948	247	41	14	0.708711	4	A
CuRP3d	Regia Piana	41°21'46''N	14°32'09''E	0.2	ostreid shell	1455	362	35	9	0.708655	5	PA
CuRP3e	Regia Piana	41°21'46''N	14°32'09''E	0.2	pectinid shell	2472	679	49	17	0.708525	8	Pr
CuRP3M	Regia Piana	41°21'46''N	14°32'09''E	0.2	matrix bulk	3103	227	55	18	0.708608	11	
CuRP4a	Regia Piana	41°21'46''N	14°32'09''E	0.93	ostreid shell	1026	222	21	11	0.708682	5	A
CuRP4d	Regia Piana	41°21'46''N	14°32'09''E	0.93	ostreid shell	1543	389	57	11	0.708661	7	PA
CuRP4M	Regia Piana	41°21'46''N	14°32'09''E	0.93	matrix bulk	3958	309	77	19	0.708620	11	
CuRP8a	Regia Piana	41°21'46"N	14°32'09"E	2	ostreid shell	2500	560	60	12	0.708692	12	PA
CuRP8b	Regia Piana	41°21'46"N	14°32'09"E	2	pectinid shell	769	362	36	9	0.708510	5	PA
CuRP8c	Regia Piana	41°21'46"N	14°32'09"E	2	ostreid shell	1607	1060	36	12	0.708503	11	PA
CuRP8d	Regia Piana	41°21'46"N	14°32'09"E	2	ostreid shell	2314	571	231	5	0.708658	8	PA
CuRP8M	Regia Piana	41°21'46"N	14°32'09"E	2	matrix bulk	3626	297	88	22	0.708543	6	
CuCAM1a	Mt. Rosa	41°10'33"N	14°34'41"E	0.5	ostreid shell	1975	998	9	4	0.708713	8	Pr
CuCAM1b	Mt. Rosa	41°10'33"N	14°34'41"E	0.5	pectinid shell	2011	670	188	11	0.708690	7	Pr
CuCAM1b4	Mt. Rosa	41°10'33"N	14°34'41"E	0.5	ostreid shell	1939	527	24	7	0.708737	6	PA
CuCAM1c	Mt. Rosa	41°10'33"N	14°34'41"E	0.5	ostreid shell	2164	482	66	11	0.708735	6	PA
CuCAM1e	Mt. Rosa	41°10'33"N	14°34'41"E	0.5	ostreid shell	2236	489	6	8	0.708729	6	PA
CuCAM1f	Mt. Rosa	41°10'33"N	14°34'41"E	0.5	pectinid shell	1847	745	6	8	0.708715	6	Pr
CuCAM1g	Mt. Rosa	41°10'33"N	14°34'41"E	0.5	ostreid shell	2519	529	2	7	0.708706	10	Pr
CuCAM1M	Mt. Rosa	41°10'33"N	14°34'41"E	0.5	matrix bulk	4556	312	123	13	0.708704	6	

[a] Sr isotope ratios measured in the lab have been corrected for interlaboratory bias; see the methods section of the text for further explanations.

4.4. Results

4.4.1 Stratigraphy and facies

In the study area, the regional forebulge unconformity between the syn-orogenic lower Miocene shallow-water carbonates and the pre-orogenic substrate is represented by a paraconformity or a disconformity at the scale of the outcrop (Fig. 4.4a, c). The unconformity surface is generally marked by pressure solution structures such as stylolites (Figs. 4.5a, 4.6a). At the top of the Cretaceous substrate, breccia levels, sometimes accompanied by red crusts, are reported in some localities of the Mt. Camposauro area (Carannante et al., 2013). The uppermost levels of the Cretaceous substrate range in age from the Early Cretaceous (i.e., Aptian at Pietraroja and Mt. Rosa sections) to the Late Cretaceous (i.e. Coniacian at Regia Piana) (Simone et al., 2003; Carannante et al., 2013).

At Pietraroja, the Miocene carbonates of the Cusano Fm. cover a Lower Cretaceous substrate, which can be dated as Aptian due to the presence of the foraminifers *Sabaudia capitata* Arnaud-Vanneau, *Sabaudia minuta* (Hofker), *Cuneolina laurentii* (Sartoni and Crescenti) and *Nezzazata isabellae* Arnaud-Vanneau and Sliter (Chiocchini et al., 1994). The first Miocene level in the Pietraroja section (BLL-1 lithofacies in Bassi et al., 2010), is composed of about 4-5 meters of bryozoan and rhodolith floatstone with a fine-grained matrix containing serpulids, echinoid fragments and spines, thin-shelled bivalves, benthic foraminifers (including *Heterostegina* sp., *Amphistegina* sp., *Operculina* sp. and *Sphaerogypsina* sp.) and few planktonic foraminifers (Fig. 4.6b). This interval is truncated upward by a submarine hardground with evidence of intense bioperforation (Fig. 4.5c, d) (Bassi et al., 2010). Above the hardground, sedimentation resumed with deposition of bryozoan and rhodolith floatstone to rudstone with a coarser-grained matrix (Figs. 4.5b-f; 4.6c, d) (BLL-2 lithofacies in Bassi et al., 2010), containing ostreids, pectinids, echinoid fragments and spines, benthic foraminifers (including *Amphistegina* sp., *Sphaerogypsina* sp. and small rotaliids), some planktonic foraminifers and also re-sedimented clasts of the underlying BLL-1 lithofacies.

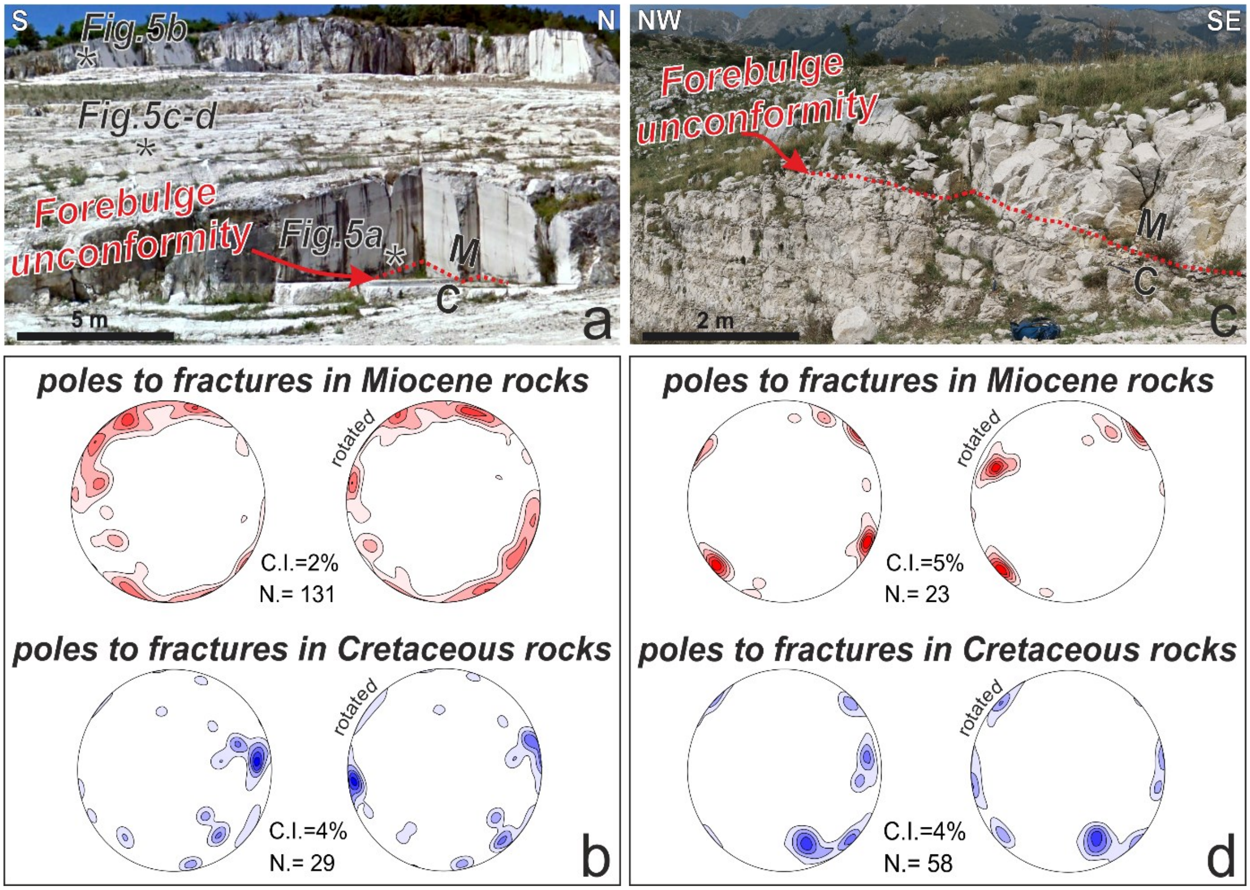

Figure 4.4. a) Pietraroja section, well-exposed in an abandoned quarry. Forebulge unconformity between the lower Miocene Cusano Fm. (M) and the Lower Cretaceous (Aptian) Calcari a Requienie Fm. (C). The black stars indicate the location of Fig. 4.5a, c, d. b) Contouring of poles to fractures analyzed at the Pietraroja site at the top of the Cretaceous substrate and within the Miocene carbonates (in blue and red, respectively), in their present-day configuration and after bedding-dip removal. c) Forebulge unconformity at the Regia Piana between the Upper Cretaceous Calcari a Radiolitidi Fm. (C) and the lower Miocene Cusano Fm. (M). d) Contour plots of poles to fractures analyzed at Regia Piana at the top of the Cretaceous substrate and within the Miocene carbonates (in blue and red, respectively), in their present-day configuration and after bedding-dip removal. C.I.: contour increment; N.: data number.

In the Regia Piana section, the contact between the Miocene limestones and the Upper Cretaceous substrate, dated as Coniacian due to the occurrence of the foraminifers *Accordiella conica* Farinacci, *Dicyclina schlumbergeri* Munier-Chalmas, *Moncharmontia apenninica* (De Castro) and *Rotalispira* *scarsellai* (Torre) (Chiocchini et al., 1994), is marked by a stylolitic surface (Figs. 4c, 6a) and is usually densely bored by lithophagous organisms (Fig. 4.6a). The basal interval of the Cusano Fm. consists of a rhodolith floatstone with bryozoans, ostreids, pectinids, echinoid fragments and spines, benthic foraminifers (such as *Amphistegina* sp., *Sphaerogypsina* sp., and rotaliids), and few planktonic foraminifers (Fig. 4.6a).

In the Mt. Camposauro area, the Cusano Fm. overlies a Lower Cretaceous substrate, which can be dated as upper Aptian due to the presence of *Archaeoalveolina reicheli* (De Castro) and *Cuneolina laurentii* (Sartoni and Crescenti). In the studied outcrop, the contact is sharp and marked by a stylolitic surface. The basal lower Miocene deposits consist of rhodolith rudstone to floatstone, with subordinated bryozoans, ostreids, pectinids, echinoid fragments and spines, and benthic foraminifers (*Amphistegina* sp. and some rotalids) (Fig. 4.6e). *Miogypsina intermedia* Drooger was reported by Schiavinotto (1985) in a level about 1 m above the base of the Cusano Fm.

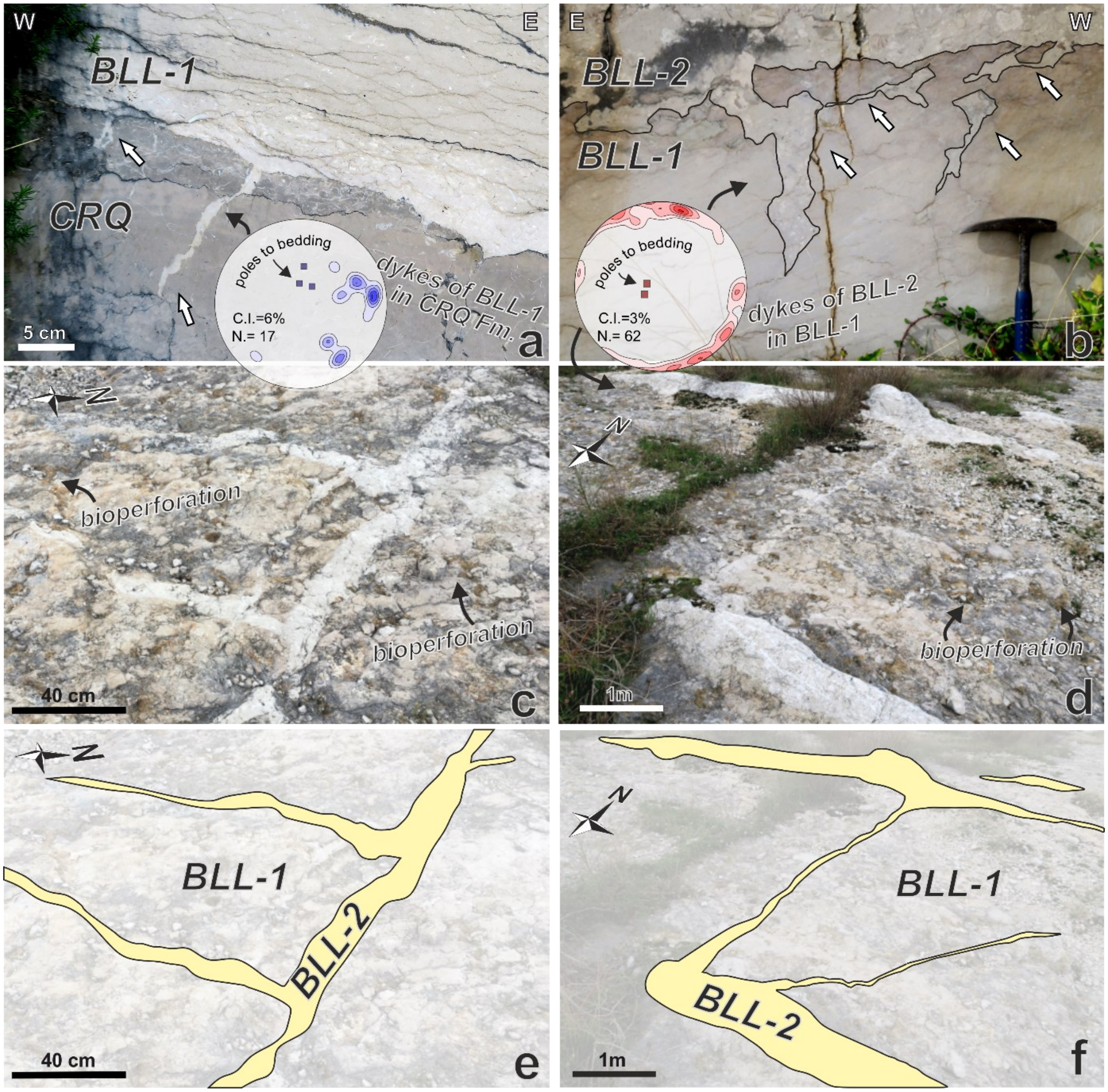

Figure 4.5. a) Detail of two sedimentary dykes (white arrows) cutting the Calcari a Requienie Fm. (CRQ) of Pietraroja site, filled by the first Miocene deposits (BBL-1) of the Cusano Fm. b) Contact between the rhodolith float-rudstones, facies BLL-2 (above), and the bryozoan-rhodolith floatstones, BLL-1 (below), of the Cusano Fm in the Pietraroja site. These two lithofacies are separated by a hardground (pinkish level). White arrows indicate sedimentary dykes filled by BLL-2 sediments in BBL-1 bedrock, oriented almost N-S and subordinately E-W. c, d) sedimentary dykes in the basal lithofacies (BLL-1) of Cusano Fm., filled by sediments of the overlying lithofacies (BLL-2). e,f) Line-drawing of the sedimentary dykes showing the predominant E-W and N-S orientations. Contour plots indicate poles to planes of dykes hosted on top of pre-orogenic carbonates (CRQ, blue-colored) and in basal levels of syn-orogenic carbonates (BLL-1, red-colored). The blue and red squares represent the poles to bedding planes of Cretaceous and Miocene carbonates, respectively.

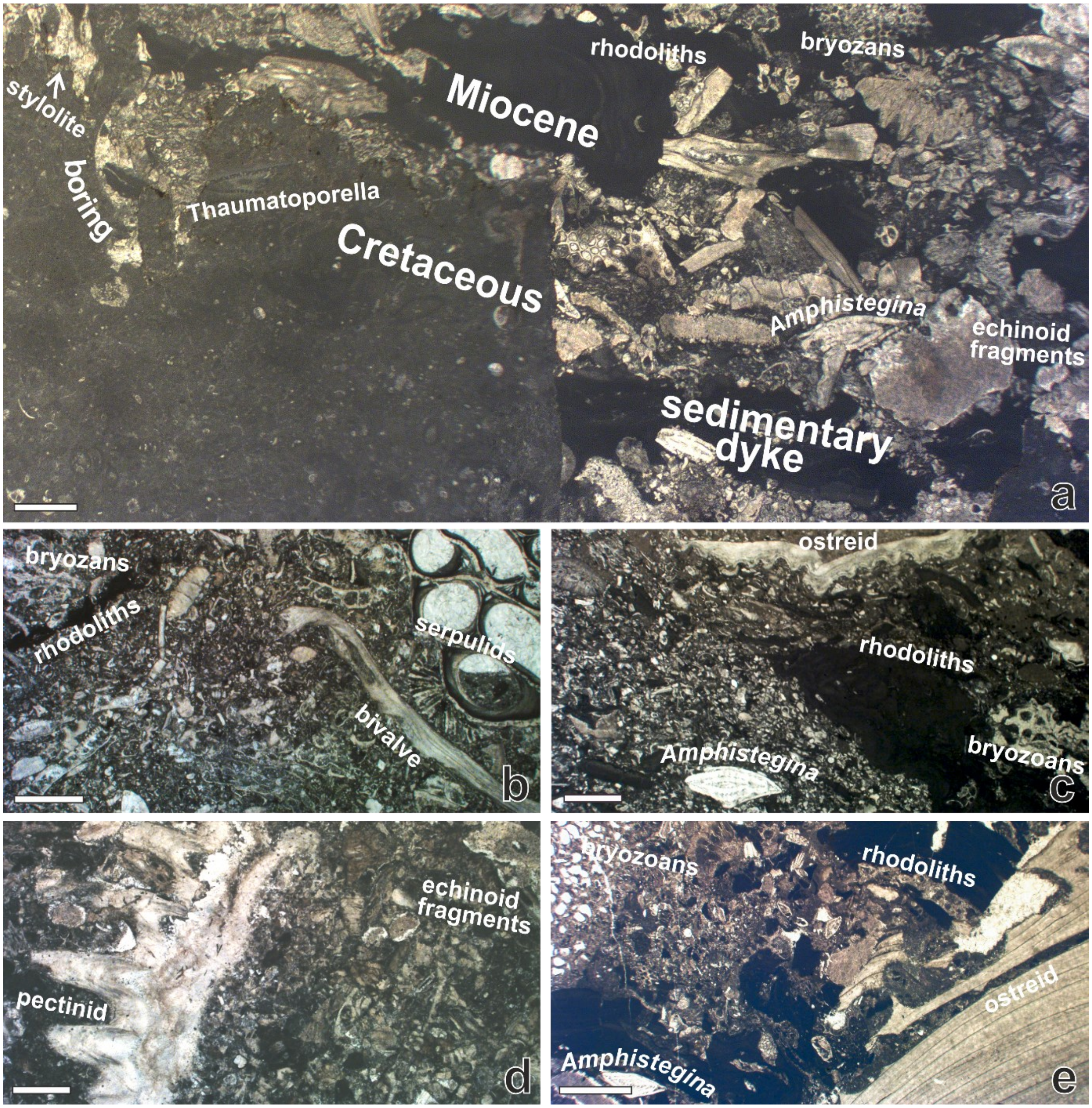

Figure 4.6. Microfacies of the lower Miocene (Burdigalian) Cusano Fm. in the studied sections. a) Detail of the stylolitic contact between the Cusano Fm. and the Upper Cretaceous pre-orogenic carbonates at Regia Piana. The lower Miocene sediments fill borings and sedimentary dykes in the Cretaceous substrate. The basal levels of the Cusano Fm. are a rhodolith floatstone. b) The lithofacies BLL-1 (Bassi et al., 2010) at Pietraroja is a bryozoan and rhodolith floatstone with a fine-grained matrix. c) Above the hardground at Pietraroja, the BLL-2 facies is characterized by a bryozoan and rhodolith rudstone to floatstone with a coarser-grained matrix. d) Rudstone of the Cusano Fm, about 2 m above the hardground. e) The basal deposits of the Cusano Fm. at Mt. Camposauro are a rhodolith rudstone to floatstone. See the text for more detailed descriptions. Scale bar = 1 mm in all photographs.

4.4.2 Strontium isotope stratigraphy

4.4.2.1 Pietraroja

The dataset for the locality of Pietraroja consists of four samples from four different stratigraphic levels (Table 41; Figs. 4.3, 4.7c, d, e). The lowest one (CuPRJ0) was taken very close to the base of the Cusano Fm., within the unit labelled BLL1 by Bassi et al. (2010). The other three come from unit BLL2, which is separated from BLL1 by a bioeroded hardground (Fig. 4.3).

The Sr concentration of the two shell fragments of undetermined bivalves of sample CuPRJ0 (445-457 ppm) is below the 600 ppm threshold value proposed by Scasso et al. (2001) for well-preserved Miocene pectinids. However, the microstructure of these two shell fragments is well preserved, with no evidence of diagenetic recrystallization. Moreover, the Sr isotope ratio of the two shell fragments is almost within analytical error while it is significantly different from the value of the bulk matrix enclosing the shells (Fig. 4.8a). For these reasons, we consider that the $^{87}Sr/^{86}Sr$ value of the shells has not been significantly altered by diagenesis. The mean value of the Sr isotope ratio calculated for CuPRJ0 gives an age of 18.7 Ma (Table 4.2).

Of the five shells fragments obtained from sample CuPRJ1 (Fig. 4.7c), CuPRJ1c was discarded, because of petrographic evidence of recrystallization. Its Sr isotope ratio has most probably been significantly altered by diagenesis, as it differs significantly from the values obtained from the other shells of the same sample, while it is very similar to the value obtained from the bulk matrix (Table 4.2, Fig. 4.8a). CuPRJ1b2 shows minor evidence of recrystallization. Moreover, its Sr concentration and Sr isotope ratio plot halfway between the well-preserved shells and the bulk matrix (Fig. 4.8a). For these reasons, this shell was considered as partially altered and was not used for SIS.

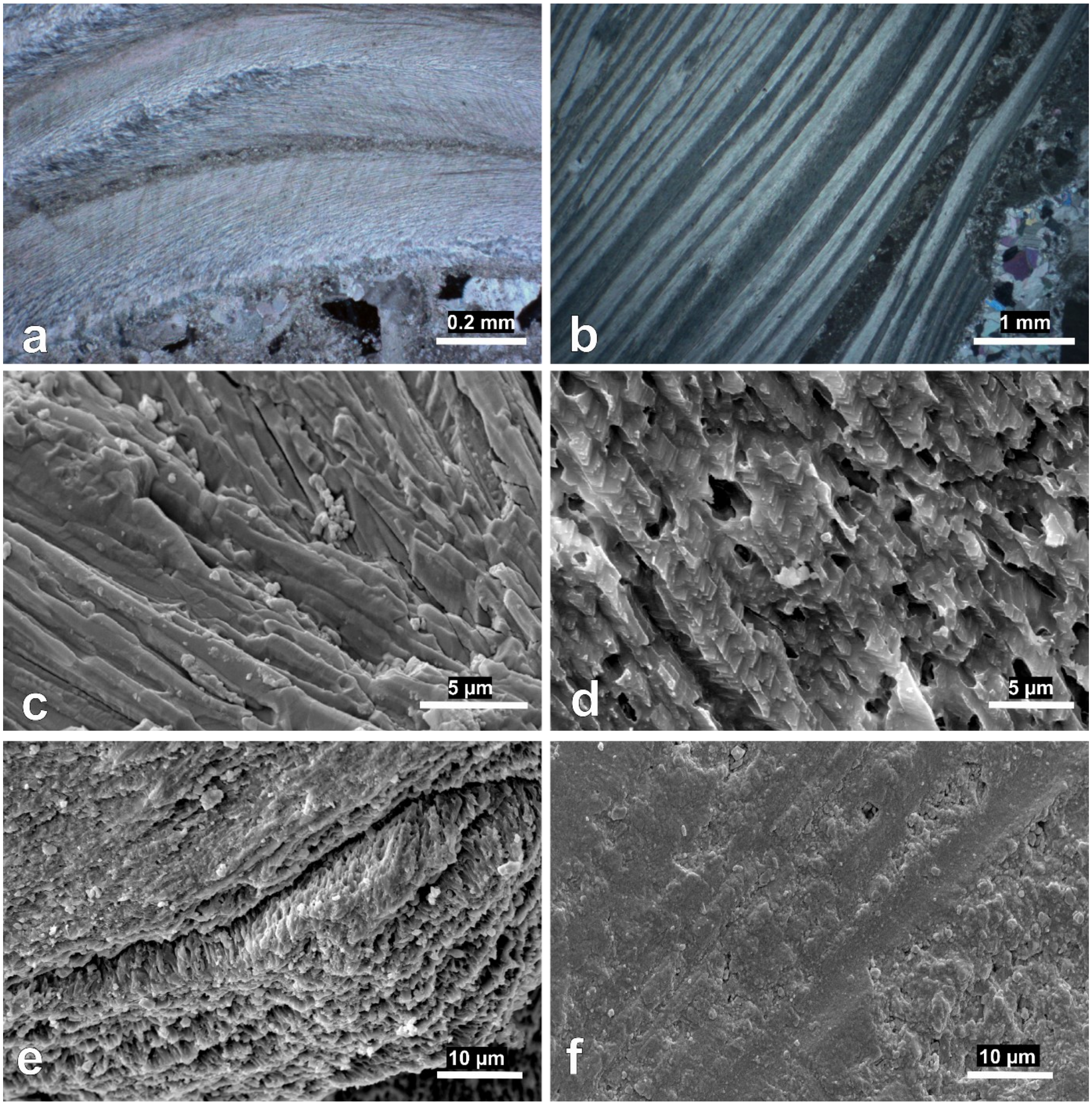

Figure 4.7. Microphotographs of Miocene pectinid and ostreid shells under optical and scanning electron microscopy. a, b) Ostreid shells at crossed nicols: in a) sample CuRP8c shows parts in which the lamellar microstructure is well-preserved; in b) sample CUCAM1a has a perfectly pristine lamellar microstructure. c, d) Pectinid shells of samples CuPRJ2b and CuPRJ1b1, showing well-preserved lamellar and cross-lamellar ultrastructure with single well-recognizable calcite fibers. e), f) Ostreid shells of samples CuPRJ3b and CuRP3b, showing different alteration degrees: in e) the original lamellar microstructure is still visible, but it has been altered by diagenesis, while in f) the microstructure has been almost completely obliterated by recrystallization.

The three pectinid shells of sample CuPRJ2 are well preserved, with no petrographic evidence of recrystallization (Fig. 4.7d). Their Sr isotope ratios are analytically indistinguishable, while they are significantly different from the values obtained from the bulk matrix enclosing the shells (Table 4.2, Fig. 4.8a). For all these reasons, their $^{87}Sr/^{86}Sr$ values are considered as pristine (i.e. not altered by diagenesis). The stratigraphic distance between samples CuPRJ1 and CuPRJ2 is just 0.5 m and there is no sedimentological evidence of stratigraphic breaks between them. Therefore, as the Sr isotope values of the well-preserved shells of these samples define a very narrow range (0.708537-0.708562), they have been lumped together for SIS. The mean $^{87}Sr/^{86}Sr$ value calculated for CuPRJ1-CuPRJ2, after excluding the altered shells, is 0.708546, corresponding to a numerical age of 18.3 Ma (Table 4.2).

The three ostreid shell fragments of sample CuPRJ3 show petrographic evidence of recrystallization (Fig. 4.7e). Moreover, their Sr isotope ratios are very discordant (0.708506-0.708712) (Fig. 4.8a). For these reasons, they are considered to have been significantly altered by diagenesis and were not used for SIS.

4.4.2.2 Regia Piana

The dataset for the locality Regia Piana consists of three samples from three different stratigraphic levels, within two meters stratigraphic distance from the base of the Cusano Fm (Fig. 4.3). The three shell fragments of sample CuRP3, give very discordant Sr isotope ratios (0.708525-0.708711). The two ostreid shells show evidence of recrystallization and have very low Sr concentrations, similar to that of the enclosing matrix (Table 4.1, Fig. 4.8b). Their Sr isotope ratios are significantly higher than that of the pectinid shell (CuRP3e), which has a well-preserved microstructure and a Sr concentration falling within the range of well-preserved Miocene pectinids defined by Scasso (2001). For these reasons, only CuRP3e was used for SIS (Fig. 8b). Its $^{87}Sr/^{86}Sr$ value corresponds to a numerical age of 18.6 Ma (Table 4.2).

All the shell fragments of samples CuRP4 and CuRP8, mostly consisting of ostreids, notwithstanding preserved areas (Fig. 4.7a), show petrographic and geochemical evidence of diagenetic alteration and were not used for SIS (Table 4.1, Fig. 4.8b).

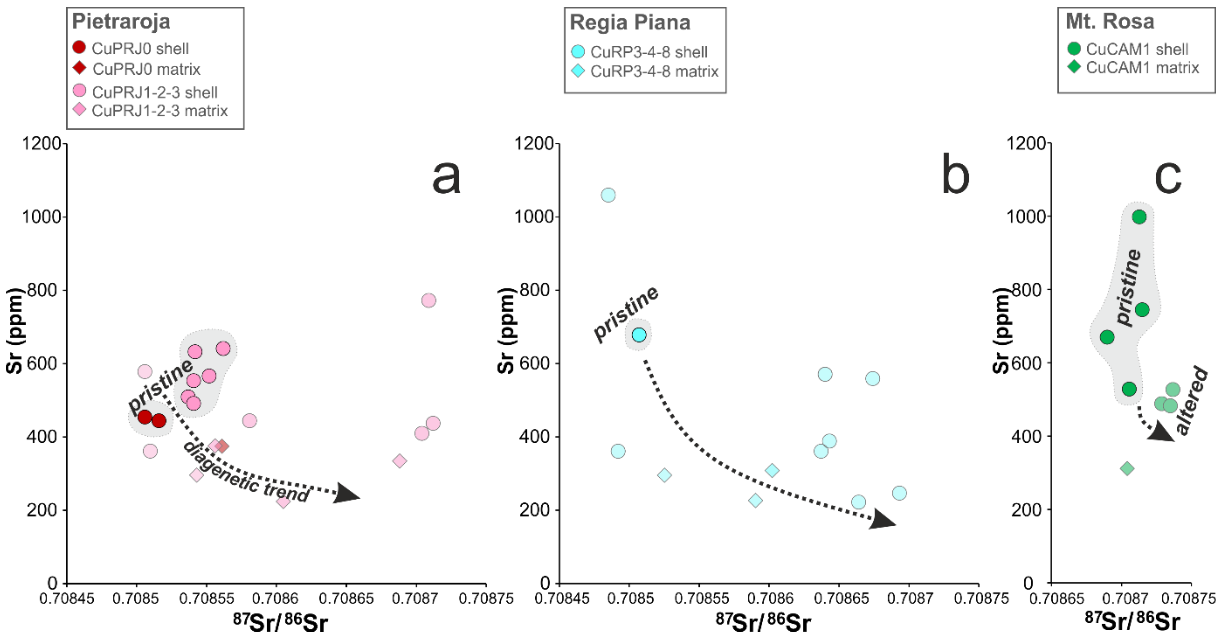

Figure 4.8. Bivariate scatterplot of Sr concentration vs $^{87}Sr/^{86}Sr$ ratio of the analyzed samples a) at Pietraroja, b) Regia Piana, and c) Camposauro sites.

4.4.2.3 Mt. Camposauro

The dataset for the Mt. Camposauro area consists of seven shell fragments (two pectinids and five ostreids) coming from a single stratigraphic level 0.5 m above the base of the Cusano Fm. (Fig. 4.3). On a plot of Sr concentration vs Sr isotope ratio, the shell fragments define two separate clusters (Fig. 4.8c). One cluster is made by three shell fragments of ostreids, characterized by petrographic evidence of recrystallization and by higher Sr isotope ratios (0.708729-0.708737) with lower Sr concentration (482-527ppm) (Fig. 4.8c). The other cluster consists of four shell fragments (two pectinids and two ostreids) with well-preserved microstructure (Fig. 4.7b), lower Sr isotope ratios (0.708690-0.708715) and higher Sr concentrations (539-998 ppm). These four shell fragments are considered to have retained their pristine Sr isotope ratios and were used for SIS (Fig. 4.8c). Their mean $^{87}Sr/^{86}Sr$ value corresponds to a numerical age of 16.3 Ma (Table 4.2).

Table 4.2. Strontium isotope stratigraphy of basal levels of the Cusano Fm. in the studied localities.

Sample	Section locality	m from the base	$^{87}Sr/^{86}Sr^{a}$	2 se (*10^{-6})	$^{87}Sr/^{86}Sr$ mean	2 se (*10^{-6})	numerical age (Ma) [b]		
							min	mean	max
CuPRJ0a	Pietraroja	0	0.708516	7	0.708511	10	18.5	18.7	18.9
CuPRJ0b		0	0.708506	7					
CuPRJ1a		4.5	0.708542	8	0.708546	8	18.2	18.3	18.5
CuPRJ1b1		4.5	0.708552	7					
CuPRJ1d		4.5	0.708562	5					
CuPRJ2a		5	0.708537	5					
CuPRJ2b		5	0.708541	5					
CuPRJ2c		5	0.708541	5					
CuRP3e	Regia Piana	0.2	0.708525	8	0.708525	15	18.4	18.6	18.9
CuCAM1a	Mt. Rosa	0.5	0.708713	8	0.708706	11	16	16.3	16.5
CuCAM1b		0.5	0.708690	7					
CuCAM1f		0.5	0.708715	6					
CuCAM1g		0.5	0.708706	10					

[a] Sr isotope ratios measured in the lab have been corrected for interlaboratory bias; see the methods section of the text for further explanations.
[b] The preferred numerical age has been derived from the look-up table of MacArthur et al. (2001, version 5: 04/13). The minimum and max age are calculated by combining the statistical uncertainty of the samples (2 se of the mean) with the uncertainty of the reference curve (see the methods section in Frijia et al., 2015, for a detailed explanation of the procedure).

4.4.3 Fracture pattern analysis

The structural analysis, performed on both the pre-orogenic carbonate megasequence and the basal part of the syn-orogenic carbonates, shows the occurrence of a fracture network mostly made of two sets, oriented orthogonal to each other and nearly perpendicular to bedding. A total of more than 300 meso-structural data, including bedding surfaces, joints, veins, and sedimentary dykes, were collected at Pietraroja and Regia Piana sites (Figs.

4.4, 4.5). In different outcrops, joints, veins, and sedimentary dykes display the same orientation, suggesting a common extensional origin. Accordingly, these structures are grouped together in the plots of Fig. 4.4, and they are termed “fractures”. Fracture orientation data are displayed in their present-day orientation and in the unfolded state (i.e., removing the bedding dip), in order to better visualize the pre-folding fracture sets (Tavani et al., 2018). The difference between the present-day and unfolded analysis is minimal, due to the very gently dips which characterize the bedding surfaces. The fractures measured on top of the Cretaceous substrate at the Pietraroja site are characterized by poles forming two clusters corresponding to bedding-perpendicular fractures striking N-S and, subordinately, E-W (contour plot in blue, Fig. 4.4b). In the same section, poles to fractures, hosted in the Miocene limestones, are clustered in three sets, corresponding to bedding perpendicular surfaces striking E-W, N-S, and NE-SW (contour plot in red, Fig. 4.4b). Figure 5a shows in detail sedimentary dykes cutting the Cretaceous bedrock in the Pietraroja site (CRQ, Calcari a Requienie Fm.) and filled by the first sediments of the Cusano Fm. (BLL-1). Data on sedimentary dykes collected in this portion of the multilayer are shown in Fig. 4.5b-f, with their contour plots in the present-day orientation showing the same clustering as those of Fig. 4.4b, i.e. dykes are bedding-perpendicular and striking N-S and E-W. These dykes, appearing only on top of the BLL-1 interval of the Cusano Fm. (Bassi et al., 2010), are the result of sedimentary infilling of open fractures by sediments of the lithofacies BLL-2 of the Cusano Fm. (Bassi et al., 2010).

At the Regia Piana section, fractures collected in Cretaceous rocks (RDT - Calcari a Radiolitidi Fm.) underlying the forebulge unconformity, define two mutually orthogonal sets of bedding perpendicular surfaces, striking nearly NNW-SSE and WSW-ENE (Fig. 4.4d). The orientation of fractures measured in the Miocene rocks is quite similar. These fractures, indeed, are bedding-perpendicular and oriented NE-SW and NW-SE (Fig. 4.4d).

4.5. Discussion

The SIS data presented in this paper supply for the first-time precise constraints on the age of the first lower Miocene deposits overlying the forebulge unconformity in the northern sector of the southern Apennines. The age for the base of the syn-orogenic sequence is rather diachronous, varying from 18.7 Ma at Pietraroja, 18.6 Ma at Regiapiana to 16.3 Ma in the Mt. Camposauro area.

The forelandward migration of a foreland basin system can be constrained by dating the first syn-orogenic deposits overlying the forebulge unconformity (DeCelles and Giles, 1996; DeCelles, 2012). Such migration is driven by the interplay of the load of the orogenic wedge, the load of the downgoing plate and the trench retreat, which define the tectonic setting. The latter also delineates the architecture, sedimentology and structure of the foreland basins (DeCelles, 2012). Accordingly, three main types of contractional foreland basin settings can be defined: retroarc, collisional, and collisional with retreating subducting slabs (DeCelles, 2012, pp. 411-416, for a detailed review). In these settings, four depozones are generally observed: wedge-top, foredeep, forebulge and back-bulge (DeCelles and Giles, 1996). The Apennines represent a typical example of a retreating collisional belt, characterized by narrow but thick foredeep and wedge-top depozones, and very narrow forebulge and back-bulge depozones (DeCelles, 2012). The vertical “Waltherian sequence” of foreland basin depozones (DeCelles, 2012) for the Apennine foreland basin is represented by the basal subaerial forebulge unconformity overlain by three diachronous lithostratigraphic units (Fig. 4.9). From bottom to top these are: (i) a shallow-water carbonate unit, (ii) a hemipelagic marl unit overlain by (iii) a siliciclastic turbidite unit ("underfilled trinity"; Sinclair, 1997).

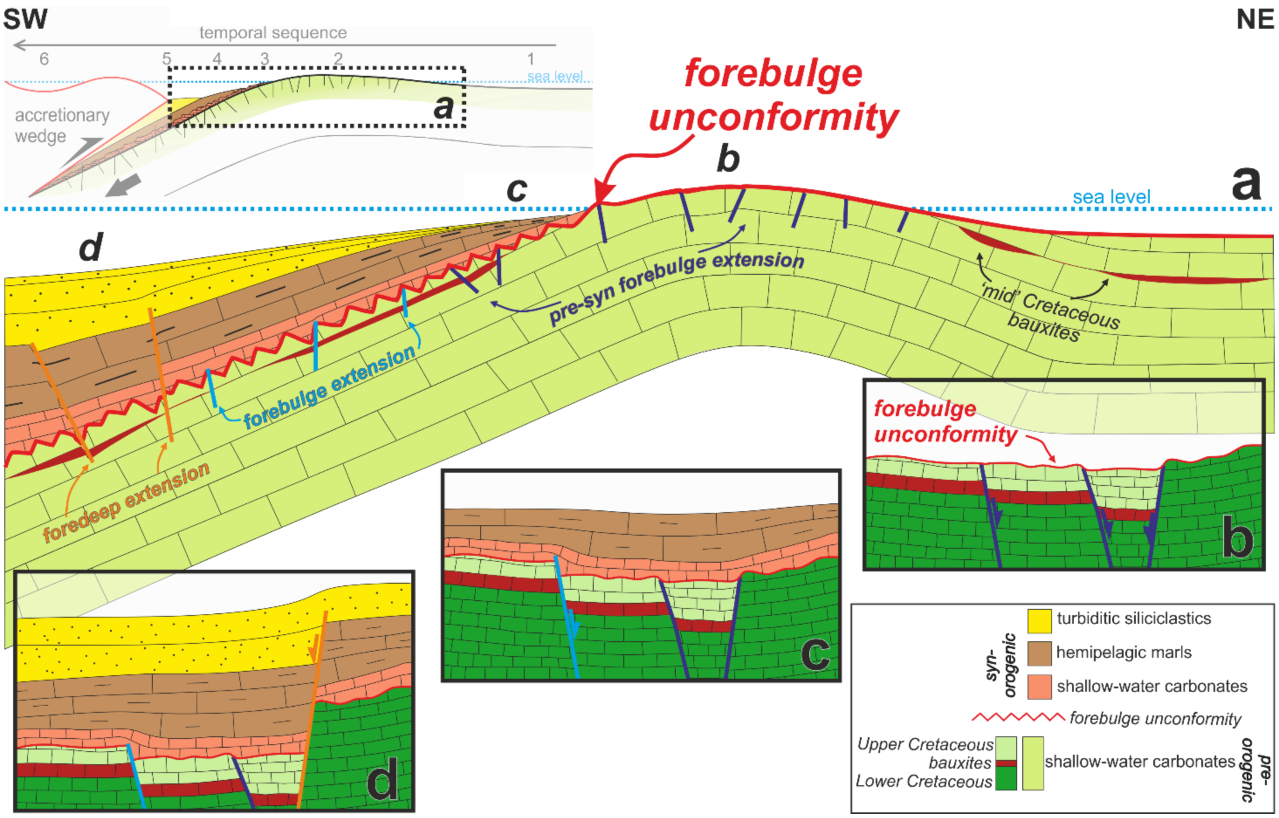

Figure 4.9. Sketch showing the tectono-stratigraphic evolution of the foreland basin system at a regional scale (a) with details evidencing how, on a more local scale (b), the articulated topography created before/during the onset of foreland basin subsidence influences the syn-orogenic stratigraphic record from the shallow-water, hemipelagic (c), to siliciclastics turbiditic (d) deposition.

The rate of migration of the southern Apennine foreland basin-belt system and the amount of shortening are highly debated (e.g., Dewey et al., 1989; Faccenna et al., 2001; Vitale and Ciarcia, 2013) with stratigraphic constraints derived exclusively from the deposits of the wedge-top and foredeep depozones (Cosentino et al., 2010; Vitale and Ciarcia, 2013 and references therein). However, the siliciclastic turbidite deposits of foredeep and wedge-top depozones are characterized by poorly fossiliferous micro- and nannofossil assemblages generally dominated by reworked taxa (De Capoa et al., 2003), which have resulted in uncertain and controversial biostratigraphic dating (e.g., Bonardi et al.,1985; Baruffini et al., 2000; Noguera and Rea, 2000). On the other hand, the deposits of the forebulge and back-bulge depozones have been poorly investigated, leaving a gap in the knowledge of the first steps of the foreland basin evolution. The first shallow-water sediments overlying the forebulge unconformity are generally represented in the study area by middle ramp deposits. These deposits do not record the first marine ingression, because above the fair-weather wave-base the platform was shaved by wave and currents (Brandano, 2017) and sediments did not accumulate. Therefore, the first marine sediments preserved above the unconformity track the time when the sea bottom subsided below the fair-weather wave base. They give, hence, the age of the base of the forebulge depozone, which is a significant point in the evolution of the foreland basin.

4.5.1 Age constraints

The age of the base of the lower Miocene limestones of the Matese Mts was previously poorly constrained. A Burdigalian age was proposed, based on the presence of the bivalve *Pecten pseudobeudanti* (Carannante and Simone, 1996). More to the north, at Mt. Cairo, in the Aurunci Mts, *Miogypsina globulina* (Michelotti) has been found at the base of the Calcari a Briozoi e Litotamni Fm. (Brandano et al., 2007), which represents the equivalent of the Cusano Fm. in the central Apennines. The same species is also reported in the lower Miocene limestones of the Roccadaspide Fm. at Capaccio (Cilento promontory; unpublished data cited in Brandano et al., 2007). *Miogypsina globulina* is a marker for the lower part of the Shallow Benthic Zone 25 of Cahuzac and Poignant (1997). This larger foraminiferal biozone is considered to span the entire Burdigalian (Cahuzac and Poignant, 1997; Hilgen et al., 2012), which is characterized, in the Mediterranean realm, by the sequence of chronospecies *M. globulina, M. intermedia, M. cushmani* and *M. mediterranea* (Drooger, 1993, and references therein). Based on its evolutionary stage, the *M. globulina* population of the Mt. Cairo section, was considered indicative of the middle part of the lower Burdigalian (Brandano et al., 2007, pp. 226). However, it must be stressed that the chronostratigraphic calibration of the ranges of different chronospecies and, even more, of the different evolutionary stages of the same chronospecies, is very poorly constrained. For this reason, SIS offers a much more precise and reliable tool for high-resolution dating and correlation of lower Miocene shallow-water carbonates. The ages of 18.7-18.6 Ma for the base of the Cusano Fm. in the Matese Mts (Pietraroja and Regia Piana) fall within the middle portion of the Burdigalian, according to the GTS2012. Moreover, these ages, considering their error band, are within error from the age of 18.8 Ma obtained with SIS for the base of the Calcari a Briozoi and Litotamni Fm. in the Mt. Lungo section (Aurunci Mts, central Apennines) by Brandano and Policicchio (2012).

A considerably younger age, 16.3 Ma, is given by SIS for the base of the Cusano Fm. in the Mt. Camposauro area. A younger age for the base of the Miocene transgressive deposits overlying the forebulge unconformity at Mt. Camposauro, is consistent with the occurrence in this locality of a rather advanced population of *Miogypsina intermedia* (Schiavinotto, 1985). The SIS age obtained for the base of the syn-orogenic sequence at Mt. Camposauro would correspond to the uppermost part of the SBZ 25 and would extend the range of *M. intermedia* almost to the end of the Burdigalian. To this regard, it is worth mentioning that the range of *M. intermedia* is considered to extend into the N7 planktic foraminiferal zone (De Mulder, 1975), which corresponds to the upper part of the Burdigalian (Hilgen et al., 2012).

A precise reconstruction of the timing of the Miocene transgression over the whole central and southern Apennines, recorded by the base of the first shallow-water carbonates overlying the forebulge unconformity, is at the moment hindered by the absence of precisely constrained ages. In any case, this task is definitely beyond the resolution attainable with biostratigraphy. The available data indicate that from the Pollino massif in northern Calabria to the Aurunci Mts in Lazio, the first transgressive deposits contain *Miogypsina globulina* (Selli, 1957; Brandano et al., 2007). Specimens of the older *Miogypsina socini* were found only in few localities of the Cilento area (Fig. 4.10) (Carannante et al., 1988a; Carannante and Simone, 1996). The range of *M. socini* is referable to the middle-upper Aquitanian, while the range of *M. globulina,* most probably extending over a time interval of some million years, is at present considered to start at the Aquitanian-Burdigalian boundary (Cahuzac and Poignant, 1997; Hilgen et al., 2012). However, their calibration to the geological time scale is very poorly constrained. A much better resolution can at present only be pursued by SIS (Fig. 4.10).

4.5.2 The forebulge unconformity

The occurrence of the Miocene Apennine forebulge is testified by a regional unconformity separating the passive margin megasequence from syn-orogenic sediments (Figs.1, 9) (Crampton and Allen, 1995). In the study area, the mid-upper Burdigalian syn-orogenic deposits lie on a passive margin paleosubstrate, which is Lower to Upper Cretaceous in age (Fig. 4.9, the "mid-Cretaceous" bauxites represent a guide level separating Lower from Upper Cretaceous limestones). Few and scattered localities witness also the deposition of Paleogene shallow-water carbonates (Selli, 1962; Chiocchini et al., 1994). Overall, from the southern to central Apennines, the age of the first syn-orogenic deposits overlying the unconformity ranges from early to late Miocene (Selli, 1957; Carannante et al. 1988a; Patacca et al., 2008; Carnevale et al., 2011; Brandano and Policicchio, 2012). A different interpretation is presented by Carminati et al. (2007), who proposed that the first interval of Miocene shallow-water carbonates was deposited during a phase of moderate uplift or stability related to the development of protothrusts or to foreland propagation of compressive stresses. The development of the forebulge unconformity and depozone shows differences in function of the environmental setting (Crampton and Allen, 1995). The latter is in turn related to geodynamics (e.g., flexural rigidity of the foreland lithosphere; Watts, 2001; DeCelles, 2012) and eustatism (Giles and Dickinson, 1995). Generally, in submarine deep-water settings, the stratigraphic record of the bulging and of the onset of flexural subsidence has a good potential of preservation, such as in the Aruma Group on the Wasia-Aruma Break unconformity in Oman and UAE (Robertson, 1987; Boote et al., 1990; Robertson and Searle, 1990; Ali and Watts, 2009; Cooper et al., 2014), the Gurpi-Pabdeh Group in Zagros (Alavi, 2004; Vergés et al., 2011; Saura et al., 2015), and in the Pinecone Sequence in Antler foreland of Nevada-Utah (Giles and Dickinson, 1995). In the Apennines, the peripheral bulge developed in subaerial conditions. The system thus evolved from subaerial to shallow-water, with generally incomplete preservation of the stratigraphic record. The facies transition from pre-, syn-, and post-bulging is only sporadically fully recorded in the Apennines, such as in the Cilento area of southern Apennines (Boni, 1974; Carannante et al., 1988a, Bianca et al., 2009; Monti et al., 2014) and in Scontrone and Palena areas of the central Apennines (Patacca et al., 2008; Carnevale et al., 2011). In most parts of the central-southern Apennines, including the study area, a paraconformity/disconformity (Bassi et al., 2010; Brandano, 2017) (Figs. 4.4a-c, 4.5a, 4.6a) is the only record left by the passage of the forebulge. This can be explained considering that, when sedimentation resumes in shallow-water environment (Fig. 4.9c), the marine transgression can be accompanied by erosion – i.e. ravinement – and sediment bypass, which can smooth the unconformity and remove the continental deposits of the subaerial phase and the transitional marine deposits of the first phase of the transgression (e.g., White et al., 2002; Babić and Zupanič, 2012; Brandano, 2017).

4.5.3. Local effects on a regional framework

In the study area, compared to the general regional configuration (Fig. 4.9a), the local topography of the top of the pre-orogenic sequence - Lower to Upper Cretaceous in age - appears more articulated. This influenced the development of the unconformity and the onset of syn-orogenic sedimentation (Fig. 4.9b). Accordingly, the diachrony between the first deposits of the Cusano Fm. at the Matese and Camposauro sites is likely related to such articulated topography. Prior to becoming the paleosubstrate of the foreland basin, the top of the passive margin sequence formed a locally articulated and tectonically controlled paleotopography, as documented in the present Apulian forebulge (Doglioni et al., 1994; Mariotti and Doglioni, 2000; Billi and Salvini, 2003) and in the Hyblean Plateau (Billi et al., 2006). In particular, horst and graben structures were inherited by previous tectonic events (see the blue colored faults in Fig. 4.9b) (e.g., Calabrò et al., 2003; Vitale et al., 2018) and subsequently reactivated during the forebulge stage (e.g., Tavani et al., 2015b) (see the pale blue colored faults in Fig. 4.9c). In support of this reactivation, we also present data on meso-structures affecting the sedimentary rocks below and above the forebulge unconformity. Joints and veins in the Cretaceous and Miocene sedimentary rocks display similar orientations, i.e. bedding-perpendicular and striking mostly NNW-SSE to N-S and WSW-ENE to E-W, which are identical to the orientation of sedimentary dykes filled with Miocene sediments. This feature indicates a Miocene age for these extensional structures. Studies on the early-orogenic fracture patterns of the Apennines recognize similar trends both in the fold and thrust belt (e.g., Vitale et al., 2012; Carminati et al., 2014; Tavani et al., 2015b; Corradetti et al., 2018; La Bruna et al., 2018) and in the present-day forebulge (Billi and Salvini, 2003). In agreement with our interpretation, these studies have attributed the development of these extensional structures to the flexing of the lithosphere during the development of the forebulge. The ongoing flexure-related extension carried on with the acceleration of the subsidence (Carminati et al., 2007) and led to the drowning of the platform below the photic zone in the early Serravallian (Fig. 4.9c) (i.e., hemipelagic marls deposition of the

Longano Fm., Lirer et al., 2005). Progressively, the system became involved in the foredeep setting (Pietraroja Fm., middle Tortonian; Selli, 1957; Lirer et al., 2005), where further structures were reactivated and formed (see the orange-colored faults in Fig. 4.9d) (Tavani et al., 2015b). At this stage, the syn-orogenic sedimentation definitively switched into siliciclastic deposition (Fig. 4.9d).

The effect of eustatic sea-level changes on the first stages of the Miocene transgression in the southern Apennines should also be taken into account for a complete tectono-stratigraphic reconstruction. In this regard, Crampton and Allen (1995) stressed the role of long-term sea-level changes (i.e., second-order cycles of Haq et al., 1988) on the development of the forebulge unconformity. These long-term sea-level changes, lasting a similar amount of time to the duration of forebulge uplift, can have a greater impact than rapid oscillations. In our case, the onset of syn-orogenic sedimentation at the Matese and Camposauro sites occurred during a global (2nd order) sea-level lowstand (Haq et al., 1988; Brandano and Corda, 2002; Brandano and Policicchio, 2012), which further emphasizes the role of tectonic subsidence in driving the transgression. On the other hand, the age of the first syn-orogenic sediments at Camposauro can also reflect the influence of the higher-order sea-level rise in the latest Burdigalian (John et al., 2011; Kominz et al., 2016). Currently, the sedimentary record of the Miocene foreland of the central-southern Apennine belt is exposed in patches in different localities of the central-southern Apennines belt (Fig. 4.10) and this further complicates reconstructing the complete tectono-stratigraphic evolution of the foreland basin. Precise dating of the very first syn-orogenic deposits has been obtained through SIS only for some areas of the central Apennines (Brandano and Corda, 2002; Brandano and Policicchio, 2012) and for the Matese and Camposauro (this study). For other areas, only biostratigraphic ages are available, which are inadequate to constrain the evolution and migration of the foreland basin and orogenic belt system. In Fig. 4.10, the example of the poor resolution attained by biostratigraphy versus high resolution attained by SIS is illustrated considering the ages of Cerchiara, Roccadaspide and Recommone Fms (Selli, 1957; De Blasio et al., 1981; Carannante et al., 1988a), Cusano Fm. (this study) for the southern Apennines and Lithothamnium Limestone Fm. (Tortonian – lower Messinian, Patacca et al., 2008) for the central Apennines.

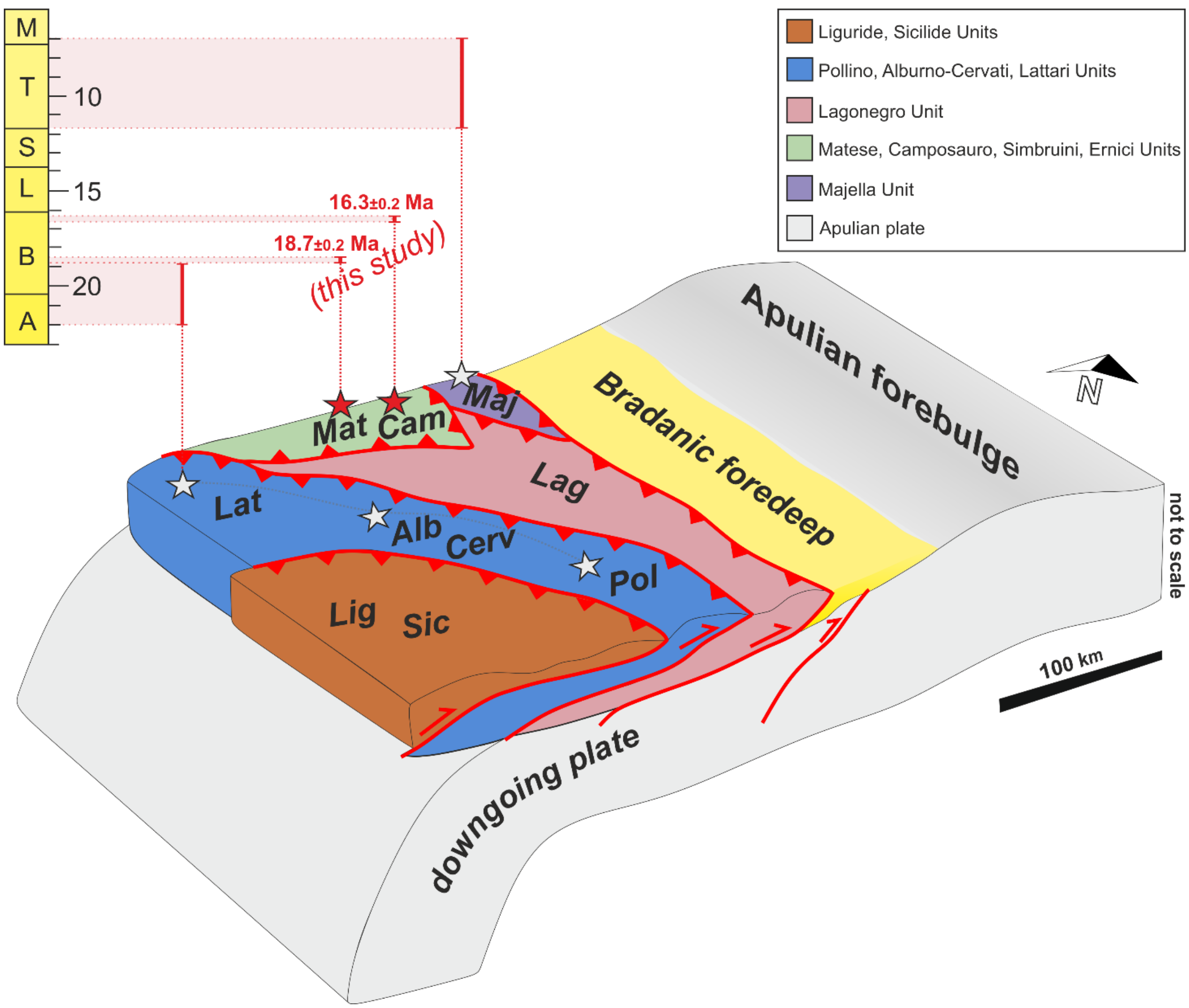

Figure 4.10. Schematic reconstruction of the central-southern Apennines fold and thrust belt and of their foreland in the present-day configuration. The figure shows the age of the first syn-orogenic shallow-water carbonates at different locations within the Apennine orogenic belt. Biostratigraphic ages (white stars) are from the literature (Selli, 1957; De Blasio et al., 1981; Carannante et al., 1988b; Patacca et al., 2008). The strontium isotope ages for the Matese and Camposauro (red stars) are from the present study.

4.6. Conclusions

The Miocene Apennine foreland basin system developed in a collisional-retreating setting, in which local and regional factors played a role in the development and configuration of forebulge unconformity and first syn-orogenic transgression. The ages of the first shallow-water carbonates overlying the forebulge unconformity provide a prime constraint to unravel the evolution of the Miocene foreland basin of the southern Apennine fold and thrust belt. Precise dating and correlation of these deposits by strontium isotope stratigraphy reveal a strongly diachronous timing of the onset of the syn-orogenic sedimentary sequence between the Matese Mts (18.7-18.6 Ma) and the Mt. Camposauro area (16.3 Ma), in the northern sector of the southern Apennines. We discussed the possible reasons for the observed diachrony and finally identified that it can be explained as a smaller-scale local complication of inherited topography along with forebulge extension in the framework of a regional foreland basin system.

We observed and discussed that the development of the forebulge unconformity was accompanied by extensional deformation. Joints, veins, and sedimentary dykes developed during this stage pointing to an extensional regime. This indicates the flexing of the lithosphere during the forebulge stage.

We finally conclude that by extending the same approach of this work to other sectors of the southern Apennines, we could define for the first time the timing of deformation, and thus better constrain the amount and rate of shortening and trench retreat in the Apennine fold and thrust belt. Ultimately, the workflow used in this study could be applied to other fold and thrust belts where subaerial exposure has produced an incomplete record of the transition from bulging to foredeep.

4.8 Supplementary material

4.8.1. Diagenetic screening

The best-preserved shells were selected in the field, using color preservation as a first guidance. The biotic calcite of pristine shells is generally honey-colored to dark brown or dark grey, as opposed to the whitish or dull light grey color of shells replaced by diagenetic calcite. Then, the preservation of the original shell microstructure was checked with a low-magnification lens. For each stratigraphic level, at least 4-5 shells and shell fragments were collected, along with a sample of the bulk matrix enclosing the shells. Having more than one shell from a single bed is fundamental to generate a more robust isotopic dataset and to further assess the degree of diagenetic alteration (McArthur, 1994). Different shells from the same bed (i.e., same age) should be characterized by a very narrow range of Sr isotope ratios (i.e., the Sr isotope ratio of marine water at the time of their precipitation), while diagenetic alteration would move the isotope ratio of the shells to different values. On the other hand, the bulk matrix represents a mixture dominated by diagenetic material (cements, recrystallized grains). Comparing its strontium isotope ratio with the ratio shown by the shells can be further used to assess their preservation (i.e., a shell that has a Sr isotope ratio very close to that of the matrix has been most probably altered by diagenesis). Selected shells were then passed through a petrographic screening, consisting in optical microscope, cathodoluminescence and scanning electron microscope (SEM) observations, in order to further assess the preservation of the original microstructure (McArthur, 1994; Ullmann and Korte, 2015). All the samples observed through cathodoluminescence microscopy revealed very low (essentially intrinsic) luminescence.

The elemental (Mg, Sr, Mn and Fe) composition of the shells, and of the micritic matrix of the samples, were analyzed as a further screening step, in order to evaluate their diagenetic evolution. Powder for geochemical analyses was obtained by scraping the polished surfaces of rocks exposing bivalve shells by means of a hand-operated microdrill, equipped with thin tungsten drill bits (0.5-1 mm). Before microdrilling the polished slabs and the isolated shell fragments were cleaned in an ultrasonic bath with a weak acid (acetic acid 4%), in order to remove surficial diagenetic coatings. Microsampling was performed under the binocular microscope.

4.8.2. Analytical procedures

The samples used for this work were analyzed over a period of about 2 years from 2017 to 2019 in three different geochemistry laboratories using different analytical methods.

4.8.2.1 Minor and trace elements concentration

The first batch of samples (CuPRJ0a, CuPRJ0b, CuPRJ0M, CuPRJ1b2, CuPRJ2a, CuPRJ2b, CuPRJ2c, CuPRJ2M, CuPRJ3a, CuPRJ3b, CuPRJ3c, CuPRJ3M, CuRP3c, CuRP8d, CuCAM1a, CuCAM1b, CuCAM1b42, CuCAM1c, CuCAM1e, CuCAM1f, CuCAM1g, CuCAM1M) was analyzed at the Institut für Geologie, Mineralogie und Geophysik of the Ruhr-Universität of Bochum. An aliquot of the carbonate powder was dissolved in 1 ml 3 M HNO3 and then diluted with 2 ml H2O for analysis with a Thermo Fisher Scientific iCAP6500 Dual View inductively coupled plasma optical emission spectroscopy (ICP-OES). The external reproducibility, expressed as relative standard deviation (RDS), is ±1% of the measured concentrations for Mg and Sr, ± 2% for Mn and ± 5.6% for Fe.

The second batch of samples (CuPRJ1a, CuPRJ1b, CuPRJ1c, CuPRJ1d, CuPRJ1d, CuPRJ1M, CuRP3b, CuRP3d, CuRP3M, CuRP4a, CuRP4d, CuRP4M, CuRP8a, CuRP8b, CuRP8c, CuRP8M) was analyzed at the Department of

Chemistry and Earth Science of the University of Modena and Reggio Emilia. An aliquot of each sample was dissolved in 4 ml 3 M HNO_3 and then diluted with 1 ml H_2O for elemental concentration determination using a Perkin Elmer Optima 4200 DV ICP-OES. Each sample was analyzed three times and precisions were typically better than 5% RSD for Mg, Sr and Fe and better than 20% for Mn.

4.8.2.2 Sr-isotope ratios analysis

The strontium isotope ratio was analyzed on a split of the same samples analyzed for elemental concentrations after separation of Sr with standard ion-exchange separation methods.

A first batch of samples (CuPRJ2a, CuPRJ2b, CuPRJ2c, CuPRJ2M, CuPRJ3a, CuPRJ3b, CuPRJ3c, CuPRJ3M) was analyzed with a Finnigan MAT 262 thermal ionization mass spectrometer (TIMS) at the Institut für Geologie, Mineralogie und Geophysik of the Ruhr-Universität of Bochum. 87Sr/86Sr ratios were normalized to an 86Sr/88Sr value of 0.1194. The long term mean of NIST SRM 987 at Bochum laboratory was 0.710240 ± 0.000002 (2 s.e., n= 386). The $^{87}Sr/^{86}Sr$ ratios of the samples have been corrected for the inter-laboratory bias by adjusting the long term mean value of NIST SRM 987 at Bochum laboratory to the value of 0.710248 used by McArthur et al. (2012) for the compilation of the ‘‘look-up’’ table (McArthur et al., 2001).

A second group of samples (CuPRJ1a, CuPRJ1b1, CuPRJ1c, CuPRJ1d, CuPRJ1d, CuPRJ1M, CuRP3b, CuRP3d, CuRP3M, CuRP4a, CuRP4d, CuRP4M, CuRP8a, CuRP8b, CuRP8c, CuRP8M) was analyzed by means of a Thermo Scientific Neptune high-resolution multi-collector inductively coupled plasma mass spectrometer (MC-ICP-MS) at the Centro Interdipartimentale Grandi Strumenti of the University of Modena and Reggio. The Sr-isotope values were determined following the same procedure reported by Vescogni et al. (2014) and the samples were run using a bracketing sequence blank-standard-blank-sample-blank to correct for possible instrumental drifts. The mean value of the NIST SRM 987 standards run together with the samples was 0.710214 ± 0.000007 (2 s.e., n= 23). The $^{87}Sr/^{86}Sr$ ratios of the samples were first corrected from isobaric interferences of 86Kr and 87Rb on ^{86}Sr and ^{87}Sr, and then adjusted to the value of 0.710248 of NIST SRM 987 (McArthur et al., 2012) by multiplying each Sr-isotope ratio for the C-factor value calculated dividing the measured isotope ratio by the average value of the two standards measured before and after each sample in the bracketing sequence.

A third group of Sr-isotopes measurements were obtained with a Thermo Fisher Triton multi-collector TIMS housed at the National Institute of Geophysics and Volcanology, Vesuvius Observatory (INGV-OV) in Naples. The samples were analyzed in four analytical sequences (1. CuPRJ0a, CuPRJ0M, CuRP8d, CuCAM1a, CuCAM1b; 2. CuPRJ1b2; CuCAM1e, CuCAM1f, CuCAM1M; 3. CuPRJ0b, CuCAM1b4; 4. CuRP3e, CuCAM1c, CuCAM1g).

The mean values of NIST SRM 987 standards run together with the four sequences of samples are: 1) 0.710248 ± 0.000007 (2 s.e., n=2); 2) 0.710246 ± 0.000006 (2 s.e., n=2); 3) 0.710246 ± 0.000006 (2 s.e., n=2); 4) 0.710279 ± 0.000006 (2 s.e., n=2). The long term mean of NIST SRM 987 at INGV-OV laboratory was 0.710244 ± 0.000006 (2 s.e., n=55) for a period and 0.710266 ± 0.000007 (2 s.e., n=37) for a second period. The $^{87}Sr/^{86}Sr$ ratios of the samples have been corrected for the inter-laboratory bias by adjusting the long term mean values of NIST SRM 987 at INGV-OV laboratory to the value of 0.710248 used by McArthur et al. (2012) for the compilation of the look-up table (McArthur et al., 2001).

4.9 Data availability

This chapter is extracted from a journal paper that was published in Sedimentary Geology, doi:10.1016/j.sedgeo.2020.105634

Supplementary data can be found online at https://doi.org/10.1016/j.sedgeo.2020.105634

CHAPTER 5. INSIGHTS ON THE PALEOECOLOGY OF AMMONIA (FORAMINIFERA, ROTALIOIDEA) FROM MIOCENE CARBONATES OF CENTRAL AND SOUTHERN APENNINES (ITALY)

Consorti, L., ***Sabbatino, M.****, & Parente, M.*

This chapter has been published in *Palaeogeography, Palaeoclimatology, Palaeoecology* **562**, (2021)

Abstract

The Miocene transgression in central and southern Apennines is commonly represented by a sharp contact between shallow-water open-marine bioclastic limestones and the underlying Cretaceous or Eocene bedrock. Only in a few areas, very proximal marine or paralic deposits, witnessing the first stage of the transgression, have been preserved. These deposits contain rich foraminiferal assemblages commonly dominated by specimens of the genus *Ammonia*. The paleontological and paleoenvironmental analysis revealed that the Miocene *Ammonia* shared the same habitat and ecological requirements of living representatives from recent shoreline environments. Small *Ammonia* forma '*tepida*' have been found in Miocene marginal paralic organic-rich bottoms with restricted water circulation and possibly under natural metal pollution. Big *Ammonia* forma '*beccarii*' characterize Miocene nearshore marine bottoms with vegetated areas under fresh water inputs. The endoskeletal lamellar folding called tooth-plate, which characterizes recent representatives, is observed in fossil specimens of both *tepida* and *beccarii* morphogroups, testifying that there were no major changes in the shell architecture of *Ammonia* since the early Miocene.

Keywords: Paralic environments; Miocene transgression; Ecophenotypic variation; Estuarine bay; Coastal lagoon

5.1. Introduction

Ammonia Brünnich is a benthic foraminifer dwelling in littoral and neritic environments of both siliciclastic and carbonate marine systems. Its recent geographic distribution is extremely wide, extending from the north-eastern Atlantic to Australia, New Zealand and southern Argentina (Walton and Sloan, 1990; Hayward et al., 2019). Ammonia usually thrives in estuarine, brackish and saltmarsh environments (Jorissen, 1988; Haynes, 1992; Murray, 2006; Dupuy et al., 2010, among others) or under the influence of fluctuating water salinity, temperature and nutrient input (Schnitker, 1974; Debenay et al., 1998). It is mostly considered a deposit-feeding foraminifer with different ecological strategies, from epiphytic to shallow infaunal (Langer et al., 1989; Takata et al., 2009; Dupuy et al., 2010), and is capable to incorporate nitrates in low-oxygen environments (Nomaki et al., 2016). It can also tolerate a wide range of water temperatures, from 5°C to 35°C (Bradshaw, 1961; Walton and Sloan, 1990; Weinmann and Langer, 2017) but the optimum for reproduction and shell growth is established between 25°C and 30°C (Bradshaw, 1961).

When present in the foraminiferal assemblage, *Ammonia* is often dominant and commonly shows a remarkable morphological variability, expressed both in test size and ornamentation. Such variability has been generally referred to genetic plasticity (Haynes, 1992) or to ecotypic variations (Schnitker, 1974; Holzmann and Pawlowski, 1997). Relative abundance and dominance of different Ammonia morphotypes could be linked to the environmental conditions. For instance, small 'tepida' morphotypes thrive generally in organic-rich bottoms, while big 'beccarii' morphotypes abound under more open marine conditions or estuaries with fluctuating water salinity. Morphologic variability caused in the taxonomy of Ammonia what Holzmann and Pawlowski (1997) and Haynes (1992) called 'nomenclatural chaos', a situation that makes difficult the assignment of species and has produced redundancy or proliferation of synonyms. *Ammonia parkinsoniana*, *A. aomoriensis*, *A. langeri* and species described in Billman et al. (1980), among others, may be considered endemic. However, the dispersal mechanism in *Ammonia* remains not completely understood (see also discussion in Walton and Sloan, 1990 and Schweizer et al., 2011) as suggested by the synchronous occurrence of *A. pawlowskii* both into the Mediterranean Sea and West Indian Ocean (Hayward et al., 2019), which are two different foraminiferal bioprovinces (Langer and Hottinger, 2000). A further complication is introduced by the existence of teratologic forms (Schnitker, 1974; Melis and Covelli, 2013) sometimes linked to stressed conditions, such as mesotrophic hyposaline low-oxygen bottoms (Stouff et al., 1999). Moreover, Hayward et al. (2019) have demonstrated that the molecular phylogenetic tree of Ammonia is significantly diverse, thus probably representing many more molecular species than those previously recorded. In spite of these problems, there is a general consensus among the authors that studied recent Ammonia species (Schnitker, 1974; Jorissen, 1988; Pawlowski et al., 1995; Debenay et al., 1998; Hayvward et al., 2004; Dupuy et al., 2010; Richirt et al., 2019 among others) that at least two morphogroups can be easily sorted up: *Ammonia forma beccarii* and *Ammonia forma tepida*. However, especially in fossil assemblages, when molecular analysis is not available, it could be preferable to treat these morphogroups as ecophenotypes, i.e. morphotypes linked with the environmental parameters and not necessarily to genotypic differences (Schitker, 1974; Jorissen, 1988; Walton and Sloan, 1990; Debenay et al., 1998; Takata et al., 2009).

Ammonia appears in the geological record from the early Miocene. According to Billman et al. (1980), there are several lineages from that time interval. Fossil representatives have been recovered worldwide in paralic, brackish and shallow-marine settings of Africa (Hottinger, 1966; Ramihangihajason et al., 2014; Amakrane et al., 2016), America (Sen Gupta et al., 1986; Patterson, 1987; Boonstra et al., 2015; Gurocak-Orhun and Collins, 2017), Europe (Baldi and Hohenegger, 2008; Filipescu et al., 2011), and Asia (Ujiié, 1965; Billman et al., 1980; Hasegawa and Takahashi, 1992; Roslim et al., 2019), especially within Miocene-Pliocene rocks. Fossil *Ammonia* have been commonly used as paleoenvironmental indicators (Van der Zwaan, 1982; Amakrane et al., 2016; Gurocak-Orhun and Collins, 2017, among others). In this paper, we report some rich *Ammonia* assemblages from the Miocene paralic to proximal marine shallow-water deposits of the central and southern Apennines. These deposits are found at the base of the transgressive Miocene units and rest onto the Cretaceous or Eocene carbonate substrate, generally with the interposition of residual clays, exposure-related breccias and/or *Microcodium* caliches. Paralic (*sensu* Guelorget and Perthuisot, 1983) and very proximal marine sediments were most probably widespread in several areas of the central and southern Apennines during the Miocene. However, they may have been partially washed out or eroded during the ravinement phase of the transgression (see discussion in Patacca et al., 2008). Outcrops of limited extension and thickness have been preserved only locally and they have been often overlooked in the literature. These sediments represent the main target of the present study. We give a morphological description and paleoecological interpretation of the benthic foraminiferal assemblages. In this contribution, we also reviewed the (paleo)-environmental information available from the literature on the recent Mediterranean and western Atlantic *Ammonia* morphostock *sensu* Poag (1978) to test if the paleoecology of fossil *Ammonia* fits with that of recent representatives. Our main aim is to investigate whether the distribution of fossil *tepida*-like and *beccarii*-like morphotypes found in the studied deposits correspond to their facies and environmental distribution in modern marine environments. Being *Ammonia* widely occurring along present shorelines, this contribution wishes to provide useful insight into the early paleoecological history of the genus which is critical to explain its wide range of molecular species in the Recent (Holzmann et al., 1998; Hayward et al., 2019; Richirt et al., 2019).

5.2. Taxonomy of the Ammonia shell in thin section

Ammonia is a lamellar perforated foraminifer with a set of inflated slightly trapezoidal chambers that are trochospirally arranged. There is a maximum of four whorls; the dorsal side is evolute whereas the umbilical side is involute. The canal system is composed by a spiral canal connected to an intraseptal interlocular network. There are some typical features of *Ammonia* that can be distinguished not only studying isolated individuals or oriented sectioned cuts (see Fig. 5.1), but also in some non-oriented sub-axial and transversal sections, which are the ones mostly used in this work. The occurrence of the endoskeletal shell structure called umbilical tooth-plate (see Hottinger, 2006 for definition), together with the occurrence of a well-rounded periphery, are the distinctive traits of *Ammonia*, as first reported by Hofker (1971), and they are easily observable in thin section (Fig. 5.1). A tooth-plate is observed in several different rotaliid Foraminifera (Revets, 1993; Hottinger et al., 1991; Benedetti et al., 2020) like in the genus *Pararotalia* Le Calvez (see e.g. Hottinger et al., 1991; Piuz and Meister, 2013) and is classically used to split the group of pararotaliids within Rotalioidea (Hottinger, 2014; Consorti et al., 2017a, Consorti et al., 2017b). However, when comparing sections with similar orientation, Pararotalia can be distinguished from *Ammonia* because of the lower trochospire, of the occurrence of a very angular chamber periphery bearing few spines and the presence of deeper umbilical chamber sutures (see Hottinger et al., 1991). The tooth-plate is visible in several sections of *Ammonia* illustrated by Hansen and Reiss (1971), and Billman et al. (1980), as well as in illustrations of its junior synonym, *Strebulus beccarii*, by Hofker

(1971). The umbilical plug, deriving by the umbilical extension of the pile, occurs as well, but this is visible in external view, especially in the *beccarii* morphotype. The genera *Helenina* Saunders and *Monspeliensina* Glacon and Lys differ from *Ammonia* for the almost flat profile; for the lack of a marked ornamentation (e.g., sutural ridges or ventral feathering) and the absence of the tooth-plate.

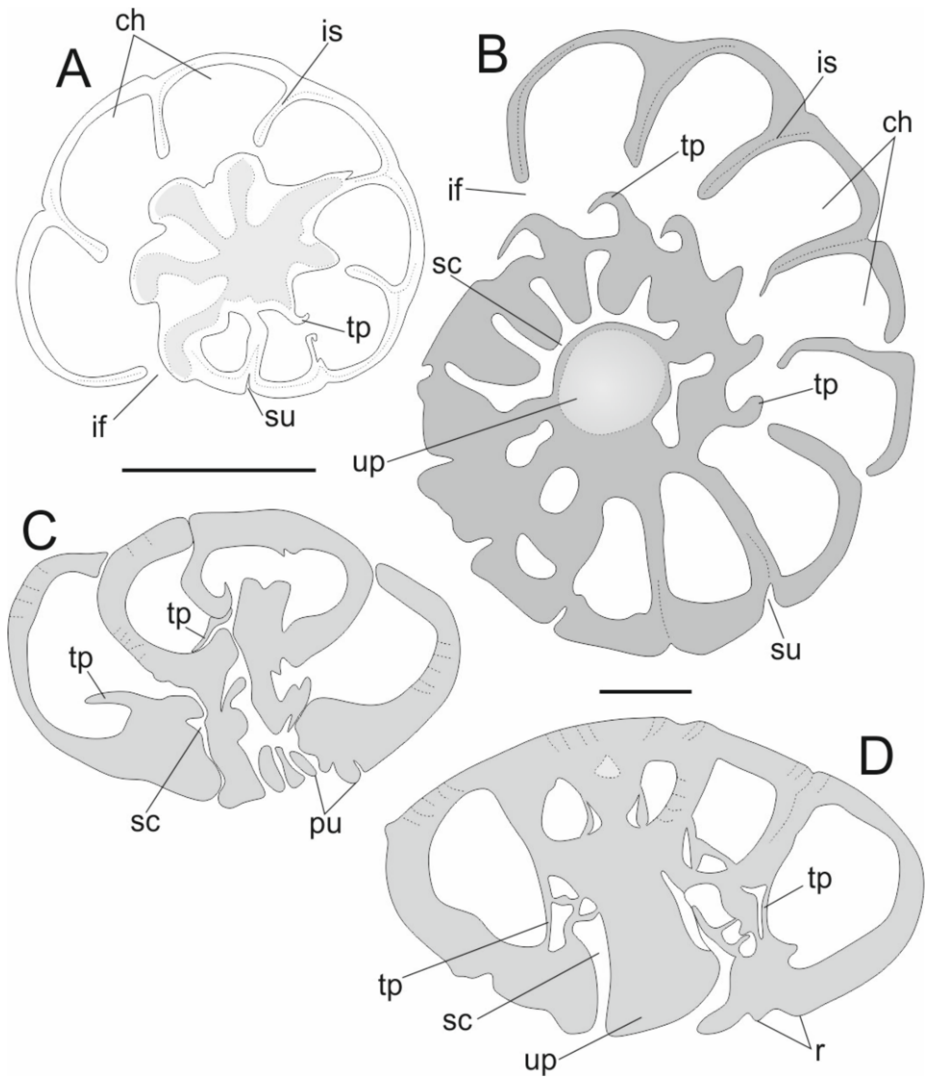

Figure 5.1. Drawings of *Ammonia* in oriented transversal (A, B) and axial (C, D) sections. A, C. *Ammonia tepida*. B, D. *Ammonia beccarii*. Redrawn from Hansen and Reiss (1971), Loeblich and Tappan (1987) and Woods et al. (2019). Scale bar 0.2 mm. ch: chamber lumen; if: intercameral foramen; is: intraseptal interlocular canal; pu: pustules (umbilical ornamentation); r: ridges (umbilical ornamentation); sc: spiral canal; su: sutural canal; up: umbilical pile; tp: tooth-plate.

The tooth-plate has been figured in thin sections of lower Miocene *Ammonia* specimens by Billman et al. (1980) and Ujiié (1965). This supports the idea that this shell structure was fully developed since the first radiation of the group. For working purposes, and in absence of molecular indications we have grouped the fossil morphotypes studied in this paper in two main ecophenotypic clusters: *Ammonia* forma *beccarii* and *Ammonia* forma *tepida*. This in turn is based on the taxonomic differences observed among the lectotype of *A. beccarii* (following Vaiani et al., 2019) and that of *A. tepida* (following Hayward et al., 2003), which are the only specimens that unarguably carry the species names. Although these Ammonia lectotypes are illustrated with isolated specimens, the characters here exposed may easily be observed in thin section too, as well as in most benthic foraminifera (see Flügel, 2004; Hottinger, 2006, Hottinger, 2014). *A. beccarii* is the biggest, reaching 1.5 mm in diameter; it possesses almost 30 chambers at the last whorl. The shell wall is relatively thick. The shell surface is heavily ornamented by ridges and furrows (feathering), locally associated with pustules over the umbilical area that bears an evident umbilical plug. *A. tepida* test is small (0.25 mm to 0.35 mm in diameter), with a maximum of 6-8 chambers per whorl, whereas its shell wall is relatively thin and the surface less ornamented. Based on the lectotype figured in Hayward et al. (2003) the umbilical area of *A. tepida* seems not occupied by a plug but rather by few shallow pustules. However, being *A. tepida* lectotype not axially sectioned, the umbilical pile might be present (as displayed in the type-taxon *A. beccarii*) but engulfed and hidden within the last whorl of chambers. As also reported by Hayward et al. (2019) for the Recent, the specific diversity of *Ammonia* was presumably high in the Miocene as well. The population studied for each Miocene deposit of central and southern Apennines may represent a single genetically related assemblage composed by co-specific entities.

5.3. *Ammonia* ecophenotypes and their environmental meaning

Based on a survey of literature on recent *Ammonia* (Schnitker, 1974; Jorissen, 1988; Langer et al., 1989; Walton and Sloan, 1990; Debenay et al., 1998; Stouff et al., 1999; Hayward et al., 2004; Carboni et al., 2009; Takata et al., 2009; Dupuy et al., 2010; Haller et al., 2019; Hayward et al., 2019, among others), we subdivide the ecopenotypes morphospace as follows.

5.3.1. Ammonia forma beccarii

Differences in test ornamentation and chamber volume allow identifying two end-members. The first one is here denominated *Ammonia* forma *beccarii* A and corresponds to a group of morphotypes including *Ammonia beccarii* forma *beccarii* in Jorissen (1988, pl. 5) or *Ammonia beccarii* forma *beccarii* in Walton and Sloan (1990, pl. 1). The diameter of the test of this morphotype ranges from 300 µm to 1000 µm. It shows dorsal ornamentation composed by ridges along chamber sutures and deep interlocular space in the umbilical area. Chambers outline is rectangular, with acute termination in the adaxial directions. The umbilical plug is distinct. Defined piles are composed of axial lamellar thickenings lying on the acute adaxial chamber termination. Test thickness of last chambers is moderate. Pores are comparatively large.

Jorissen (1988) found the forma *beccarii* A at 15 m to 20 m depth, in sediment samples with intermediate proportions of organic matter and at least a very little percentage of sand and variable amount of clay. This morphotype seems absent under direct fresh-water runoff, such as delta inlets, but it occurs in the surroundings of these areas. The forma *beccarii* A is a shallow-infaunal deposit feeder, with occasionally epifaunal or epiphytic behaviour (Jorissen, 1988; Debenay et al., 1998).

The second form, here designated as *Ammonia* forma *beccarii* B, corresponds to a group of morphotypes including the Ammonia beccarii forma inflata of Jorissen (1988, pl. 6), the *Ammonia beccarii* forma *beccarii* of Walton and Sloan (1990, pl.3); the *Ammonia beccarii* in Debenay et al. (1998), the *Ammonia reyi* of Cornée et al. (2006), as well as the adult specimens of Northern Adriatic Sea described in Hayward et al. (2019; figs. 1.13-1.18). We include within this group all the ornamented, probably endemic, *Ammonia* species figured in Hottinger (1966) and Billman et al. (1980). The diameter of the test is generally bigger compared to forma *beccarii* A, reaching sometimes more than 1 mm. Chambers are inflated, with acute termination in the adaxial umbilical direction. According to the description of Debenay et al. (1998), this morphotype is biconvex and trochospiral, with about 10 chambers in the last whorl. The umbilical ornamentation consists of granules, ridges or shallow spines (lamellar thickenings), and moderate to heavily feathered sutures. Feathering usually runs through the entire suture, from side to side of the shell. Ridges along chamber sutures and deep interlocular spaces in the umbilical area build the shell ornamentation. Adult specimens usually display a large umbilical plug, but in some specimens the umbilical area is occupied by a columellar infilling (see pl. I, fig. 3 in Debenay et al., 1998). The wall of adult chambers is thick, with large pores.

This morphotype is found in many different habitats. According to literature, it mostly prefers an epiphytic suspension-feeder life style, both on seagrass leaves or on calcareous algae (Debenay et al., 1998). Jorissen (1988) observed *Ammonia* forma *beccarii* B on sandy bottoms along or in the surroundings of seagrass meadows, thriving under the influence of moderate salinity variation and in conditions of nutrient enrichment such as upwelling zones, phytoplankton blooms or well-oxygenated habitat rich in organic matter. Although these *Ammonia* prefer environments with fresh-water inputs, such as river deltas, the correlation with runoff zones is not always clear, suggesting a possible, but not proven, change in feeding strategy with the incorporation of symbiotic microalgae (Jorissen, 1988 and the references cited herein). In Jorissen et al. (2018), the species here grouped as forma *beccarii* B are ecologically considered as indifferent to opportunistic. Their functional morphology suggests motility at the sediment-water interface and temporarily screwing into stressed microenvironments to feed within organic-rich bottoms (Hottinger, 1986; Jorissen, 1999).

5.3.2. Ammonia forma tepida

There are two end-members in this morphogroup (Jorissen, 1988; Walton and Sloan, 1990), mostly differing for the shape of chambers, dimension of pores, quality of sutures and presence/absence of umbilical infillings. Both are very small, with a maximum shell diameter of 500 µm. These differences are supported by molecular analysis and considered diagnostic to separate at least two species (see Richirt et al., 2019). According to literature, there is no direct correlation between the morphology and the ecological behavior of these two end-members, which we assume thriving under equivalent environmental conditions. The *Ammonia* here indicated as forma *tepida* A is close to *Ammonia batava* (Hofker, 1951), to the *Ammonia parkinsoniana* forma *parkinsoniana* of Jorissen (1988), to *Ammonia tepida* of Debenay et al. (1998, their pl. 1, fig. 6), to *Ammonia* "*beccarii*" (Linne') forma 1 of Takata et al. (2009) and to *Ammonia parkinsoniana* in Haller et al. (2019, their fig. 2.21). We consider in this group also the small, poorly ornamented morphotypes included by Hayward et al. (2019) into the *beccarii* cluster as *A. falsobeccarii*. This morphotype shows a slightly flat morphology; mostly flat dorsal side, a distinct umbilical plug, acute adaxial termination of chambers and lack of suture feathering and dorsal ornamentation (see also Jorissen, 1988). The chamber wall is usually thin or very thin, with small to medium pores.

The *Ammonia* here indicated as forma *tepida* B corresponds to what figured as *Ammonia beccarii* forma *tepida* in Walton and Sloan (1990), *Ammonia parkinsoniana* forma *tepida* in Jorissen (1988) and as *Ammonia tepida* in Dupuy et al. (2010) and Haller et al. (2019, their fig. 2.22). We comprise in this group also the small *A. langeri* in Hayward et al. (2019) and the *Ammonia* figured by Holzmann et al. (1998). Differently to forma A, in this variant the chambers of the last whorl appear slightly inflated with a rounded outline. An umbilical plug may or may not be present. Massive presence of *Ammonia* forma *tepida* indicates stressed environments with clay inputs, low-oxygen and nutrient-rich bottoms. It has been reported in transitional marine environments at shallow depth (10 m to 25 m) such as estuaries (Haller et al., 2019), but also in paralic environments such as suboxic mudflats (Thibault de Chanvalon et al., 2015), marginal marshes and brackish lagoons (Walton and Sloan, 1990; Debenay et al., 1998, Debenay et al., 2000; Debenay and Guillou, 2002; Takata et al., 2009; Dupuy et al., 2010; Melis and Covelli, 2013), and even in inland brackish lakes (Wennrich et al., 2007). Its distribution also includes inland saline-water bodies (Walton and Sloan, 1990; Almogi-Labin et al., 1992) lying very far from the sea (Wennrich et al., 2007). According to Jorissen et al. (2018), *Ammonia tepida* ecologically behaves as a second order opportunistic benthic foraminifer. Forma *tepida* shows a wide range of ecological adaptations, screwing into soft muddy sediments (Langer et al., 1989) or living attached to hydrozoan, nematode or hard substrates in estuarine areas. Teratologies indicate tolerance to environmental stress, including pollution (Jorissen, 1988; Melis and Covelli, 2013), anoxia (Koho et al., 2018) or hypersaline conditions (Almogi-Labin et al., 1992; Stouff et al., 1999). Under irradiance, this ecophenotype can incorporate a very limited number of chloroplasts (Jauffrais et al., 2016). *Ammonia* forma *tepida* feeds on nematodes, copepods and larval gastropods (Dupuy et al., 2010). Coloured tests may indicate a shallow-infaunal life style (Jorissen, 1988).

5.4. Geological setting and stratigraphy of the study sections

The *Ammonia* assemblages studied in the present paper come from Miocene rocks of different localities of the central and southern Apennines. The Apennines are a fold-and-thrust belt resulting from the eastward retreating subduction of the Adria plate beneath the European plate (Malinverno and Ryan, 1986; Doglioni, 1991; Faccenna et al., 1996). The present-day configuration is the result of the tectonic superposition of several thrust sheets made up of Meso-Cenozoic deep basin to shallow-water successions of the Adria passive margin. More than 4000 m of shallow-water carbonate rocks were deposited during the Late Triassic to Miocene (Fig. 5.2) time interval in two platform domains: the Apennine and the Apulia carbonate platforms (D'Argenio and Alvarez, 1980; Bernoulli, 2001; Bosellini, 2002, Bosellini, 2004; Frijia et al., 2015 and references therein). Shallow-water carbonate sedimentation was relatively continuous over very wide areas from the Late Triassic to the Late Cretaceous (middle Campanian), while the Paleogene of the Apennines is mostly lacking and recorded only locally by a few meters to one hundred meters of Eocene to upper Oligocene bioclastic limestones (Chiocchini et al., 1994; Brandano, 2017) in central Apennines and by the Eocene Trentinara Formation (Selli, 1962) in the southern Apennines.

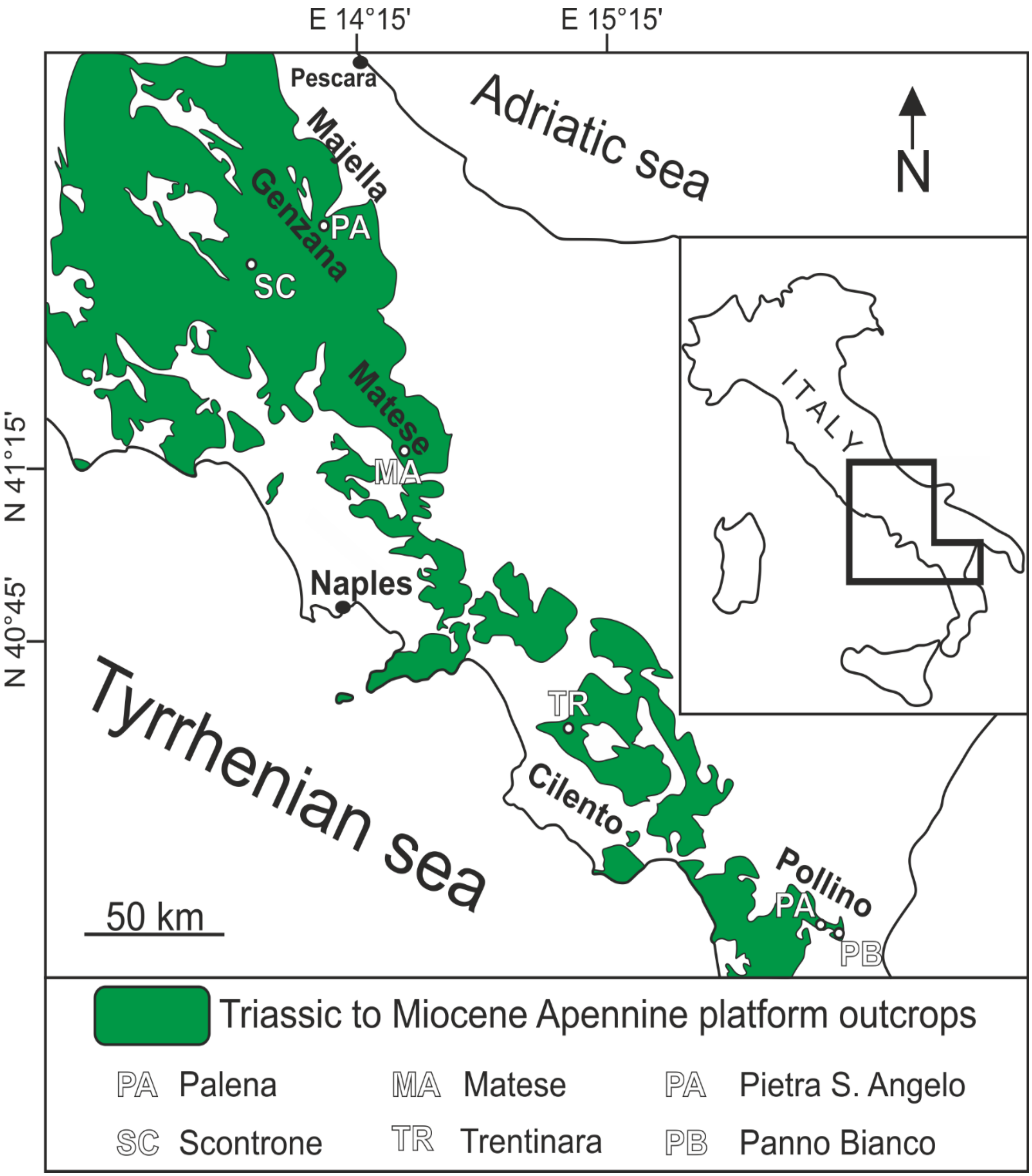

Figure 5.2. Map of the distribution of the Triassic to Miocene platform carbonates of the central and southern Apennines with the indication of the sampled localities.

During the Miocene eastward migration of the accretionary wedge, the Apennine foreland underwent bending, uplift, and erosion in the peripheral-bulge area, followed by flexural subsidence. The stratigraphic expression of this tectonic stage is a regional forebulge unconformity (Crampton and Allen, 1995; Cipollari and Cosentino, 1995) at the top of the pre-orogenic passive margin mega-sequence, overlaid by the first syn-orogenic carbonates of the so-called "Miocene transgression" (Selli, 1957), which record the onset of flexural subsidence (Carminati et al., 2007; Brandano e Policicchio, 2012; Sabbatino et al., 2020). In different areas, the Miocene carbonates overlie either a Cretaceous and/or an Eocene-Oligocene substrate (Selli, 1962; Chiocchini et al., 1994; Brandano et al., 2010). The Miocene carbonates are dominated by red algae, bryozoans and variable amounts of large benthic foraminifers, and are considered a typical expression of a "rhodalgal" -type carbonate factory, ("foramol" sensu lato; Simone and Carannante, 1985, Simone and Carannante, 1988; Carannante and Simone, 1996 and references therein). Shallow-water carbonate sedimentation ended in the middle Miocene by drowning of the platform below the photic zone, recorded by the Orbulina Marls of the Longano Fm in Matese Mts (Selli, 1957; Lirer et al., 2005), followed by deposition of deep-water siliciclastics and calciclastics in foredeep and wedge-top basins (Patacca and Scandone, 2007). In the southern Apennines, the Miocene carbonates overlying the forebulge unconformity are Aquitanian to Langhian in age and are represented by the Cerchiara Fm in North Calabria (Selli, 1957), by the Roccadaspide Fm in the Cilento area (Carannante et al., 1988b; A.P.A.T., Geological map 503 Vallo della Lucania, 2005), by the Calcareniti di Recommone Fm in the Sorrento Peninsula (De Blasio et al., 1981) and by the Cusano Fm in the Matese-Camposauro Mts (Selli, 1957; Carannante and Simone, 1996).

In the central Apennines, the Miocene carbonates are referred to the "Calcari a Briozoi e Litotamni" Fm (Accordi and Carbone, 1988; Civitelli and Brandano, 2005) of Aquitanian-Serravallian age (Brandano et al., 2010). In the Majella Mts and Genzana Mts (south-eastern Abruzzo), which belong to the Apulian platform domain, the Tortonian-Messinian Lithothamnion Limestone Fm (Mutti et al., 1997; Carnevale et al., 2011; Patacca et al., 2008, Patacca et al., 2013) is considered equivalent of the "Calcari a Briozoi e Litotamni" of Brandano et al. (2016) and Cornacchia et al. (2017). The diachronous age of the Miocene transgressive shallow-water carbonates, which become younger toward the northeast, is considered to be the effect of the progressive flexural subsidence following the Apennine orogenic wedge migration (Doglioni, 1991; Sabbatino et al., 2020). In this paper we have studied the facies and the foraminiferal assemblages of the basal levels of the Miocene transgression in four different areas, from the Mt Pollino massif in northern Calabria, to the Cilento promontory and the Matese massif in Campania, and to the Majella and Genzana Mts of Abruzzo (Fig. 5.2).

5.4.1. North Calabria, Cerchiara Formation

The samples containing *Ammonia* from the Pollino massif belong to the Cerchiara Fm. These deposits are Aquitanian-Burdigalian in age (Selli, 1957). We sampled two outcrops at Pietra S. Angelo, near the San Lorenzo Bellizzi village and Panno Bianco, near Cerchiara di Calabria (indicated respectively as PA and PB, in Fig. 5.2). The Cerchiara Fm is part of the Alburno-Cervati-Pollino tectonic unit and consists of bio-lithoclastic grainstone-packstone with bivalve shells and fragments, echinoids, bryozoans, and red algae. In the Pollino area these rocks rest on the Eocene substrate of the Trentinara Fm. In the Pietra S. Angelo section the studied samples have been collected from the basal levels of the formation, between an oyster bank with shells in life-position and a caliche level (Fig. 5.3). In the Panno Bianco section, the samples with Ammonia have been collected just above the contact between the Cerchiara Fm and the underlying Eocene Trentinara Fm (Fig. 5.3).

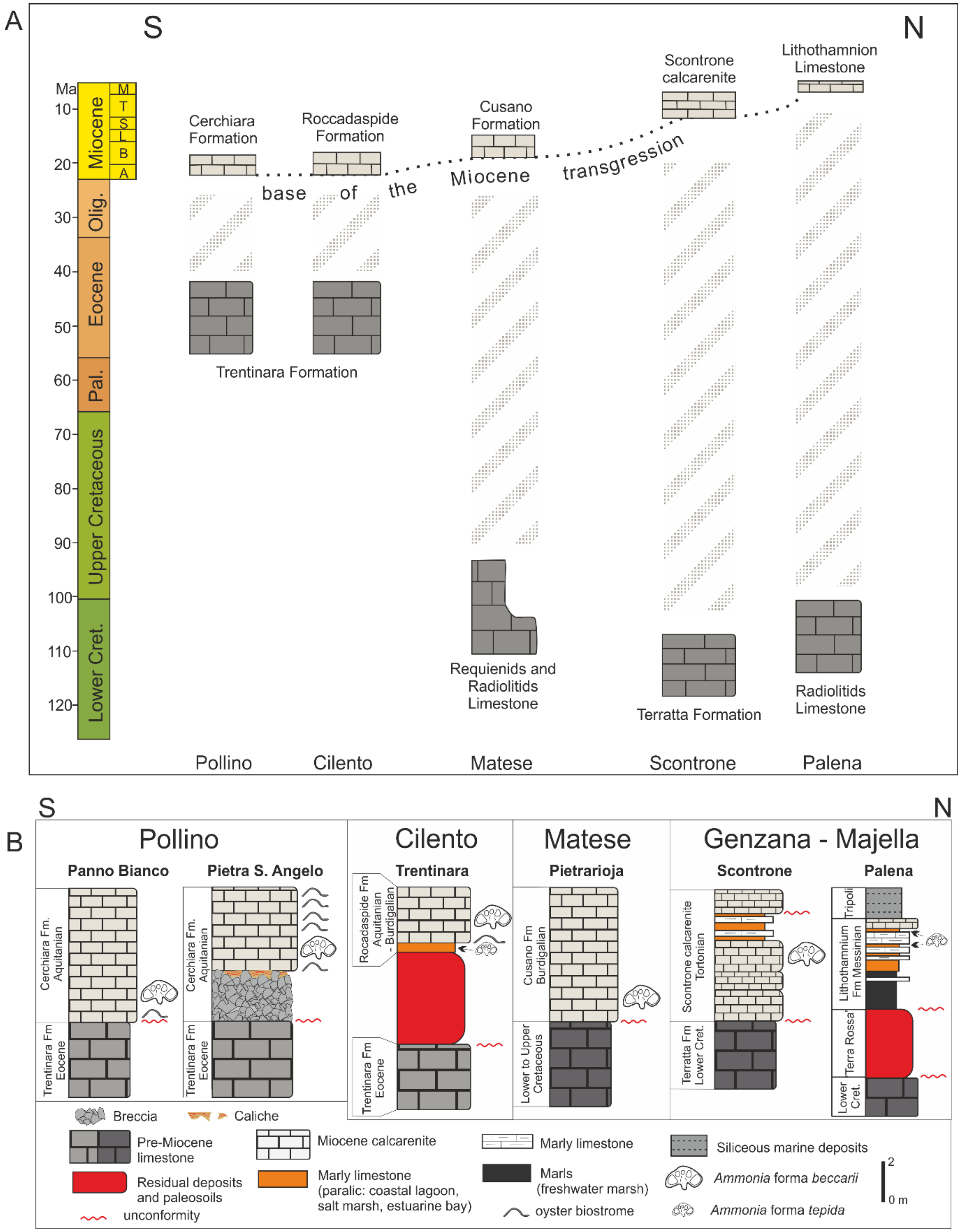

Figure 5.3. Stratigraphic information. A. Chronostratigraphic diagram. B. Stratigraphic logs of the sampled localities; age of Miocene refer to the base of the successions. The Palena log has been redrawn after Carnevale et al. (2011), the Scontrone log has been modified from Patacca et al. (2013).

5.4.2. Cilento, Roccadaspide Formation

The *Ammonia*-bearing samples from the Cilento area have been collected in the basal levels of the Roccadaspide Fm (Selli, 1957) cropping out near the village of Trentinara (TR in Fig. 5.2). The Roccadaspide Fm is a glauconitic bio-lithoclastic grainstone-packstone with red algae, echinoids fragments and benthic foraminifers (Carannante et al., 1988b; Carannante and Simone, 1996). Biostratigraphy suggests a late Aquitanian (Carannante et al., 1988b) to Burdigalian age (Selli, 1957). In the Trentinara outcrop, the basal level of the Roccadaspide Fm is represented by a thin marly limestone here interpreted as deposited within a paralic environment. These rocks lie paraconformably on a paleokarstified substrate of the Eocene Trentinara Fm, with the interposition of lenses of residual clays, which are also present in other localities of the Cilento area (Boni, 1974; Boni et al., 1978). In other outcrops (e.g., Roccadaspide village) the contact between the Roccadaspide Fm and the Eocene Trentinara Fm is marked by levels of *Microcodium* and rhizocretions, and by lenses of grey clays with fresh-water ostracods and cerithid gastropods (Carannante et al., 1988b). The depositional environment of the Roccadaspide Fm, has been interpreted as evolving from transitional paralic to open-marine shelf conditions (Carannante et al., 1988b).

5.4.3. Matese mountains, Cusano Formation

The *Ammonia* assemblages from the Matese Mts come from the basal levels of the Cusano Fm. This formation is Burdigalian-Langhian in age and consists mainly of floatstone-rudstone with red algae and bryozoans (Carannante and Simone, 1996; Bassi et al., 2010; Sabbatino et al., 2020). The Cusano Fm is overlain by the Serravallian-Tortonian hemipelagic marly limestones and marls of the Longano Fm (also known as the *Orbulina* marls; Lirer et al., 2005). The contact is marked by a m-thick phosphatic hardground (Carannante, 1982). In the Pietraroja sections, the Cusano Fm was deposited in an open-marine channelized carbonate shelf setting (Carannante and

Vigorito, 2001; Vigorito et al., 2005). The samples with *Ammonia* studied in the present paper come from two different outcrops: i) the basal levels of the Cusano Fm in the Regia Piana section and ii) and a level at about 5 m from the base of the formation in the Pietraroja section (MA in Fig. 5.2). In both these localities, the contact between the Miocene Cusano Fm and the Cretaceous substrate is represented by a stylolitic surface (see figs 5a and 6a in Sabbatino et al., 2020).

5.4.4. Scontrone and Palena (Abruzzo), Lithothamnion Limestone

The samples with *Ammonia* from the eastern side of central Apennines belong to the Tortonian-Messinian deposits cropping out in Scontrone and Palena (SC and PA in Fig. 5.2). The sedimentological and paleontological features of the continental to transitional marine successions exposed in these localities have been studied in detail by Carboni et al. (1992), Carnevale et al. (2011) and Patacca et al., 2008, Patacca et al., 2013. We refer to these papers for an accurate description of the vertical evolution of facies and for biostratigraphy. The upper Miocene deposits of Scontrone belong to the structurally complex Gran Sasso-Genzana tectonic unit (Patacca et al., 2008) and crop out along its southernmost edge. The studied samples come from the "Scontrone Calcarenite", which is the basal interval of the "*Lithothamnion* Limestone" in the 'Scontrone south' section of Patacca et al. (2013). More precisely they have been collected from "level d", at the top of the "Scontrone calcarenites", just below the surface with root traces and rizhocretions (see fig. 5 in Patacca et al., 2013). The microfacies of these samples show a well-sorted bioclastic calcarenite with echinoids fragments (Fig. 5.4G), which was interpreted by Patacca et al. (2008) as deposited under the action of coastal currents in a paralic environment. The "Scontrone calcarenite" has been indirectly dated as Tortonian in age (see discussion in Patacca et al., 2013).

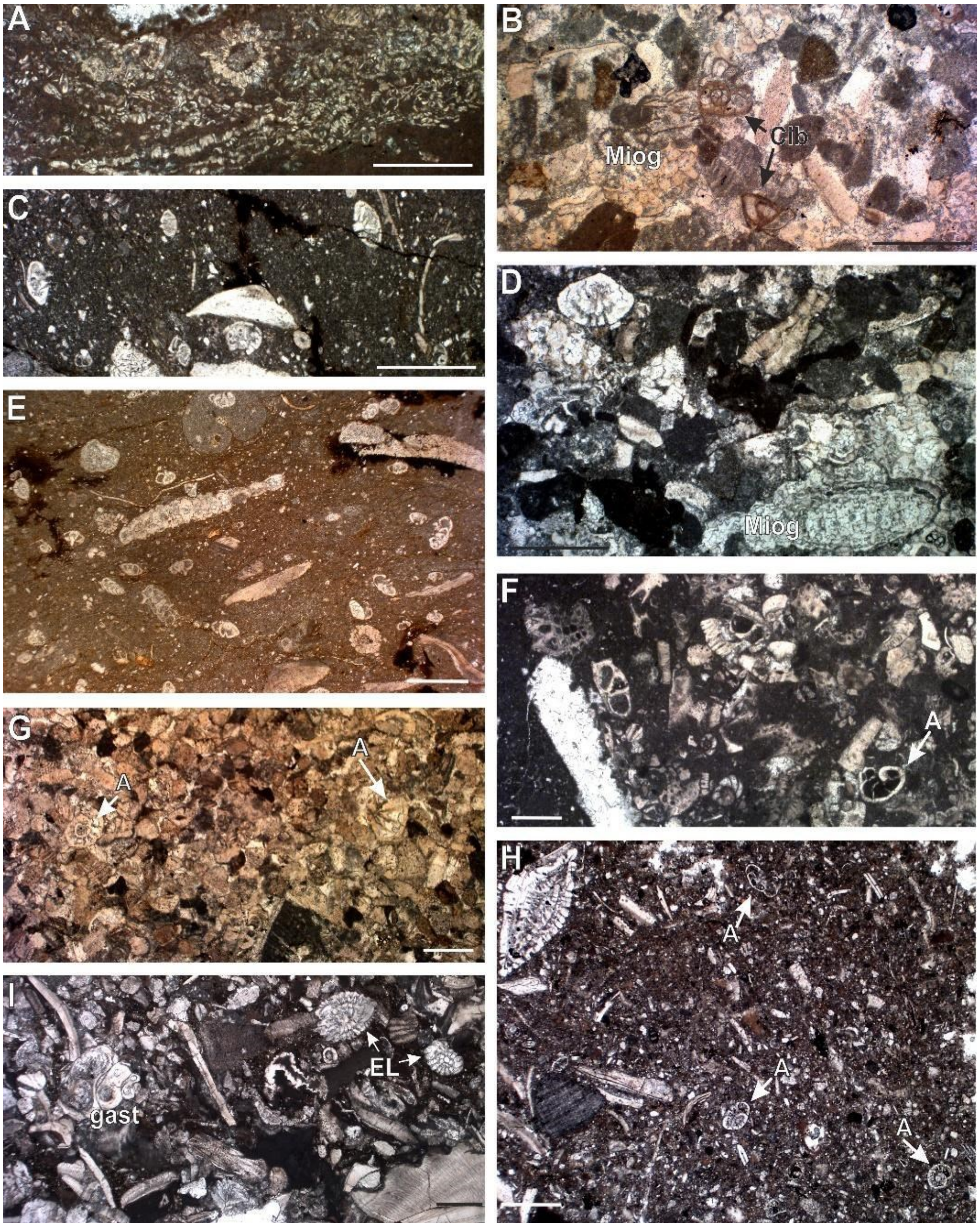

Figure 5.4. Microfacies of the basal levels of the Miocene transgressive deposits. All scale bars are 0.5 mm. A. *Microcodium* calcite aggregates and alveolar texture within a caliche crust. Calabria, Pietra S. Angelo section. B. Calcarenite with *Cibicides* sp. (Cib) and *Miogypsina* fragments (Miog). Calabria, Panno Bianco section. C, E. Coastal lagoon wackestone with *Ammonia* forma *tepida* along with oyster fragments and echinoid spines. Cilento, Trentinara section. D. *Miogyspina*-rich calcarenite with *Ammonia* forma *beccarii*. Cilento, Trentinara section. F. Bioclastic packstone with *Ammonia*. Matese, Pietraroja section. G. Scontrone calcarenite with *Ammonia* forma *beccarii* (A). H. Estuarine deposits from the Palena section with *Elphidium* and *Ammonia* forma *tepida* (A). I. Packstone with marly matrix rich in echinoderm and bivalve fragments. Note the presence of *Elphidium* (EL) and gastropods (Gast). Palena; bioclastic calcarenite with marly matrix above the estuarine level.

The Miocene deposits of Palena lie on a karstified Cretaceous substrate (Fig. 5.3) of the Porrara tectonic unit (Carboni et al., 1992; Carnevale et al., 2011). The *Ammonia*-bearing samples studied for the present paper have been collected from the lower part of the *Lithothamnion* Limestone Fm, in a marly bed labelled c3 in Carnevale et al. (2011; fig. 1 of "The Capo di Fiume Stratigraphic Section" chapter) and in the marly limestone resting above it. The microfacies of the c3 marly bed is a bioclastic wackestone with bivalve fragments, *Elphidium* sp. and few glauconite grains. It has been interpreted by Carnevale et al. (2011) as deposited in a restricted coastal bay under the effect of estuarine currents. The microfacies of the marly limestone overlying the c3 marly bed is a bioclastic packstone rich in bivalve fragments, gastropods and sparse, well preserved *Cibicides* and *Elphidium* (Figs. 4I and 5F). This level has been interpreted by Carnevale et al. (2011) as deposited in more open marine conditions. The fossil vertebrate fauna, the fossil flora and the benthic foraminifers of Palena point out to a Messinian age (Carboni et al., 1992; Carnevale et al., 2011).

5.5. Material and methods

An extensive field sampling has been carried out along the Apennine backbone, from the Pollino massif in northern Calabria to the Majella Mts in Abruzzo. From south to north the localities reported in this work are: Panno Bianco (Pollino; coordinates: 39°51'02″N 16°22'17″E); Pietra Sant'Angelo (Pollino; coordinates: 39°52'31″N 16°21'03″E); Trentinara (Cilento; coordinates: 40°24'38.59″N 15°06'12.78″E); Pietraroja (Matese; coordinates: 41°20'59″N 14°33'08″E); Regia Piana (Matese; coordinates: 41°21'46″N 14°32'09″E); Scontrone (coordinates: 41°44'28.3"N 14°02'22.1"E) and Palena (Majella; coordinates: 41°57'50"N 14°07'12 "E). In each of these localities a short succession has been logged across the unconformity separating the Cretaceous or Eocene substrate from the Miocene transgressive deposits (Fig. 5.3). Sixty-five carbonate samples have been collected from the lowermost levels of the Miocene shallow-water transgressive sequence, from which 53 thin sections have been obtained. A total of 345 specimens of *Ammonia* have been studied under the optical microscope in random and oriented sections. In particular, following Ujiié (1965), Billmann et al. (1980) and Hottinger, 2006, Hottinger, 2014, we relied on shell diameter, thickness of the wall, presence/absence of feathered sutures or umbilical plug to define the architecture of Ammonia morphotypes studied in thin sections. Serial acetate peels have been produced from the Scontrone and Trentinara samples in order to better define the umbilical ornamentation and the presence of tooth-plate.

5.6. Results

5.6.1. Pollino Massif

Specimens of *Ammonia* forma *beccarii* with relatively thick chamber wall, slightly angular chamber profile, pronounced umbilical plug and deep umbilical interlocular spaces occur in the lowermost levels of the Cerchiara Fm (Fig. 5.3). At Pietra S. Angelo, thick-shelled specimens of *Ammonia*, with a test diameter ranging between 0.3 mm and 0.4 mm, are found in bioclastic packstones occurring just above a 2m-thick brecciated interval capped by a caliche level with *Microcodium*, fecal pellets and alveolar texture ("beta microfabric" of Wright and Tucker, 1991; Alonso-Zarza and Wright, 2010; Fig. 5.3, 4A). *Ammonia* specimens have been here observed in the micritic matrix of dense accumulations of oyster and balanid shells occurring at the base of the Cerchiara Fm, just above the caliche level. At Panno Bianco the *Ammonia*-bearing facies is represented by a well-sorted bioclastic packstone. Abraded specimens of *Ammonia* forma *beccarii* A, with a thin surficial coating of iron oxydes, have been found at 5 m from the oyster bank at the base of the formation, together with rounded red algae and oyster fragments, echinoids, miogypsinids, and planorbulinids (Fig. 5.4B), and large to small reworked clasts of the underlying Trentinara Fm. The deposit also contains numerous well-preserved specimens of the foraminifer *Cibicides* sp. (Figs. 5.4B, 5.5B-D).

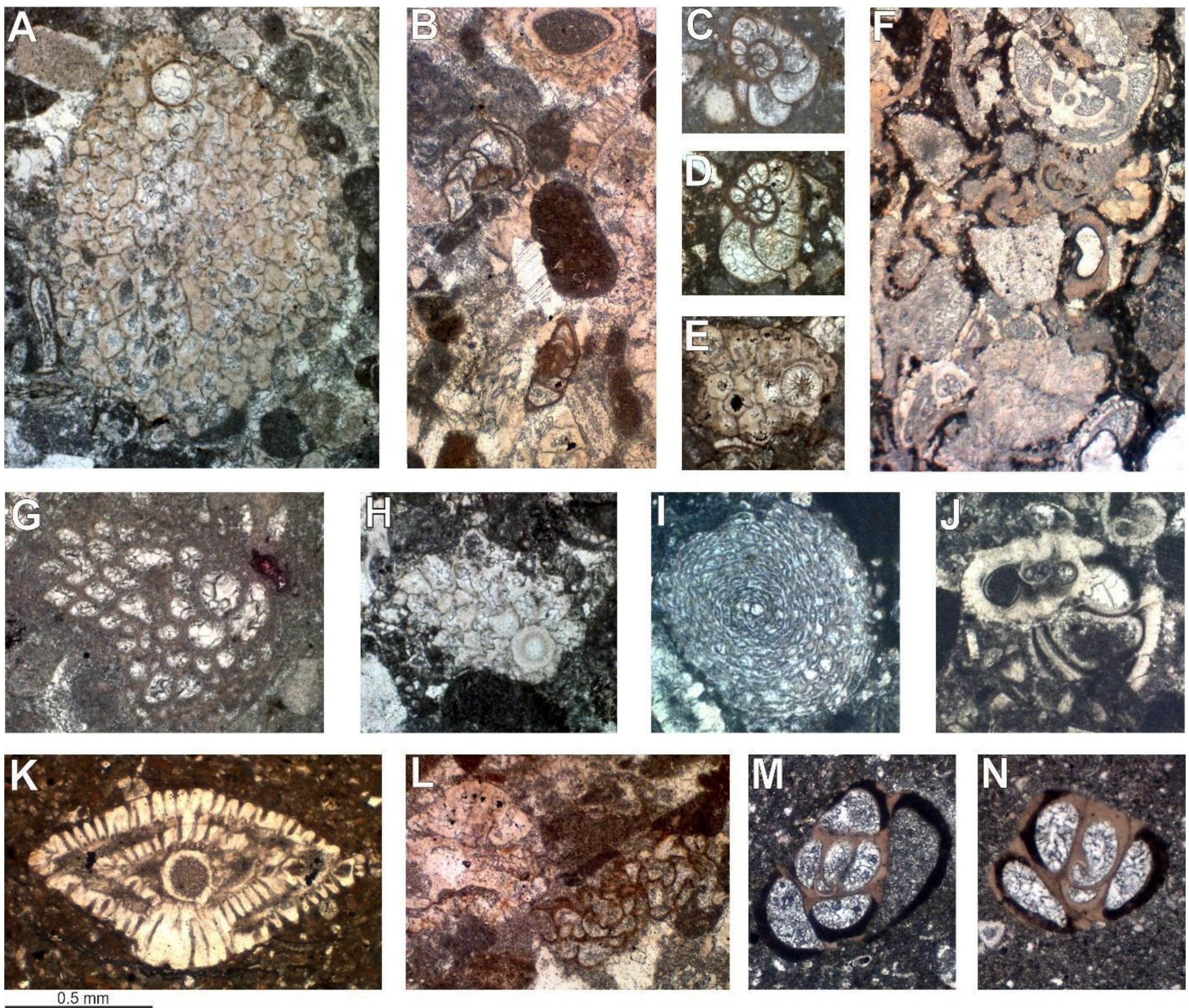

Figure 5.5. Associated fauna. Scale bar is 0.5 mm. A. *Miogypsina* cf. *globulina*. Pollino Mt., Panno Bianco section. B, C, D. *Cibicides* sp. Pollino Mt, Panno Bianco section. E, G, H. *Miogypsina* cf. *globulina*. Cilento, Trentinara section. F. *Cibicides* sp., Majella Mt, Palena section (acetate peel). I. *Sphaerogypsina globulus*. Matese, Regia Piana section. J. *Mississippina* sp. Matese, Regia Piana section. K. *Elphidium* sp. Majella Mt, Palena section. L. *Planorbulina* and *Ammonia*. Pollino, Panno Bianco section. M, N. Miliolids. Trentinara paralic level.

The sedimentological characters of both outcrops point out to a very proximal sector of the Miocene carbonate platform of the Cerchiara Fm. The occurrence of a caliche with *Microcodium* at Pietra S. Angelo witnesses subaerial conditions and a probable colonization of the substrate by land plants, followed by marine flooding during the transgression, recorded by the occurrence of a thick oyster bank. At Panno Bianco, the occurrence of marine facies at the base of the Cerchiara Fm and the presence of reworked clasts of the substrate (Trentinara Fm.), suggest an environment slightly deeper than at the Pietra S. Angelo. The occurrence of epiphytic planorbulinids and *Cibicides* suggests the presence of seagrass meadows (Langer, 1993). Specimens of *Miogypsina* cf. *globulina* have been found at Panno Bianco (Fig. 5.5A), pointing to an upper Aquitanian to lower Burdigalian age (Cahuzac and Poignant, 1997).

5.6.2. Cilento

Numerous *Ammonia* forma *tepida*, represented by both A and B end-members (Fig. 5.4C, E; Fig. 5.6), occur at the base of the Roccadaspide Fm (Trentinara section, Fig. 5.3) in a thin marly limestone bed. The *Ammonia* recovered within such level are small, with a shell diameter ranging from 0.2 mm to 0.4 mm, without dorsal ornamentation. Most specimens are composed by 2 whorls of chambers and display a clear umbilical plug. The microfacies is a slightly argillaceous bioclastic wackestone to floatstone with an oligotypic foraminiferal assemblage dominated by Ammonia and miliolids (Fig. 5.5M, N), associated to *Nonion* (Fig. 5.6P) and seriate hyaline forms (Fig. 5.4E). The microfacies contains also ostracods with articulated valves (Fig. 5.6R), few reworked fragments of miogypsinids, oyster and balanid fragments, echinoderm spines and thin unidentified bioclasts.

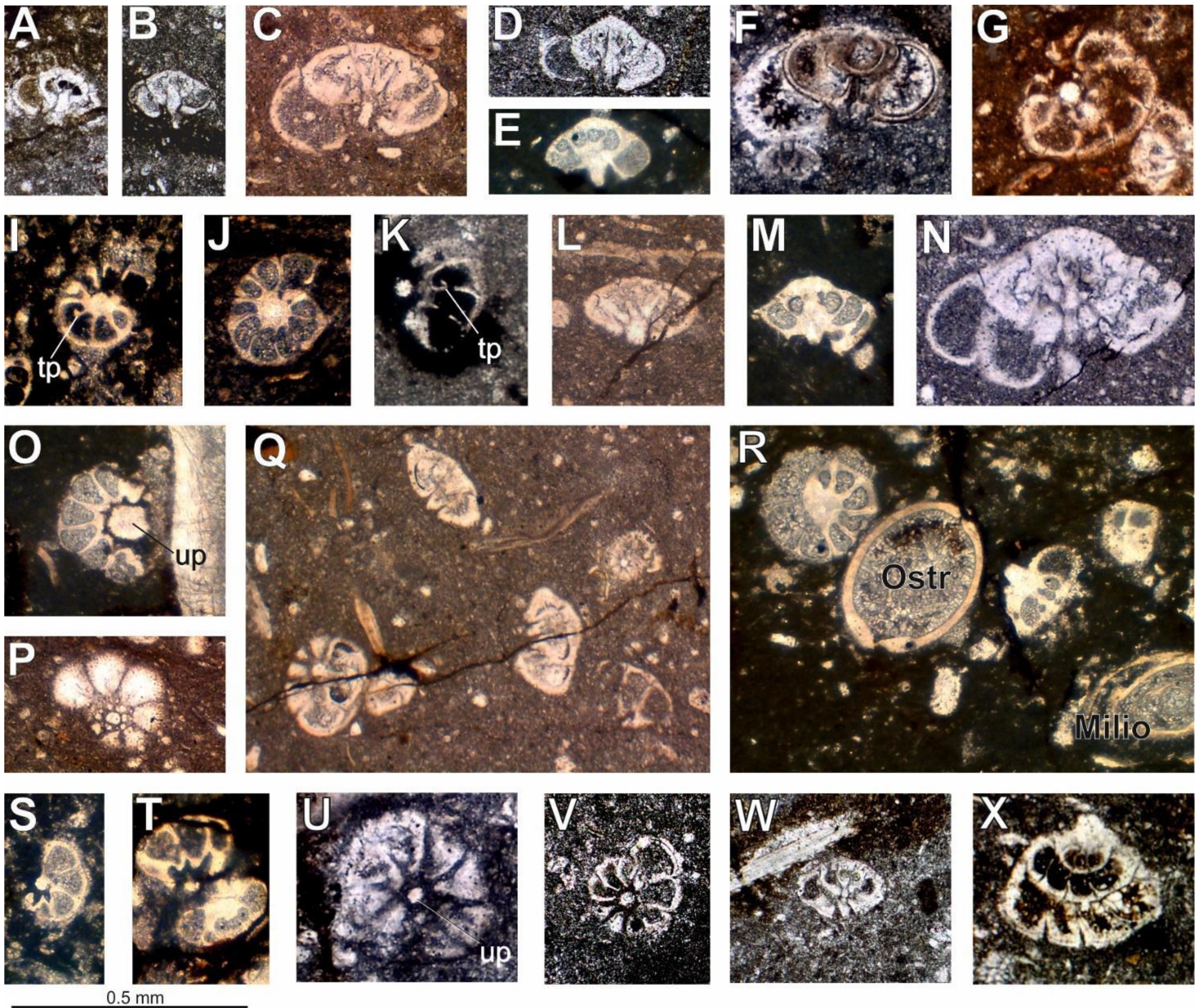

Figure 5.6. *Ammonia* forma *tepida* from Trentinara paralic deposit. Scale bar is 0.5 mm. E, I, J, M, O, R, S, T from acetate peels, all the other from thin sections. A-F, L, M, W. Axial and subaxial sections. G-J, O, S-W. Transverse basal and oblique sections. P. *Nonion* sp. N, Q, X. Oblique sections. Note in I and K the tooth plate. tp: tooth plate; up: umbilical plug; Ostr: ostacod; Milio: miliolid shell.

The marly limestone with *Ammonia* forma *tepida* directly overlies a thick level of residual clays (Boni, 1974; Boni et al., 1978) and is sporadically incrusted by ostreids in living position. The substrate of the residual clays is represented by the limestones of the Trentinara Fm, which are locally bioeroded by lithophagous organisms. Overall, the sedimentological features and the fossil assemblage shown by the tepida-rich level point out to a low-energy coastal lagoon with a probably estuarine circulation (Inden and Moore, 1983; Guelorget and Perthuisot, 1983). The marly limestone is overlain by a bioclastic calcarenite with abundant *Miogypsina* cf. *globulina*, echinoids, reworked *Microcodium* and red algae fragments. This calcarenite contains thick-shelled *Ammonia* forma *beccarii* (Fig. 5.4D). These deposits indicate an open marine carbonate environment (Carannante et al., 1988b; Carannante and Simone, 1996). The presence of *Miogypsina* cf. *globulina* (Fig. 5.5G, H) supports an upper Aquitanian to lower Burdigalian age (Cahuzac and Poignant, 1997) for the base of the Roccadaspide Fm in the Trentinara section.

5.6.3. Matese

The *Ammonia* specimens found at the base of the Cusano Fm in the Matese area are relatively small, with a shell diameter ranging from 0.3 mm to 0.5 mm. The umbilical plug is relatively big; the periphery of the shell is slightly acute, whereas the whole shell thickness is comparatively high. Based on these parameters, we consider these specimens under the forma *beccarii* A. In the Pietraroja section, *Ammonia* is found at 5 m from the base of the Miocene deposits, within a red algae and bryozoan floatstone with a fine-grained matrix. In the Regia Piana section *Ammonia* is found in the basal levels of the Cusano Fm, overlying the Cretaceous (probably Coniacian) bedrock. The Miocene carbonates of the Cusano Fm in the Matese Mts are characterized by typical foramol grain associations (Simone and Carannante, 1988; Carannate and Simone, 1996). The most common components are red algae, bryozoans, oysters, pectinids, large echinoderm fragments, serpulids, and foraminifers such as *Elphidium* sp., *Sphaerogypsina globulus* (Fig. 5.5I), *Amphistegina* sp., *Operculina* sp., *Mississipina* sp., *Cibicides* sp. and globigerinids (see also Bassi et al., 2010; Carannante, 1982, Carannante et al., 1988a, Carannante and Simone, 1996). This biotic association suggests more open marine and higher water depth than in Cilento and Pollino. The presence of re-sedimented bioclasts suggests repeated re-working events from more proximal to deeper environments, as confirmed by Bassi et al. (2010). The Cusano Fm has been considered as late Burdigalian to early Langhian in age (Barbera et al., 1980; Schiavinotto, 1985; Carannante and Simone, 1996). A middle Burdigalian age (18.7±0.2 Ma) has been obtained by strontium isotope stratigraphy for the basal levels of the Cusano Fm in the Pietraroja and Regia Piana sections (Sabbatino et al., 2020)

5.6.4. Majella

The *Ammonia* specimens found in the samples of the Palena section are small to very small, frequently less than 0.3 mm in diameter (Fig. 5.7). Very few specimens display a marked umbilical plug and a thicker chamber wall. The whole assemblage is dominated by specimens with thin chamber wall, which can be placed into the *Ammonia* forma *tepida* group. The microfacies shows the occurrence of sparse specimens of Ammonia in a muddy matrix rich in bivalve (*Corbula gibba*) fragments together with few and relatively less fragmented *Elphidium* sp., bryozoan remains and few sparse glauconite grains (Fig. 5.4H). Most of the Palena specimens can be assigned to the B variant of the forma *tepida*. The occurrence of *Ammonia* at Palena was also mentioned by Carboni et al. (1992), as *Ammonia beccarii*. The association studied in this work comes from the marly bed in the *Litothamnium* Fm equivalent labelled as c3 in Carnevale et al. (2011; fig. 1 of "The Capo di Fiume Stratigraphic Section" chapter). This level has been referred to a paralic environment, interpreted as a proximal estuarine bay (Carnevale et al., 2011). The marly calcarenite resting above the c3 marly bed (Fig. 5.3) has also been analysed. The microfacies is rich in bivalve and gastropod fragments. The benthic foraminiferal assemblage is dominated by *Cibidices* sp. and *Elphidium* sp., which are most probably epiphytic species (Langer, 1993), along with sparse porcelaneous taxa (Figs. 5.4I; 5.5F). We interpret this calcarenite as deposited in a restricted marine environment, with probably vegetated bottom, adjacent to the estuarine bay. A Messinian age has been assigned to the Palena succession (Carboni et al., 1992).

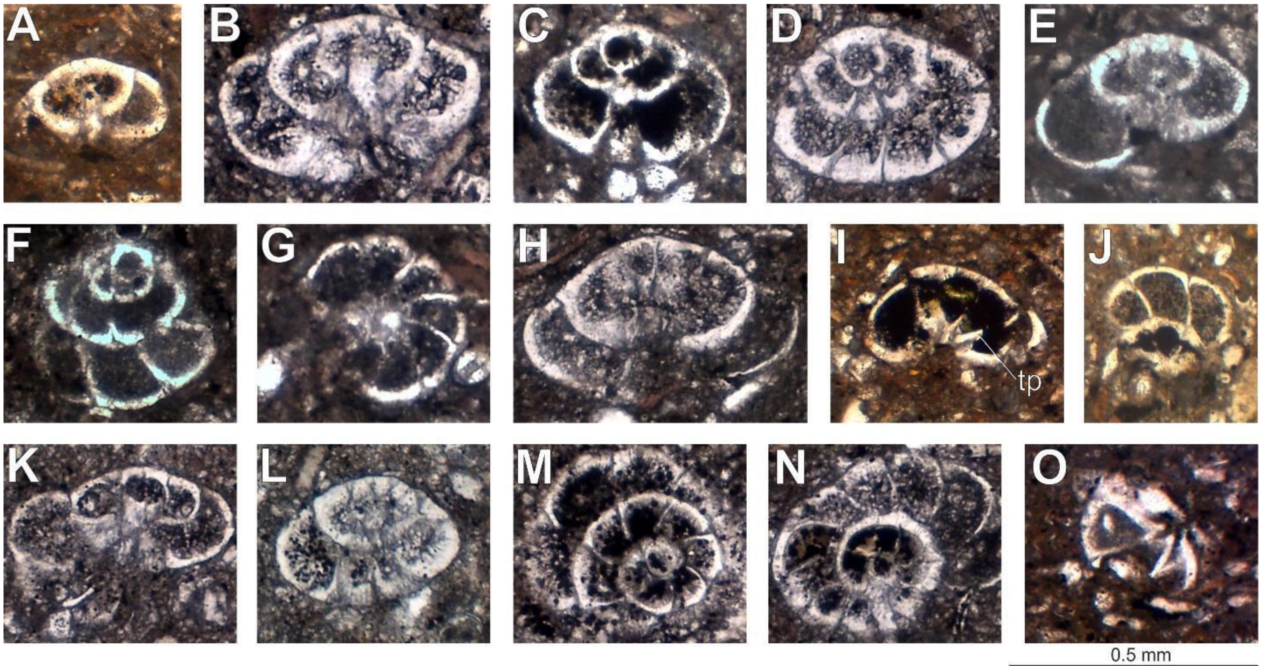

Figure 5.7. *Ammonia* forma *tepida* from Palena paralic deposit. Scale bar is 0.5 mm. A, B, C, E, H, K. Axial and subaxial sections. D, F. Oblique centred sections. I, J, L, O. Oblique sections. G, M, N. Transverse sections. tp: tooth-plate.

5.6.5. Genzana Mts, Scontrone

The *Ammonia* association recovered in the "Scontrone calcarenite" at Scontrone consists of very abundant, big (shell diameter up to >1 mm), thick-shelled and heavily ornamented specimens with deep and ornamented umbilical sutures (Fig. 5.8). These specimens can be assigned to the *Ammonia* forma *beccarii* B and are fully comparable with the living representative of this morphogroup, based on the large diameter (commonly comprised between 0.5 mm and 1.1 mm) and heavy umbilical ornamentation with feathered sutures. The shell wall is comparatively thick, around 0.08 mm, and its periphery is well rounded. In the microfacies, *Ammonia* occurs together with echinoderm fragments, *Elphidium* sp. and *Cibicides* sp. and few porcelaneous foraminifers (Fig. 5.4G). The *Ammonia* shells have been probably transported in the coastal tidal flat, which was the site of deposition of the calcarenite, from a lagoon or a tidal inlet, as pointed out by Patacca et al. (2008). Patacca et al. (2008 pl. 1, fig. b; 2013 fig. 7a) figured forma *beccarii* B in association with porcelaneous and agglutinated serial benthic foraminifera within an analogous coastal barrier level (level a) of the "Scontrone calcarenite". Patacca et al., 2008, Patacca et al., 2013 assigned the age of these deposits to the Tortonian.

5.7. Discussion

Ammonia is a quite common component of shallow marine Miocene-Pleistocene deposits and has been reported from many localities with a wide geographic distribution (see table 5.1). In Europe, Van der Zwaan (1982) reported *Ammonia* forma *tepida* from the Messinian of Crete; Poignant (1997) cited *Ammonia* in the lower Miocene of the Aquitaine basin; Báldi and Hohenegger (2008) refers to *Ammonia* gr. *beccarii* from the Middle Miocene of Vienna basin; Filipescu et al. (2011) collected *Ammonia* from the Miocene of Romania. In America, Ammonia has been figured from the Miocene of California (Patterson, 1987); Costa Rica (Sen Gupta et al., 1986) and Amazonia (Boonstra et al., 2015), among other localities. In Africa *Ammonia* is reported from the Miocene of Morocco to Madagascar (Ramihangihajason et al., 2014; Amakrane et al., 2016, among others), while in the Middle East Roozpeykar and Moghaddam (2016) figured an oligotypic assemblage, probably referable to *Ammonia* forma *tepida*, in the Aquitanian-Burdigalian of the Asmari Fm in Iran. In Asia there are records of *Ammonia* from the Miocene of Japan (Ujiié, 1965; Hasegawa and Takahashi, 1992) and Borneo (Billmann et al., 1980; Roslim et al., 2019), among other localities. In the Miocene of Italy, Patacca et al. (2013) recognized *Ammonia beccarii* in the 'Scontrone calcarenite', whereas Danese (1999) figured an *Ammonia* from the upper Miocene reef deposits of Guado di Coccia, in the southern Majella. *Ammonia* has also been mentioned by Carboni et al. (1992) at Palena. However, none of these papers investigated in detail the ecological distribution during the Miocene neither discussed if it conforms to the distribution of living representatives of the genus (see Tab. 5.2).

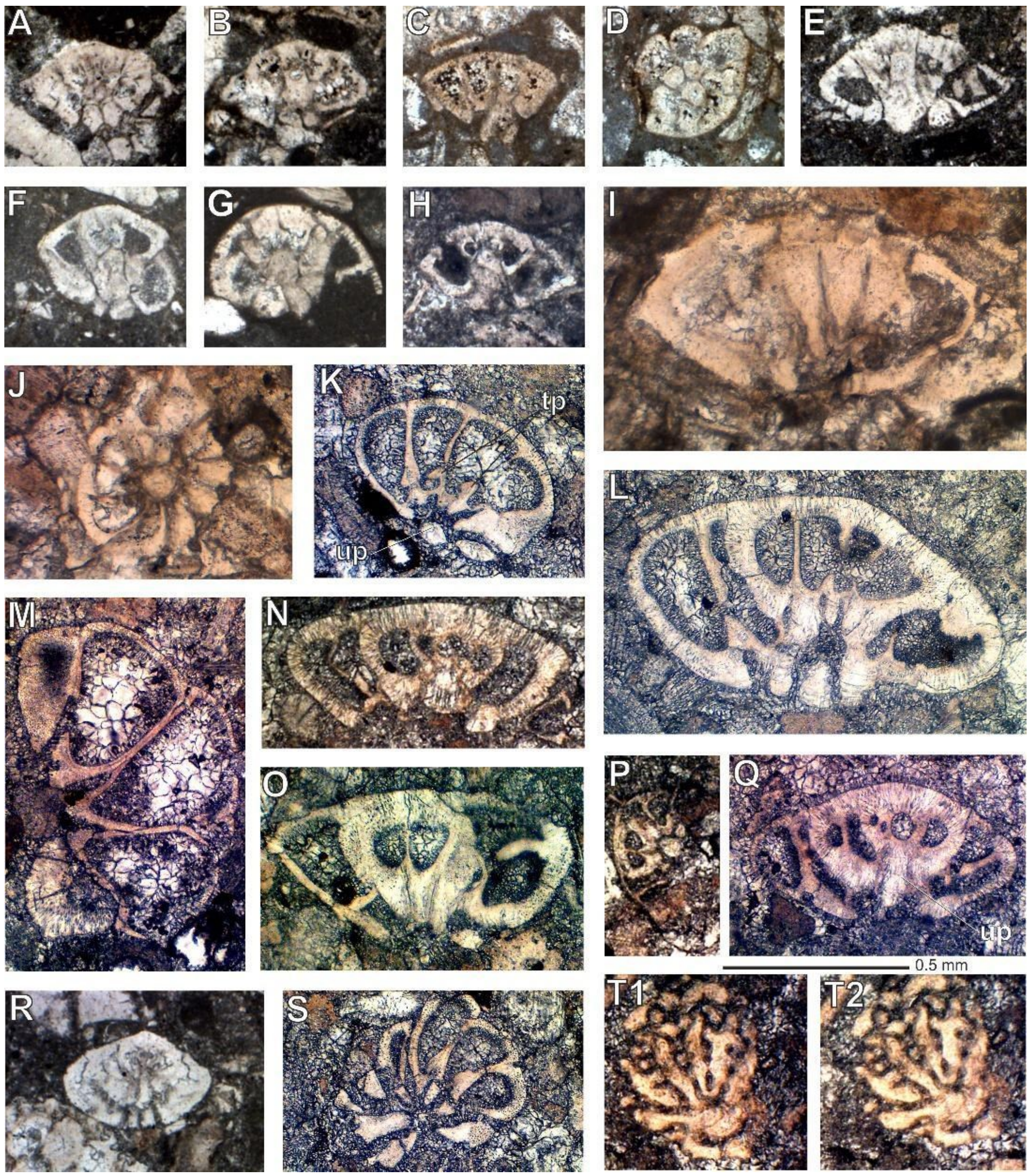

Figure 5.8. Ammonia forma beccarii. Scale bar is 0.5 mm. K-Q, S, T1, T2 are acetate peels, all the others are from thin sections. A-D. Oblique sections. Pietra S. Angelo. E-G. Oblique sections. Panno Bianco. H. Axial section. Matese. I-Q. Specimens from Scontrone. J, K, P, S. Transverse oblique sections. I, M, O. Tangential and oblique sections. L, N, O, Q. Axial and subaxial sections. T1, T2. Serial acetate peel sections of the same specimen, showing the umbilical feathering. tp: tooth plate; up: umbilical plug.

Table 5.1. Literature records of fossil Ammonia with reference to the morphotypes discussed in this work.

Ammonia morphotype (this work)	Geographic area	reference
Ammonia forma *tepida*	Greece	van der Zwaan (1982); pl. 1
Ammonia forma *tepida*	SW France	Poignant (1997); pl.4, fig. 16
Ammonia forma *tepida*	Romania	Filipescu et al. (2011), figs. 6.1-4
Ammonia forma *beccarii*	West USA	Patterson (1987), pl.1, figs. 1,2
Ammonia forma *tepida*	Costa Rica	Sen Gupta et al. (1986), fig. 3
Ammonia forma *tepida*	Amazonia (Colombia/Perú)	Boonstra et al. (2015), pl. 2
Ammonia forma *beccarii* (Lectotype of *A. beccarii*)	Italy	Vaiani et al. (2019)
Ammonia forma *beccarii*?	Madagascar	Ramihangihajason et al. (2014), fig. 4.15
Ammonia forma *beccarii*?	Morocco	Amakrane et al. (2016), fig. 5.1
Ammonia forma *tepida*	Iran	Roozpeykar and Moghaddam (2016), fig. 7E
Ammonia forma *beccarii*	Japan	Ujiié (1965), Pl. 18, 19
Ammonia forma *beccarii*	Japan	Hasegawa and Takahashi (1992), figs. 10.1-10.3
Ammonia forma *tepida*	Japan	Hasegawa and Takahashi (1992), 10.4-10.6
Ammonia forma *tepida* (Lectotype of *A. tepida*)	Puerto Rico	Hayward et al. (2003)
Ammonia forma *beccarii*	Borneo	Billmann et al. (1980), pls. 1-11
Ammonia forma *tepida*	Brunei Darussalam	Roslim et al. (2019), figs. 4.29-30
Ammonia forma *beccarii*	Italy	Patacca et al. (2008), pl. 1b; 5f Patacca et al. (2013), fig. 7a, 7c
Ammonia forma *tepida*	Italy	Patacca et al. (2008), pl. 4b. Patacca et al. (2013), fig. 11b
Ammonia forma *beccarii*	Italy	Danese (1999), pl. 10, fig. 2

Table 5.2. Ecological parameters of recent and Miocene Ammonia.

Ammonia morphotypes	Environmental and ecological parameters					
	Recent[1]			Miocene (this study)		
	Habitat	***Life style***	***Feeding strategy***	***Habitat***	***Life style***	***Feeding strategy***
Ammonia forma *beccarii* A	Coastal marine areas near to delta inlets; bottoms with intermediate proportions of organic matter	Shallow-infaunal; occasionally epifaunal or epiphytic	deposit feeder	Shallow-marine coastal settings under high-nutrient input; well-oxygenated bottoms.	Shallow-infaunal or epifaunal	Deposit feeder
	Well-oxygenated bottoms rich in organic matter. Direct fresh-water inputs	Epiphytic on seagrass leaves or calcareous algae. Epifaunal.	Suspension or deposit feeder	Vegetated bottoms of a proximal shoreface setting, under quite normal marine salinity.	Epiphytic or epifaunal in organic-rich bottoms.	Suspension or deposit feeder
Ammonia forma *tepida* A and B	Stressed paralic or estuarine environments with clay inputs, low-oxygen and nutrient-rich bottoms under metal pollution, hypersaline conditions and anoxia.	Shallow-infaunal or attached to hydrozoan, nematode or hard substrates.	Deposit feeder	Moderate to low hydrodynamic energy. Hyposaline or metahaline Organic-rich paralic estuarine bay sometimes hypersaline intervals and heavy metal pollution.	Shallow-infaunal or attac	

[1]information on the ecology of recent *Ammonia* is mainly from Jorissen (1988); Langer et al. (1989); Walton and Sloan (1990); Debenay et al. (1998); Stouff et al. (1999); Murray (2006); Dupuy et al. (2010); Hayward et al. (2019). See text for a more complete list of relevant papers.

5.7.1. Paleoenvironmental distribution of Miocene Ammonia forma tepida

Ecophenotypes referable to *Ammonia* forma tepida reported in this work have been found in paralic facies both at Trentinara (Cilento) and at Palena (Majella). The *Ammonia* and miliolid of Trentinara can be interpreted as in-situ components, since they are well preserved and are found in a low-energy mud-supported texture, with no evidence of sedimentary reworking. The occurrence of articulated ostracod valves further supports moderate to low hydrodynamic energy. The dominance of *Ammonia* forma tepida and miliolids (Fig. 5.4C, E) suggests the occurrence of non-normal marine waters. Miliolids supports the regular influx of marine waters, but they may thrive in hypersaline (Murray, 2006) or metahaline (Haig et al., 2020) conditions. Restricted marine environments, characterized by mud-supported textures with dominance of miliolid and small lamellar hyaline foraminifers are commonly identified in Mesozoic and Cenozoic carbonate platforms (e.g., facies with *Discorbidae* and *Miliolidae* of Chiocchini et al., 1994, Chiocchini et al., 2012; Mossadegh et al., 2009). Salinity fluctuations are expected in the Trentinara coastal lagoon, as they are commonly recorded in other fossil (Flügel, 2004; Haig et al., 2020) and recent (Debenay et al., 2000, Debenay et al., 2001; Melis and Covelli, 2013) marginal marine environments. The salinity gradient in coastal lagoons or proximal marine environments depends on fresh water input and tidal regime, with conditions that may range from brackish to hypersaline, depending on climate (Murray, 2006; Mossadegh et al., 2009). Salinity variations could have been influenced by seasonality, but the lack of evaporitic minerals and the absence of shells with teratological morphological aberrations allow us to exclude persistent high evaporation rates and highly hypersaline conditions (Almogi-Labin et al., 1992; Debenay et al., 2001; Carboni et al., 2009). In the Trentinara section, the paralic deposits rest unconformably on a thick lens of residual clays, whose erosion and discharge into the coastal lagoon where the *Ammonia* thrived could have caused i) heavy metal pollution and ii) increased amount of suspended material, adding a further factor of ecological stress (Melis and Covelli, 2013). Summing up, the sedimentological and paleontological evidence suggests that the Ammonia forma tepida populations found at the base of the Trentinara Fm thrived mostly in a hyposaline brackish paralic coastal lagoon influenced by some hypersaline intervals, i.e. they lived under ecological conditions comparable to their recent counterparts (Debenay et al., 1998, Debenay et al., 2001; Debenay and Guillou, 2002; Murray, 2006; Wennrich et al., 2007; Takata et al., 2009; Dupuy et al., 2010, among others). The same indication is given by the dominance of *Ammonia* tepida with brackish or lacustrine ostracods in the distinctive Messinian "Lago–Mare" facies of the Mediterranean (van de Poel, 1992; Pierre et al., 2006). The overlying calcarenite beds containing *Miogypsina*, red algae, bryozoans and *Ammonia* forma beccarii indicate the onset of normal marine conditions, likely with vegetated bottoms. Small *Ammonia* forma *tepida* (roughly 0.3 mm in shell diameter) are figured by Patacca et al. (2013; fig 10C) into a 'Lago-Mare' brackish-water lagoon of the Scontrone calcarenite, suggesting a parallelism to what we have observed at the base of the Trentinara Fm. The lack of miliolids and the abundance of brackish mollusks in these deposits indicate, however, constant fresh water run-off and no hypersaline conditions.

The *Ammonia* forma *tepida* of the Palena section are embedded in a marly matrix and are mainly composed by three whorls. The dominance of advanced growth stages suggests optimum environmental conditions and warm waters, at least with seasonal recurrence. The specimens appear well-preserved or affected only by minor abrasion, suggesting that they occur in situ. The texture of the embedding deposits suggests a low energy depositional environment. The co-occurrence of *Corbula gibba* indicates organic-rich bottoms (Nicoletti et al., 2004). The black organic matter filling some specimens (Fig. 5.7C, I) is presumably due to accumulation of undecomposed detritus that commonly characterize estuary deposits under fluvial dominance (Goñi et al., 2003). According to Carboni et al. (1992) and Carnevale et al. (2011) the paralic facies of Palena were deposited in a marginal marine environment or in a restricted estuarine bay. Salinity fluctuations, due to stratification of marine and continental waters, were presumably occurring in the setting under which such *Ammonia* population thrived. This is supported by i) the presence of a mixed continental-brackish malacofauna in the level with *Ammonia* (Carboni et al., 1992), ii) the presence at the base of the Palena series of a continental fossil flora and of a mixed marine-continental fossil fauna, suggesting the discharge of a river mouth (see Carnevale et al., 2011). Ecological stress for the foraminiferal assemblages could have been further increased by the input of trace metals and clays deriving from the washing of the 'Terra rossa' bed cropping out some meter below.

Summing up, the sedimentological characters and the fossil associations of the *Ammonia*-rich levels at Palena point out to a paralic salt marsh environment rich in organic matter, under fresh water (hypohaline) input. Comparable oligotypic *Ammonia* forma *tepida* associations appear in recent athalassic (non-marine) settings (Cann and Deckker, 1981; Wennrich et al., 2007) and in river delta or paralic brackish settings (Debenay and Guillou, 2002; Murray, 2006; Thibault de Chanvalon et al., 2015 among others). The marly calcarenite level overlying the *Ammonia*-rich estuarine bay deposits contains Cibicides, Elphidium (Fig. 5.4I, 5.5F), echinoids and bivalve fragments. This deposit witnesses the onset of more open marine conditions in a seagrass vegetated area colonized by epiphytic communities including bryozoans (Langer, 1993).

5.7.2. Paleoenvironmental distribution of Miocene Ammonia forma beccarii

Ecophenotypes referable to *Ammonia* forma *beccarii* have been found in shallow-water carbonate facies of Pollino (Calabria), Trentinara (Cilento), Matese and at Scontrone (Genzana Mts). The *Ammonia* forma *beccarii* assemblages of the lower Miocene of Pollino and Cilento occur in calcarenite beds with fragments of bryozoan, bivalves, red algae and foraminifers like *Cibicides* and *Miogypsina*. The *Ammonia* specimens are relatively small, even if the shell thickness and the occurrence of umbilical plug indicates robust affinities with forma *beccarii* A. Several specimens from Pollino appear oxidized, due to post-mortem reworking (Fig. 5.8B-D). This suggests that these *Ammonia* thrived in a very proximal marine setting. The paleoenvironment inferred for the Miocene *Ammonia* forma *beccarii* assemblages of the Pollino and Cilento areas can be compared with those documented by the recent distribution of the forma *beccarii* A (Jorissen, 1988), which prefers nutrient-rich but well-oxygenated bottoms. A relatively high nutrient input is expected in shallow-marine coastal settings near to emerged areas, whose presence is documented in the Pollino area by the occurrence of caliche and exposure-related breccias and at Trentinara by residual clays and coastal lagoon facies immediately underlying the levels with *Ammonia* forma *beccarii*.

The specimens from the Matese area have been found in a slightly deeper setting, characterized by the abundance of red algae and bryozoans and by the occurrence of some planktonic foraminifera. However, in accordance with Bassi et al. (2010), it might be possible that the carbonate bioclasts found in this setting, including *Ammonia*, were displaced from a shoreface proximal environment and re-deposited into the channels system in an open-shelf setting (Carannante, 1982; Carannante and Simone, 1996). The *Ammonia* specimens from the Tortonian ‘Scontrone calcarenite’ are referable to the forma *beccarii* B. The *Ammonia* population is mostly composed by big adult specimens (roughly 1 mm, Fig. 5.8I-Q), ornamented with deep umbilical feathering (Fig. 8T1-2), associated with abundant *Elphidium*. These *Ammonia* have been collected from high-energy coastal bar deposits. We interpret these shells as resedimented from nearby coastal settings. Patacca et al. (2008, pl.2, fig. f; pl.4, fig. b) figured *Ammonia* forma *beccarii* from a high intertidal to supratidal marsh deposits and in facies with reworked cerithids remains, ostracods and oyster fragments, interpreted as a storm layer accumulated within the coastal lagoon. The presence of seagrass meadows at Scontrone is supported by *Elphidium crispum* (see also Patacca et al., 2008; pl. 1, fig. b) that, in recent seas, lives around Posidonia rhizomes or attached to shallow-water green algae (Langer, 1993). The shell features of the *Ammonia* forma *beccarii* B of Scontrone, as the presence of deep interlocular umbilical cavities, support an epiphytic life style, as observed for the same morphotype in the Recent by Debenay et al. (1998). The 'Scontrone calcarenite' is interpreted as deposited in a wave-dominated river-mouth by Patacca et al. (2013). In this setting, we expect salinity fluctuations, driven by the river seasonality. The vertical stacking pattern of the Scontrone succession shows alternation of coastal lagoon-marsh and coastal bar environments (see fig. 2 and fig. 5 of Patacca et al., 2013). In these highly variable environments, the microhabitat may have changed from epiphytic in vegetated areas to epifaunal in more organic-rich bottoms, as in recent allies (Jorissen, 1988; Debenay et al., 1998). Comparable fossil *Ammonia* forma *beccarii* were reported from vegetated bottoms of a proximal shoreface setting, thriving under quite normal marine salinity in Plio-Pleistocene sediments of Greece (Hageman, 1979).

5.8. Conclusions

The Miocene transgressive deposits of central and southern Apennines, which are usually represented by open shelf shallow-water carbonates directly overlying the Cretaceous or Eocene substrate, show in some localities the interposition of residual clays, paleosoils and transitional coastal sediments with *Ammonia*. Autochthonous *Ammonia* assemblages are observed in Trentinara (Cilento, southern Apennines), Scontrone and Palena (Genzana and Majella, central Apennines), whereas in the other studied localities the assemblages are interpreted as parautochthonous. The 'Scontrone calcarenite' contains a rich assemblage of epiphytic foraminifers, maybe associated with seagrass meadows. The functional morphology of *Ammonia* forma *beccarii* B, along with the comparison with recent allies, confirms that they thrived under conditions of fluctuating salinity due to the discharge of a river mouth. Similar to the present, *Ammonia* occurs frequently associated with *Elphidium* and *Cibicides*, which characterized the nearshore, estuarine or paralic facies during the Miocene.

Ammonia was present in the peri-Mediterranean area since the early Miocene. The morphological varieties observed in the fossil representatives are here considered as ecophenotypes. The paleoenvironmental conditions inferred for the Miocene *Ammonia* suggest a strict parallelism with the ecological distribution of recent allies. Big *Ammonia* forma *beccarii* thrived under fluctuating water salinity and moderate trophic conditions, predominantly with an epiphytic or epibenthic habit. The small *Ammonia* forma *tepida* dwelled mostly as shallow-infauna in paralic, coastal lagoon to estuarine bay brackish settings, characterized by eutrophic conditions and pronounced seasonal salinity changes. Forma *tepida* may also indicate natural metal pollution due to its occurrence to deposits of residual clays. Our data suggest that the ecological behavior of *Ammonia*, as well as its morphological diversity, has remained almost unchanged for roughly 20 my. The tooth-plate, an endoskeletal element produced by the lamellar flap, occurs early in the *Ammonia* evolutionary stages, one example is here reported from the early Miocene (late Aquitanian to early Burdigalian) of the Roccadaspide Fm at Trentinara. This finding could be important to reconstruct the phylogenetic history of the group, which includes several recent representatives.

5.9 Data availability

This chapter is extracted from a journal paper that was published in Palaeogeography, Palaeoclimatology, Palaeoecology, doi:10.1016/j.palaeo.2020.110105

CHAPTER 6. FOREBULGE MIGRATION IN THE FORELAND BASIN SYSTEM OF THE CENTRAL-SOUTHERN APENNINE BELT (ITALY): NEW HIGH-RESOLUTION SR-ISOTOPE DATING CONSTRAINTS

Sabbatino, M., *Tavani, S., Vitale, S., Ogata, K., Corradetti, A., Consorti, L., Arienzo, I., Cipriani, A., & Parente, M.*

This chapter is under review in *Basin Research*, (2021)

Abstract

The Apennines are a retreating collisional belt where the foreland basin system, in large domains, is floored by a subaerial forebulge unconformity developed due to bulge uplift and erosion. This unconformity is overlain by a diachronous sequence of three lithostratigraphic units made of: (i) shallow-water carbonates, (ii) hemipelagic marls and shales, and (iii) siliciclastic turbidites. Typically, the latter have been interpreted regionally as the onset of syn-orogenic deposition in the foredeep depozone, while little attention has been given to the underlying units. Accordingly, the rate of migration of the southern Apennine foreland basin-belt system has been constrained, so far, exclusively considering the age of the turbidites, which largely postdate the onset of foredeep depozone.

In this work we provide new high-resolution ages obtained by strontium isotope stratigraphy applied to calcitic bivalve shells sampled at the base of the first syn-orogenic deposits overlying the Eocene-Cretaceous pre-orogenic substratum. Integration of our results with published data indicates progressive rejuvenation of the strata sealing the forebulge unconformity toward the outer portions of the belt. In particular, the age of the forebulge unconformity linearly scales with the position of the analyzed sites in their pre-orogenic position, pointing to a constant velocity of the forebulge wave in the last 25 Myr.

Keywords: Foreland basin system; Forebulge; Foredeep; Strontium isotope stratigraphy; Fold and thrust belt; Central-Southern Apennines (Italy)

6.1. Introduction

The Apennines are a fold and thrust belt belonging to the Western Mediterranean subduction zone: a narrow, arcuate, low-elevation orogenic system formed by the convergence between African and Eurasian continents which rims most of the western Mediterranean Basin (Royden and Faccenna, 2018 and references therein) (Fig. 6.1A). Such a system includes, beyond the Apennine, the Calabria, Maghebride, Rif, and external Betic thrust belts, along with associated back-arc and foreland basins. In this framework, the Apennines form the northern limb of the Apennines-Calabria-Sicily orocline, developed due to the SE-ward retreating subduction of the Alpine Tethys (e.g., Malinverno and Ryan, 1986; Royden et al., 1987; Doglioni, 1991; Faccenna et al., 1997; Carminati and Doglioni, 2012).

In this subduction system, information about the timing of the orocline development has been derived mainly by the age of syn-orogenic deposits filling the fossil foreland basins (Ori et al., 1986; Cipollari and Cosentino, 1995; Cavinato and DeCelles, 1999; Bigi et al., 2009; Vezzani et al., 2010; Vitale and Ciarcia, 2013). Indeed, the architecture and stratigraphy of foreland basins provide constraints on the evolution of the associated thrust belts (e.g., Allen et al., 1986; Ori et al., 1986; DeCelles and Giles, 1996; DeCelles, 2012). Typically, foreland basin systems host four depozones: wedge-top, foredeep, forebulge and back-bulge (DeCelles and Giles, 1996). The Apennines, being a retreating collisional belt, are characterized by narrow but thick foredeep and wedge-top depozones, and very narrow forebulge and back-bulge depozones (DeCelles, 2012). In this context, the architecture and stratigraphy of the central and southern Apennines, including its fossil foreland basins, have been extensively studied in the last decades (e.g., Patacca and Scandone, 2007; Cosentino et al., 2010; Vezzani et al., 2010; Critelli et al., 2011; Vitale and Ciarcia, 2013 among others). Typically, the timing of migration and deformation of the Apennine belt-foreland basin system has been constrained using the ages of the siliciclastic sedimentary rocks filling the foredeep and wedge-top depozones. However, those strata do not represent the first syn-orogenic depositional event on the foreland plate. In fact, the earliest stage of a foreland basin system history predates the passage of the forebulge and it is recorded by the slow accumulation in the back-bulge depozone, which, in retreating collisional settings like the Apennines, may be removed by erosion during passage of the forebulge itself (e.g., DeCelles, 2012). During forebulge uplift, the lithosphere flexes upward, causing stratigraphic condensation, erosion and development of a forebulge unconformity in shallow-water settings (Crampton and Allen, 1995). In these cases, the deposits directly overlying the unconformity constitute the first record of syn-orogenic deposition associated with the most distal foredeep depozone, not reached by siliciclastic input (Fig. 6.2).

The importance of the forebulge unconformity and the following syn-orogenic sedimentation for evaluating the dynamics of foreland basin system development was already remarked in several orogenic belt-basin systems, such as in the Appalachians (e.g., Hiscott et al., 1986) Carpathians (e.g., Leszczyński and Nemec, 2015), Dinarides (e.g., Babić and Zupanič, 2012), Himalayas (e.g., DeCelles et al., 1998), Northern Alps (e.g., Crampton and Allen, 1995; Sinclair, 1997), Oman-UAE (e.g., Glennie et al., 1973; Robertson, 1987), Papuan Basin (e.g., Pigram et al., 1990); Pyrénées (e.g., Vergés et al., 1998), Taiwan (e.g., Yu and Chou, 2001), Timor Trough (e.g., Veevers et al., 1978), North American Cordillera (e.g., White et al., 2002), and Zagros (e.g., Homke et al., 2009; Saura et al., 2015; Pirouz et al., 2015, 2017a,b). Furthermore, the geometry of the forebulge unconformity and the progressive time-transgressive onlap of overlying sediments are of fundamental importance for understanding the history of foreland sedimentation associated with the events of the advancing orogen. In the central-southern Apennines, these deposits are typically represented by shallow-water carbonates, which have been described under different lithostratigraphic units, such as the Cerchiara, Roccadaspide, Recommone, and Cusano formations, the Bryozoan and Lithothamnium Limestones, and the Gravina Calcarenite (Selli, 1957; De Blasio et al., 1981; Carannante et al., 1988a; Taddei Ruggiero, 1996; Civitelli and Brandano, 2005; Patacca et al., 2008). To date, the early evolutionary stage in the syn-orogenic history of the central-southern Apennines has not been investigated in detail: filling this gap constitutes the main aim of this contribution. In particular, we aim at constraining precisely the age of the first carbonate sediments overlying the forebulge unconformity by means of Sr-isotope stratigraphy (SIS). This method is particularly suitable for high-resolution dating and correlation of Miocene marine carbonates because the reference curve for this stratigraphic interval is characterized by a very narrow statistical uncertainty and by a very high slope (i.e., rapid unidirectional change of $^{87}Sr/^{86}Sr$ ratio of the ocean through time) (McArthur, 1994). For these reasons, a resolution of up to 0.1 Ma can be potentially attained in Miocene marine deposits. Moreover, Miocene shallow-water carbonate units of the Apennines contain low-Mg calcite shells of pectinid and ostreid bivalves, which are one of the best materials for SIS (McArthur et al., 2020 and references therein).

Building on the work by Sabbatino et al., 2020, who presented a first case study in the southern Apennines, we assembled a more complete dataset for the base of the central-southern Apennine foreland basin - i.e. the first syn-orogenic deposits associated with the most distal foredeep depozone directly overlying the forebulge unconformity - widening the area of investigation to a large transect of the orogenic belt, extending from inner to outer sectors (i.e., from W to E/NE; Fig. 1B). Integration of these new data with previously published ages of syn-orogenic deposits allows us to better constrain the evolution of the Apennine belt and foreland basin.

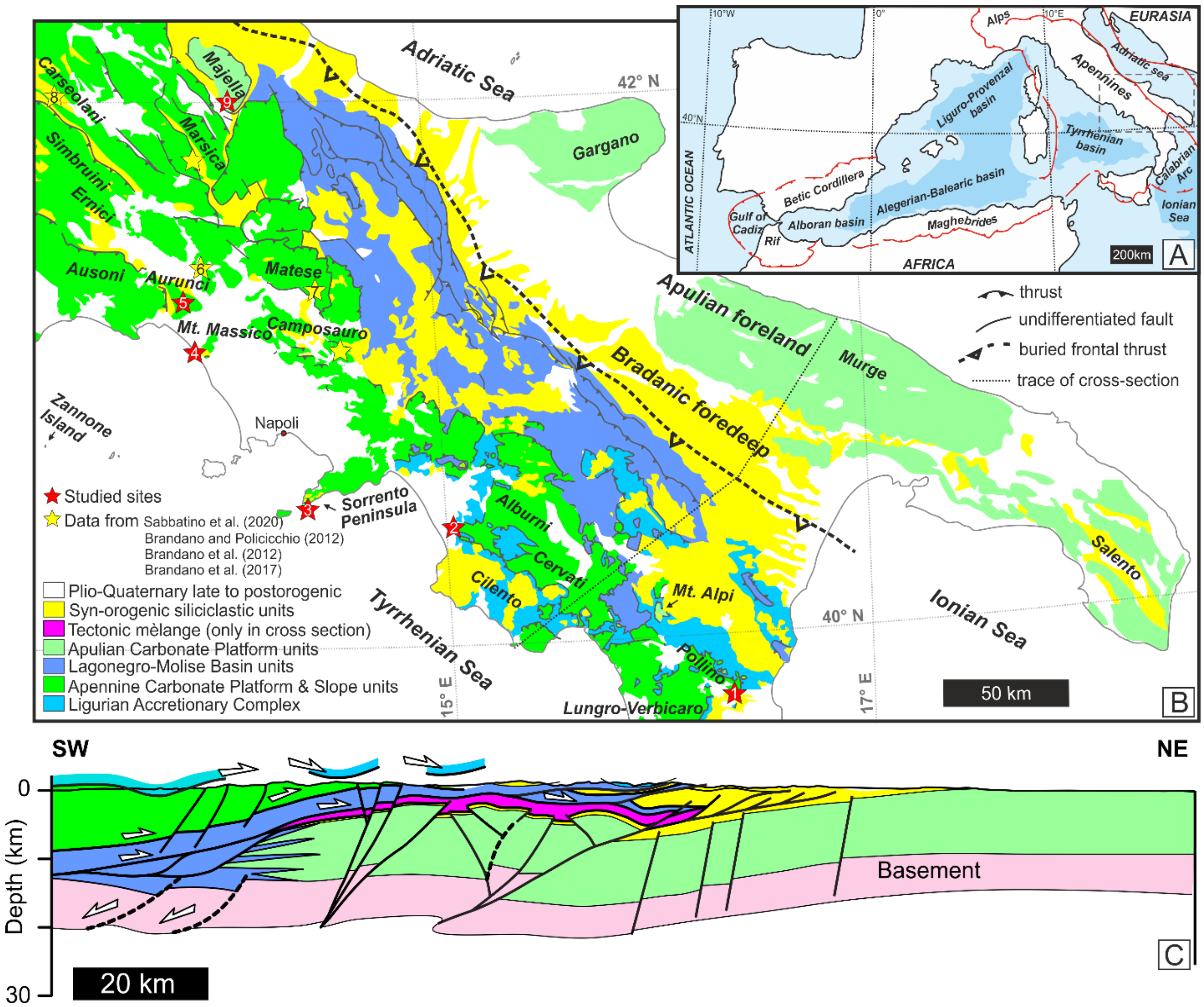

Figure 6.1. A) Tectonic sketch map of the Western Mediterranean subduction zone; B) schematic geological map of the central and southern Apennines showing the locations of the studied sites (modified after Vitale and Ciarcia, 2013). Numbered symbols refer to the stratigraphic logs of Fig. 6.3). C) Cross-section across the southern Apennines (modified after Tavani et al., 2021).

6.2. Geological setting

The Apennines are part of the Western Mediterranean subduction zone that evolved in the framework of the Alpine-Himalayan geodynamic system (Fig. 6.1A) (e.g., Faccena et al., 2001; Royden and Faccena, 2018). The orogenic system formed by the westward subduction of Adria beneath Europe (Malinverno and Ryan, 1989) and evolved in the context of a retreating collisional system, characterized by a progressive arching of an originally nearly linear belt, following the E-ward retreat of the trench and the opening of the Tyrrhenian back-arc basin (e.g., Dewey et al., 1989; Malinverno and Ryan, 1986; Doglioni, 1991; Mazzoli and Helman, 1994; Faccenna et al., 2014). During such convergence, several tectonic units, originally deposited in a system of carbonate platforms and intervening deep basins that developed on the southern margin of the Alpine Tethys ocean since the Triassic (Bosellini, 2004), were imbricated to form the Apennine thrust belt.

In more detail, the Apennines can be further subdivided into two main arcs: the northern and the southern Apennines, which connect in the central Apennines. The present-day tectonic architecture of the southern Apennines is made up of the thrust sheets of the Mesozoic Lagonegro-Molise Basin successions, sandwiched between thrust sheets composed of the overlying Apennine and underlying Apulian Mesozoic shallow-water platforms. The Apennine platform is in turn overthrust by the deep basinal units of the Ligurian accretionary complex, which was deposited on top of the Jurassic oceanic and thinned continental crust and exhumed oceanic lithosphere (e.g., Cello and Mazzoli, 1998; Mazzoli et al., 2008, Tavani et al., 2021). The western part of the Apulian platform is deformed under a thick tectonic pile, and is now exposed in the Mount Alpi, in the southern Apennines, and Majella Mountains in the central Apennines. The outer (eastern) sector of the Apulian platform is exposed in the foreland region of the southern Apennines to the NE, where it is locally buried underneath a Plio-Pleistocene sedimentary cover.

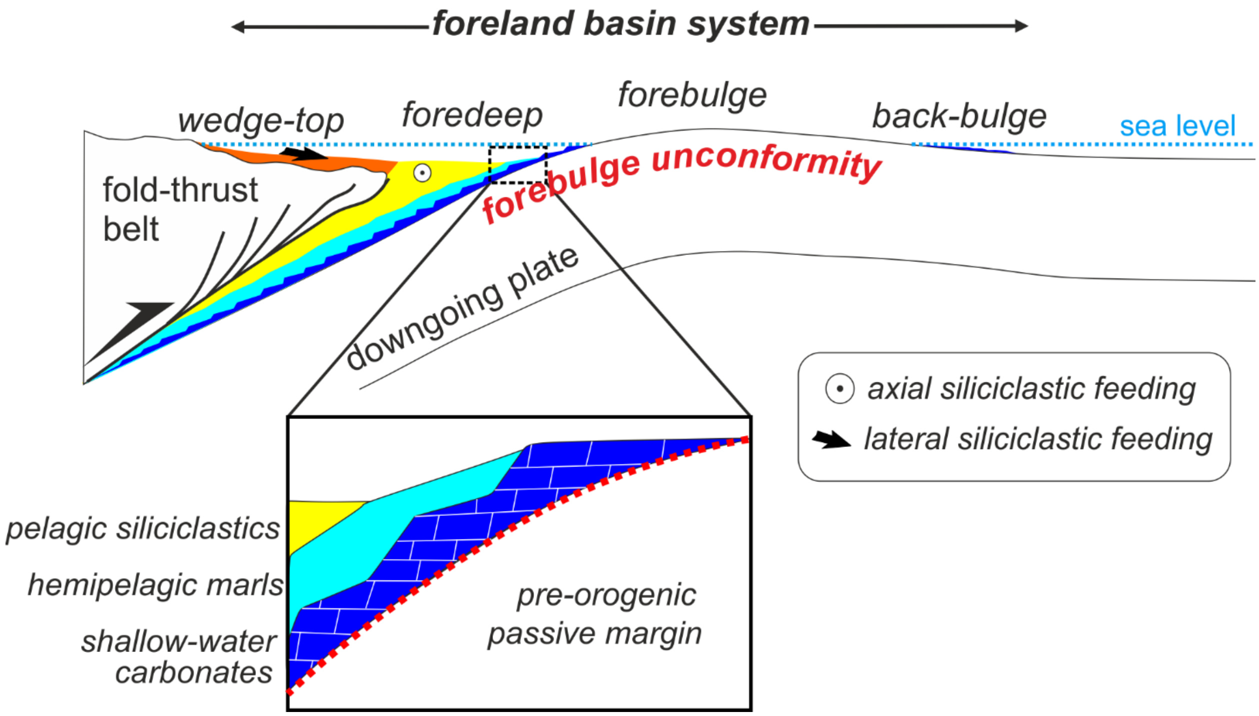

Figure 6.2. Schematic cross-section of a foreland basin system with the back-bulge, forebulge, foredeep, and wedge-top depozones (modified after DeCelles and Giles, 1996; Sinclair, 1997; and Sabbatino et al., 2020).

The foreland basin, which developed ahead of the central-southern Apennine tectonic edifice, was progressively filled with syn-orogenic sediments, following a younging trend toward the east/north-east. The Miocene to Pleistocene syn-orogenic carbonates, object of this study, unconformably overlie the Apennine and Apulia carbonate platform pre-orogenic units. The Apennine and Apulia platform units represent allochthonous and (partly) autochthonous respectively paleogeographic domains witnessing a long-term record of pre-orogenic passive margin shallow-water carbonate sedimentation. Thick platform successions (up to 6000m; Ricchetti et al., 1988) developed from the Late Triassic to the Late Cretaceous (Bernoulli, 2001), with the only long-lasting interruption by prolonged subaerial exposure recorded in some areas by 'middle' Cretaceous karst bauxites (Mindszenty et al., 1995). Shallow-water carbonate sedimentation resumed in some sparse areas in the Paleogene and is now represented by much less widespread, thin, and stratigraphically discontinuous deposits (Selli, 1962; Chiocchini et al., 1994) overlying unconformably Upper Cretaceous platform carbonates. In the southern Apennines, this stratigraphic interval is represented by an up to 150 m-thick sequence of lower-middle Eocene limestones, known as the Trentinara Formation (Selli, 1962), which is widely exposed in the Alburno-Cervati (Cilento Promontory) and Pollino Mountains (Fig. 6.1). In the central Apennines analogous facies, described as "*Spirolina* sp. Limestones" (Chiocchini and Macinelli, 1977; Romano and Urgera, 1995; Vecchio et al., 2007), are much less widespread and reach a maximum thickness of about 30 m (Romano and Urgera, 1995). After this prolonged phase of passive margin sedimentation and a long-lasting Cretaceous/Eocene to Miocene hiatus, a new phase of shallow-water carbonate sedimentation occurred starting from the early Miocene, related to the development of the Apennine belt.

6.2.1 The central-southern Apennine foreland basin system

Starting from the Miocene, the foreland of the central-southern Apennines has experienced pre-thrusting bulging, uplift, and erosion, caused by the bending of the subducting lithosphere and by the E/NE-ward migration of the accretionary wedge (e.g., Doglioni, 1995). This tectonic stage is recorded by a regional unconformity, by extensional fracturing and faulting in the uppermost part of the lithosphere, and by the onset of flexural subsidence, conforming to the models of foreland basin evolution in retreating collision systems (Turcotte and Schubert, 1982; Bradley and Kidd, 1991; Crampton and Allen, 1995; Doglioni, 1995; DeCelles and Giles, 1996; DeCelles, 2012; Carminati et al., 2014). The onset of flexural subsidence is recorded by time-transgressive deposits overlying the pre-orogenic substrate. In absence of records of the earliest syn-orogenic back-bulge depozone, the Miocene shallow-water carbonates of the central-southern Apennines represent the base of the foreland basin mega-sequence (Sabbatino et al., 2020). The vertical stacking pattern of the Apennine foreland basin conforms to the "Waltherian sequence" of DeCelles (2012), recording the spatial-temporal evolution and migration of syn-orogenic depozones in front of the migrating orogenic belt. The sequence is composed of the basal subaerial forebulge unconformity at the top of the pre-orogenic passive margin megasequence, overlain by three diachronous lithostratigraphic units, which from bottom to top are: (i) a shallow-water carbonate unit, (ii) a hemipelagic marly unit, and (iii) a siliciclastic turbiditic unit (Fig. 2) ("underfilled trinity"; Sinclair, 1997).

The syn-orogenic shallow-water carbonate unit records the sedimentation on a carbonate ramp dominated by red algae and bryozoans, with variable amounts of benthic foraminifers. This fossil assemblage is typical of a temperate-type foramol (*sensu* Lees, 1975) or foramol/rhodalgal carbonate factory (*sensu* Carannante et al., 1988b). The shallow-water carbonate ramp sedimentation was not able to keep up with accelerating flexural subsidence and it was eventually terminated by drowning below the photic zone, as recorded by the deposition of hemipelagic marls with planktonic foraminifera (Lirer et al., 2005). The switch from hemipelagic deposits to Mio-Pliocene turbiditic siliciclastics is the further step (Sgrosso, 1998; Patacca and Scandone, 2007) within the frame of the abovementioned evolution of an underfilled foreland basin (Sinclair, 1997). Finally, foredeep deposits were incorporated into the accretionary wedge and overlain by unconformable sediments deposited in wedge-top basins (e.g., Ascione et al., 2012). In the regional literature of the Apennines, different names have been used for lithostratigraphic units representing the same evolutive stage in different areas. To make easier the understanding of the Apennine foreland basin evolution, we group the different formations according to the abovementioned nomenclature of Sinclair (1997). Groups of formations, biostratigraphic age, and related lithostratigraphic units are listed in the Table S6.1 of the Supporting information section.

6.3. Material and methods

Strontium Isotope Stratigraphy (SIS) is a well-established tool for high-resolution dating and correlation of marine carbonates (DePaolo and Ingram, 1985; Palmer and Elderfield, 1985; Hodell, 1991; McArthur, 1994; McArthur et al., 2020). This method is based on the empirical observation that the Sr-isotope ratio of the oceanic waters has varied through geological time and on the assumption that the $^{87}Sr/^{86}Sr$ ratio at any time is homogeneous, given the long residence time of Sr in seawater compared to the ocean mixing time.

A total of 61 samples, collected from the basal levels of the transgressive syn-orogenic shallow-water carbonates of the Apennines, were used for SIS. All geochemical data, details on sample preparation, analytical procedures, precision and reproducibility of the analyses, the values of the laboratory standards, and the mean values used for the SIS age determinations are reported in the Supplementary material 6.2, 6.3, and 6.4 of the Supporting Information. The new Sr isotope data and SIS ages produced for this paper are listed in Table 6.1, along with previously published data (i.e., Brandano and Policicchio, 2012; Brandano et al., 2012; Brandano et al., 2017b; Sabbatino et al., 2020).

In order to correct for interlaboratory bias, the Sr isotope ratios were normalized to the value of the NIST–SRM 987 standard used by McArthur et al. (2020) for their compilation. Only the Sr isotope ratios of bivalve shell material (i.e., compact lamellar and prismatic shell layers of ostreid and pectinid bivalves, respectively) which has not been affected by diagenesis (i.e., that is considered to have retained its pristine Sr isotope value) were used for SIS. The diagenetic screening process followed the multistep procedure outlined in Frijia and Parente (2008). This procedure incorporates petrographic observation of the shell microstructure, sample by sample geochemical screening based on trace element composition of the different components (well-preserved shells, altered shells, and bulk matrix), and internal consistency of the Sr isotope ratios of different well-preserved shells from the same stratigraphic level. Numerical ages were derived from the Sr isotope ratios by means of the look-up table of McArthur et al. (2020; version 6: 03/20). When more than one shell was available for the same stratigraphic level, the SIS age was derived from the mean value calculated from all the shells. Minimum and maximum ages were obtained by combining the statistical uncertainty of the samples, given by 2 standard errors (2 s.e.; McArthur, 1994) of the mean value, with the uncertainty of the reference curve (see Steuber, 2003, for an explanation of the method). When fewer than four shells per level were analyzed, the precision of the mean value was considered to be not better than the average precision of single measurements, given as 2 s.e. of the mean value of the standards. The numerical ages obtained from the look-up table were translated into chronostratigraphic ages by reference to the Geological Time Scale of Gradstein et al. (2020), to which the look-up table is tied. To compare the SIS ages produced for this paper with the ones provided in previous works, we have revised all the numerical ages from the Sr isotope ratios, using the new version of the look-up table of McArthur et al. (2020; version 6: 03/20).

6.4. Results

The sections that we studied for this work are located along the southern and central Apennines in the following areas (Fig. 6.1B): 1. Pollino Massif, 2. Alburno-Cervati, 3. Sorrento Peninsula, 4. Massico, 5. Aurunci, 6. Ernici, 7. Matese, 8. Carseolani, and 9. Majella Mountains. (Fig. 6.3). The geographical coordinates of each studied section are given in table S6.2 (supplementary information); table S6.4 lists the samples that were selected to calculate the mean values used for the SIS age determination. We complete a transect across the whole central-southern Apennine foreland basin by considering additionally the sections of Camposauro and Marsica Mountains. We refer to Sabbatino et al. (2020) for the details on the Matese and Camposauro sections, and to Brandano and Policchio (2012), Brandano et al. (2012), and Brandano et al. (2017b) for the detailed descriptions of the Ernici, Carseolani, and Marsica Mountains sections.

Table 6.1. Strontium Isotope Stratigraphy of the base of syn-orogenic carbonate deposits in the studied localities.

Formation	Secion locality	$^{87}Sr/^{86}Sr$ mean†	2 se (*10^{-6})	numerical age (Ma) ‡ min	mean	max	Chronostratigraphic age§
Cerchiara Fm.	Panno Bianco (Pollino Mts)	0.708389	8	20.7	20.8	21	upper Aquitanian
Cerchiara Fm.	Pietra S. Angelo (Pollino Mts)	0.708405	22	20.2	20.6	21	Aquitanian-Burdigalian
Cerchiara Fm.	SS92 Cerchiara (Pollino Mts)	0.708427	11	20.1	20.3	20.5	lower Burdigalian
Roccadaspide Fm.	Trentinara (Alburno-Cervati Mts)	0.708341	9	21.4	21.6	21.8	upper Aquitanian
Roccadaspide Fm.	Trentinara (Alburno-Cervati Mts)	0.708378	8	20.8	21	21.2	upper Aquitanian
Recommone Calcarenites Fm.	Mt. San Costanzo (Sorrento Peninsula)	0.708335	8	21.5	21.7	21.9	upper Aquitanian
Cusano Fm.	Mt. Rosa (Camposauro Mts)	0.708706¶	11	16.3	16.6	16.7	upper Burdigalian
Cusano Fm.	Pietraroja (Matese Mts)	0.708511¶	10	18.9	19.1	19.3	middle Burdigalian
Cusano Fm.	Massico Mt.	0.708577	18	17.9	18.3	18.5	middle Burdigalian
Bryozoan and Lithothamnium Limestone Fm.	Castelforte (Aurunci Mts)	0.708504	31	18.7	19.2	19.7	middle Burdigalian
Bryozoan and Lithothamnium Limestone Fm.	Mt Lungo (Aurunci Mts)	0.708521¶			19		middle Burdigalian
Bryozoan and Lithothamnium Limestone Fm.	Pietrasecca (Carseolani Mts)	0.708542¶	6	18.5	18.7	18.8	middle Burdigalian
Bryozoan and Lithothamnium Limestone Fm.	Gioia dei Marsi (Marsica Mts)	0.708678¶	15	16.7	16.9	17.1	upper Burdigalian
Lithothamnium Limestone Fm.	Guado di Coccia (Majella Mts)	0.708926	18	7.1	8.4	9.4	upper Tortonian

† Sr isotope ratios measured in the lab have been corrected for interlaboratory bias; see the methods section of the text for further explanations.
‡ The preferred numerical age has been derived from the look-up table of MacArthur et al. (2020, version 6: 03/20). The minimum and max age are calculated by combining the statistical uncertainty of the samples (2 se of the mean) with the uncertainty of the reference curve (see the methods section in Frijia and Parente, 2008, for a detailed explanation of the procedure).
§ The chronostratigraphy and biochronology have been derived from the numerical age using the Geological Time Scale of Gradstein et al. (2020) to which the the look-up table of MacArthur et al. (2020, version 6: 03/20) is calibrated.
¶ The $^{87}Sr/^{86}Sr$ ratios are taken from Brandano and Policicchio (2012), Brandano et al. (2012, 2017), and Sabbatino et al., 2020.

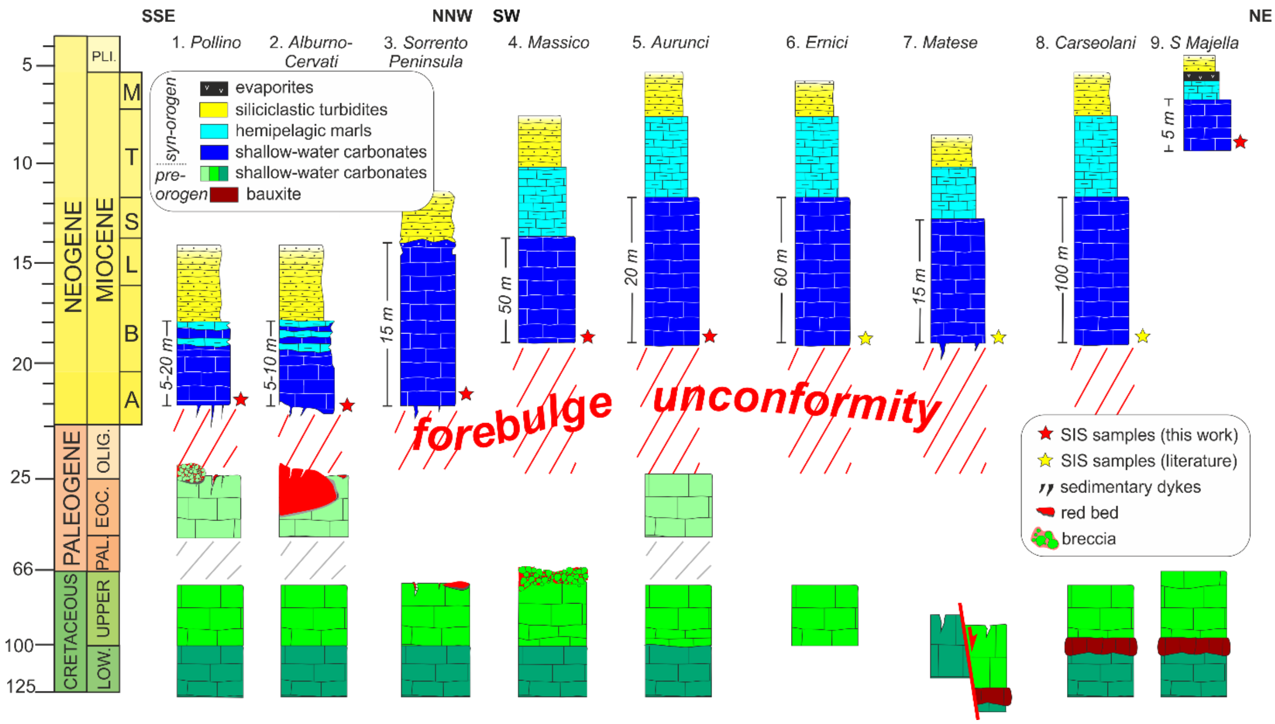

Figure 6.3. Stratigraphic logs of the studied sections in the southern and central Apennines. Numbers correspond to numbered symbols on Fig. 6.1B. Section 1 summarizes the three stratigraphic logs of Panno Biano, Pietra Sant'Angelo, and SS92 Road; section 3 summarizes the two logs of Recommone and Mount San Costanzo. See the text for further details.

6.4.1 Site 1: Pollino Massif and Cilento promontory

The study area belonging to the Pollino Massif consists of three distinct stratigraphic sections located 2-3 km far from each other (Panno Bianco, Pietra S. Angelo, and Cerchiara-SS92-road) at the southern termination of the southern Apennine chain (Fig. 6.1B). The stratigraphy of these three sections has been summarized in the Pollino section of Fig. 6.3. In the Pollino Massif, the shallow-water carbonate post-bulge unit (i.e., the Cerchiara Formation) lies unconformably (paraconformably at the scale of the outcrop; Fig. 6.4A) above a karstified Eocene substrate, locally brecciated and with lenses of residual clays. The thickness of the shallow-water carbonate unit decreases from 20m to less than 10m moving from south to north/northeast. The base of the shallow-water carbonate unit is marked by an oyster bank (Fig. 6.4A) in all the three studied sections. The facies progressively pass upward into proximal marine to more open marine shallow-water facies (Consorti et al., 2020). Pristine shells sampled from the oyster bank were used for SIS. The mean value of the Sr isotope ratio calculated for the basal level of the shallow-water carbonate unit in the abovementioned Panno Bianco, Pietra S. Angelo, Cerchiara SS92 road sites give the following ages: 20.8, 20.6, and 20.3 Ma (see Table 6.1 for the associated uncertainty bar). These numerical ages correspond to a chronostratigraphic age ranging from the upper Aquitanian to the lowermost Burdigalian. Moving toward N-NE, in the Alburno-Cervati Mountains of the Cilento promontory (Fig. 6.1B), Miocene post-bulge shallow-water carbonates (Roccadaspide Formation) seal the forebulge unconformity on top of an Eocene substrate showing evidence of subaerial exposure, including residual clays (up to 10 meters of 'lateritic clays' in: Boni, 1974) (Fig. 6.3). The base of the shallow-water carbonate unit is marked by an oyster bank, passing upward into paralic facies evolving to more open marine calcarenites (Consorti et al., 2020). The SIS results produced for shells of the basal oyster bed sampled at this site provide a numerical age of 21.6-21 Ma, corresponding to an upper Aquitanian chronostratigraphic age. The shallow-water carbonate unit is overlain by middle Burdigalian calciclastic-siliciclastic deposits which are then capped by wedge-top siliciclastic deposits, latest Burdigalian - earliest Tortonian in age (see Table S6.1).

6.4.2 Site 2: Sorrento Peninsula

In the Sorrento Peninsula, we have studied two outcrops: Recommone and Mount San Costanzo. These sections have been merged into the log of Fig. 6.3 (see Table S6.2, in the Supplementary material 2, for the geographic position of the sections). The post-bulge Miocene shallow-water carbonate deposits (i.e., Recommone Calcarenites) overlie paraconformably an highly bioeroded Upper Cretaceous pre-orogenic substrate (Fig. 6.4B-C). Evidence of subaerial exposure is here represented by paleokarstic cavities and sedimentary dykes in the Cretaceous bedrock, filled by the bioclastic Miocene calcarenite. The Miocene deposits cropping out in these sites are up to a few tens of meters thick and are representative of an open marine environment. The shallow-water carbonate unit passes gradually upward to Serravallian sandstones, which are then capped by wedge-top siliciclastic deposits late Tortonian in age (see Table S6.1).

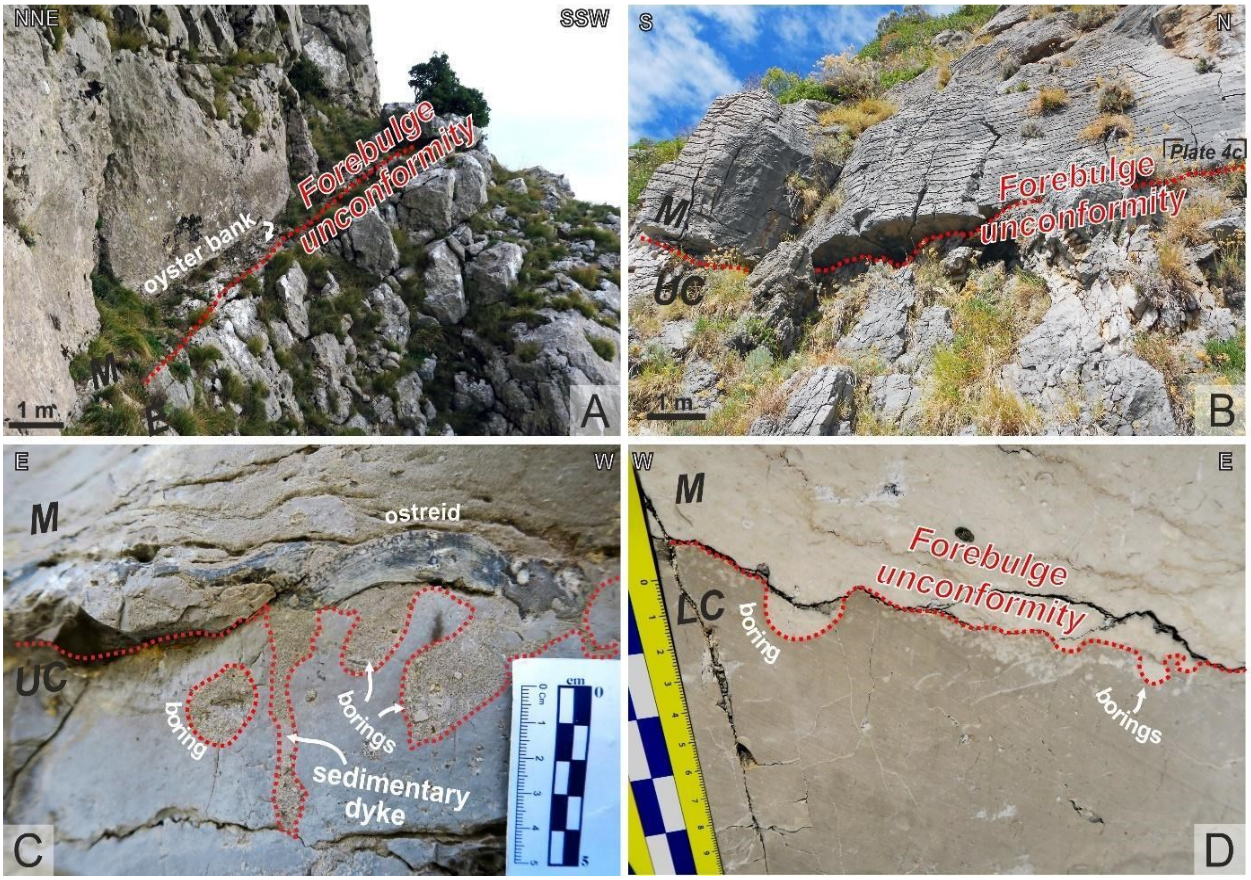

Figure 6.4. Exposures of the forebulge unconformity (paraconformity at the scale of the outcrop) separating Miocene syn-orogenic deposits from the Cretaceous/Eocene pre-orogenic substrate in the central-southern Apennines. A) Mount Panno Bianco site near Cerchiara di Calabria (Pollino Massif; 39°50'59''N 16°22'17''E): Eocene carbonate (E) covered by the Miocene shallow-water carbonate deposits (M). The sharp contact is marked by an oyster bank in life-position. B, C) Recommone site (Sorrento Peninsula; 40°35'03"N 14°21'54''E): overview and detail of the sharp contact between the Miocene shallow-water carbonate deposits (M) and the Upper Cretaceous substrate (UC). The contact is marked by a level with ostreids in life-position and by dykes and boring filled and sealed by Miocene sediments. D) Pietraroja site (Matese Mountains; 41°20′59″N 14°33′09″E). The Miocene shallow-water carbonate deposits (M) lie on top of Lower Cretaceous carbonates (LC). The contact is marked by a stylolite surface and borings.

The shells sampled from the basal oyster level at the Mount San Costanzo site give a numerical age of 21.7 Ma (late Aquitanian) (Table 6.1). The material sampled at Recommone site showed important signs of diagenetic alteration and was not used for calculating a SIS age (see Table S6.2).

6.4.3 Site 3: Massico, Aurunci, and Ernici Mountains

At Mount Massico site, the post-bulge shallow-water carbonate unit (i.e., Bryozoan and Lithothamnium Limestone; Table S6.1), crops out on top of locally brecciated Upper Cretaceous carbonates (Fig. 6.3). It is made of about 50 meters of carbonate ramp facies, consisting mainly of bryozoan and rhodolith rudstone-floatstone with shells and fragments of bivalves, balanids, echinoid fragments and spines, benthic foraminifers, few rotalids, and rare planktic foraminifers. The age obtained by SIS for the basal levels of the shallow-water carbonate unit in the Massico site is 18.2 Ma, corresponding to the middle Burdigalian. In the Castelforte section (Aurunci Mountains), Miocene deposits of the post-bulge carbonates overlie Eocene carbonates (Fig. 6.3). The basal facies correspond to a middle ramp environment. The Sr-isotope value obtained by analyzing bivalve shell fragments from basal levels of the formation provides a numerical age of 19.2 Ma, which corresponds to the middle Burdigalian. About 17 km north of Castelforte, in the Cassino plain, the Mount Lungo section (Ernici Mountains) exposes 60 meters of shallow-water carbonate rocks resting on top of Upper Cretaceous limestones (Fig. 6.3) (Damiani et al. 1992; Brandano and Policchio, 2012). The basal facies are representative of an inner ramp environment and grade upward to middle and outer ramp (Brandano and Policicchio, 2012). A numerical age of 19 Ma was calculated using the Sr-isotope value given by Brandano and Policicchio (2012) for the base of these deposits.

In these sites, the ramp carbonate facies pass upward to Serravallian-Tortonian hemipelagic deposits evolving in turn to siliciclastic turbidites. Upper Tortonian to lower Messinian wedge-top siliciclastic deposits cap the foredeep sequence (see Table S6.1).

6.4.4 Site 4: Matese and Camposauro Mountains

Sixty km east of Massico site, in the Matese and Camposauro Mountains sites (Figs 6.1B, 6.3), the shallow-water carbonate unit is the first syn-orogenic deposit unconformably overlying the top of the Cretaceous substrate, which ranges in age from the Early Cretaceous to the Late Cretaceous. The contact between pre-orogenic and syn-orogenic rocks is marked by a stylolitic surface, borings, and sedimentary dykes filled by the syn-orogenic deposits (Fig. 6.4D). The Miocene deposits are representative of open marine facies deposited in middle ramp environments. Recently, Sabbatino et al. (2020) reported Sr-isotope values corresponding to a SIS numerical age of 16.3 and 19.1 Ma (middle Burdigalian) for the base of the shallow-water carbonates at Camposauro and Matese sites, respectively. The authors interpret the diachrony between the base of the shallow-water carbonate unit in these two sites as related to a locally complex paleotopography, with horst and graben extensional structures inherited by previous tectonic events and subsequently active again during the forebulge stage.

In both the Matese and Camposauro Mountains areas, the shallow-water carbonate unit passes upward to the Serravallian – lower Tortonian hemipelagic marly unit and then to lower-middle Tortonian siliciclastic turbiditic unit. The foredeep siliciclastic deposits are topped by upper Tortonian - lower Messinian wedge-top deposits (see Table S6.1).

6.4.5 Site 5: Marsica and Carseolani Mountains

In the Marsica Mountains (Fig. 6.1B), up to 70-80 m of Miocene post-bulge shallow-water carbonate units are exposed. The basal facies are attributed to middle ramp environments and dated as 16.9 Ma (upper Burdigalian) by Brandano et al. (2012). In the area of the Carseolani Mountains (Figs 6.1B, 3), at the Pietrasecca site, up to 100 meters of shallow-water carbonate rocks cover paraconformably an Upper Cretaceous substrate (Brandano et al., 2017b). The post-bulge shallow-water carbonate unit in this site comprises three main facies types that can be ascribed to an outer ramp environment (Brandano et al., 2017b). The SIS numerical age calculated from the Sr-isotope value given by Brandano et al. (2017b) is 18.7 Ma, corresponding to the middle Burdigalian (Table 6.1). In both these sites, the shallow-water carbonate unit passes upward to upper Tortonian – lower Messinian hemipelagic marly deposits and then to siliciclastic turbiditic deposits. The latter are topped by Messinian wedge-top siliciclastic deposits (see Table S6.1).

6.4.6 Site 6: South Majella Mountains

In the studied site at South Majella Mountains (Fig. 6.1B, 6.3), the first syn-orogenic carbonates (i.e., Lithothamnium Limestone; Table S6.1) cover unconformably uppermost Cretaceous pre-orogenic carbonates. The unconformity surface is marked by non-depositional and/or erosional features and locally it is intensely bioeroded (Danese, 1999). In the section of Capo di Fiume, about 4 km east of Guado di Goccia, syn-orogenic shallow-water carbonates overlie paleosols that lie in turn on an uppermost Cretaceous substrate. The basal facies of the shallow-water carbonate unit at the Guado di Coccia site consist of a few meters of bioclastic calcarenites, rich in red algae and corals, representative of an open marine environment, passing upward into deposits of a coastal-transitional marine environment with an evolution from wetland to estuarine conditions at the Capo di Fiume site (Danese, 1999; Carnevale et al., 2011). The $^{87}Sr/^{86}Sr$ mean value of pectinid and ostreid shells collected from basal levels of the syn-orogenic sequence gives a numerical age of 8.4 Ma, which corresponds to the late Tortonian (Table 6.1). The shallow-water carbonates pass upward into Messinian hemipelagic deposits and then to evaporite levels (Gessoso-Solfifera Formation; Danese, 1999). The latter is topped by early Pliocene siliciclastic turbiditic deposits and then by middle-upper Pliocene wedge-top siliciclastic deposits (see Table S6.1).

6.5. Discussion

The discussion is organized in two subsections. In the first one, we summarize our findings in terms of age and characters of the base of the syn-orogenic sequence in the different areas (Fig. 6.5, 6.6A). In the second subsection, we compare the time-transgressive age of the base of the distal foredeep carbonates with the age of the onset of siliciclastic sedimentation in foredeep and wedge-top depozones, and all these ages are plotted against their pre-orogenic positions, to discuss mode and rate of the flexural wave migration (Fig. 6.6B, C).

6.5.1 Dating the base of the syn-orogenic megasequence in the southern-central Apennines

Here we provide a detailed discussion for each study site. Additionally, although not covered by this work, we intend to complete the picture of the Apennine foreland basin depozones by mentioning shortly the first syn-orogenic deposition in the innermost sectors of the Apennine foreland and in the external sectors of the Apulian foreland domain that are exposed at Mount Alpi and in the present-day Apulian foreland (Figs 6.1, 6.5).

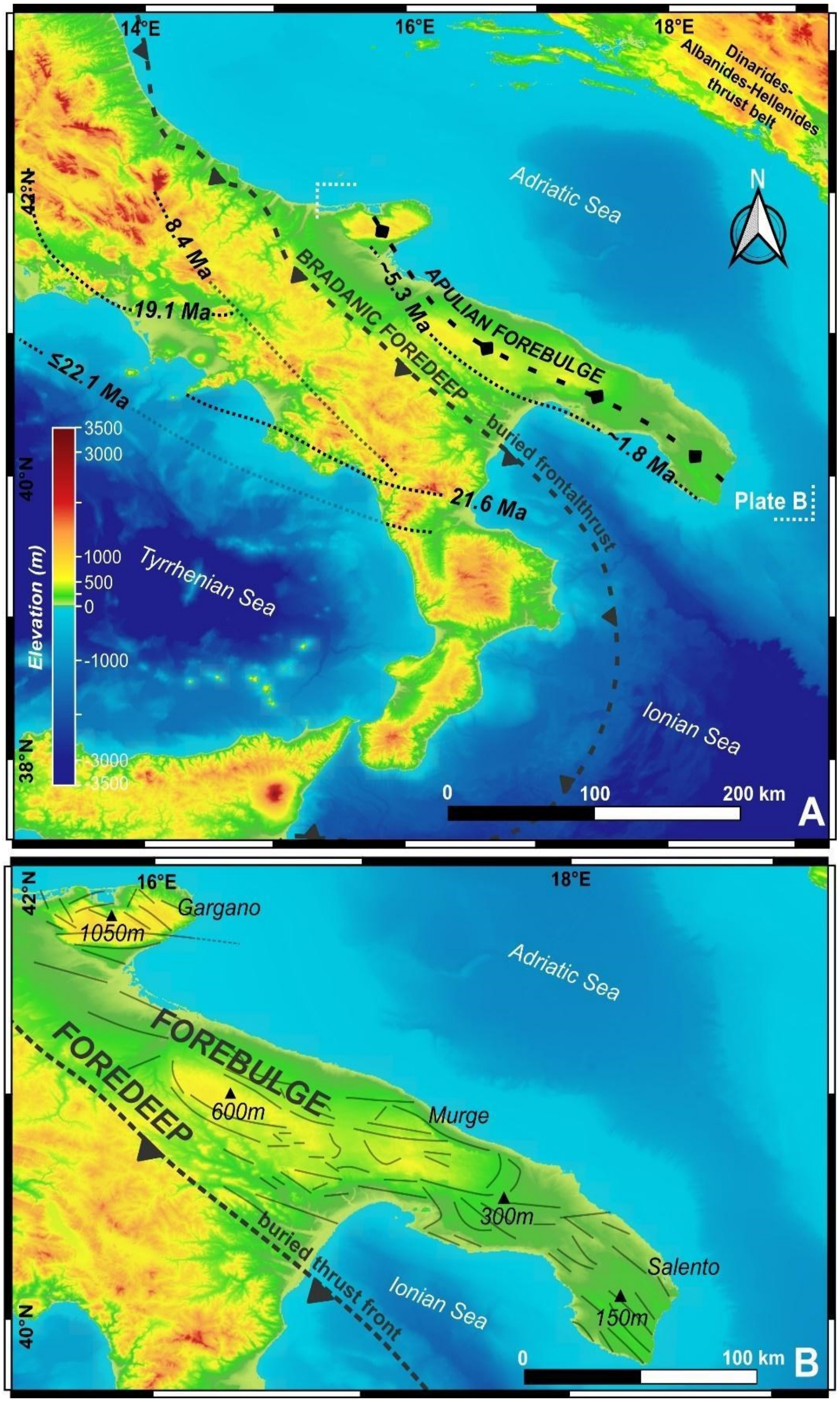

Figure 6.5. A) Isochrones of the base of the foredeep depocenters. B) Modern Apulian foreland. The mapped faults are taken from Doglioni et al. (1994) and Pieri et al. (1997). Bathymetry and outside Italy land elevation were obtained from GEBCO 2020 Grid (doi: 10/dtg3) with a spatial resolution of 15 arc seconds. Land elevation for Italy territory was downloaded from the Institute for Environmental Protection and Research of Italy (ISPRA) website (http://www.sinanet.isprambiente.it/it/sia-ispra/download-mais/dem20/view).

6.5.1.1 Lungro-Verbicaro and Zannone Island

In the Lungro-Verbicaro site (Fig. 6.1B), middle Eocene to Aquitanian calcareous breccias, with platform-derived limestone clasts, alternating with marls and shales (i.e., the Colle Trodo Formation; Iannace et al., 2007) lie transgressively on a Maastrichtian-Paleocene paleosubstrate and grade upward to siliciclastic deposits of Aquitanian age (i.e., Scisti del Fiume Lao Formation; D'Errico and Di Stasio, 2010; Table S6.1). These Aquitanian deposits are substantially coeval with the Flysch unit of the Zannone Island, located W of Mount Massico (Fig. 6.1B), which have been recently interpreted as the oldest foredeep depozone of the central Apennines by Curzi et al. (2020). The authors constrained the age of those deposits as spanning from late Oligocene to early Aquitanian (not younger than 22.1 ± 0.6 Ma) by K-Ar dating of fault gauge clay related to the end of thrusting leading the Mesozoic carbonate rocks onto the turbidites. We infer that both the deposits of the Lungro-Verbicaro area and of Zannone Island were part of the same innermost and oldest foredeep depozone (Fig. 6.5A).

6.5.1.2 Pollino Massif and of the Cilento Promontory

In these areas, the forebulge stage is testified by continental red beds and breccia-conglomerate levels that overlie the pre-orogenic Eocene substrate (Fig. 6.6A). Evidence of syn-bulging subaerial exposure is also represented by paleokarstic cavities present within the topmost strata of the pre-orogenic rocks, along with sedimentary dykes filled and sealed by meteoric cements and continental to marine sediments belonging to the overlying deposits. The overlying carbonate rocks had been dated only by biostratigraphy (Selli, 1957; Carannante et al., 1988a). In detail, the occurrence of *Miogypsina socini* and *M. globulina*, markers of the shallow benthic zones (SBZ) 24 and 25 (Cahuzac and Poignant, 1997), provided an age ranging from the early Aquitanian to the end of the Burdigalian. The limitations of these biostratigraphic data are twofold: 1) the SBZ zonal scheme has a resolution of 2-4 Ma for the early Miocene; 2) miogypsinids are rare in these formations and they are not present in the basal levels, so that the age of a single level with miogypsinids is generally extended to the whole section. Our SIS ages of 20.8, 20.6, 20.3, 21.6, and 21 Ma, for the base of the shallow-water carbonate unit in different sites (i.e., Cerchiara Panno Bianco, Pietra Sant'Angelo, and SS92, and two sites at Trentinara; Table 6.1) (Fig. 6.5A), are compatible with the biostratigraphic data but they allow a much greater time resolution. The slightly variable ages of such deposits can be attributed to a complex paleotopography affecting the foreland through horst and graben structures before the onset of syn-orogenic sedimentation, as documented in other sites of the central-southern Apennines and in the present Apulian foreland (Fig. 6.5B and section 6.1.6) (e.g., Doglioni et al., 1994; Billi and Salvini, 2003; Sabbatino et al., 2020). Such inherited paleotopography has also influenced the depositional environment and thickness of the shallow-water carbonate units in the different studied sites.

The age of the base of the siliciclastic foredeep deposits overlying the basal carbonate unit in the Pollino Massif and Cilento Promontory (Fig. 6.1, 6.3) falls in the middle Burdigalian (Tab. S6.1).

6.5.1.3 Sorrento Peninsula

In this area, the syn-bulging emersion is evidenced by a sharp unconformity surface, sedimentary dykes, and paloekarstic cavities on top of the Upper Cretaceous substrate, filled and sealed by very thin continental deposits and open-marine carbonates (Fig. 6.4B, C; 6.6A). The post-bulging shallow-water carbonate unit was previously attributed to the Burdigalian-Langhian, based on the occurrence of miogypsinids (De Blasio et al., 1981). Our SIS results on the basal shallow-water carbonate unit at Mount San Costanzo site constrain the age of the base of this formation at 21.7 Ma (late Aquitanian) (Fig. 6.5A; Table 6.1). The age of the first siliciclastic deposits is considered not older than Serravallian (Table S6.1).

6.5.1.4 Massico, Aurunci, Ernici, Matese, Camposauro, Marsica, and Carseolani Mountains

In this large area, which extends from the northern termination of the southern Apennines to the central Apennines, the base of the syn-orogenic deposition overlying the pre-orogenic Cretaceous carbonates of the Apennine Carbonate Platform varies from 18.3, 19.2, 19, 19.1, 16.6, 18.7, and 16.9 Ma (i.e., middle to late Burdigalian) in the sites of Massico, Aurunci (Castelforte site), Ernici (Mount Lungo site), Matese (Pietraroja site), Camposauro, Carseolani (Pietrasecca site), and Marsica Mountains respectively (Fig. 6.1, 6.3, 6.5A; Table 6.1). The basal facies are also variable from inner to outer ramp. The Miocene shallow-water carbonates evolve upward to hemipelagic marls, which testify the acceleration of the flexural subsidence (Carminati et al., 2007), and then to siliciclastic turbidites. The age of the base of siliciclastics varies from the middle Tortonian to the early Messinian (Table S6.1).

6.5.1.5 South Majella and Mount Alpi

In the S Majella Mountains, the transgressive shallow-water carbonate unit covers a strongly bioeroded pre-orogenic Maastrichtian limestone substrate of the Apulian Carbonate Platform (e.g., Danese, 1999). Our SIS age for the basal levels of the syn-orogenic sequence at the Guado di Coccia site (Figs. 6.1, 6.3, 6.5A) is 8.4 Ma, which corresponds to the late Tortonian. An uppermost Tortonian-Messinian age was reported by Danese (1999), based on the presence of the nannofossil *Amaurolithus* sp. in the matrix of the basal bioclastic calcarenites levels. The SIS age is compatible with the biostratigraphic age if we consider the error band (7.1 - 9.4 Ma; Table 6.1). Moreover, the slight mismatch could be due to infiltration of a slightly younger matrix with nannoplankton into the biocalcarenite, for instance, from the overlying marly deposits. The shallow-water carbonate unit evolves upward to hemipelagic marls during the Messinian. The onset of the siliciclastic sedimentation is here dated as early Pliocene (Table S6.1).

Mount Alpi exposes an inner sector of the Apulian platform exhumed from underneath its tectonic cover of allochthonous Lagonegrese and Liguride Units in the axial zone of the Apennine belt (Fig. 6.1) (Mazzoli et al., 2006). In this site, syn-orogenic carbonate deposits overlie paranconformably pre-orogenic Lower Cretaceous carbonates (Vezzani et al., 2010; La Bruna et al., 2018). The age of the syn-orogenic deposition is constrained by the presence of *Turborotalia multiloba* and *Amaurolithus primus*, planktic and nannofossil assemblages, respectively, pointing to a latest Tortonian - early Messinian age (Taddei and Siano, 1992; Bonardi et al., 2016). The shallow-water carbonate deposits evolve to hemipelagic marls, which are overlaid by siliciclastic deposits. The age of the latter, albeit not well-constrained, is considered not older than late Messinian (Table S6.1).

6.5.1.6 Apulian foreland

The first syn-orogenic shallow-water carbonate rocks of the current Apulian Foreland onlap Upper Cretaceous pre-orogenic carbonates in the three isolated structural domains of Gargano, Murge, and Salento (Fig. 6.1, 6.5A) (Tropeano and Sabato, 2000). In response to the foreland flexural subsidence, these domains were progressively drowned (Iannone and Pieri, 1983), and the Murge and Salento domains became archipelagos (see fig. 2 in Pomar and Tropeano, 2001). The base of the shallow-water carbonate unit is attributed to the middle-late Pliocene in the NW sectors of the Apulia region (i.e., Gargano; Fig. 6.5A), due to the occurrence of *Globigerinoides obliquus extremus*, *Globigerina pachyderma*, *Globorotalia crassaformis*, and *G. hirsuta aemiliana*, included within the *Globorotalia margaritae* planktic zone (Moretti et al., 2011). Moving from NW to SE, toward the Murge and Salento areas, the same formation is dated progressively younger, until Calabrian (Fig. 6.5A), due to the presence of *Arctica islandica*, *Hyalinea baltica*, and *Globorotalia* *truncatulinoides* (Ricchetti and Ciaranfi, 2009). The onset of the siliciclastic deposition into the foredeep, which represents the current Adriatic-Bradanic Foredeep (Casnedi, 1988), spans from Pliocene to Holocene (Table S6.1).

The Apulian foreland is of particular interest since it represents the best modern analog of the Miocene paleotopography of the Apennines foreland region, strongly affected by inherited structures and newly forming foreland faults and fractures (e.g., La Bruna et al., 2018; Sabbatino et al., 2020). The modern Apulian foreland is characterized by a bulge of about 100 km wide with a height of 300 m on average (Fig. 6.5B). Such a complex topography is tectonically controlled (Fig. 6.5B) (e.g., Doglioni et al., 1994; Pieri et al., 1997; Billi and Salvini, 2002) and it has influenced the deposition of the Plio-Pleistocene foredeep depocenter as well (e.g., Pomar and Tropeano, 2002).

6.5.2 The flexural wave migration of the Apennine forebulge-foredeep

In figure 6.6 we integrate the above discussed newly presented high-resolution dataset on the age of the first deposits of the foreland basin with the previous knowledge on the whole central-southern Apennine foreland basin. In detail, figure 6.6B sums up, for different areas, the age of the distinct lithostratigraphic units of the underfilled foreland basin as listed by Sinclair (1997), i.e., (i) basal shallow-water carbonate unit, (ii) hemipelagic marl unit, and (iii) siliciclastic turbiditic unit, (iv) wedge-top sediments. In Figure 6.6C, these ages are plotted on a restored section of the Adria passive margin. For the sites located far away from the section (i.e., 3 to 7), the position has been projected based on the structural position within the thrust belt. This solution entails a significant but poorly constrained error for sites 3 to 7, which has been arbitrarily taken as 33% of the distance from the section. In addition to this error, the uncertainty on the age due to the scarce biostratigraphic resolution (affecting the age of the base of the turbidites) has to be taken into account. Despite all these issues, our reconstruction suggests that the migration velocity of the base of the syn-orogenic post-bulge shallow-water carbonate unit was almost constant in the last 25 Myr at nearly 15mm/yr. It is to note that the linear regression well fits the entire dataset, with the exception of point 6, which is however positioned more than 200 km away from the section trace, thus representing the less constrained part of the restored section.

6.5.2.1 Dating the forebulge emersion interval

Constraining directly the timing of forebulge migration would entail dating the continental red bed forebulge deposits, which is very challenging or even impossible in many cases, due to their absence. Accordingly, it is only possible to bracket the onset of the forebulge unconformity development, considering the youngest strata underlying the unconformity and the first Miocene shallow-water carbonates above the unconformity. This approach does not take into account the amount of erosion of the pre-orogenic substrate and introduces a great uncertainty, especially where the Miocene carbonate rocks sit directly on Cretaceous substratum. However, in several localities of the central-southern Apennines, Eocene strata are found beneath the unconformity, so it can be safely assumed that the onset of forebulge arching postdates the Eocene. In such cases the time span of passage of the forebulge would include all of the Oligocene plus the very earliest million or two million years of the Miocene (the SIS ages indicate max Miocene ages of 21.7 Ma, suggesting an age span of ca. 10-13 Myr). The time-span recorded by the forebulge unconformity can provide geodynamic information, because it records the time it took for the forebulge to pass a given location, which is related to the rheology of the foreland plate (Flemings and Jordan, 1990). The foreland lithosphere can be considered as an elastic plate responding to standard equations for flexure models (Turcotte and Schubert, 2006). Assuming for the Apennine an elastic plate thickness of 20 km and a flexural rigidity of ca. $6*10^{22}$ N m (Royden et al. 1987), it turns out a forebulge roughly

100-150 km wide and a few tens to a few hundred meters high. Dividing the width of the forebulge by the age span of the unconformity, provides a flexural wave velocity of ca. 7.5-15 mm/yr, fitting with the results presented above.

6.5.2.2 Onset of siliciclastic sedimentation vs flexuring

Figure 6.6C well illustrates the poorly organized trend of the younging of the base of the siliciclastic and wedge top deposits, until present considered indicative of the style and rate of foreland basin migration in the Apennines (e.g., Patacca and Scandone, 2007; Cosentino et al., 2010; Vezzani et al., 2010; Critelli et al., 2011; Vitale and Ciarcia, 2013). In fact, these deposits retrace the E-ward younging age of the base of the syn-orogenic post-bulge shallow-water carbonate unit, but significantly deviates from its linear trend. These differences are due to the fact that siliciclastic sediments do not testify the first phase of syn-orogenic sedimentation in the foreland, but rather the first siliciclastic input to the system, not necessarily related to the flexure itself (DeCelles, 2012) and subject to many different controls, including sediment routing. In particular, a few to several million years of geological history could get missed using the first arrival of siliciclastic sediments, since the siliciclastic rocks represent neither the base of the foredeep depozone nor the onset of syn-orogenic sedimentation. The arrival of siliciclastic sediments into the foredeep depozone, in fact, is driven by the rates of erosion and propagation of turbidite lobes longitudinally from the Apennine front or axially from far away sources (e.g., the Alps for the northern Apennines foredeep; Ricci Lucchi, 1986) and this can occur several million years after the onset of orogeny.

6.5.2.3 Base of the post-bulging carbonates as a proxy for the flexural wave

The earliest onset of syn-orogenic sedimentation occurs within the back-bulge depozone and subsequently within the forebulge depozone following a "flexural wave" pattern. In retreating collisional belts like the Apennines, in absence of a dynamic load (i.e., forearc settings), the forebulge and back-bulge depozones are generally poorly preserved or completely absent (DeCelles, 2012). In the central-southern Apennines, the back-bulge is indeed not preserved but a few meters of forebulge depozone are recorded in only a few sectors of the Apennine belt (Fig. 6.6A). Our computation of the bulge migration velocity, based on elastic parameters and on the age of forebulge unconformity (section 6.5.2.1), indicates a wave velocity of 7.5 to 15 mm/yr. This value is in agreement with the migration rate of the distal foredeep depozone, calculated from the age of first post-bulge carbonates, which represents to date the most reliable constraint on the velocity of flexural wave migration.

Shallow-water carbonates of the distal foredeep have already been successfully used in many other orogenic belts to derive a detailed record of the first phases of foreland basin evolution (Dorobek, 1995; Galewsky, 1998; Bosence, 2005). In this framework, here we have shown that central-southern Apennines offer a good example of ramp profiles on the foreland margin, characterized by backstepping geometries in front of positive and underfilled accommodation (Fig. 6.2) (Sinclair, 1997; Catuneanu et al., 2011). Such carbonate platform dynamics are particularly suitable to constrain the diachronous migration of an entire orogenic system, as demonstrated worldwide also for many other orogenetic systems such as the Alps (Allen et al., 1991; Sinclair, 1997), Pyrenees (Vergés et al., 1998), Taiwan (You and Chou, 2001), Timor Trough (Veevers, et al., 1978), Papuan Basin (Galewsky et al., 1996), and Zagros (Pirouz et al., 2017).

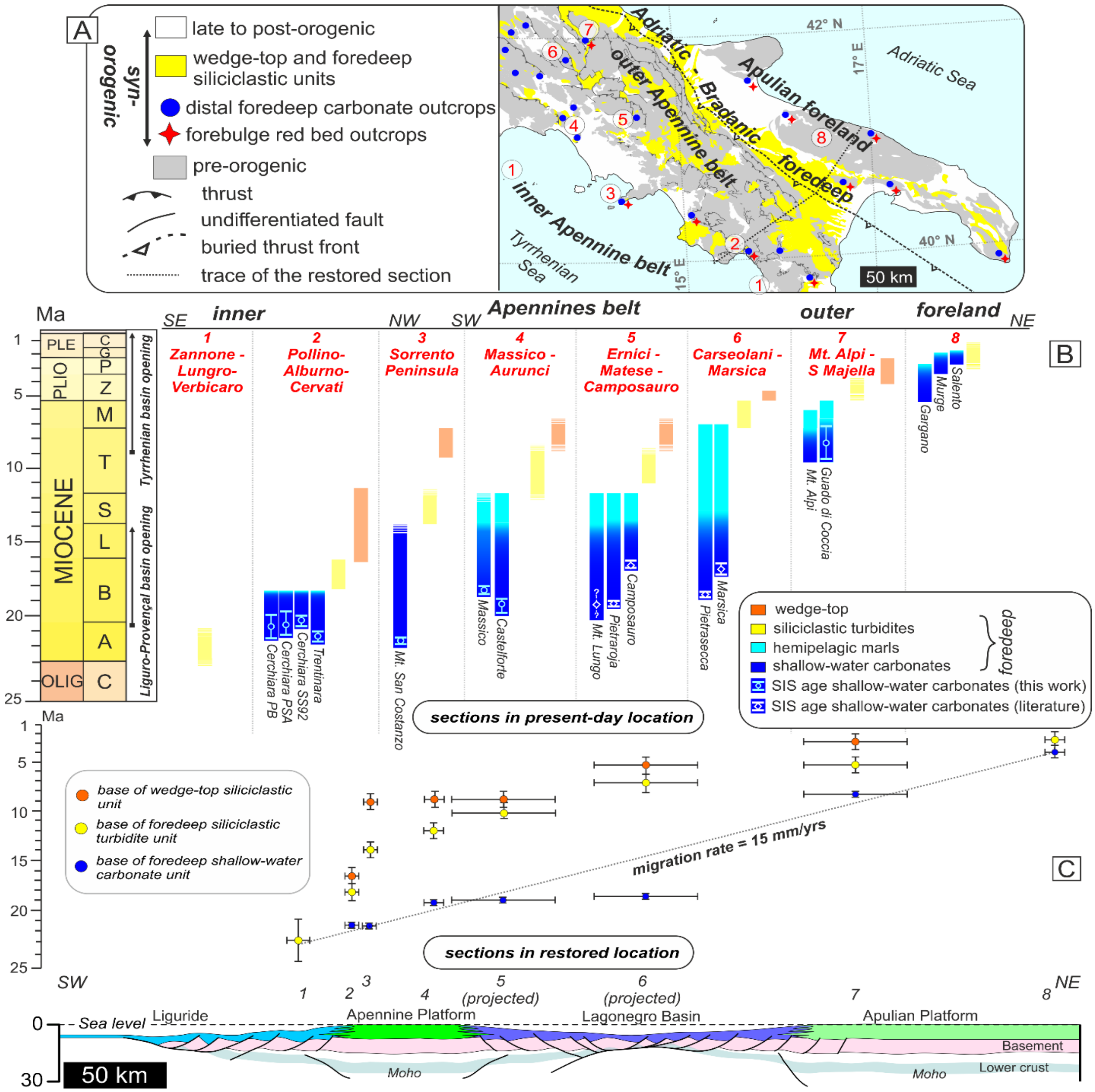

Figure 6.6. A) Simplified geological map of the central-southern Apennines summarizing the syn-orogenic deposits in the different sites of the thrust belt and foreland. B) Time framework for the evolution of the central-southern Apennine foreland basin. The ages of the first syn-orogenic deposits are constrained by high-resolution SIS (this work). The ages of the other lithostratigraphic units are constrained by biostratigraphy (taken from the literature). C) Ages of the base of the syn-orogenic lithostratigraphic units plotted on a restored section of the pre-orogenic Adria passive margin (modified after Tavani et al., 2021).

6.7. Conclusion

In this work we have provided a new high-resolution regional Sr isotope stratigraphy dataset for the base of the time-transgressive shallow-water carbonate unit at the bottom of the foreland basinal megasequence sealing the forebulge unconformity in the central-southern Apennines. Integration with previously published data on syn-orogenic sediments of the area demonstrates that, among the different lithostratigraphic units of the foreland megasequence, dating the base of the post-bulging carbonates is the best tool to constrain the style and rate of the foreland flexuring. Our newly presented dataset allowed us to constrain, with unprecedented resolution, the migration rate of the foreland system, which was nearly constantly 15mm/yr in the last 25 Myr interval.

6.8. Supplementary material

6.8.1 Supplementary Table S6.1.

Summary of the syn-orogenic lithostratigraphic units and formations of the central-southern Apennines.

Depozone	Lithostratigraphic unit	Location site	Formation	Biostratigraphic age	References
FOREDEEP	shallow-water carbonate unit	Pollino Mts.	*Cerchiara Formation*	Aquitanian - Burdigalian	Selli, 1957
		Alburno-Cervati Mts.	*Roccadaspide Formation*	Aquitanian - Burdigalian	Selli, 1957; Carannante et al., 1988
		Sorrento Peninsula	*Recommone Calcarenites*	Burdigalian - Langhian (?)	De Blasio et al., 1981
		Matese-Camposauro Mts.	*Cusano Formation*	Burdigalian - Langhian	Carannante et al., 1996
		Massico-Aurunci-Ernici-Carseolani-Marsica Mts.	*Bryozoan and Lithothamnium Limestone*	Burdigalian - Serravallian	Civitelli and Brandano, 2006
		Majella Mts.	*Lithothamnium Limestone*	Tortonian - Messinian	Patacca et al., 2008
		Mt. Alpi	*Lower Unit*	upper Tortonian (?) - Messinian	Sgrosso, 1988; Taddei and Siano, 1992; La Bruna et al., 2018
		Apulian foreland	*Gravina Calcarenite*	middle Pliocene - Pleistocene	Taddei, 1996; Ricchetti and Ciaranfi, 2009; Moretti et al., 2011
	hemipelagic marl unit	Matese-Camposauro Mts.	*Longano Formation*	Serravallian	Lirer et al., 2005
		Massico-Aurunci-Ernici-Carseolani-Marsica Mts.	*Orbulina Marls*	Serravallian - lower Messinian	Pampaloni et al., 1994
		Majella Mts.	*Turborotalia multiloba marls*	Messinian	Carnevale et al., 2011
		Mt. Alpi	*Upper Unit*	Messinian (?)	Sgrosso, 1988; Taddei and Siano, 1992; La Bruna et al., 2018
		Apulian foreland-Bradanic foredeep	*Subappeninic Clays*	Pliocene - Pleistocene	Casnedi, 1988; Pieri et al., 1996
	siliciclastic turbidite unit	Zannone Island	*Zannone Flysch*	Oligocene (?) - upper Aquitanian	Curzi et al., 2020
		Lungro-Verbicaro Mts.	*Scisti del Fiume Lao*	Aquitanian	Burton et al., 1971; Iannace et al., 2007; D'Errico and Di Stasio, 2010
		Pollino-Alburno-Cervati Mts.	*Bifurto Formation*	middle Burdigalian	Sgrosso et al., 2010
		Sorrento Peninsula	*Nerano-Termini Formation*	Serravallian	De Blasio et al., 1981
		Matese-Camposauro Mt.s	*Pietraroja Formation*	middle Tortonian	Selli, 1957; Lirer et al., 2005
		Aurunci-Ernici Mts.	*Frosinone Formation*	Tortonian	Cipollari and Cosentino, 1995
		Carseolani-Marsica Mts.	*Arenaceo-pelitica' Unit - Brecce della Renga*	Tortonian - Messinian	Cipollari and Cosentino, 1995; Fabbi and Rossi, 2014
		Majella Mts.	*Majella Flysch*	lower Pliocene	Cipollari et al., 2003
		Apulian foreland-Bradanic foredeep	*Subappenninic Clays*	Pliocene - Pleistocene	Casnedi, 1988; Pieri et al., 1996
WEDGE-TOP	clastic unit	Pollino-Alburno-Cervati Mts.	*Cilento Group - Albidona Formation*	uppermost Burdigalian - lowermost Tortonian	Bonardi et al., 1985; Amore et al., 1988
		Sorrento Peninsula	*Brecce Punta del Capo*	upper Tortonian	Iananace et al., 2015
		Matese-Camposauro-Massico Mts.	*Castelvetere Group*	upper Tortonian - lower Messinian	Patacca et al., 1992; Vitale et al., 2018, 2020
		Aurunci-Ernici Mts.	*Gavignano and Gorga Formation*	upper Tortonian - lower Messinian	Alberti et al., 1975
		Ernici-Simbruini Mts.	*Arenarie di Torrice - Argille con gessi*	Messinian	Cipollari and Cosentino, 1993
		Carseolani-Marsica Mts.	*Le Vicenne conglomerates*	late Messinian - early Pliocene	Cipollari et al., 1999
		Majella Mts.	*Castilenti Formation*	middle - late Pliocene	Cipollari et al., 2003

6.8.2 Supplementary Table S6.2

Geochemistry of the basal levels of the syn-orogenic carbonates in the studied localities. Pr = preserved, PA = partially altered, A = Altered.

Sample	Section locality	Latitude	Longitude	Material	Mg (ppm)	Sr (ppm)	Fe (ppm)	Mn (ppm)	$^{87}Sr/^{86}Sr$ (corrected)	2 se ($*10^{-6}$)	Preservation
FDC-PB1	Panno Bianco Mt	39°51'02''N	16°22'17''E	shell	344	3518	55	2	0.708364	5	PA
FDC-PB2	Panno Bianco Mt	39°51'02''N	16°22'17''E	shell	453	3980	180	3	0.708363	5	PA
FDC-PB3	Panno Bianco Mt	39°51'02''N	16°22'17''E	shell	1546	768	283	41	0.708395	5	Pr
FDC-PB4	Panno Bianco Mt	39°51'02''N	16°22'17''E	shell	1532	948	230	36	0.708395	6	Pr
FDC-PB5	Panno Bianco Mt	39°51'02''N	16°22'17''E	matrix bulk	2576	304	1618	111	0.708212	6	
FDC-PB6	Panno Bianco Mt	39°51'02''N	16°22'17''E	shell	634	3087	70	11	0.708334	4	A
FDC-PB7	Panno Bianco Mt	39°51'02''N	16°22'17''E	shell	1046	663	99	58	0.708345	11	A
FDC-PB8	Panno Bianco Mt	39°51'02''N	16°22'17''E	matrix bulk	1323	484	202	91	0.708247	6	
FDC-PB9	Panno Bianco Mt	39°51'02''N	16°22'17''E	shell	1610	286	346	1191	0.708361	10	PA
FDC-PB10	Panno Bianco Mt	39°51'02''N	16°22'17''E	shell	2787	2666	75	279	0.708389	5	Pr
FDC-PB11	Panno Bianco Mt	39°51'02''N	16°22'17''E	shell	1762	770	147	87	0.708380	6	Pr
FDC-PB12	Panno Bianco Mt	39°51'02''N	16°22'17''E	shell	337	2783	37	8	0.708379	4	PA
FDC-PB13	Panno Bianco Mt	39°51'02''N	16°22'17''E	matrix bulk	2874	491	430	149	0.708278	7	A
FDC-PB14	Panno Bianco Mt	39°51'02''N	16°22'17''E	shell	1112	779	97	36	0.708402	4	Pr
FDC-PB15	Panno Bianco Mt	39°51'02''N	16°22'17''E	shell	2656	739	572	180	0.708385	5	Pr
FDC-PSA17	Pietra S. Angelo Mt	39°52'31''N	16°21'03''E	shell	1516	694	78	25	0.708405	6	A
FDC-PSA18	Pietra S. Angelo Mt	39°52'31''N	16°21'03''E	shell	2064	788	219	32	0.708377	7	PA
FDC-PSA19	Pietra S. Angelo Mt	39°52'31''N	16°21'03''E	shell	2300	1154	694	37	0.708345	7	A
FDC-PSA22	Pietra S. Angelo Mt	39°52'31''N	16°21'03''E	matrix bulk	2201	586	492	146	0.708285	7	
FDC-PSA20	Pietra S. Angelo Mt	39°52'31''N	16°21'03''E	shell	3719	2073	961	314	0.708402	5	Pr
FDC-PSA21	Pietra S. Angelo Mt	39°52'31''N	16°21'03''E	shell	1484	852	598	49	0.708408	5	Pr
FDC-SS22	SS92 Cerchiara	39°52'11''N	16°22'08''E	shell	867	690	118	23	0.708412	7	Pr
FDC-SS23	SS92 Cerchiara	39°52'11''N	16°22'08''E	shell	1779	267	647	77	0.708426	15	A
FDC-SS24	SS92 Cerchiara	39°52'11''N	16°22'08''E	shell	1400	442	157	78	0.708438	9	PA
FDC-SS25	SS92 Cerchiara	39°52'11''N	16°22'08''E	matrix bulk	3038	243	587	124	0.708376	11	
FDC-SS26	SS92 Cerchiara	39°52'11''N	16°22'08''E	shell	1709	750	320	37	0.708430	5	Pr
FDR-TR1	Trentinara	40°23'55''N	15°07'26''E	shell	2421	947	433	365	0.708308	4	A
FDR-TR2	Trentinara	40°23'55''N	15°07'26''E	shell	1986	797	253	327	0.708335	6	PA
FDR-TR3	Trentinara	40°23'55''N	15°07'26''E	shell	1614	717	472	199	0.708337	6	PA
FDR-TR4	Trentinara	40°23'55''N	15°07'26''E	shell	1289	853	237	130	0.708350	6	PA
FDR-TR5	Trentinara	40°23'55''N	15°07'26''E	shell	1296	866	319	286	0.708373	6	PA
FDR-TR6	Trentinara	40°23'55''N	15°07'26''E	shell	1075	908	134	150	0.708362	6	A
FDR-TR7	Trentinara	40°23'55''N	15°07'26''E	matrix bulk	3588	290	2047	376	0.708033	6	
FDR-TR8	Trentinara	40°24'39''N	15°06'13''E	shell	2107	892	646	1970	0.708378	7	Pr
FDR-TR9	Trentinara	40°24'39''N	15°06'13''E	shell	1048	834	617	997	0.708377	8	PA
FDR-TR10	Trentinara	40°24'39''N	15°06'13''E	shell	1479	929	647	1210	0.708378	7	Pr
FDR-TR11	Trentinara	40°24'39''N	15°06'13''E	matrix bulk	4534	324	3246	5330	0.708370	10	
CDR-MSC1	Mt. San Costanzo	40°24'39''N	15°06'13''E	shell	1382	378	30	11	0.708346	10	Pr
CDR-MSC2	Mt. San Costanzo	40°24'39''N	15°06'13''E	shell	1238	392	33	9	0.708330	6	Pr

Sample	Section locality	Latitude	Longitude	Material	Mg (ppm)	Sr (ppm)	Fe (ppm)	Mn (ppm)	$^{87}Sr/^{86}Sr$ (corrected)	2 se ($*10^{-6}$)	Preservation
CDR-MSC3	Mt. San Costanzo	40°24'39''N	15°06'13''E	shell	1066	403	18	8	0.708329	10	Pr
CDR-MSC4	Mt. San Costanzo	40°24'39''N	15°06'13''E	shell	1207	501	5	6	0.708333	7	Pr
CDR-MSC5	Mt. San Costanzo	40°24'39''N	15°06'13''E	shell	1761	301	19	12	0.708296	10	PA
CDR-MSC6	Mt. San Costanzo	40°24'39''N	15°06'13''E	matrix bulk	2504	195	466	12	0.707873	7	
CDR-RE7	Recommone	40°35'03"N	14°21'54"E	shell	1309	358	53	10	0.708340	6	PA
CDR-RE8	Recommone	40°35'03"N	14°21'54"E	shell	1643	360	26	17	0.708260	6	A
CDR-RE9	Recommone	40°35'03"N	14°21'54"E	matrix bulk	3649	562	359	36	0.708126	6	A
CDR-RE10	Recommone	40°35'03"N	14°21'54"E	shell	2481	412	463	12	0.708245	8	PA
CDR-RE11	Recommone	40°35'03"N	14°21'54"E	shell	1167	488	19	8	0.708223	9	A
CDR-RE12	Recommone	40°35'03"N	14°21'54"E	matrix bulk	2155	250	1006	14	0.707739	10	A
CDR-RE13	Recommone	40°35'03"N	14°21'54"E	shell	2418	356	335	12	0.708192	12	A
CDR-RE14	Recommone	40°35'03"N	14°21'54"E	shell	2909	200	552	13	0.708055	6	A
CDR-RE15	Recommone	40°35'03"N	14°21'54"E	shell	1469	420	40	12	0.708247	8	A
CDR-RE16	Recommone	40°35'03"N	14°21'54"E	shell	1696	390	55	11	0.708283	6	PA
CDR-RE17	Recommone	40°35'03"N	14°21'54"E	shell	1979	382	52	13	0.708237	8	PA
CDR-RE18	Recommone	40°35'03"N	14°21'54"E	shell	1187	472	35	7	0.708314	10	PA
CDR-RE19	Recommone	40°35'03"N	14°21'54"E	shell	1457	433	46	10	0.708297	8	PA
CDR-RE20	Recommone	40°35'03"N	14°21'54"E	shell	1715	777	588	8	0.707596	6	A
CDR-RE21	Recommone	40°35'03"N	14°21'54"E	matrix bulk	2866	207	911	13	0.708001	6	
CU-MA1	Massico	41°10'0''N	13°53'30''E	shell	2455	497	120	26	0.708568	8	PA
CU-MA2	Massico	41°10'0''N	13°53'30''E	shell	1197	682	115	8	0.708586	8	Pr
CU-MA3	Massico	41°10'0''N	13°53'30''E	shell	1707	527	75	10	0.708607	7	PA
CU-MA4	Massico	41°10'0''N	13°53'30''E	matrix bulk	2849	505	247	15	0.708572	6	
CBL-CA1	Castelforte	41°17'53"N	13°49'53"E	shell	1784	362	2793	42	0.708504	5	Pr
CBL-CA2	Castelforte	41°17'53"N	13°49'53"E	matrix bulk	3802	250	335	7	0.708454	5	
CBL-CA3	Castelforte	41°17'53"N	13°49'53"E	matrix bulk	2949	250	224	109	0.708628	5	
CL-MAJ1	Guado di Coccia	42° 0'8"N	14° 4'58"E	shell	3233	768	34	40	0.708867	6	PA
CL-MAJ2	Guado di Coccia	43° 0'8"N	15° 4'58"E	shell	2429	690	35	53	0.708887	4	PA
CL-MAJ3	Guado di Coccia	44° 0'8"N	16° 4'58"E	shell	2374	738	40	33	0.708927	5	Pr
CL-MAJ4	Guado di Coccia	45° 0'8"N	17° 4'58"E	matrix bulk	22930	347	269	126	0.708585	5	PA
CL-MAJ5	Guado di Coccia	46° 0'8"N	18° 4'58"E	shell	959	708	59	22	0.708930	5	Pr
CL-MAJ6	Guado di Coccia	47° 0'8"N	19° 4'58"E	shell	1587	783	40	31	0.708920	5	Pr
CL-MAJ7	Guado di Coccia	48° 0'8"N	20° 4'58"E	shell	5889	400	254	147	0.708786	5	PA
CL-MAJ8	Guado di Coccia	49° 0'8"N	21° 4'58"E	matrix bulk	4397	293	218	160	0.708767	6	

[a] Sr isotope ratios measured in the lab have been corrected for interlaboratory bias; see the methods section of the text for further explanations.

6.8.3 Supplementary Table S6.3.

Samples and their mean values used for Strontium Isotope Stratigraphy.

Sample	Section locality	$^{87}Sr/^{86}Sr$ †	2 se (*10^{-6})	$^{87}Sr/^{86}Sr$ mean	2 se (*10^{-6})	numerical age (Ma) ‡		
						min	mean	max
FDC-PB3	Panno Bianco	0.708395	5	0.708389	0.000008	20.7	20.8	21
FDC-PB4		0.708395	6					
FDC-PB11		0.708380	6					
FDC-PB15		0.708385	5					
FDC-PSA17	Pietra Sant'Angelo	0.708405	6	0.708405	0.000022	20.2	20.6	21
FDC-SS22	SS92 Cerchiara	0.708412	7	0.708427	0.000011	20.1	20.3	20.5
FDC-SS23		0.708426	15					
FDC-SS24		0.708438	9					
FDC-SS26		0.708430	5					
FDR-TR2	Trentinara	0.708335	6	0.708341	0.000009	21.4	21.6	21.8
FDR-TR3		0.708337	6					
FDR-TR4		0.708350	6					
FDR-TR8		0.708378	7	0.708378	0.000008	20.8	21	21.2
FDR-TR9		0.708377	8					
FDR-TR10		0.708378	7					
CDR-MSC1	Mt. San Costanzo	0.708346	10	0.708335	0.000008	21.5	21.7	21.9
CDR-MSC2		0.708330	6					
CDR-MSC3		0.708329	10					
CDR-MSC4		0.708333	7					
CU-MA1	Massico	0.708568	8	0.708577	0.000018	17.9	18.3	18.5
CU-MA2		0.708586	8					
CBL-CA1	Castelforte	0.708504	5	0.708504	0.000031	18.7	19.2	19.7
CL-MAJ3	Guado di Coccia	0.708927	5	0.708926	0.000018	7.1	8.4	9.4
CL-MAJ5		0.708930	5					
CL-MAJ6		0.708920	5					

† Sr isotope ratios measured in the lab have been corrected for interlaboratory bias; see the methods section of the text for further explanations.

‡ The preferred numerical age has been derived from the look-up table of MacArthur et al. (2020, version 6: 03/20). The minimum and max age are calculated by combining the statistical uncertainty of the samples (2 se of the mean) with the uncertainty of the reference curve (see the methods section in Frijia et al., 2015, for a detailed explanation of the procedure).

6.8.4 Supplementary material S6.4

6.9.4.1. Diagenetic screening

The diagenetic screening followed the procedure described in Frijia and Parente (2008), Frijia et al. (2015), and Sabbatino et al. (2020), i.e. combining petrographic observation of the shell microstructure with the analysis of the geochemical composition of the different components (well-preserved shells, altered shells and bulk matrix), and assessing the internal consistency of the Sr isotope ratios of different shells from the same stratigraphic level. See the table S6.2 and S6.3 for the complete details.

6.8.4.2. Analytical procedures

The samples used for this work were analyzed over a period of about 2 years from 2017 to 2019.

6.9.4.2.1 Minor and trace elements concentration

The first batch of samples (FDC-PB1 to FDC-PB5, and CDR-RE7 to CDR-RE21, FDC-PB14 and FDC-PB15, FDC-PSA20 and FDC-PSA21, FDC-SS26; FDR-TR1 to FDR-TR11, CDR-MSC1 to CDR-MSC6, CU-MA1 to CU-MA4, CBL-CA1 to CBL-CA3, and CL-MAJ1 to CL-MAJ8) was analyzed at the Institut für Geologie, Mineralogie und Geophysik of the Ruhr-Universität of Bochum. An aliquot of the carbonate powder was dissolved in 1 ml 3 M HNO_3 and then diluted with 2 ml H_2O for analysis with a Thermo Fisher Scientific iCAP6500 Dual View inductively coupled plasma optical emission spectroscopy (ICP-OES). The external reproducibility, expressed as relative standard deviation (RDS), is ±1% of the measured concentrations for Mg and Sr, ± 2% for Mn and ± 5.6% for Fe.

The second batch of samples (FDC-PB6 to FDC-PB13; FDC-PSA17 to 19; FDC-SS22-25) was analyzed at the Department of Chemistry and Earth Science of the University of Modena and Reggio Emilia. An aliquot of each sample was dissolved in 4 ml 3 M HNO_3 and then diluted with 1 ml H_2O for elemental concentration determination using a Perkin Elmer Optima 4200 DV ICP-OES. Each sample was analyzed three times and precisions were typically better than 5% RSD for Mg, Sr, and Fe and better than 20% for Mn.

6.8.4.2.2 Sr-isotope ratio analysis

The strontium isotope ratio was analyzed on a split of the same samples analyzed for elemental concentrations after separation of Sr with standard ion-exchange separation methods.

Two batches of samples (1. FDC-PB1 to FDC-PB5 and CDR-RE7 to CDR-RE9; 2. FDC-PB14 and FDC-PB15, FDC-PSA20 and FDC-PSA21, FDC-SS26;

FDR-TR1, CU-MA1 to CU-MA4, CBL-CA1 to CBL-CA3, and CL-MAJ1 to CL-MAJ8) were analyzed with a Finnigan MAT 262 thermal ionization mass spectrometer (TIMS) at the Institut für Geologie, Mineralogie und Geophysik of the Ruhr-Universität of Bochum. $^{87}Sr/^{86}Sr$ ratios were normalized to an $^{86}Sr/^{88}Sr$ value of 0.1194. The long term mean of NIST SRM 987 at Bochum laboratory was 0.710240 ± 0.000002 (2 s.e., n= 386) for the first batch of analyses and 0.710247 ± 0.000001 (2 s.e., n= 488) for the second one. The $^{87}Sr/^{86}Sr$ ratios of the samples have been corrected for the inter-laboratory bias by adjusting the long term mean value of NIST SRM 987 at Bochum laboratory to the value of 0.710248 used by McArthur et al. (2020) for the compilation of the ‘‘look-up’’ table.

A second group of samples (FDC-PB6 to FDC-PB13; FDC-PSA17 to 19; FDC-SS22-25) was analyzed by means of a Thermo Scientific Neptune high-resolution multi-collector inductively coupled plasma mass spectrometer (MC-ICP-MS) at the Centro Interdipartimentale Grandi Strumenti of the University of Modena and Reggio. The Sr-isotope values were determined following the same procedure reported by Vescogni et al. (2014) and the samples were run using a bracketing sequence blank-standard-blank-sample-blank to correct for possible instrumental drifts. The samples were analyzed in two analytical sessions where the mean value of the NIST SRM 987 standards run together with the samples were 0.710218 ± 0.000012 (2 s.e., n= 3) and 0.710252 ± 0.000007 (2 s.e., n= 8). The $^{87}Sr/^{86}Sr$ ratios of the samples were first corrected from isobaric interferences of 86Kr and 87Rb on ^{86}Sr and ^{87}Sr, and then adjusted to the value of 0.710248 of NIST SRM 987 (McArthur et al., 2020) by multiplying each Sr-isotope ratio for the C-factor value calculated dividing the measured isotope ratio by the average value of the two standards measured before and after each sample in the bracketing sequence.

A third group of Sr-isotopes measurements were obtained with a Thermo Fisher Triton multi-collector TIMS housed at the National Institute of

Geophysics and Volcanology, Vesuvius Observatory (INGV-OV) in Naples in two periods.

The $^{87}Sr/^{86}Sr$ ratios of the samples have been corrected for the inter-laboratory bias by adjusting the long term mean value of NIST SRM 987 at Bochum laboratory to the value of 0.710248 used by McArthur et al. (2020) for the compilation of the ‘‘look-up’’ table.

The long term mean of NIST SRM 987 at INGV-OV laboratory was 0.710244 ± 0.000006 (2 s.e., n=55) for a period and 0.710266 ± 0.000007 (2 s.e., n=37) for a second period. The $^{87}Sr/^{86}Sr$ ratios of the samples have been corrected for the inter-laboratory bias by adjusting the long term mean values of NIST SRM 987 at INGV-OV laboratory to the value of 0.710248 used by McArthur et al. (2020) for the compilation of the look-up table.

6.9 Disclosure

The present form of this chapter is currently under review in Basin Research. The final version in its published form may vary accordingly.

CONCLUDING REMARKS

This research has provided a new high-resolution regional Sr-isotope stratigraphy dataset for the base of the time-transgressive shallow-water carbonate unit at the bottom of the foreland basinal megasequence sealing the forebulge unconformity in the central-southern Apennines. These strata represent the onset of flexural subsidence in a given location, that, in absence of records of the earliest syn-orogenic back-bulge depozone, represent the base of the foreland basin mega-sequence of the central-southern Apennines.

Additionally, I have reported on red beds followed by very proximal marine or paralic deposits with rich assemblages of *Ammonia*. This more complete record of the transition from the forebulge depozone to the first stage of the syn-orogenic transgression in the distal foredeep depozone is preserved only in a few localities of the southern and central Apennines. To date, the early evolutionary stage in the syn-orogenic history of the central-southern Apennines had not been investigated in detail and this research project has contributed to fill this gap.

Integration with previously published data on syn-orogenic sediments of the central-southern Apennines demonstrates that, among the different lithostratigraphic units of the foreland megasequence, dating the base of the post-bulging carbonates is the best tool to constrain the style and rate of the foreland flexuring.

This newly presented dataset allows to constrain, with unprecedented resolution, the migration rate of the foreland system, which was nearly constantly 15mm/yr in the last 25 Myr interval.

Ultimately, the workflow used in this study could be applied to other fold and thrust belts where subaerial exposure has produced an incomplete record of the transition from bulging to foredeep.

BIBLIOGRAPHY

Accordi, G., & Carbone, F. (1988). Lithofacies map of Latium-Abruzzi and neighbouring areas. Scale 1:250000. *Quaderni Della Ricerca Scientifica*, *114*, 11–89.

Alavi, M. (2004). Regional stratigraphy of the Zagros fold-thrust belt of Iran and its proforeland evolution. *American Journal of Science*, *304*(1), 1–20. https://doi.org/10.2475/ajs.304.1.1

Alberti, A., Bergomi, C., Catenacci, V., Centamore, E., Cestar, G., Chiocchini, M., Chiocchini, U., Manganelli, V., & Tilia Zuccari, A. (1975). *Note illustrative della carta geologica d'Italia alla scala 1:50.000 Foglio 389 Anagni*. *Servizio Geologico d'Italia, ISPRA*.

Ali, M. Y., & Watts, A. B. (2009). Subsidence history, gravity anomalies and flexure of the United Arab Emirates (UAE) foreland basin. *GeoArabia*, *14*(2), 17–44.

Allen, P. A., Homewood, P., & Williams, G. D. (1986). Foreland basins: an introduction. In *Foreland basins, Inter. Assoc. Sediment., Spec. Pub.*, 8, pp. 3-12.

Allen, P. A., Crampton, S. L., & Sinclair, H. D. (1991). The inception and early evolution of the north Alpine foreland basin, Switzerland. *Basin Research*, *3*(3), 143–163. https://doi.org/10.1111/j.1365-2117.1991.tb00124.x

Almogi-Labin, A., Perelis-Grossovicz, L., & Raab, M. (1992). Living Ammonia from a hypersaline inland pool, Dead Sea area, Israel. *The Journal of Foraminiferal Research*, *22*(3), 257–266.

Alonso-Zarza, A. M., & Wright, V. P. (2010). Calcretes. *Developments in Sedimentology*, *61*, 225–267.

Amore, F. O., Bonardi, G., Ciampo, G., De Capoa, P., & Perrone, V. (1988). Relazioni tra Flysch interni e domini Appenninici: Reinterpretazione delle formazioni di Pollica, San Mauro e Albidona e il problema dell'evoluzione inframiocenica delle zone esterne Appenniniche. *Memorie Della Società Geologica Italiana*, *41*, 285–297.

Ascione, A., Ciarcia, S., Di Donato, V., Mazzoli, S., & Vitale, S. (2012). The Pliocene-Quaternary wedge-top basins of southern Italy: an expression of propagating lateral slab tear beneath the Apennines. *Basin Research*, *24*(4), 456–474. https://doi.org/10.1111/j.1365-2117.2011.00534.x

Babić, L., & Zupani, J. (2008). Evolution of a river-fed foreland basin fill: The north dalmatian flysch revisited (Eocene, Outer Dinarides). *Natura Croatica*, *17*(4), 357–374.

Babić, L., & Zupanič, J. (2012). Laterally variable development of a basin-wide transgressive unit of the North Dalmatian Foreland Basin (Eocene, Dinarides, Croatia). *Geologia Croatica*, *65*(1), 1–28. https://doi.org/10.4154/gc.2012.01

Baldi, K., & Hohenegger, J. (2008). Paleoecology of benthic foraminifera of the Baden-Sooss section (Badenian, Middle Miocene, Vienna Basin, Austria). *Geologica Carpathica*, *59*(5), 411–424.

Barbera, C., Carannante, G., D'argenio, B., & Simone, L. (1980). Il Miocene calcareo dell'Appennino Meridionale: contributo della paleoecologia alla costruzione di un modello ambientale. *Annali Università Di Ferrara (NS), Sez. IX*, *6*, 281–289.

Barbin, V. (2000). Cathodoluminescence of Carbonate Shells: Biochemical vs Diagenetic Process. In *Cathodoluminescence in Geosciences* (pp. 303–329). Springer. https://doi.org/10.1007/978-3-662-04086-7_12

Baruffini, L., Lottaroli, F., Torricelli, S., & Lazzari, D. (2000). Stratigraphic revision of the Eocene Albidona Formation in the type locality (Calabria, Southern Italy). *Rivista Italiana Di Paleontologia e Stratigrafia (Research In Paleontology and Stratigraphy)*, *106*(1). https://doi.org/10.13130/2039-4942/5391

Bassi, D., Carannante, G., Checconi, A., Simone, L., & Vigorito, M. (2010). Sedimentological and palaeoecological integrated analysis of a Miocene channelized carbonate margin, Matese Mountains, Southern Apennines, Italy. *Sedimentary Geology*, *230*(3–4), 105–122. https://doi.org/10.1016/j.sedgeo.2010.07.002

Benedetti, A., Consorti, L., Schlagintweit, F., & Rashidi, K. (2020). Ornatorotalia pila n. sp. from the late Palaeocene of Iran: ecological, evolutionary and paleobiogeographic inferences. *Historical Biology*, 1–8.

Bernoulli, D. (2001). Mesozoic-Tertiary carbonate platforms, slopes and basins of the external Apennines and Sicily. In *Anatomy of an Orogen: the Apennines and Adjacent Mediterranean Basins* (pp. 307–325). Dordrecht: Springer Netherlands. https://doi.org/10.1007/978-94-015-9829-3_18

Bianca, M., Festa, A., Mammino, P., & Monaco, C. (2009). Geological Map of Italy, scale 1: 50000, sheet 535 (Trebisacce). ISPRA, Rome. In *Geological Map of Italy, scale 1: 50000, sheet 535 (Trebisacce). ISPRA, Rome* (p. 104).

Bigi, S., Milli, S., Corrado, S., Casero, P., Aldega, L., Botti, F., Moscatelli, M., Stanzione, O., Falcini, F., Marini, M., & Cannata, D. (2009). Stratigraphy, structural setting and burial history of the Messinian Laga basin in the context of Apennine foreland basin system. *Journal of Mediterranean Earth Sciences*, *1*(2009), 61–84. https://doi.org/10.3304/JMES.2009.006

Billi, A., Porreca, M., Faccenna, C., & Mattei, M. (2006). Magnetic and structural constraints for the noncylindrical evolution of a continental forebulge (Hyblea, Italy). *Tectonics*, *25*(February 2005), 1–15. https://doi.org/10.1029/2005TC001800

Billi, A., & Salvini, F. (2003). Development of systematic joints in response to flexure-related fibre stress in flexed foreland plates: the Apulian forebulge case history, Italy. *Journal of Geodynamics*, *36*(4), 523–536. https://doi.org/10.1016/S0264-3707(03)00086-3

Billman, H. (1980). Neogene to Recent rotaliid Foraminifera from the Indo-Pacific Ocean: their canal system, their classification and their stratigraphic use.

Bonardi, G., Cinque, A., De Capoa, P., Di Staso, A., Esposito, P., Guida, D., Mazzoli, S., Parente, M., Radoičić, R., Sgrosso, A., Siervo, V., & Zamparelli, V. (2016). *Note illustrative della Carta Geologica d'Italia alla scala 1: 50.000 - Foglio 521 "Lauria." Servizio Geologico d'Italia, ISPRA*.

Bonardi, G., Ciarcia, S., Di Nocera, S., Matano, F., Sgrosso, I., & Torre, M. (2009). Carta delle principali unità cinematiche dell'appennino meridionale. nota illustrative. *Bollettino Della Società Geologica Italiana*, *128*(1), 47–60.

Bonardi, G., Perrone, V., Ciampo, G., & Perrone, V. (1985). La Formazione di Albidona nell'Appennino calabro-lucano: ulteriori dati stratigrafici e relazioni con le unità esterne appenniniche. *Boll. Soc. Geol. It.*, *104*, 539–549.

Boni, M. (1974). Le argille rosse continentali del passaggio Paleocene-Miocene nella piattaforma carbonatica campano-lucana. *Bollettino Della Societa Geologica Italiana*, *93*(4), 1059–1094.

Boni, M., Stanzione, D., & Zenone, F. (1978). I depositi argillosi dal Cretacico Superiore al Miocene Inferiore nella piattaforma carbonatica Campano-Lucana: variazione mineralogiche ed evoluzione paleoambientale. *Rend. Acc. Sci. Fis. Mat., Soc. Naz. Sci. Lett. Arti Nap*, *45*(4), 1–21.

Boonstra, M., Ramos, M. I. F., Lammertsma, E. I., Antoine, P. O., & Hoorn, C. (2015). Marine connections of Amazonia: Evidence from foraminifera and dinoflagellate cysts (early to middle Miocene, Colombia/Peru). *Palaeogeography, Palaeoclimatology, Palaeoecology*, *417*, 176–194.

Boote, D. R. D., Mou, D., & Waite, R. I. (1990). Structural evolution of the Suneinah Foreland, Central Oman Mountains. *Geological Society Special Publication*, *49*(49), 397–418. https://doi.org/10.1144/GSL.SP.1992.049.01.25

Bosellini, A. (2004). The western passive margin of Adria and its carbonate platforms. In *Special volume of the Italian Geological Society for the IGC* (pp. 79–92).

Bosellini, A. (2002). Dinosaurs “re-write” the geodynamics of the eastern Mediterranean and the paleogeography of the Apulia Platform. *Earth-Science Reviews*, *59*(1–4), 211–234.

Bosence, D. (2005). A genetic classification of carbonate platforms based on their basinal and tectonic settings in the Cenozoic. *Sedimentary Geology*, *175*(1-4 SPEC. ISS.), 49–72. https://doi.org/10.1016/j.sedgeo.2004.12.030

Bradley, D. C., & Kidd, W. S. F. (1991). Flexural extension of the upper continental crust in collisional foredeeps. *Geological Society of America Bulletin*, *103*(11), 1416–1438. https://doi.org/10.1130/0016-7606(1991)103<1416:FEOTUC>2.3.CO;2

Bradshaw, J. S. (1961). Laboratory experiments on the ecology of foraminifera. *Cushman Foundation for Foraminiferal Research Contributions*, *12*, 87–106.

Brandano, M. (2017). Unravelling the origin of a Paleogene unconformity in the Latium-Abruzzi carbonate succession: A shaved platform. *Palaeogeography, Palaeoclimatology, Palaeoecology*, *485*, 687–696. https://doi.org/10.1016/j.palaeo.2017.07.025

Brandano, M., & Corda, L. (2002). Nutrients, sea level and tectonics: constrains for the facies architecture of a Miocene carbonate ramp in central Italy. *Terra Nova*, *14*(4), 257–262. https://doi.org/10.1046/j.1365-3121.2000.00419.x

Brandano, M., Corda, L., & Castorina, F. (2012). Facies and Sequence Architecture of a Tropical Foramol-Rhodalgal Carbonate Ramp: Miocene of the Central Apennines (Italy). In *Carbonate Systems during the Oligocene-Miocene Climatic Transition* (pp. 107–127). Oxford, UK: Wiley-Blackwell. https://doi.org/10.1002/9781118398364.ch7

Brandano, M., Cornacchia, I., & Tomassetti, L. (2017a). Global versus regional influence on the carbonate factories of Oligo-Miocene carbonate platforms in the Mediterranean area. *Marine and Petroleum Geology*, 87, 188–202. https://doi.org/10.1016/j.marpetgeo.2017.03.001

Brandano, M., Cornacchia, I., Raffi, I., Tomassetti, L., & Agostini, S. (2017b). The Monterey Event within the Central Mediterranean area: The shallow-water record. *Sedimentology*, *64*(1), 286–310. https://doi.org/10.1111/sed.12348

Brandano, M., Giannini, E., Schiavinotto, F., & Verrubbi, V. (2007). Miogypsina Globulina (Michelotti) From Lower Miocene Villa S . Lucia Section (M.Te Cairo - Central Apennines). *Geologica Romana*, *40*, 119–127.

Brandano, M., & Policicchio, G. (2012). Strontium stratigraphy of the Burdigalian transgression in the Western Mediterranean. *Lethaia*, *45*(3), 315–328. https://doi.org/10.1111/j.1502-3931.2011.00285.x

Burton, A. N. (Compiler). (1971). *Carta Geologica della Calabria, scale 1:25000, sheets 228–229*. (R. Cassa per il Mezzogiorno, Ed.).

Cahuzac, B., & Poignant, A. (1997). An attempt of biozonation of the Oligo-Miocene in the European basins, by means of larger neritic foraminifera. *Bulletin de La Societe Geologique de France*, *168*(2), 155–169.

Calabrò, R. A., Corrado, S., Di Bucci, D., Robustini, P., & Tornaghi, M. (2003). Thin-skinned vs. thick-skinned tectonics in the Matese Massif, Central-Southern Apennines (Italy). *Tectonophysics*, *377*(3–4), 269–297. https://doi.org/10.1016/j.tecto.2003.09.010

Cann, J. H., & De Deckker, P. (1981). Fossil Quaternary and living foraminifera from athalassic (non-marine) saline lakes, southern Australia. *Journal of Paleontology*, 660–670.

Carannante, G., Cesarano, M., Pappone, G., & Putignano, M. L. (2013). Illustrative Notes of the Geological Map of Italy, scale 1:50000, sheet 431 (Caserta est). ISPRA, Rome. In *Illustrative Notes of the Geological*

Map of Italy, scale 1:50000, sheet 431 (Caserta est). ISPRA, Rome (p. 140).

Carannante, G. (1982). La Valle del Canale (Civita di Pietraroia, Matese) una incisione miocenica riesumata sul margine della piattaforma carbonatica abruzzese-campana. *Geologica Romana*, *21*, 511–521.

Carannante, G, Esteban, M., Milliman, J. D., & Simone, L. (1988a). Carbonate lithofacies as paleolatitude indicators: problems and limitations. *Sedimentary Geology*, *60*(1–4), 333–346.

Carannante, G, Matarazzo, R., Pappone, G., Severi, C., & Simone, L. (1988b). Le calcareniti mioceniche della Formazione di Roccadaspide (Appennino campano-lucano). *Mem. Soc. Geol. It*, *41*, 775–789.

Carannante, G, & Vigorito, M. (2001). A channelized temperate-type carbonate margin: geometries and controlling factors. *Géologie Méditerranéenne*, *28*, 41–44.

Carannante, G., & Simone, L. (1996). Rhodolith facies in the central-southern Apennines mountains, Italy.

Carboni, M. G., Civitelli, G., Corda, L., Esu, D., Matteucci, R., & Palagi, I. (1992). Evoluzione delle facies e delle comunità bentoniche dal continentale al marino del Miocene superiore della valle del fiume Aventino. In *Proceedings of the Libro-Guida Delle Escursioni. Quinto Simposio di Ecologia e Paleoecologia delle Comunità Bentoniche, Roma, Italy* (pp. 110–119).

Carboni, M.G., Succi, M. C., Bergamin, L., Di Bella, L., Frezza, V., & Landini, B. (2009). Benthic foraminifera from two coastal lakes of southern Latium (Italy). Preliminary evaluation of environmental quality. *Marine Pollution Bulletin*, *59*(8–12), 268–280.

Carminati, E., Corda, L., Mariotti, G., & Brandano, M. (2007). Tectonic control on the architecture of a Miocene carbonate ramp in the Central Apennines (Italy): Insights from facies and backstripping analyses. *Sedimentary Geology*, *198*(3–4), 233–253. https://doi.org/10.1016/j.sedgeo.2006.12.005

Carminati, E., & Doglioni, C. (2012). Alps vs. Apennines: The paradigm of a tectonically asymmetric Earth. *Earth-Science Reviews*, *112*(1–2), 67–96. https://doi.org/10.1016/j.earscirev.2012.02.004

Carminati, E., Fabbi, S., & Santantonio, M. (2014). Slab bending, syn-subduction normal faulting, and out-of-sequence thrusting in the Central Apennines. *Tectonics*, *33*(4), 530–551. https://doi.org/10.1002/2013TC003386

Carnevale, G., Patacca, E., Scandone, P., & Pisa, U. (2011). Field Guide to the Post-Conference Excursions (Scontrone , Palena and Montagna della Majella). In *Field Guide to the Post-Conference Excursions (Scontrone, Palena and Montagna della Majella)* (pp. 4–5).

Casnedi, R. (1988). La Fossa Bradanica: origine, sedimentazione e migrazione. *Memorie Della Società Geologica Italiana*, *41*(1988), 439–448.

Catuneanu, O., Galloway, W. E., Kendall, C. G. S. C., Miall, A. D., Posamentier, H. W., Strasser, A., & Tucker, M. E. (2011). Sequence Stratigraphy: Methodology and nomenclature. *Newsletters on Stratigraphy*, *44*(3), 173–245. https://doi.org/10.1127/0078-0421/2011/0011

Cavinato, G. P., & De Celles, P. G. (1999). Extensional basins in the tectonically bimodal central Apennines fold-thrust belt, Italy: Response to corner flow above a subducting slab in retrograde motion. *Geology*, *27*(10), 955–958. https://doi.org/10.1130/0091-7613(1999)027<0955:EBITTB>2.3.CO;2

Cello, G., & Mazzoli, S. (1998). Apennine tectonics in southern Italy: a review. *Journal of Geodynamics*, *27*(2), 191–211.

Chiocchini, M., Farinacci, A., Mancinelli, A., Molinari, V., & Potetti, M. (1994). Biostratigrafia a foraminiferi, dasicladali e calpionelle delle successioni carbonatiche mesozoiche dell'Appennino centrale (Italia) - Tav.1. In *Biostratigrafia dell'Italia centrale: Studi Geologici Camerti* (pp. 9–129).

Chiocchini, M., Pampaloni, M. L., & Pichezzi, R. M. (2012). Microfacies and microfossils of the Mesozoic carbonate successions of Latium and

Abruzzi (Central Italy). *Memorie per Servire Alla Descrizione Della Carta Geologica D'Italia, ISPRA, Dipartimento Difesa Del Suolo, Roma*, 269.

Cipollari, P, & Cosentino, D. (1993). Le Arenarie di Torrice : Un deposito di bacino di piggy-back del Messiniano nell'Appennino centrale. *Bollettino Della Società Geologica Italiana*, *112*(2), 497–505.

Cipollari, P., Cosentino, D., Esu, D., Girotti, O., Gliozzi, E., & Praturlon, A. (1999). Thrust-top lacustrine-lagoonal basin development in accretionary wedges: Late Messinian (Lago-Mare) episode in the central Apennines (Italy). *Palaeogeography, Palaeoclimatology, Palaeoecology*, *151*(1–3), 149–166. https://doi.org/10.1016/S0031-0182(99)00026-7

Cipollari, Paola, & Cosentino, D. (1995). Miocene unconformities in the Central Apennines: geodynamic significance and sedimentary basin evolution. *Tectonophysics*, *252*(1–4), 375–389. https://doi.org/10.1016/0040-1951(95)00088-7

Civitelli, G., & Brandano, M. (2005). The «Calcari a Briozoi e Litotamni» in the Latium-Abruzzi carbonate platform (Central Apennines, Italy): Atlas of the lithofacies and depositional model. *Bollettino Della Societa Geologica Italiana*, *124*(3), 611–643. Retrieved from http://www.scopus.com/inward/record.url?eid=2-s2.0-33750432876&partnerID=40&md5=0cacd6f1b8822069dd36e13847414d0e

Consorti, L., Frijia, G., & Caus, E. (2017). Rotaloidean foraminifera from the Upper Cretaceous carbonates of Central and Southern Italy and their chronostratigraphic age. *Cretaceous Research*, *70*, 226–243.

Consorti, L., Sabbatino, M., & Parente, M. (2021). Insights on the paleoecology of Ammonia (Foraminifera, Rotalioidea) from Miocene carbonates of central and southern Apennines (Italy). *Palaeogeography, Palaeoclimatology, Palaeoecology*, *562*, 110105. https://doi.org/10.1016/j.palaeo.2020.110105

Consorti, L., Villalonga, R., & Caus, E. (2017). New Rotaliids (benthic Foraminifera) from the Late Cretaceous of the Pyrenees in northeastern Spain. *Journal of Foraminiferal Research*, *47*(3), 284–293. https://doi.org/10.2113/gsjfr.47.3.284

Cooper, D. J. W., Ali, M. Y., & Searle, M. P. (2014). Structure of the northern Oman Mountains from the Semail Ophiolite to the Foreland Basin. *Geological Society, London, Special Publications*, *392*(1), 129–153. https://doi.org/10.1144/SP392.7

Cornacchia, I., Andersson, P., Agostini, S., Brandano, M., & Di Bella, L. (2017). Strontium stratigraphy of the upper Miocene Lithothamnion Limestone in the Majella Mountain, central Italy, and its palaeoenvironmental implications. *Lethaia*, *50*(4), 561–575. https://doi.org/10.1111/let.12213

Corradetti, A., Spina, V., Tavani, S., Ringenbach, J., Sabbatino, M., Razin, P., Laurent, O., Brichau, S., & Mazzoli, S. (2020). Late-stage tectonic evolution of the Al-Hajar Mountains, Oman: new constraints from Palaeogene sedimentary units and low-temperature thermochronometry. *Geological Magazine*, *157*(7), 1031–1044. https://doi.org/10.1017/S0016756819001250

Corradetti, A., Tavani, S., Parente, M., Iannace, A., Vinci, F., Pirmez, C., Torrieri, S., Giorgioni, M., Pignalosa, A., & Mazzoli, S. (2018). Distribution and arrest of vertical through-going joints in a seismic-scale carbonate platform exposure (Sorrento peninsula, Italy): insights from integrating field survey and digital outcrop model. *Journal of Structural Geology*, *108*, 121–136. https://doi.org/10.1016/j.jsg.2017.09.009

Cosentino, D, Cipollari, P., & Pipponzi, G. (2003). Evoluzione cinematica del sistema orogenico dell'Appennino centro-meridionale: caratterizzazione stratigrafico-strutturale dei bacini sintettonici. In *Convegno-escursione COFIN'99* (p. 85).

Cosentino, Domenico, Cipollari, P., Marsili, P., & Scrocca, D. (2010). Geology of the central Apennines: a regional review. *Journal of the Virtual Explorer*, *36*(January). https://doi.org/10.3809/jvirtex.2010.00223

Crampton, S. L., & Allen, P. A. (1995). Recognition of Forebulge Unconformities Associated with Early Stage Foreland Basin Development: Example from the North Alpine Foreland Basin. *AAPG Bulletin*, *79*(10), 1495–1514. https://doi.org/10.1306/7834DA1C-1721-11D7-8645000102C1865D

Critelli, S., Muto, F., Tripodi, V., & Perri, F. (2011a). Relationships between Lithospheric Flexure, Thrust Tectonics and Stratigraphic Sequences in Foreland Setting: the Southern Apennines Foreland Basin System, Italy. https://doi.org/http://dx.doi.org/10.5772/57353

Critelli, S., Muto, F., Tripodi, V., & Perri, F. (2011b). Relationships between Lithospheric Flexure, Thrust Tectonics and Stratigraphic Sequences in Foreland Setting: the Southern Apennines Foreland Basin System, Italy. *New Frontiers in Tectonic Research - At the Midst of Plate Convergence*. https://doi.org/10.5772/24120

Curzi, M., Billi, A., Carminati, E., Rossetti, F., Albert, R., Aldega, L., Cardello, G. L., Conti, A., Gerdes, A., Smeraglia, L., Van der Lelij, R., Vignaroli, G., & Viola, G. (2020). Disproving the Presence of Paleozoic-Triassic Metamorphic Rocks on the Island of Zannone (Central Italy): Implications for the Early Stages of the Tyrrhenian-Apennines Tectonic Evolution. *Tectonics*, *39*(12), 1–25. https://doi.org/10.1029/2020TC006296

D'Argenio, B., & Alvarez, W. (1980). Stratigraphic evidence for crustal thickness changes on the southern Tethyan margin during the Alpine cycle. *Bulletin of the Geological Society of America*, *91*(12), 681–689. https://doi.org/10.1130/0016-7606(1980)91<681:SEFCTC>2.0.CO;2

D'Errico, M., & Di Staso, A. (2010). Stratigraphic revision of the Cenozoic deposits of the Lungro-Verbicaro Unit (Northern Calabria): New data for the reconstruction of tectonic evolution of the southern Apennines. *Italian Journal of Geosciences*, *129*(3), 450–456. https://doi.org/10.3301/IJG.2010.14

Damiani, A. V, Chiocchini, M., Colacicchi, R., Mariotti, G., Parotto, M., Passeri, L., & Praturlon, A. (1991). Elementi litostratigrafici per una sintesi delle facies carbonatiche meso-cenozoiche dell'Appennino centrale. *Studi Geologici Camerti*, *1991*, 187–213.

Danese, E. (1999). Upper Miocene carbonate ramp deposits from the southernmost part of Maiella Mountain (Abruzzo, Central Italy). *Facies*, (41), 41–54.

De Blasio, I., Lima, A., Perrone, V., & Russo, M. (1981). Nuove vedute sui depositi miocenici della Penisola Sorrentina. *Bollettino Della Societa Geologica Italiana*, *100*(1), 57–70.

De Capoa, P., Di Donato, V., Di Staso, A., Giardino, S., & Rinaldi, S. (2003). Preparation techniques and methodological approach to calcareous nannoplankton analysis in silico- and calciclastic turbidites. *Courier Forschungsinstitut Senckenberg*, 105–128.

DeCelles, P. G., & DeCelles, P. C. (2001). Rates of shortening, propagation, underthrusting, and flexural wave migration in continental orogenic systems. *Geology*, 29(2), 135–138. https://doi.org/10.1130/0091-7613(2001)029<0135:ROSPUA>2.0.CO;2

de Mulder, E. F. J. (1975). Microfauna and sedimentary-tectonic history of the Oligo-Miocene of the Ionian Islands and Western Epirus (Greece). Utrecht University.

Debenay, J.-P., Bénéteau, E., Zhang, J., Stouff, V., Geslin, E., Redois, F., & Fernandez-Gonzalez, M. (1998). Ammonia beccarii and Ammonia tepida (Foraminifera): morphofunctional arguments for their distinction. *Marine Micropaleontology*, *34*(3–4), 235–244.

Debenay, J.-P., Geslin, E., Eichler, B. B., Duleba, W., Sylvestre, F., & Eichler, P. (2001). Foraminiferal assemblages in a hypersaline lagoon, Araruama (RJ) Brazil. *The Journal of Foraminiferal Research*, *31*(2), 133–151.

Debenay, J. P., & Guillou, J. J. (2002). Ecological transitions indicated by foraminiferal assemblages in paralic environments. *Estuaries*, *25*(6), 1107–1120.

Debenay, J. P., Guillou, J. J., Redois, F., & Geslin, E. (2000). Distribution trends of foraminiferal assemblages in paralic environments. In *Environmental micropaleontology* (pp. 39–67). Springer.

DeCelles, P. G. (2012). Foreland Basin Systems Revisited: Variations in Response to Tectonic Settings. In *Tectonics of Sedimentary Basins* (pp. 405–426). Chichester, UK: John Wiley & Sons, Ltd. https://doi.org/10.1002/9781444347166.ch20

DeCelles, P. G., & Giles, K. A. (1996). Foreland basin systems. *Basin Research*, *8*(2), 105–123. https://doi.org/10.1046/j.1365-2117.1996.01491.x

DeCelles, P. G., & DeCelles, P. C. (2001). Rates of shortening, propagation, underthrusting, and flexural wave migration in continental orogenic systems. Geology, 29(2), 135–138. https://doi.org/10.1130/0091-7613(2001)029<0135:ROSPUA>2.0.CO;2

DeCelles, P. G., Gehrels, G. E., Quade, J., & Ojha, T. P. (1998). Eocene-early Miocene foreland basin development and the history of Himalayan thrusting, western and central Nepal. *Tectonics*, *17*(5), 741–765. https://doi.org/10.1029/98TC02598

DePaolo, D. J., & Ingram, B. L. (1985). High-resolution stratigraphy with strontium isotopes. *Science*, *227*(4689), 938–941. https://doi.org/10.1126/science.227.4689.938

Dewey, J. F., Helman, M. L., Knott, S. D., Turco, E., & Hutton, D. H. W. (1989). Kinematics of the western Mediterranean. *Geological Society, London, Special Publications*, *45*(1), 265–283. https://doi.org/10.1144/GSL.SP.1989.045.01.15

Doglioni, C. (1991). A proposal for the kinematic modelling of W-dipping subductions - possible applications to the Tyrrhenian-Apennines system. *Terra Nova*, *3*(4), 423–434. https://doi.org/10.1111/j.1365-3121.1991.tb00172.x

Doglioni, C. (1995). Geological remarks on the relationships between extension and convergent geodynamic settings. *Tectonophysics*, *252*(1–4), 253–267. https://doi.org/10.1016/0040-1951(95)00087-9

Doglioni, C., Mongelli, F., & Pieri, P. (1994). The Puglia uplift (SE Italy): An anomaly in the foreland of the Apenninic subduction due to buckling of a thick continental lithosphere. *Tectonics*, *13*(5), 1309–1321. https://doi.org/10.1029/94TC01501

Dorobek, S. L. (1995). Synorogenic carbonate platforms and reefs in foreland basins: controls on stratigraphic evolution and platform/reef morphology. In *Stratigraphic Evolution of Foreland Basins* (pp. 127–147). SEPM (Society for Sedimentary Geology). https://doi.org/10.2110/pec.95.52.0127

Drooger, C. W. (1993). *Radial Foraminifera; morphometrics and evolution*. *Verhandelingen der Koninklijke Akademie van Wetenschappen. Afdeeling Natuurkunde. Eerste sectie*. North-Holland.

Dupuy, C., Rossignol, L., Geslin, E., & Pascal, P.Y. (2010). Predation of mudflat meio-macrofaunal metazoans by a calcareous foraminifer, Ammonia tepida (Cushman, 1926). *The Journal of Foraminiferal Research*, *40*(4), 305–312.

Fabbi, S. (2016). Geology of the Northern Simbruini Mts. (Abruzzo–Italy). *Journal of Maps*, *12*, 441–452. https://doi.org/10.1080/17445647.2016.1237899

Fabbi, S., & Rossi, M. G. (2014). The Brecce della Renga Formation: Age and sedimentology of a syn-tectonic clastic unit in the upper Miocene of Central Apennines. Insights from field geology. *Rivista Italiana Di Paleontologia e Stratigrafia*, *120(2)*(7), 225–242. https://doi.org/10.13130/2039-4942/6062

Faccenna, C., Becker, T. W., Auer, L., Billi, A., Boschi, L., Brun, J. P., Capitanio, F. A., Funiciello, F., Horvàth, F., Jolivet, L., Piromallo, C., Royden, L., Rossetti, F., & Serpelloni, E. (2014). Mantle dynamics in the Mediterranean. *Reviews of Geophysics*, *52*(3), 283–332. https://doi.org/10.1002/2013RG000444

Faccenna, C., Davy, P., Brun, J. P., Funiciello, R., Giardini, D., Mattei, M., & Nalpas, T. (1996). The dynamics of back-arc extension: An experimental approach to the opening of the Tyrrhenian Sea.

Geophysical Journal International, *126*(3), 781–795. https://doi.org/10.1111/j.1365-246X.1996.tb04702.x

Faccenna, C., Mattei, M., Funiciello, R., & Jolivet, L. (1997). Styles of back-arc extension in the Central Mediterranean. *Terra Nova*, *9*(3), 126–130. https://doi.org/10.1046/j.1365-3121.1997.d01-12.x

Filipescu, S., Wanek, F., Miclea, A., DeLeeuw, A., & Vasiliev, I. (2011). Micropaleontological response to the changing paleoenvironment across the Sarmatian-Pannonian boundary in the Transylvanian Basin (Miocene, Oarba de Mures section, Romania). *Geologica Carpathica*, *62*(1), 91.

Flemings, P. B., & Jordan, T. E. (1990). Stratigraphic modeling of foreland basins: Interpreting thrust deformation and lithosphere rheology. *Geology*, *18*(5), 430–434.

Flugel, E., & Flügel, E. (2004). *Microfacies of carbonate rocks: analysis, interpretation and application*. Springer Science & Business Media.

Frijia, G., & Parente, M. (2008). Strontium isotope stratigraphy in the upper Cenomanian shallow-water carbonates of the southern Apennines: Short-term perturbations of marine 87Sr/86Sr during the oceanic anoxic event 2. *Palaeogeography, Palaeoclimatology, Palaeoecology*, *261*(1–2), 15–29. https://doi.org/10.1016/j.palaeo.2008.01.003

Frijia, G., Parente, M., Di Lucia, M., & Mutti, M. (2015a). Carbon and strontium isotope stratigraphy of the Upper Cretaceous (Cenomanian-Campanian) shallow-water carbonates of southern Italy: Chronostratigraphic calibration of larger foraminifera biostratigraphy. *Cretaceous Research*, *53*, 110–139. https://doi.org/10.1016/j.cretres.2014.11.002

Galewsky, J. (1998). The dynamics of foreland basin carbonate platforms: Tectonic and eustatic controls. *Basin Research*, *10*(4), 409–416. https://doi.org/10.1046/j.1365-2117.1998.00079.x

Galewsky, J., Silver, E. A., Gallup, C. D., Edwards, R. L., & Potts, D. C. (1996). Foredeep tectonics and carbonate platform dynamics in the Huon Gulf, Papua New Guinea. *Geology*, *24*(9), 819–822.

https://doi.org/10.1130/0091-7613(1996)024<0819:FTACPD>2.3.CO;2

GEBCO Bathymetric Compilation Group 2020 (2020). The GEBCO_2020 Grid - a continuous terrain model of the global oceans and land. British Oceanographic Data Centre, National Oceanography Centre, NERC, UK. doi:10/dtg3.

Giles, K. A., & Dickson, A. J. (1995). The interplay of eustasy and lithospheric flexure in forming stratigraphic sequences in foreland settings: An example from the Antler foreland, Nevada and Utah. In *Stratigraphic Evolution of Foreland Basins* (pp. 187–211). SEPM (Society for Sedimentary Geology). https://doi.org/10.2110/pec.95.52.0187

Glennie, K. W., Boeuf, M. G. A., Hughes Clarke, M. W., Moody-Stuart, M., Pilaar, W. F. H., & Reinhardt, B. M. (1973). Late Cretaceous Nappes in Oman Mountains and Their Geologic Evolution. *AAPG Bulletin*, *58*(5), 895–898. https://doi.org/10.1306/819A4240-16C5-11D7-8645000102C1865D

Goñi, M. A., Teixeira, M. J., & Perkey, D. W. (2003). Sources and distribution of organic matter in a river-dominated estuary (Winyah Bay, SC, USA). *Estuarine, Coastal and Shelf Science*, *57*(5–6), 1023–1048.

Gradstein, F M, Ogg, J. G., Schmitz, M. D., & Ogg, G. M. (2020). *Geologic Time Scale 2020*. Elsevier.

Gradstein, Felix M, Ogg, J. G., Schmitz, M., & Ogg, G. (2012). *The geologic time scale 2012*. (F M Gradstein, J. G. Ogg, M. Schmitz, & G. Ogg, Eds.). Boston: Elsevier.

Guelorget, O., & Perthuisot, J. P. (1983). Le domaine paralique. Expressions géologiques, biologiques et économiques du confinement.

Hageman, J. (1979). Benthic foraminiferal assemblages from the Plio-Pleistocene open bay to lagoonal sediments of the western Peloponnes (Greece). *Utrecht Micropaleontol. Bull.*, *20*, 1–180.

Haig, D. W., Smith, M. G., Riera, R., & Parker, J. H. (2020). Widespread seagrass meadows during the Early Miocene (Burdigalian) in southwestern Australia paralleled modern seagrass distributions. *Palaeogeography, Palaeoclimatology, Palaeoecology*, *555*, 109846.

Haller, C., Smith, C. G., Hallock, P., Hine, A. C., Osterman, L. E., & McCloskey, T. (2019). Distribution of modern salt-marsh foraminifera from the eastern Mississippi Sound, USA. *Journal of Foraminiferal Research*, *49*(1), 29–47.

Handy, M. R., M. Schmid, S., Bousquet, R., Kissling, E., & Bernoulli, D. (2010). Reconciling plate-tectonic reconstructions of Alpine Tethys with the geological-geophysical record of spreading and subduction in the Alps. *Earth-Science Reviews*. https://doi.org/10.1016/j.earscirev.2010.06.002

Hansen, H. J., & Reiss, Z. (1971). Electron microscopy of rotaliacean wall structures. *Bulletin of the Geological Society of Denmark*, *20*(part 4), 329–346.

Haq, B. U., Hardenbol, J., & Vail, P. R. (1988). Mesozoic and Cenozoic chronostratigraphy and cycles of sea-level change. In W. C.K., H. C.A., H. Ross, J. Posamentier, C. G. Van Wagoner, & C. G. S. C. Kendal (Eds.), *Sea-Level Changes: An Integrated Approach* (pp. 71–108). SEPM (Society for Sedimentary Geology). https://doi.org/10.2110/pec.88.01.0071

Hasegawa, S., & Takahashi, T. (1992). Faunal succession of benthic foraminifera in the upper Yatsuo Group of the Hokuriku district, central Japan—A temporal faunal trend during an early—middle Miocene transgression in Japan. *Centenary of Japanese Micropaleontology*, 51–66.

Haynes, J. R. (1992). Supposed pronounced ecophenotypy in foraminifera. *Journal of Micropalaeontology*, *11*(1), 59–63.

Hayward, B. W., Holzmann, M., Grenfell, H. R., Pawlowski, J., & Triggs, C. M. (2004). Morphological distinction of molecular types in Ammonia–towards a taxonomic revision of the world's most commonly misidentified foraminifera. *Marine Micropaleontology*, *50*(3–4), 237–271.

Hayward, B. W., Holzmann, M., & Tsuchiya, M. (2019). Combined molecular and morphological taxonomy of the Beccarii/T3 group of the foraminiferal genus ammonia. *Journal of Foraminiferal Research*, *49*(4), 367–389.

Hilgen, F. J., Lourens, L. J., Van Dam, J. A., Beu, A. G., Boyes, A. F., Cooper, R. A., Krijgsman, W., Ogg, J.G., Piller, W.E., & Wilson, D.S. (2012). *The Neogene Period*. *The Geologic Time Scale 2012* (Vol. 1–2). Gradstein, F. M., Ogg, J. G., Schmitz, M., and Ogg, G. https://doi.org/10.1016/B978-0-444-59425-9.00029-9

Hiscott, R. N., Pickering, K. T., & Beeden, D. R. (1986). Progressive filling of a confined Middle Ordovician foreland basin associated with the Taconic Orogeny, Quebec, Canada. *Foreland Basins*, 307–325.

Hodell, D. A., Mueller, P. A., & Garrido, J. R. (1991). Variations in the strontium isotopic composition of seawater during the Neogene. *Geology*, *19*(1), 24–27. https://doi.org/10.1130/0091-7613(1991)019<0024:VITSIC>2.3.CO;2

Hofker, J. (1971). Studies of Foraminifera. Part 3. Systematic Problems. In *Publicaties van het Natuurhistorisch genootshap in Limburg* (p. 202).

Holzmann, M., Piller, W. E., Zaninetti, L., Fenner, R., Martini, R., Serandrei-Barbero, R., & Pawlowski, J. (1998). Molecular versus morphologic variability in Ammonia spp.(Foraminifera, Protozoa) from the Lagoon of Venice, Italy. *Revue de Micropaléontologie*, *41*(1), 59–69.

Homke, S., Vergés, J., Serra-Kiel, J., Bernaola, G., Sharp, I., Garcés, M., Montero-Verdú, I., Karpuz, R., & Goodarzi, M. H. (2009). Late Cretaceous–Paleocene formation of the proto–Zagros foreland basin, Lurestan Province, SW Iran. *GSA Bulletin*, *121*(7–8), 963–978. https://doi.org/10.1130/B26035.1

Hottinger, L. (1966). Les ammonia dans le Miocène supérieur et Pliocène marocain. In *Committee on Mediterranean Neogene stratigraphy. Session. 3* (pp. 117–123).

Hottinger, L. (2006). Illustrated glossary of terms used in foraminiferal research. In *Notebooks on Geology, Brest, Memoir* (p. 126).

Hottinger, L, Leadbeater, B., & Riding, R. (1986). Construction, structure, and function of foraminiferal shells. *Biomineralization in Lower Plants and Animals*, *219*, 235.

Hottinger, Lukas, & Bassi, D. (2014). *Paleogene larger rotaliid foraminifera from the Western and Central Neotethys*. Springer.

Hottinger, Lukas, Halicz, E., & Reiss, Z. (1991). The foraminiferal genera Pararotalia, Neorotalia, and Calcarina: taxonomic revision. *Journal of Paleontology*, *65*, 18–33.

Iannace, A., Merola, D., Perrone, V., Amato, A., & Cinque, A. (2014). *Note illustrative della carta geologica d'Italia alla scala 1:50.000 Foglio 466-485 Sorrento-Termini*. *Servizio Geologico d'Italia, ISPRA*.

Iannace, A., Vitale, S., D'Errico, M., Mazzoli, S., Di Staso, A., Macaione, E., Messina, A., Reddy, S. M., Somma, R., Zamparelli, V., Zattin, M. & Bonardi, G. (2007). The carbonate tectonic units of northern Calabria (Italy): A record of Apulian palaeomargin evolution and Miocene convergence, continental crust subduction and exhumation of HP-LT rocks. *Journal of the Geological Society*, *164*(6), 1165–1186. https://doi.org/10.1144/0016-76492007-017

Iannone, A., & Pieri, P. (1983). Rapporti fra i prodotti residuali del carsismo e la sedimentazione quaternaria nell'area delle Murge. *Rivista Italiana Di Paleontologia e Stratigrafia*, *88*, 319–330.

Inden, R.F., & Moore, C.H., 1983. Beach Environment. In (Eds.): Scholle, P.A., Debout, D., Moore H.M., Carbonate depositional environments. AAPG Memories 33, 345–462.

Jauffrais, T., Jesus, B., Metzger, E., Mouget, J. L., Jorissen, F., & Geslin, E. (2016). Effect of light on photosynthetic efficiency of sequestered chloroplasts in intertidal benthic foraminifera (Haynesina germanica and Ammonia tepida). *Biogeosciences*, *13*(9), 2715–2726.

John, C. M., Karner, G. D., Browning, E., Leckie, R. M., Mateo, Z., Carson, B., & Lowery, C. (2011). Timing and magnitude of Miocene eustasy derived from the mixed siliciclastic-carbonate stratigraphic record of the northeastern Australian margin. *Earth and Planetary Science Letters*, *304*(3–4), 455–467. https://doi.org/10.1016/j.epsl.2011.02.013

Jordan, T. E. (1981). Crustal Loading and Foreland Basin Evolution, Cretaceous, Western United States. *AAPG Bulletin*, 65(12), 2506–2520. https://doi.org/10.1306/2f919f3a-16ce-11d7-8645000102c1865d

Jorissen, F., Nardelli, M.P., Almogi-Labin, A., Barras, C., Bergamin, L., Bicchi, E., El Kateb, A., Ferraro, L., McGann, M., Morigi, C., Romano, E., Sabbatini, A., Schweizer, M., & Spezzaferri, S. (2018). Developing Foram-AMBI for biomonitoring in the Mediterranean: Species assignments to ecological categories. *Marine Micropaleontology*, *140*, 33–45.

Kenyon, N. H., & Millington, J. (1995). Contrasting deep-sea depositional systems in the Bering Sea. In K. T. Pickering, R. N. Hiscott, N. H. Kenyon, F. Ricci Lucchi, & R. D. A. Smith (Eds.), *Atlas of Deep Water Environments: Architectural style in turbidite systems: London, Chapman & Hall* (1st ed., pp. 196–202).

Koho, K.A., LeKieffre, C., Nomaki, H., Salonen, I., Geslin, E., Mabilleau, G., Søgaard Jensen, L.H., & Reichart, G.J. (2018). Changes in ultrastructural features of the foraminifera Ammonia spp. in response to anoxic conditions: Field and laboratory observations. *Marine Micropaleontology*, *138*, 72–82.

Kominz, M. A., Miller, K. G., Browning, J. V., Katz, M. E., & Mountain, G. S. (2016). Miocene relative sea level on the New Jersey shallow continental shelf and coastal plain derived from one-dimensional backstripping: A case for both eustasy and epeirogeny. *Geosphere*, *12*(5), 1437–1456. https://doi.org/10.1130/GES01241.1

La Bruna, V., Agosta, F., Lamarche, J., Viseur, S., & Prosser, G. (2018). Fault growth mechanisms and scaling properties in foreland basin system: The case study of Monte Alpi, Southern Apennines, Italy. *Journal of Structural Geology*, *116*(August), 94–113. https://doi.org/10.1016/j.jsg.2018.08.009

Langer, M., Hottinger, L., & Huber, B. (1989). Functional morphology in low-diverse benthic foraminiferal assemblages from tidal flats of the North Sea. *Senckenbergiana Maritima*, *20*(3–4), 81–99.

Langer, M. R. (1993). Epiphytic foraminifera. *Marine Micropaleontology*, *20*(3–4), 235–265.

Langer, M. R., & Hottinger, L. (2000). Biogeography of selected" larger" foraminifera. *Micropaleontology*, *46*, 105–126.

Lees, A. (1975). Possible influence of salinity and temperature on modern shelf carbonate sedimentation. *Marine Geology*, *19*(3), 159–198.

Leszczyński, S., & Nemec, W. (2015). Dynamic stratigraphy of composite peripheral unconformity in a foredeep basin. *Sedimentology*, *62*(3), 645–680. https://doi.org/10.1111/sed.12155

Lirer, F., Persico, D., & Vigorito, M. (2005). Calcareous plankton biostratigraphy and age of the Middle Miocene deposits of Longano Formation (eastern Matese Mountains, southern Apennines). *Rivista Italiana Di Paleontologia e Stratigrafia (Research In Paleontology and Stratigraphy)*, *111*(1). https://doi.org/https://doi.org/10.13130/2039-4942/6277

Malinverno, A., & Ryan, W. B. F. (1986). Extension in the Tyrrhenian Sea and shortening in the Apennines as result of arc migration driven by sinking of the lithosphere. *Tectonics*, *5*(2), 227–245.

Mariotti, G., & Doglioni, C. (2000). The dip of the foreland monocline in the Alps and Apennines. *Earth and Planetary Science Letters*, *181*(1–2), 191–202. https://doi.org/10.1016/S0012-821X(00)00192-8

Martelli, L., Nardi, G., Bravi, S., Cavuoto, G., Toccacerli, R. M., Cammarosano, A., Danna, M., de Rienzo, F., Sgrosso, A., De Capoa, P., Di Staso, A., Giardino, S., & Valente, A. (2005). *Note illustrative* *della carta Geologica d'Italia alla scala 1:50000 - Foglio 503 "Vallo della Lucania", Servizio Geologico d'Italia, ISPRA*.

Martinelli, M., Bistacchi, A., Balsamo, F., & Meda, M. (2019). Late Oligocene to Pliocene Extension in the Maltese Islands and Implications for Geodynamics of the Pantelleria Rift and Pelagian Platform. *Tectonics*, *38*(9), 3394–3415. https://doi.org/10.1029/2019TC005627

Mazzoli, S., Aldega, L., Corrado, S., Invernizzi, C., & Zattin, M. (2006). Pliocene-quaternary thrusting, syn-orogenic extension and tectonic exhumation in the Southern Apennines (Italy): Insights from the Monte Alpi area. *Special Paper of the Geological Society of America*, *414*(414), 55–77. https://doi.org/10.1130/2006.2414(04)

Mazzoli, S., D'Errico, M., Aldega, L., Corrado, S., Invernizzi, C., Shiner, P., & Zattin, M. (2008). Tectonic burial and "young" (<10 Ma) exhumation in the southern Apennines fold-and-thrust belt (Italy). *Geology*, *36*(3), 243–246. https://doi.org/10.1130/G24344A.1

Mazzoli, Stefano, & Helman, M. (1994). Neogene patterns of relative plate motion for Africa-Europe: some implications for recent central Mediterranean tectonics. *Geologische Rundschau*, *83*(2), 464–468. https://doi.org/10.1007/BF00210558

McArthur, J. M., & Howarth, R. J. (2005). Strontium isotope stratigraphy. In F M Gradstein, J. G. Ogg, M. D. Schmitz, & G. M. Ogg (Eds.), *A Geologic Time Scale 2004* (pp. 96–105). Cambridge University Press. https://doi.org/10.1017/CBO9780511536045.008

McArthur, J. M., Howarth, R. J., & Bailey, T. R. (2001). Strontium Isotope Stratigraphy: LOWESS Version 3: Best Fit to the Marine Sr-Isotope Curve for 0–509 Ma and Accompanying Look-up Table for Deriving Numerical Age. *The Journal of Geology*, *109*(2), 155–170. https://doi.org/10.1086/319243

McArthur, J. M., Howarth, R. J., & Shields, G. A. (2012). *Strontium Isotope Stratigraphy*. *The Geologic Time Scale 2012* (Vol. 1–2). Gradstein, F. M., Ogg, J. G., Schmitz, M. D., & Ogg, G. Elsevier, 127-144. https://doi.org/10.1016/B978-0-444-59425-9.00007-X

McArthur, J. M., Howarth, R. J., Shields, G. A., & Zhou, Y. (2020). Chapter 7 - Strontium Isotope Stratigraphy. In F. M. Gradstein, J. G., Ogg, Schmitz, M. D., & Ogg. G. M. (Eds.). Elsevier, 211–238. https://doi.org/https://doi.org/10.1016/B978-0-12-824360-2.00007-3

McArthur, J. M. M. (1994). Recent trends in strontium isotope stratigraphy. *Terra Nova*, *6*(4), 331–358. https://doi.org/10.1111/j.1365-3121.1994.tb00507.x

Mearon, S., Paytan, A., & Bralower, T. J. (2003). Cretaceous strontium isotope stratigraphy using marine barite. *Geology*, *31*(1), 15–18. https://doi.org/10.1130/0091-7613(2003)031<0015:CSISUM>2.0.CO;2

Melis, R., & Covelli, S. (2013). Distribution and morphological abnormalities of recent foraminifera in the Marano and Grado Lagoon (North Adriatic Sea, Italy). *Mediterranean Marine Science*, *14*(2), 432–450.

Mindszenty, A., D'Argenio, B., & Aiello, G. (1995). Lithospheric bulges recorded by regional unconformities. The case of mesozoic-tertiary apulia. *Tectonophysics*, *252*(1–4), 137–161. https://doi.org/10.1016/0040-1951(95)00091-7

Monti, L., Sgrosso, I., Graziano, R., Amore, F. O., Morabito, S., Santini, U., & Ferraro, L. (2014). *Geological Map of Italy, scale 1:50000, sheet 520 (Sapri), ISPRA, Rome*.

Moretti, M., Pieri, P., Ricchetti, G., & Spalluto, L. (2011). Note Illustrative della Carta Geologica d'Italia alla scala 1: 50.000, Foglio 396 "San Severo." In *Servizio Geologico d'Italia, ISPRA* (p. 145).

Murray, J. W. (2006). *Ecology and applications of benthic foraminifera*. Cambridge university press.

Mutti, M., Bernoulli, D., & Stille, P. (1997). Temperate carbonate platform drowning linked to Miocene oceanographic events: Maiella platform margin, Italy. *Terra Nova*, *9*(3), 122–125. https://doi.org/10.1046/j.1365-3121.1997.d01-19.x

Nicoletti, L., La Valle, P., & Chimenz Gusso, C. (2004). Indicator species: The Corbula Gibba (Olivi, 1792) case. *Biologia Marina Mediterranea*, *11*(2), 273–277.

Noguera, A. M., & Rea, G. (2000). Deep structure of the Campanian-Lucanian Arc (Southern Apennine, Italy). *Tectonophysics*, *324*(4), 239–265. https://doi.org/10.1016/S0040-1951(00)00137-2

Nomaki, H., Bernhard, J.M., Ishida, A., Tsuchiya, M., Uematsu, K., Tame, A., Kitahashi, T., Takahata, N., Sano, Y., & Toyofuku, T. (2016). Intracellular isotope localization in Ammonia sp. (Foraminifera) of oxygen-depleted environments: results of nitrate and sulfate labeling experiments. *Frontiers in Microbiology*, *7*, 163.

Ogniben, L. (1958). *Stratigrafia e microfaune del terziario della zona di Caiazzo, Caserta*.

Ori, G. G., Roveri, M., & Vannoni, F. (1986). Plio-Pleistocene sedimentation in the Apenninic-Adriatic foredeep (Central Adriatic Sea, Italy). In *Foreland basins* (Vol. 8, pp. 183–198). International Association of Sedimentologists.

Otoničar, B. (2007). Upper Cretaceous to Paleogene Forbulge Unconformity Associated With Foreland Basin Evolution (Kras, Matarsko Podolje and Istria; SW Slovenia and NW Croatia). *Acta Carsologica*, *36*(1), 101–120. https://doi.org/10.3986/ac.v36i1.213

Palmer, M. R., & Elderfield, H. (1985). Sr isotope composition of sea water over the past 75 Myr. *Nature*, *314*(6011), 526–528. https://doi.org/10.1038/314526a0

Pampaloni, M. L., Pichezzi, R. M., Raffi, I., & Rossi, M. (1994). Calcareous planktonic biostratigraphy of the marne a Orbulina unit (Miocene, central Italy). *Giornale Di Geologia*, *56*(1), 139–153.

Patacca, E., & Scandone, P. (2007). Geology of the Southern Apennines. *Bollettino Della Societa Geologica Italiana, Supplemento*, *7*(April 2007), 75–119.

Patacca, E, Sartori, R., & Scandone, P. (1992). Tyrrhenian and Apennine. Kinematic evolution and related dynamic constraints. *Proceedings of* *the Course on Recent Evolution and Seismicity of the Mediterranean Area; Erice, September*, 1–10.

Patacca, E, Scandone, P., Bellatalla, M., & Santini, U. (1992). The Numidian-sand event in the Southern Apennines. *Mem. Sci. Geol. Padova*, *43*, 297–337.

Patacca, Etta, Sartori, R., & Scandone, P. (1990). Tyrrhenian basin and Apenninic arcs: kinematic relations since Late Tortonian times. *Memorie Della Società Geologica Italiana*, *45*, 425–451.

Patacca, Etta, Scandone, P., & Carnevale, G. (2013). The Miocene vertebrate-bearing deposits of Scontrone (Abruzzo, Central Italy): Stratigraphic and paleoenvironmental analysis. *Geobios*, *46*(1–2), 5–23. https://doi.org/10.1016/j.geobios.2012.11.001

Patacca, Etta, Scandone, P., & Mazza, P. (2008). The Miocene land-vertebrate fossil site of Scontrone (Central Apennines, Italy). *Ital. J. Geosci.*, *127*(1), 51–73.

Patterson, R. T. (1987). Arcellaceans and foraminifera from Pleistocene Lake Tecopa, California. *Journal of Foraminiferal Research*, *17*(4), 333–343. https://doi.org/10.2113/gsjfr.17.4.333

Perrone, V. (1987). I depositi miocenici della dorsale di M Soprano (Appennino campano): segnalazione di vulcanismo andesitico e nuova interpretazione. *Bollettino Della Società Geologica Italiana*, *106*(1), 3–12.

Pieri, P., Sabato, L., & Tropeano, M. (1996). Significato geodinamico dei caratteri deposizionali e strutturali della fossa bradanica nel Pleistocene. *Memorie Della Società Geologica Italiana Geologica Italiana*, *51*, 501–515.

Pierre, C., Caruso, A., Blanc-Valleron, M. M., Rouchy, J. M., & Orzsag-Sperber, F. (2006). Reconstruction of the paleoenvironmental changes around the Miocene–Pliocene boundary along a West–East transect across the Mediterranean. *Sedimentary Geology*, *188*, 319–340.

Pigram, C. J., Davies, P. J., Feary, D. A., Symonds, P. A., & Chaproniere, G. C. H. (1990). Controls on Tertiary carbonate platform evolution in the Papuan Basin: new play concepts. Papua New Guinea (PNG) Petroleum Convention Proceedings.

Pirouz, M., Simpson, G., & Chiaradia, M. (2015). Constraint on foreland basin migration in the Zagros mountain belt using Sr isotope stratigraphy. *Basin Research*, *27*(6), 714–728. https://doi.org/10.1111/bre.12097

Pirouz, M., Avouac, J. P., Hassanzadeh, J., Kirschvink, J. L., & Bahroudi, A. (2017a). Early Neogene foreland of the Zagros, implications for the initial closure of the Neo-Tethys and kinematics of crustal shortening. *Earth and Planetary Science Letters*, *477*, 168–182. https://doi.org/10.1016/j.epsl.2017.07.046

Pirouz, M., Simpson, G., Castelltort, S., Gorin, G., & Bahroudi, A. (2017b). Controls on the sequence stratigraphic architecture of the Neogene Zagros foreland basin. In *Tectonic Evolution, Collision, and Seismicity of Southwest Asia: In Honor of Manuel Berberian's Forty-Five Years of Research Contributions*. Geological Society of America, 525. https://doi.org/10.1130/2016.2525(12)

Piuz, A., & Meister, C. (2013). Cenomanian rotaliids (Foraminiferida) from Oman and Morocco. *Swiss Journal of Palaeontology*, *132*(2), 81–97.

Poag, C. W. (1978). Paired foraminiferal ecophenotypes in Gulf Coast estuaries: ecological and paleoecological implications. *Revue de Micropaléontologie*, *40*, 71–96.

Poignant, A. (1997). Smaller benthic foraminifera and microproblematica of the Aquitaine (southwestern France) Miocene–biostratigraphical distribution–taxonomical and biostratigraphical results. *Revue de Micropaléontologie*, *40*(1), 71–96.

Pomar, L., & Tropeano, M. (2001). The Calcarenite di Gravina Formation in Matera (southern Italy): New insights for coarse-grained, large-scale, cross-bedded bodies encased in offshore deposits. *AAPG Bulletin*, *85*(4), 661–690. https://doi.org/10.1306/8626C979-173B-11D7-8645000102C1865D

Ramihangihajason, T. N., Andrianavalona, T. H., Razafimbelo, R., Rahantarisoa, L., Ali, J. R., & Samonds, K. E. (2014). Miocene benthic foraminifera from Nosy Makamby and Amparafaka, Mahajanga Basin, northwestern Madagascar. *Journal of African Earth Sciences*, *100*, 409–417.

Revets, S. A. (1993). The foraminiferal toothplate, a review. *Journal of Micropalaeontology*, *12*(2), 155–169.

Ricchetti, G., & Ciaranfi, N. (2009). *Note illustrative della Carta Geologica d'Italia alla scala 1:50.000, foglio 536 "Ugento" Servizio Geologico d'Italia, ISPRA*.

Ricchetti, G., Ciaranfi, N., Luperto Sinni, E., Mongelli, F., & Pieri, P. (1988). Geodinamica ed evoluzione sedimentaria e tettonica dell'avampaese apulo. *Memorie Della Società Geologica Italiana*, *41*, 57–82.

Ricci Lucchi, F. (1986). The Oligocene to Recent foreland basins of the northern Apennines. In *Foreland basins, 8,* 105–139. Blackwell Scientific Oxford.

Richirt, J., Schweizer, M., Bouchet, V. M. P., Mouret, A., Quinchard, S., & Jorissen, F. J. (2019). Morphological distinction of three Ammonia phylotypes occurring along European coasts. *Journal of Foraminiferal Research*, *49*(1), 76–93.

Robertson, A. H. F. (1987). Upper Cretaceous Muti Formation: transition of a Mesozoic carbonate platform to a foreland basin in the Oman Mountains. *Sedimentology*, *34*(6), 1123–1142.

Robertson, A. H. F., & Searle, M. P. (1990). The northern Oman Tethyan continental margin: stratigraphy, structure, concepts and controversies. *Geological Society, London, Special Publications*, *49*(1), 3–25.

Romano, A., & Urgera, A. (1995). Geologia del Paleogene dei Monti Aurunci orientali (Lazio meridionale). *Studi Geol. Camerti*, *XIII*, 29–38.

Roslim, A., Briguglio, A., Kocsis, L., Ćorić, S., & Gebhardt, H. (2019). Large rotaliid foraminifera as biostratigraphic and palaeoenvironmental indicators in northwest Borneo: An example from a late Miocene section in Brunei Darussalam. *Journal of Asian Earth Sciences*, *170*, 20–28.

Roure, F., Casero, P., & Vially, R. (1991). Growth processes and melange formation in the southern Apennines accretionary wedge. *Earth and Planetary Science Letters*, *102*(3–4), 395–412. https://doi.org/10.1016/0012-821X(91)90031-C

Royden, L., & Faccenna, C. (2018). Subduction Orogeny and the Late Cenozoic Evolution of the Mediterranean Arcs. *Annual Review of Earth and Planetary Sciences*, *46*(1), 261–289. https://doi.org/10.1146/annurev-earth-060115-012419

Royden, L., Patacca, E., & Scandone, P. (1987). Segmentation and configuration of subducted lithosphere in Italy An important control on thrust-belt and foredeep-basin evolution. *Geology*, *15*(August), 714–717.

Sabbatino, M., Vitale, S., Tavani, S., Consorti, L., Corradetti, A., Cipriani, A., Arienzo, I., & Parente, M. (2020). Constraining the onset of flexural subsidence and peripheral bulge extension in the Miocene foreland of the southern Apennines (Italy) by Sr-isotope stratigraphy. *Sedimentary Geology*, *401*, 105634. https://doi.org/10.1016/j.sedgeo.2020.105634

Saura, E., Garcia-Castellanos, D., Casciello, E., Parravano, V., Urruela, A., & Vergés, J. (2015). Modeling the flexural evolution of the Amiran and Mesopotamian foreland basins of NW Zagros (Iran-Iraq). *Tectonics*, *34*(3), 377–395. https://doi.org/10.1002/2014TC003660

Scasso, R. A., McArthur, J. M., Del Río, C. J., Martínez, S., & Thirlwall, M. F. (2001). 87Sr/86Sr late miocene age of fossil molluscs in the “entrerriense” of the Valdés Peninsula (Chubut, Argentina). *Journal of South American Earth Sciences*, *14*(3), 319–329. https://doi.org/10.1016/S0895-9811(01)00032-3

Schiavinotto, F. (1979). Miogypsina e Lepidocyclina del Miocene di Monte La Serra (L’Aquila-Appennino centrale). *Geologica Romana*, *18*, 253–293.

Schiavinotto, F. (1985). Le Miogypsinidae alla base della trasgressione miocenica del Monte Camposauro (Appennino Meridionale). *Bollettino Della Società Geologica Italiana*, *104*(1), 53–63.

Schnitker, D. (1974). Ecotype variation in Ammonia beccarii (Linne). *Journal of Foraminiferal Research*, *4*, 216–223.

Schweizer, M., Polovodova, I., Nikulina, A., & Schönfeld, J. (2011). Molecular identification of Ammonia and Elphidium species (foraminifera, Rotaliida) from the Kiel Fjord (SW Baltic Sea) with rDNA sequences. *Helgoland Marine Research*, *65*(1), 1–10.

Searle, M. P., Cherry, A. G., Ali, M. Y., & Cooper, D. J. W. (2014). Tectonics of the Musandam Peninsula and northern Oman Mountains: From ophiolite obduction to continental collision. *GeoArabia*, *19*(2), 135–174. https://doi.org/10.1144/SP392.7

Selli, R. (1957). Sulla trasgressione del Miocene nell'Italia meridionale. *Giornale Di Geologia*, *26*, 1–54.

Selli R. (1962). Il Paleogene nel quadro della geologia dell'Italia meridionale. *Memorie Della Societa Geologica Italiana*, *3*(7), 737–790.

Sgrosso, I., Bonardi, G., Amore, F. O., Ascione, A. Castellano, M. C., De Vita, P., Di Donato, V. Morabito, S., Parente, M., Pescatore, E., Putignano, M.L., Sandulli, R. Schiattarella, M., & Tescione, M. (2010). *Note illustrative della carta Geologica d'Italia alla scala 1:50000 - Foglio 504 "Sala Consilina." Servizio Geologico d'Italia, ISPRA*.

Sgrosso, Italo. (1998). Possibile evoluzione cinematica miocenica nell'orogene Centro-Sud-Appenninico. *Bolletino Della Società Geologica Italiana*, *117*(3), 679–724.

Simone, L., Carannante, G., Ruberti, D., Sirna, M., Sirna, G., Laviano, A., & Tropeano, M. (2003). Development of rudist lithosomes in the Coniacian-Lower Campanian carbonate shelves of central-southern Italy: High-energy vs low-energy settings. *Palaeogeography, Palaeoclimatology, Palaeoecology*, *200*(1–4), 5–29. https://doi.org/10.1016/S0031-0182(03)00442-5

Simone, L, & Carannante, G. (1985). Evolution of a carbonate open shelf up to its drowning. *Rend. Accad. Sci. Fis. Mat., Naples, Ser. IV*, *53*, 1–43.

Simone, Lucia, & Carannante, G. (1988). The fate of foramol ("temperate-type") carbonate platforms. *Sedimentary Geology*, *60*(1–4), 347–354. https://doi.org/10.1016/0037-0738(88)90129-7

Sinclair, H. D. (1997). Tectonostratigraphic model for underfilled peripheral foreland basins: An Alpine perspective. *Bulletin of the Geological Society of America*, *109*(3), 324–346. https://doi.org/10.1130/0016-7606(1997)109<0324:TMFUPF>2.3.CO;2

Steuber, T. (2003). Strontium isotope stratigraphy of Cretaceous hippuritid rudist bivalves: Rates of morphological change and heterochronic evolution. In *Palaeogeography, Palaeoclimatology, Palaeoecology* (Vol. 200, pp. 221–243). Elsevier. https://doi.org/10.1016/S0031-0182(03)00452-8

Stouff, V., Geslin, E., Debenay, J.-P., & Lesourd, M. (1999). Origin of morphological abnormalities in Ammonia (Foraminifera): studies in laboratory and natural environments. *The Journal of Foraminiferal Research*, *29*(2), 152–170.

Taddei, A., & Siano, M. G. (1992). Analisi biostratigrafica e considerazioni paleoecologiche sulla successione Neogenica del Monte Alpi (Lucania). *Bollettino Della Società Geologica Italiana*, *111*(2), 255–272.

Taddei Ruggiero, E. (1996). Biostratigrafia e paleoecologia delle Calcareniti di Gravina nei dintorni di Cerignola (brachiopodi e foraminiferi). *Memorie Della Società Geologica Italiana*, *51*, 197–207.

Takata, H., Dettman, D. L., Seto, K., Kurata, K., Hiratsuka, J., & Khim, B. K. (2009). Novel habitat preference of Ammonia "Beccarii" forma 1 in a macrobenthos community on hard substrates in the Ohashi River, Southwest Japan. *The Journal of Foraminiferal Research*, *39*(2), 87–96.

Tavani, S., Storti, F., Lacombe, O., Corradetti, A., Muñoz, J. A., & Mazzoli, S. (2015a). A review of deformation pattern templates in foreland basin systems and fold-and-thrust belts: Implications for the state of stress in the frontal regions of thrust wedges. *Earth-Science Reviews*, *141*, 82–104. https://doi.org/10.1016/j.earscirev.2014.11.013

Tavani, S., Vignaroli, G., & Parente, M. (2015b). Transverse versus longitudinal extension in the foredeep-peripheral bulge system: Role of Cretaceous structural inheritances during early Miocene extensional faulting in inner central Apennines belt. *Tectonics*, 34(7), 1412–1430. https://doi.org/10.1002/2015TC003836

Tavani, S, Corradetti, A., Sabbatino, M., Morsalnejad, D., & Mazzoli, S. (2018). The Meso-Cenozoic fracture pattern of the Lurestan region, Iran: The role of rifting, convergence, and differential compaction in the development of pre- orogenic oblique fractures in the Zagros Belt. *Tectonophysics*, *749*, 104–119. https://doi.org/10.1016/j.tecto.2018.10.031

Tavani, S., Granado, P., Corradetti, A., Camanni, G., Manatschal, G., Mazzoli, S., & Parente, M. (2021). Rift inheritance controls the switch from thin- to thick-skinned thrusting and basal décollement re-localization at the subduction. *GSA Bulletin*, *1*, 1–15. https://doi.org/10.1130/B35800.1/5238599/b35800.pdf

Thibault de Chanvalon, A., Metzger, E., Mouret, A., Cesbron, F., Knoery, J., Rozuel, E., Launeau, Nardelli, M. P., Jorissen, F. J., & Geslin, E. (2015). Two-dimensional distribution of living benthic foraminifera in anoxic sediment layers of an estuarine mudflat (Loire estuary, France). *Biogeosciences*, *12*(20), 6219–6234.

Turcotte, D. L., & Schubert, G. (1982). *Geodynamics: Applications of continuum physics to geological problems*. New York: Wiley.

Turcotte, D. L., & Schubert, G. (2006). *Geodynamics: applications of continuum physics to geological problems*. Wiley.

Ujiié, H. (1966). Shell structure of Japanese smaller foraminifera. Part I Ammonia tochigiensis (Uchio, 1951). In *Transactions and proceedings of the Paleontological Society of Japan* (Vol. 60, pp. 156–165). Palaeontological Society Of Japan.

Ullmann, C. V., & Korte, C. (2015). Diagenetic alteration in low-Mg calcite from macrofossils: A review. *Geological Quarterly*, *59*(1), 3–20. https://doi.org/10.7306/gq.1217

Vaiani, S. C., Vai, G. B., & Borsetti, A. M. (2019). The lectotype of Ammonia beccarii (Linnaeus 1758) from Jacopo Bartolomeo Beccari's original samples. *Micropaleontology*, *65*(6), 561–566.

van de Poel, H. M. (1992). Foraminiferal biostratigraphy and palaeoenvironments of the Miocene-Pliocene Carboneras-Nijar basin (SE Spain). *Scripta Geologica*, *102*, 1–32.

van der Zwaan, G. J. (1982). Paleoecology of late Miocene Mediterranean foraminifera. Utrecht University.

Vecchio, E., Barattolo, F., & Hottinger, L. (2007). Alveolina horizons in the Trentinara Formation (southern Apennines, Italy): Stratigraphic and paleogeographic implications. *Rivista Italiana Di Paleontologia e Stratigrafia*, *113*(1), 21–42. https://doi.org/10.13130/2039-4942/6356

Veevers, J. J., Falvey, D. A., & Robins, S. (1978). Timor Trough and Australia: Facies show topographic wave migrated 80 km during the past 3 my. *Tectonophysics*, *45*(2–3), 217–227.

Vergés, J., Marzo, M., Santaeulària, T., Serra-Kiel, J., Burbank, D. W., Muñoz, J. A., & Giménez-Montsant, J. (1998). Quantified vertical motions and tectonic evolution of the SE Pyrenean foreland basin. *Geological Society Special Publication*, *134*, 107–134. https://doi.org/10.1144/GSL.SP.1998.134.01.06

Vergés, J., Saura, E., Casciello, E., Fernàndez, M., Villaseñor, A., Jiménez-Munt, I., & García-Castellanos, D. (2011). Crustal-scale cross-sections across the NW Zagros belt: implications for the Arabian margin reconstruction. *Geological Magazine*, *148*(5–6), 739–761. https://doi.org/10.1017/S0016756811000331

Vescogni, A., Bosellini, F. R., Cipriani, A., Gürler, G., Ilgar, A., & Paganelli, E. (2014). The Dagˇpazari carbonate platform (Mut Basin, Southern Turkey): Facies and environmental reconstruction of a coral reef system during the Middle Miocene Climatic Optimum.

Palaeogeography, Palaeoclimatology, Palaeoecology, *410*, 213–232. https://doi.org/10.1016/j.palaeo.2014.05.040

Vezzani, L., Festa, A., & Ghisetti, F. C. (2010). Geology and tectonic evolution of the Central-Southern Apennines, Italy. *Special Paper of the Geological Society of America*, *469*, 1–58. https://doi.org/10.1130/2010.2469

Vigorito, M., Murru, M., & Simone, L. (2005). Anatomy of a submarine channel system and related fan in a foramol/rhodalgal carbonate sedimentary setting: a case history from the Miocene syn-rift Sardinia Basin, Italy. *Sedimentary Geology*, *174*(1–2), 1–30.

Vitale, S., & Ciarcia, S. (2013). Tectono-stratigraphic and kinematic evolution of the southern Apennines/Calabria–Peloritani Terrane system (Italy). *Tectonophysics*, *583*, 164–182. https://doi.org/10.1016/j.tecto.2012.11.004

Vitale, S., & Ciarcia, S. (2018). Tectono-stratigraphic setting of the Campania region (southern Italy). *Journal of Maps*, *14*(2), 9–21. https://doi.org/10.1080/17445647.2018.1424655

Vitale, S., Dati, F., Mazzoli, S., Ciarcia, S., Guerriero, V., & Iannace, A. (2012). Modes and timing of fracture network development in poly-deformed carbonate reservoir analogues, Mt. Chianello, southern Italy. *Journal of Structural Geology*, *37*(January 2011), 223–235. https://doi.org/10.1016/j.jsg.2012.01.005

Vitale, Stefano, Amore, O. F., Ciarcia, S., Fedele, L., Grifa, C., Prinzi, E. P., Tavani, S., & Tramparulo, F. D. A. (2018). Structural, stratigraphic, and petrological clues for a Cretaceous-Paleogene abortive rift in the southern Adria domain (southern Apennines, Italy). *Geological Journal*, *53*(2), 660–681. https://doi.org/10.1002/gj.2919

Vitale, S., Prinzi, E. P., Ciarcia, S., Sabbatino, M., Tramparulo, F. D. A., & Verazzo, G. (2019). Polyphase out-of-sequence thrusting and occurrence of marble detritus within the wedge-top basin deposits in the Mt. Massico (southern Apennines): insights into the late Miocene tectonic evolution of the central Mediterranean. *International Journal* *of Earth Sciences*, *108*(2), 501–519. https://doi.org/10.1007/s00531-018-1664-0

Vitale, S., Prinzi, E. P., Tramparulo, F. D., De Paola, C., Di Maio, R., Piegari, E., Sabbatino, M., Natale, J., Notaro, P., & Ciarcia, S. (2020). Late Miocene-Early Pliocene Out-of-Sequence Thrusting in the Southern Apennines (Italy). Geosciences, 10(8), 301. https://doi.org/10.3390/geosciences10080301

Walton, W. R., & Sloan, B. J. (1990). The genus Ammonia Bruennich, 1772; its geographic distribution and morphologic variability. *The Journal of Foraminiferal Research*, *20*(2), 128–156.

Watts, A. B. (2001). *Isostasy and Flexure of the Lithosphere*. Cambridge University Press.

Weinmann, A. E., & Langer, M. R. (2017). Diverse thermotolerant assemblages of benthic foraminiferal biotas from tropical tide and rock pools of eastern Africa. *Revue de Micropaléontologie*, *60*(4), 511–523.

Wennrich, V., Meng, S., & Schmiedl, G. (2007). Foraminifers from Holocene sediments of two inland brackish lakes in central Germany. *The Journal of Foraminiferal Research*, *37*(4), 318–326.

White, T., Furlong, K., & Arthur, M. (2002). Forebulge migration in the Cretaceous Western interior basin of the Central United States. *Basin Research*, *14*(1), 43–54. https://doi.org/10.1046/j.1365-2117.2002.00165.x

Woods, M. A., Wilkinson, I. P., Leng, M. J., Riding, J. B., Vane, C. H., dos Santos, R. A. L., Kender, S., De Schepper, S., Hennissen, J. A. I., Ward, S. L., Gowing, C. J. B., Wilby, P. R., Nichols, M. D., & Rochelle C. A. (2019). Tracking Holocene palaeostratification and productivity changes in the Western Irish Sea: A multi-proxy record. *Palaeogeography, Palaeoclimatology, Palaeoecology*, *532*, 109231.

Wright, V. P. (1991). Calcretes: an introduction. In Wright, V.P. & M. E. Tucker (Eds.), *Calcretes. IAS Reprint Series, Vol.2.* (pp. 1–22). Blackwell Scientific Publications.

Yu, H. S., & Chou, Y. W. (2001). Characteristics and development of the flexural forebulge and basal unconformity of Western Taiwan Foreland Basin. *Tectonophysics*, *333*(1–2), 277–291. https://doi.org/10.1016/S0040-1951(00)00279-1

Zamparelli, V., Cirilli, S., Iannace, A., & Jadoul, F. (1999). Palaeotectonic and palaeoceanographic controls on microbial–serpulid communities in the Norian–Rhaetian carbonates of Italy: a synthesis. *Bioevents and Integrated Stratigraphy of the Triassic and the Jurassic in Italy. Paleopelagos, Special Publications*, *3*, 7–84.

ACKNOWLEDGEMENTS

First, I would like to thank my PhD supervisor Prof. Mariano Parente for his mentoring during these three fruitful years. His support and confidence have carved my human and scientific growth, without mentioning the opportunity he gave me to work in several international scientific environments.

Second, but with the same conviction, I also wish to thank my co-supervisor Prof. Stefano Tavani for his guidance and support. Without his dedication, full availability, and friendship I would have never reached this goal with the same enthusiasm.

An equally heartfelt thanks to my second co-supervisor Prof. Stefano Vitale, not only for his guidance, patience, and support but also for closeness and equally important contribution to the achievement of this goal.

My sincere thanks also go to Dr. Ilenia Arienzo and Prof. Anna Cipriani who, in different circumstances, provided me with wider knowledge concerning several aspects of the fabulous geochemical world, as well as to Dr. Sylvia Riechelmann, Dr. Dieter Buhl, and Ms. Kathrin Krimmler for hosting me in Bochum and providing additional guidance on this topic.

I am immensely grateful to Prof. Stephen Romaniello, Mr. Tyler Goepfert, Ms. Julianne Sarancha, Prof. Gwyneth Gordon, and Prof. Ariel Anbar not only for having hosted me in the US and guided me while the whole world was in lockdown during the Covid-19 pandemic but also for the wonderful time spent and their support and friendship. Their contribution and mentoring during the time I spent at the Arizona State University (USA), where I was provided full access to research facilities, was crucial for my scientific growth.

The two reviewers Prof. Eugenio Carminati and Prof. Jaume Vergés are greatly acknowledged for their review and constructive comments which greatly improved the final version of this thesis.

This research has been funded by the University of Naples Federico II (grant "Progetto di Ricerca di Ateneo" E62F17000190005, scientific coordinator Mariano Parente), which is gratefully thanked. I gratefully acknowledge additional financial support from the Ruth and

Robert Weimer Fund, the John Sanders Fund, and the Friedman Student Research Fund (SEPM Foundation Student Research Grant), from the IAS Postgraduate Grant, and from the James E. and Elloie B. Wilson Memorial Grant (American Association of Petroleum Geologists Foundation Grants-in-Aid Program).

To achieve this goal, very important was the help in the field and microscopy lab by Dr. Lorenzo Consorti who I sincerely acknowledge.

A special loving thanks goes to my partner Amerigo who firmly believes in me, patiently supporting all moments of my life. Thank you for your continuous assistance, and for your guidance and support in achieving this goal as well as in every circumstance of my life.

Several people, not yet cited, have contributed in different cases. Among them, I wish to thank Masi and Andrea.

For their help in several everyday situations during the writing of this thesis and most importantly for their friendship I would also thank Cristina and Katia.

I would also like to thank all my colleagues and all friends that I have not explicitly mentioned.

And then I will switch to my mother tongue for acknowledging my family. Grazie alla mia grande famiglia. Un grazie in particolare va ai miei genitori per avermi fornito dal nulla le basi affinché potessi arrivare fin qui, seguendo in silenzio le mie scelte, con fiducia e profonda stima nei miei confronti. A mio padre dedico ogni passo di questo percorso, a colui che avrebbe messo fieramente questo traguardo tra i suoi trofei più importanti e ora sono io a celebrare lui con grande orgoglio. Sacrificio, dedizione, coraggio e positività sono tra i migliori valori che potessi trasmettermi e attraverso i quali la tua presenza sarà sempre viva.

CURRICULUM VITAE

Monia Sabbatino

Date of birth:	*30 May 1992*
Nationality:	*Italian*
E-mail:	*monia.sabbatino@gmail.com*
E-mail2:	*monia.sabbatino@unina.it*
ORCID	*https://orcid.org/0000-0002-4693-1631*

Education

2006-2011	Pre-university education (Science School)
2011-2015	BSc in Geological Sciences (*110/110 cum laude*) University of Naples Federico II
2015-2017	MSc in Geology and Applied Geology (*110/110 cum laude*) University of Naples Federico II
2017-2021	PhD in Earth, Environment, and Resource Sciences University of Naples Federico II

Awards

2019 “Outstanding Student Poster Award” for the poster presented during the 34th International Meeting of Sedimentology.

2019 Student Assistance Grant by SEPM – Society for Sedimentary Geology.

2020 AAPG Grant-in-Aid by AAPG – American Association of Petroleum Geologists.

2020 Postgraduate Research Grant by IAS – International Association of Sedimentologists.

Publications in peer-reviewed journals

Sabbatino, M., Tavani, S., Vitale, S., Ogata, K., Corradetti, A., Consorti, L., Arienzo, I., Cipriani, A., & Parente, M. Forebulge migration in the foreland basin system of the central-southern Apennine belt (Italy): new high-resolution Sr-isotope dating constraints. *Basin Research*, 2021. (**UNDER-REVIEW**).

Tavani, S., Cardello, G.L., Vignaroli, G., Balsamo, F., Parente, M., **Sabbatino, M.**, Raffi, I., Billi, A., & Carminati, E. Segmentation of the Apennine margin of Tyrrhenian back-arc basin forced by the subduction of an inherited transform system. *Tectonics*, 2021 (**UNDER-REVIEW**).

Cardello, G. L., Vico, G., Consorti, L., **Sabbatino, M.**, Carminati, E., & Doglioni, C. (2021). Constraining the Passive to Active Margin Tectonics of the Internal Central Apennines: Insights from Biostratigraphy, Structural, and Seismic Analysis. *Geosciences*, 11, 160. doi:10.3390/geosciences11040160.

Consorti, L., **Sabbatino, M.**, & Parente, M. (2021). Insights on the paleoecology of Ammonia (Foraminifera, Rotalioidea) from Miocene carbonates of central and southern Apennines (Italy). *Palaeogeography Palaeoclimatology Palaeoecology,* 562, 110105. doi:10.1016/j.palaeo.2020.110105.

Sabbatino, M., Vitale, S., Tavani, S., Consorti, L., Corradetti, A., Cipriani, A., Arienzo, I., & Parente, M. (2020). Constraining the onset of flexural subsidence and peripheral bulge extension in the Miocene foreland of the southern Apennines (Italy) by Sr-isotope stratigraphy. *Sedimentary Geology,* 401, 105634. doi:10.1016/j.sedgeo.2020.105634.

Tavani, S., Corradetti, A., **Sabbatino, M.**, Seers, T., & Mazzoli, S. (2020). Geological record of the transition from induced to self-sustained subduction in the Oman Mountains. *Journal of Geodynamics*, 133, 101674. doi:10.1016/j.jog.2019.101674.

Vitale, S., Prinzi, E. P., Tramparulo, F. D., De Paola, C., Di Maio, R., Piegari, E., **Sabbatino, M.**, Natale, J., Notaro, P., & Ciarcia, S. (2020). Late Miocene-Early Pliocene Out-of-Sequence Thrusting in the Southern Apennines (Italy). *Geosciences*, 10, 301. doi:10.3390/geosciences10080301.

Corradetti, A., Spina, V., Tavani, S., Ringenbach, J.C., **Sabbatino, M.**, Razin, P., Laurent, O., Brichau, S., & Mazzoli, S. (2020). Late-stage tectonic evolution of the Al Hajar Mountains, Oman: new constraints from Paleogene sedimentary units and low-temperature thermochronometry. *Geological Magazine*, 7, 1031-1044. doi:10.1017/S0016756819001250.

Vitale, S., Prinzi, E. P., Ciarcia, S., **Sabbatino, M.**, Tramparulo, F. D. A., & Verazzo, G. (2019). Polyphase out-of-sequence thrusting and occurrence of marble detritus within the wedge-top basin deposits in the Mt. Massico (southern Apennines): insights into the late Miocene tectonic evolution of the central Mediterranean. *International Journal of Earth Sciences*. doi:10.1007/s00531-018-1664-0.

Tavani, S., Corradetti, A., **Sabbatino, M.**, Morsalnejad, D., & Mazzoli, S., (2018). The Meso-Cenozoic fracture pattern of the Lurestan region, Iran: The role of rifting, convergence, and differential compaction in the development of pre-orogenic oblique fractures in the Zagros Belt. *Tectonophysics*, 749, 104-119. doi:10.1016/j.tecto.2018.10.031.

Conference Abstracts and Proceedings

Sabbatino, M., Tavani, S., Vitale, S., Corradetti, A., Consorti, L, & Parente., M. (2021). Spatial-temporal migration of the central-southern Apennine belt and foreland basin system (Italy) constrained by Sr-isotope stratigraphy. *EGU General Assembly*, Vienna, 19-30 April 2021.

Sabbatino, M., Tavani, S., Vitale, S., Corradetti, A., Consorti, L, & Parente, M. (2021). Constraining the onset and migration of the central-southern Apennine foreland basin (Italy) by Sr-isotope stratigraphy. *IAS annual meeting*, Prague 22-24 June 2021.

Romaniello, S. J., Lau, K. V., **Sabbatino, M.**, & Parente, M. A revised paradigm for the interpretation of δ238U during periods of calcite seas. *Goldschmidt annual meeting,* Lione 4-9 July 2021.

Romaniello, S. J., Lau, K. V., **Sabbatino, M.**, & Parente, M. A revised paradigm for the interpretation of δ238U during periods of calcite seas. AGU fall meeting, online conference 1-17 December 2020.

Sabbatino, M., Vitale, S., Tavani, S., Consorti, L., Corradetti, A., Arienzo, I., Cipriani, A. & Parente, M.: Structural and Stratigraphic Constraints on the Deposits Bracketing the Miocene Forebulge Unconformity in the Central-Southern Apennine Fold-and-Thrust Belt (Italy). *AGU fall meeting*, San Francisco 9-13 December 2019.

Sabbatino, M., Vitale, S., Consorti, L., Corradetti, A., Arienzo, I., Cipriani, A. & Parente, M.: Multidisciplinary study of the Miocene forebulge unconformity in central-southern Apennines (2019). *SGI-SIMP-SOGEI meeting*, Parma, 16-19 September 2019.

Tavani, S., Corradetti, A., **Sabbatino, M.** & Mazzoli, S.: Geological record of the transition from induced to self-sustained subduction in the Oman Mountains (2019). *SGI-SIMP-SOGEI meeting*, Parma, 16-19 September 2019.

Sabbatino, M., Consorti, L., Vitale, S., Tavani, S., Corradetti, A., & Parente, M. (2019). The Miocene forebulge unconformity in central-southern Apennines: a sedimentological and stratigraphic study. *IAS annual meeting*, Rome 10-13 September 2019.

Sabbatino, M., Consorti, L., Vitale, S., Tavani, S., Corradetti, A., Arienzo, I., Cipriani, A., Lugli, F. & Parente, M. (2019). High-resolution stratigraphy of Late Cretaceous and Miocene shallow-water carbonates of central-southern Apennines (Italy). *IAS annual meeting*, Rome 10-13 September 2019.

Sabbatino, M., Consorti, L., Tavani, S., Vitale, S., Corradetti, A., Arienzo, I., Cipriani, A., Lugli, F. & Parente, M. (2019). From the final demise of the Mesozoic carbonate platform to the Miocene transgression: high-resolution stratigraphy of the shallow-water carbonates of southern and central Apennines (Italy). *3rd International Congress on Stratigraphy STATI 2019*, Milan, 2-5 July 2019.

Parente, M., Iannace, A., Amodio, S., & **Sabbatino, M.** (2019). Stratigraphy and facies of the Apennine Carbonate Platform (southern Italy): the shallow-water record of Mesozoic OAEs. *FT3 pre-conference field trip of the 3rd International Congress on Stratigraphy STRATI 2019*, Milan (Italy), 2-5 July 2019.

Consorti, L., Köroğlu, F., & **Sabbatino, M.** (2019). Larger Foraminifera Biostratigraphy of the Maastrichtian-Paleocene shallow-water carbonates of Şahinkaya Member (Eastern Pontides, Trabzon, NE Turkey). *3rd International Congress on Stratigraphy STATI 2019*, Milan, 2-5 July 2019.

Sabbatino, M., Tavani, S., Vitale, S., Consorti, L., Corradetti, A., Arienzo, I., Cipriani, A., Lugli, F. & Parente, M. (2019). Constraining the age of the Miocene forebulge unconformity in central-southern Apennines: a Sr-isotopes and structural study. *EGU General Assembly*, Vienna, 7-12 April 2019.

Sabbatino, M., Vitale, S., Tavani, S., Corradetti, A., Cipriani, A. & Parente, M. (2018). Structural and stratigraphic constraints of the Cretaceous to Miocene deposits bracketing the forebulge unconformity in southern Apennines by means of extensional structures pattern and Sr-isotope stratigraphy. *SGI-SIMP congress*, Catania, Italy, 12-14 September 2018, Abstract book, DOI: 10.3301/ABSGI/2018.02

Consorti, L., **Sabbatino, M.**, Cipriani, A. & Parente, M. (2018). Biostratigraphic and Sr-isotope constraints on the Miocene transgressive surface in the Southern Apennines. *SGI-SIMP congress*, Catania, Italy, 12-14 September 2018, Abstract book, DOI: 10.3301/ABSGI/2018.02

Prinzi, E., **Sabbatino, M.**, Ciarcia, S., Tramparulo, F.d'A & Vitale, S. (2017) - Late Miocene-Early Pliocene out-of-sequence thrusting in the southern Apennines (Italy). *G.I.G.S. meeting (Gruppo Italiano di Geologia Strutturale della Società Geologica Italiana)*, Padova, Italy, July 10-13.

*A detailed list of the publications and conference abstracts and proceedings published during my PhD along with associated material can be found on my ResearchGate page: https://www.researchgate.net/profile/Monia_Sabbatino